

# **Peristaltic transport of fluids with convective conditions**



*By*

*Humaira Yasmin*

**Department of Mathematics  
Quaid-i-Azam University  
Islamabad, Pakistan  
2015**

# **Peristaltic transport of fluids with convective conditions**



*By*

***Humaira Yasmin***

Supervised By

***Prof. Dr. Tasawar Hayat***

**Department of Mathematics  
Quaid-i-Azam University  
Islamabad, Pakistan**

**2015**  
**Peristaltic transport of fluids with  
convective conditions**



*By*

***Humaira Yasmin***

**A THESIS SUBMITTED IN THE PARTIAL FULFILLMENT OF THE REQUIREMENT FOR  
THE DEGREE OF  
DOCTOR OF PHILOSOPHY  
IN  
MATHEMATICS**

**Supervised By**

***Prof. Dr. Tasawar Hayat***

**Department of Mathematics  
Quaid-i-Azam University**

**Islamabad, Pakistan  
2015  
Peristaltic transport of fluids with  
convective conditions**

By

**Humaira Yasmin**

**CERTIFICATE**

**A THESIS SUBMITTED IN THE PARTIAL FULFILLMENT OF THE  
REQUIREMENTS FOR THE DEGREE OF THE DOCTOR OF  
PHILOSOPHY**

**We accept this thesis as conforming to the required standard**

1. \_\_\_\_\_  
Prof. Dr. Tasawar Hayat  
(Chairman)

2. \_\_\_\_\_  
Prof. Dr. Tasawar Hayat  
(Supervisor)

3. \_\_\_\_\_  
Dr. Muhammad Salahuddin  
(External Examiner)

4. \_\_\_\_\_  
Dr. Khalid Hanif  
(External Examiner)

**Department of Mathematics**

**Quaid-i-Azam University**  
**Islamabad, Pakistan**  
**2015**

# Preface

There is no doubt about extensive applications of peristalsis in physiology and industry. Especially the dynamics of non-Newtonian fluids by peristaltic mechanism is hot topic of research. Peristalsis is quite significant in various engineering problems associated with powder technology, sedimentation, combustion, fluidization, heart-lung machine and paint spraying. In plant physiology, such mechanism is involved in phloem translocation by driving a sucrose solution along tubules by peristaltic contractions. Heat transfer analysis in peristalsis has been also used to obtain information about the properties of tissues and thus quite significant in the biomedical sciences. In fact heat transfer is important because nutrients diffuse out from blood. Further the temperature difference in any situation results from energy flow into a system or energy flow from a system to surroundings. The former leads to heating whereas latter leads to cooling of an object. This is known as convection heat transfer. Bulk motion of fluid boosts heat transfer in many physical situations. It is supportive to predict how long it takes for a hot object to cool down at a certain temperature. Heat transfer subject to convective conditions is involved in processes such as thermal energy storage, gas turbines, nuclear plants etc. This concept is of great value because the thermodynamic aspects of blood are quite prevalent in processes such as oxygenation and hemodialysis. Moreover the energy flux is not only induced by the temperature gradient but by composition gradient as well. The simultaneous effects of heat and mass transfer with convective boundary conditions provide complicated expressions relating the fluxes and driving potentials. Keeping this in mind the present thesis highlights the heat transfer in peristaltic transport of fluids in a channel with convective boundaries. The relevant equations are modeled and solved for the approximate and numerical solutions. Salient features of heat transfer in view of convective boundary conditions are emphasized. Motivated by all such facts we structure the present thesis as follows:

The review of some existing literature relevant to peristaltic transport and some fundamental equations is given in chapter one.

Chapter two addresses the peristaltic flow of third order fluid in an asymmetric channel. Channel walls are subjected to the convective boundary conditions. The channel asymmetry is produced by choosing the peristaltic wave train on the walls to have different amplitudes and phase. Long wavelength approximation and perturbation method yield the series solutions for the stream function, temperature and longitudinal pressure gradient. Analysis has been further carried out for pressure rise per wavelength through numerical integration. Several graphs of physical interest are displayed and discussed. The results of this chapter are **published in Journal of Mechanics 29(2013) pp. 599-607.**

Chapter three deals with the peristaltic transport of viscous nanofluid in an asymmetric channel. The channel walls satisfy the convective conditions. Effects of Brownian motion and thermophoresis are taken into account. The relevant flow analysis is first modeled and then computed for the series solutions of temperature and concentration fields. Closed form expression of stream function is constructed. Plots are prepared for a parametric study reflecting the effects of Brownian motion, thermophoresis, Prandtl, Eckert and Biot numbers. The findings of this chapter have been **published in Journal of Molecular Liquids 193 (2014) pp. 74-82.**

The peristaltically driven Casson fluid flow in an asymmetric channel with convective conditions is investigated in chapter four. The Soret and Dufour effects are studied in the presence of chemical reaction. The relevant flow analysis is modelled for Casson fluid in a wave frame. Computations of solutions are made for the velocity, temperature and concentration fields. The performed analysis shows that the two yield planes exist because of channel asymmetry. These planes are described

in terms of the core width by working on the transcendental equation. Closed form expression of streamfunction is obtained. Results displayed and discussed for the effects of Casson fluid parameter, chemical reaction parameter, Prandtl, Schmidt, Soret, Dufour and Biot numbers. The research presented in this chapter is **published in Computers & Fluids 89 (2014) pp. 242-253.**

Chapter five explores the heat transfer effects in peristaltic flow of couple stress fluid. An incompressible fluid is considered in a channel with convective boundary conditions. This study is motivated towards investigating the physiological flow through particle size effect. Long wavelength and low Reynolds number approach is adopted. Effects of various physical parameters like couple stress parameter and Brinkman and Biot numbers on the velocity profile, streamlines pattern, temperature profile, pumping action and trapping are studied. Computational results are presented in graphical form. The contents of this chapter have been **accepted for publication in Heat Transfer Research (2013).**

Chapter six is concerned with the peristaltic transport of Johnson-Segalman fluid in an asymmetric channel with convective boundary conditions. Mathematical modelling is based upon the conservation laws of mass, linear momentum and energy. Resulting equations have been solved after using long wavelength and low Reynolds number considerations. Results for the axial pressure gradient, velocity and temperature profiles are obtained for small Weissenberg number. Expressions of the pressure gradient, velocity and temperature are analyzed for various embedded parameters. Pumping and trapping phenomena are also explored. The observations of conducted analysis are **published in Applied Mathematics and Mechanics-English Edition 35 (2014) pp. 697-717.**



The peristaltic flow of power law fluid in an asymmetric channel is discussed in chapter seven. The flow is generated because of peristaltic waves propagating along the channel walls. Heat transfer is examined through convective conditions at channel walls. Mathematical model is presented employing lubrication approach. The differential equations governing the flow are nonlinear and admit non-unique solutions. There exists two different physically meaningful solutions one of which satisfying the boundary conditions at the upper wall and the other at the lower wall. The effects of Biot numbers and the power-law nature of the fluid on the longitudinal velocity, temperature and pumping characteristics are studied in detail. The streamlines pattern and trapping are given due attention. Important conclusions have been pointed out. The contents of this chapter are **published in Journal of the Brazilian Society of Mechanical Sciences and Engineering 37 (2014) pp. 463-477.**

Chapter eight examines the peristaltic transport of an incompressible micropolar fluid in an asymmetric channel with heat source/sink and convective boundary conditions. Mathematical formulation is completed in a wave frame of reference. Long wavelength and low Reynolds number approach is adopted. The solutions for velocity, microrotation component, axial pressure gradient, temperature, stream function and pressure rise over a wavelength are obtained. Velocity and temperature distributions are analyzed for different parameters of interest. The findings of this chapter are **published in Zeitschrift für Naturforschung A (ZNA) 69 (2014) pp. 425-432.**

Chapter nine investigates the peristaltic flow of Sisko fluid in an asymmetric channel with sinusoidal wave propagating down its walls. The channel walls in heat transfer process satisfy the convective conditions. The flow and heat transfer equations are modeled and

nondimensionalized. The shear-thinning and shear-thickening properties of Sisko fluid in the present nonlinear analysis are examined. Comparison between the results of Sisko and viscous fluids is given. Velocity and temperature distributions, pressure gradient and streamline pattern are addressed with respect to different parameters of interest. Pumping and trapping phenomena are also analyzed. The analysis of this chapter has been **accepted for publication in International Journal of Applied Mathematics and Information Sciences (2015).**

Peristaltic motion of Carreau fluid in an asymmetric channel with convective boundary conditions is investigated in chapter ten. Mathematical formulation is first reduced in a wave frame of reference and then solutions are constructed. Expressions of the stream function, axial pressure gradient, temperature and pressure rise over a wavelength are obtained for small Weissenberg number. Velocity and temperature distributions are explored for the sundry parameters. A comparative study between the results of viscous and Carreau fluid is made. Such observations are **published in Applied Bionics and Biomechanics 11 (2014) pp. 157-168.**

Chapter eleven addresses the peristaltic flow of an incompressible and electrically conducting Williamson fluid in a symmetric planar channel with heat and mass transfer. Hall effects, viscous dissipation and Joule heating are also taken into consideration. Mathematical model is presented for long wavelength and low Reynolds number approximations. The differential equations governing the flow are highly nonlinear and thus perturbation solution for small Weissenberg number is obtained. Effects of the heat and mass transfer Biot numbers and Hall parameter on the longitudinal velocity, temperature, concentration and pumping characteristics are studied in detail. The streamlines pattern and trapping are also given due attention. Main observations of present study

are included in the concluding section. The results of this chapter are **published in International Journal of Biomathematics7 (2014) 1450058 (27 pages) DOI:10.1142/S1793524514500582.**

# Peristaltic transport of fluids with convective conditions


By


***Humaira Yasmin***


## CERTIFICATE


A THESIS SUBMITTED IN THE PARTIAL FULFILLMENT OF THE  
REQUIREMENTS FOR THE DEGREE OF THE DOCTOR OF  
PHILOSOPHY

We accept this thesis as conforming to the required standard

1.  22/5/15  
Prof. Dr. Tasawar Hayat  
(Chairman)

2.  22/5/15  
Prof. Dr. Tasawar Hayat  
(Supervisor)

3.   
Dr. Muhammad Salahuddin  
(External Examiner)

4.   
Dr. Khalid Hanif  
(External Examiner)

**Department of Mathematics  
Quaid-i-Azam University  
Islamabad, Pakistan  
2015**

# Contents

<b>1</b>	<b>Literature survey on peristalsis</b>	<b>6</b>
<b>2</b>	<b>Peristaltic flow of third-order fluid in a channel with convective boundary conditions</b>	<b>16</b>
2.1	Introduction . . . . .	16
2.2	Mathematical formulation and flow equations . . . . .	16
2.3	Method of solution . . . . .	21
2.3.1	Zeroth order system and its solution . . . . .	22
2.3.2	First order system and its solution . . . . .	23
2.3.3	Second order system and its solution . . . . .	24
2.4	Graphical analysis and discussion . . . . .	35
2.4.1	Pumping characteristics . . . . .	35
2.4.2	Velocity and temperature profiles . . . . .	38
2.4.3	Trapping . . . . .	40
2.5	Closing remarks . . . . .	41
<b>3</b>	<b>Simultaneous effects of convective conditions and nanoparticles on peristaltic motion</b>	<b>42</b>
3.1	Introduction . . . . .	42
3.2	Constitutive equations . . . . .	42
3.3	Mathematical medeling . . . . .	43
3.4	Solution procedure . . . . .	48
3.5	Results and discussion . . . . .	51

3.6	Main points . . . . .	57
<b>4</b>	<b>Soret and Dufour effects in peristaltic transport of physiological fluids with chemical reaction: A mathematical analysis</b>	<b>59</b>
4.1	Introduction . . . . .	59
4.2	Governing equation . . . . .	60
4.3	Problem formulation . . . . .	60
4.4	Solution methodology . . . . .	64
4.5	Discussion . . . . .	68
4.5.1	Yield plane locations . . . . .	68
4.5.2	Pumping characteristics . . . . .	69
4.5.3	Velocity distribution . . . . .	71
4.5.4	Temperature profile . . . . .	72
4.5.5	Concentration profile . . . . .	75
4.5.6	Streamlines and trapping . . . . .	77
4.6	Conclusions . . . . .	80
<b>5</b>	<b>Exact solution for peristaltic flow of couple stress fluid in an asymmetric channel with convective conditions</b>	<b>81</b>
5.1	Introduction . . . . .	81
5.2	Mathematical modeling and analysis . . . . .	81
5.3	Results and discussion . . . . .	87
5.3.1	Pumping characteristics . . . . .	87
5.3.2	Velocity behavior . . . . .	90
5.3.3	Temperature profile . . . . .	91
5.3.4	Trapping . . . . .	92
5.3.5	Closing remarks . . . . .	95
<b>6</b>	<b>Peristaltic flow of Johnson-Segalman fluid in an asymmetric channel with convective boundary conditions</b>	<b>97</b>
6.1	Introduction . . . . .	97

6.2	Flow equations . . . . .	97
6.3	Problem statement . . . . .	98
6.4	Solution scheme . . . . .	102
6.4.1	Zeroth order system . . . . .	103
6.4.2	First order system . . . . .	103
6.4.3	Zeroth order solution . . . . .	104
6.4.4	First order solution . . . . .	105
6.5	Discussion . . . . .	108
6.5.1	Pumping characteristics . . . . .	108
6.5.2	Velocity behavior . . . . .	111
6.5.3	Temperature profile . . . . .	113
6.5.4	Trapping . . . . .	115
6.6	Closing remarks . . . . .	118
<b>7</b>	<b>Convective heat transfer analysis on power-law fluid in a channel with peristalsis</b>	<b>119</b>
7.1	Introduction . . . . .	119
7.2	Problem formulation and flow equations . . . . .	119
7.3	Non-unique solutions of the problem . . . . .	123
7.4	Results and discussion . . . . .	127
7.5	Concluding remarks . . . . .	142
<b>8</b>	<b>Exact solution for peristaltic transport of micropolar fluid in a channel with convective conditions and heat source/sink</b>	<b>144</b>
8.1	Introduction . . . . .	144
8.2	Flow equations . . . . .	144
8.3	Exact solution . . . . .	148
8.4	Shear stress distribution at the walls . . . . .	151
8.5	Results and discussion . . . . .	151
8.6	Concluding remarks . . . . .	154

<b>9 Peristaltic flow of Sisko fluid in an asymmetric channel with convective boundary conditions</b>	<b>155</b>
9.1 Introduction . . . . .	155
9.2 Problem formulation and flow equations . . . . .	155
9.3 Method of solution . . . . .	159
9.3.1 Zeroth order system . . . . .	160
9.3.2 First order system . . . . .	161
9.3.3 Zeroth order solution . . . . .	161
9.3.4 First order solution . . . . .	163
9.4 Results and discussion . . . . .	166
9.4.1 Pumping characteristics . . . . .	166
9.4.2 Velocity behavior . . . . .	168
9.4.3 Temperature profile . . . . .	170
9.4.4 Trapping . . . . .	172
9.5 Concluding remarks . . . . .	174
<b>10 Peristaltic motion of Carreau fluid in a channel with convective boundary conditions</b>	<b>175</b>
10.1 Introduction . . . . .	175
10.2 Flow description . . . . .	175
10.3 Perturbation solution . . . . .	180
10.3.1 System of order $We^0$ . . . . .	180
10.3.2 System of order $We^2$ . . . . .	181
10.3.3 Solution for system of order $We^0$ . . . . .	181
10.3.4 Solution for system of order $We^2$ . . . . .	183
10.4 Results and discussion . . . . .	186
10.5 Concluding remarks . . . . .	191
<b>11 Convective heat and mass transfer analysis on peristaltic flow of Williamson fluid with Hall effects and Joule heating</b>	<b>192</b>
11.1 Introduction . . . . .	192



11.2	Flow equations . . . . .	193
11.3	Problem formulation . . . . .	194
11.4	Series solution . . . . .	198
11.4.1	System of order zero . . . . .	198
11.4.2	System of order one . . . . .	199
11.5	Results and discussion . . . . .	202
11.6	Concluding remarks . . . . .	211
<b>12</b>	<b>Summary</b>	<b>213</b>

# Chapter 1

## Literature survey on peristalsis

The study of peristaltic flows has been originated by pioneer experimental work of Latham [1]. He conducted the experimental study for the peristaltic motion of viscous fluid. The theoretical work by Shapiro [2] has good agreement with the experimental results in ref. [1]. Burns and Parkes [3] presented the peristaltic motion with zero Reynolds number for both planar and axisymmetric flow geometries. The series solution was acquired for small amplitude ratio. Fung and Yih [4] discussed the reflux phenomenon for small amplitude ratio in a planar channel. They concluded that the reflux occurs at the middle of the channel. They ventured that in the vasomotion of small blood vessels, the peristalsis is convoluted. The peristaltic motion in tubes is revealed by Barton and Reynor [5]. They determined the relationship among pressure difference and average flow rate through a wavelength. They expressed two types of analysis; firstly for very large wall disturbance wavelength when compared with average radius and secondly for smaller wall disturbance wavelength than the average radius of the tube. Shapiro et al. [6] discussed the peristaltic flows for both planar and axisymmetric cases. Both the geometries are investigated by means of amplitude ratios ranging from zero to full occlusion and physiological significance of reflux phenomenon is presumed to be true in ureter and the gastrointestinal systems. Another theoretical study for axisymmetric geometry is proposed by Yin and Fung [7] under the postulation of small amplitude ratio. Jaffrin and Shapiro [8] looked at the inertia-free viscous fluid movement and they offered the physical picture of peristaltic pump. Peristaltic flow for small wave number is inspected by Zein and Ostrach [9]. Their exploration was directed to the possible application of peristalsis to urine flow in the

human ureters. Lew et al. [10] discussed two solutions for the peristaltic motion of mixing and carrying chyme in small intestine; one for peristaltic carrying in which fluid motion is created in the absence of net pressure gradient and the other for peristaltic compression deprived of the net transport of fluid. Lew and Fung [11] discussed the axisymmetric flow of the Newtonian fluid at low Reynolds number through a rigid circular cylindrical tube. This analysis gave the basics for understanding the fluid flow in vessels (such as veins and lymphatic ducts) of the living body. Peristaltic pumping with the effects of inertia and streamline curvature has been seen by Jaffrin [12]. He obtained theoretical results for the peristaltic pumping in two-dimensional tube with inertia and curvature effects which physically corresponds to the case of roller pumps and the gastrointestinal tract. Semleser et al. [13] presented a mathematical model for the mechanism of swimming of spermatozoa in the cervix. Gupta and Seshadri [14] explored the mechanism of peristalsis in non-uniform channels/tubes with particular reference to the spermatoc fluid flow in the vas deferens. Liron [15] developed the solution by double expansion for Reynolds number and the square of the wave number for pipe/channel flow with peristalsis and he discussed the efficiency and performance of biological functions due to the peristaltic fluid transport. The blood flow affected by moving magnetic field is perceived by Stud et al. [16]. Srivastava and Srivastava [17] discussed the peristaltic flow of a two-phase fluid, peripheral and core fluid, model in the non-uniform tube and channel. The results obtained by Srivastava and Srivastava was applied and matched with the experiential flow rates of spermatoc fluid in vas deferens of rhesus monkeys. Agrawal and Anwaruddin [18] scrutinized the magnetic field effects on blood flow through a flexible channel which is equally branched. They deduced that the cardiac operations can be carried out under the influence of magnetic field which works as a blood pump. The mathematical aspects of intestinal peristaltic waves as a physical model were investigated by Metry and Chauvet [19]. Subsequent problem is solved by means of finite element scheme. The analysis of two immiscible viscous fluids with peristalsis is carried out by Rao and Usha [20] in a circular tube. The reflux phenomenon is observed in pumping and co-pumping regions and it is revealed that reflux occurs in pumping region and in the co-pumping region, it is vague. Chu and Fang [21] discussed two important cases i.e., the no-slip and slip flow cases with peristalsis. Eytan et al. [22] discussed the flow pattern and transport phenomena of intrauterine fluid in a finite tapered channel on account of the displacements of

symmetric and asymmetric channel walls. They explored that the results have great relevance to intrauterine fluid transport, embryo transfer and hydrosalpinx. Selverov and Stone [23] found the results for the flows along the boundary of a closed rectangular container and concluded that these results might be convenient for modeling peristaltically operated micro-electromechanical systems devices. Shehawey and Husseny [24] have talked about the viscous fluid under the transverse magnetic field effects through the porous channel with peristalsis. Shehawey et al. [25] examined the influence of constant magnetic field on an incompressible viscous fluid flow between the two inclined porous plates. Mekheimer [26] examined the effect of magnetic field on peristaltic motion of blood in a non-uniform channel. Mishra and Rao [27] studied the peristaltic flow of Newtonian fluid in an asymmetric channel. Tzirtzilakis [28] has suggested three-dimensional mathematical model depicting the Newtonian blood flows under the influence of an applied magnetic field. Teymori and Sani [29] designed and simulated the electrostatic micro-channel pump that works on the basis of peristaltic action and fulfills all the requirements of medical drug delivery. Shehawey et al. [30] employed the Adomian decomposition method to obtain the solution of the incompressible viscous fluid flow through a porous medium in an asymmetric channel. Srivastava [31] studied the effects of endoscope on the chyme movement in the small intestines. The pressure drop and frictional forces were discussed at the intestinal walls and endoscope. Design, fabrication, and experimental characterization of a peristaltic micropump for biomedical applications are discussed by Nguyen et al. [32]. Ebaid [33] studied the transport of Newtonian fluid in an asymmetric channel under the slip and magnetic field effects with peristalsis. Ali et al. [34] have discussed the slip effect on peristalsis with variable viscosity and they obtained the exact and series solutions (in the power of viscosity parameter) for hydrodynamic and magnetohydrodynamic cases. Lozano and Sen [35] investigated the peristaltic transport in two-dimensional planar and axisymmetric flow cases. They discussed the streamline patterns and their local and global bifurcations. Wave shape optimization is discussed by Walker and Shelley [36] for peristaltic pumping by using variational method in a two-dimensional channel with Navier-Stokes fluid. A compressible viscous fluid with peristalsis is discussed by Mekheimer and Abdel-Wahab [37]. Keimanesh et al. [38] explored the third grade fluid flow between two parallel plates. They have used the multi-step differential transform method to obtain the solution.

Since most of the fluids in physiology are of non-Newtonian character. Hence the mechanism of peristalsis has been also discussed for the non-Newtonian fluids in the past. The analytical properties of physiological non-Newtonian fluids with peristalsis were deliberated by Raju and Devanathan [39]. They took peristaltically driven power-law fluid and found the results in terms of the power series of wave amplitude in a tube. Casson [40] elaborated the flow equation for pigment oil-suspensions of the printing ink type fluid. The discussion on viscoelastic fluid with peristalsis is given by Raju and Devanathan [41]. They considered the solutions for small Reynolds number and no inertia force. Johnson and Segalman [42] proposed the model for viscoelastic fluid behavior with non-affine deformation. Eringen [43] described the theory of micropolar fluid which can support couple stresses, body couples and exhibits microrotation and microinertial effects. The theory of micropolar fluids is a special case of the theory of simple microfluids introduced by Eringen [44]. Bohme and Friedrich [45] studied the peristaltic motion of viscoelastic fluids with small Reynolds number and no inertia force. Srivastava and Srivastava [46] investigated the problem of peristaltic transport of blood assuming a single-layered Casson fluid and ignored the presence of a peripheral layer. The peristaltic motion in the uniform/non-uniform tubes was contributed by Srivastava and Srivastava [47] in which they have taken power-law fluid and this study was associated with pragmatic flow rates in the vas deferens and small intestine. Chaturani and Samy [48] showed the blood as Herschel-Bulkley fluid in their study. They inquired the blood flow through a stenosed artery and discussed some arterial diseases in detail. Misery [49] reflected the creeping flow assumption for Carreau fluid in a planar channel with peristalsis. Siddiqui and Schwarz [50] analyzed the flow characteristics of third order fluid through peristaltic motion. They inspected fluid flow in a planar channel and obtained perturbation solution for small Deborah number. Siddiqui and Schwarz [51] scrutinized the peristaltic pumping of a second order fluid contained in an axisymmetric duct. Perturbed solution for wave number in dimensionless form was developed. Strohmer et al. [52] found the relationship between the individual uterine size and the thickness of endomaterial in stimulated cycles. Usha and Rao [53] considered the two-layered power-law fluids within axisymmetric conduits executing peristaltic movement. Eytan and Elad [54] observed that the situation of intrauterine fluid flow due to myomaterial contractions is a peristaltic type fluid motion in a cavity. The passage of food bolus through the oesophagus is inquired by Misra and Pandey

[55]. The transfer of power-law fluid via axisymmetric peristaltic waves in a circular tube was analyzed. A mathematical study of peristaltic transport of Casson fluid is given by Mernone et al. [56] in two dimensional axisymmetric channel using the generalized form of the constitutive equation for Casson fluid. Rao and Mishra [57] studied the peristaltic flow of power-law fluid. They have made investigation in axisymmetric porous tube with slip conditions and concluded that the results of this study have obtained appreciation in observing the movement of chyme in small intestines. Nagarani and Sarojamma [58] studied the peristaltic transport of Casson fluid in an asymmetric channel. They discussed the effects of yield stress of the fluid and asymmetry of the channel. Vajravelu et al. [59] looked at the peristaltic pumping for Herschel-Bulkley fluid in a two-dimensional channel. They gave a comparison of trapping phenomenon between the Newtonian, Bingham, power-law and Herschel-Bulkley fluids. Vajravelu et al. [60] studied the peristaltic flow of Herschel-Bulkley fluid in contact with a Newtonian fluid. They explored its numerous applications to flows with biological fluids like blood, chyme, intrauterine fluid etc. Haroun [61] discussed the peristaltic motion of third order fluid in an asymmetric channel. Series solution was obtained up to second order for small Deborah number. Peristaltic flow of MHD third grade fluid in a circular cylinder-shaped tube was discussed by Hayat and Ali [62]. Hayat et al. [63] pondered the MHD peristaltic motion of third grade fluid in a planar channel and solution in the series of Deborah number is demonstrated. Hayat et al. [64] discussed the peristaltic transport of third order fluid in an asymmetric channel with slip conditions. Hayat et al. [65] discussed the peristaltic flow of third order fluid with induced magnetic field effects. The solution for stream function, axial velocity, magnetic force function and axial-induced magnetic field are obtained. Haroun [66] studied the peristaltic flow of fourth grade fluid in an asymmetric channel. Tsiklauri and Beresnev [67] have studied the viscoelasticity of fluid by considering the flow of Maxwell fluid in a circular tube with porous medium. They analyzed that such type of study have practical applications like blood flow in living creatures. Shehway et al. [68] studied the effect of slip conditions in porous media by examining the flow of Newtonian and non-Newtonian Maxwellian fluids in cylindrical axisymmetric tube. Peristaltic flow of Maxwell fluid in an asymmetric channel was probed by Hayat et al. [69]. They obtained series solutions for small values of wave number. Hayat et al. [70] studied the peristaltic motion of an Oldroyd-B fluid in a planar channel. The effects of relaxation and retardation times have been explained

by Haroun [71] while discussing an Oldroyd viscoelastic fluid with peristalsis. Hayat et al. [72] have obtained the solution for small wave number by applying regular perturbation method up to second order for peristaltic transport of Burgers' fluid in a planar channel. A detailed analysis is given on the biviscosity fluid which is electrically conducting in a non-uniform tube (see Eldabe [73]). Ali and Hayat [74, 75] discussed the peristaltic flow of micropolar and Carreau fluids in an asymmetric channel, respectively. Induced magnetic field was given due attention. Kothandapani and Srinivas [76] studied the MHD peristaltic motion of Jeffrey fluid in an asymmetric channel. This article inspected the pumping features, pressure gradient and trapping phenomenon. Wang et al. [77] examined the MHD peristaltic transport of Sisko fluid in the symmetric and asymmetric channels numerically. They obtained solution by using iterative method and analyzed the shear thinning and thickening effects. Different wave forms are discussed in a diverging tube by Hariharan et al. [78] for power-law and Bingham fluids under the influence of peristaltic mechanism. They discussed the reflux phenomenon by tracing the path lines of massless particles. Nadeem and Akbar [79] discussed the peristaltic flow of Walter's B fluid in a uniform inclined tube. Ali et al. [80] discussed the peristaltic transport of third grade fluid in a curved channel. The peristaltically driven second grade in porous medium is examined by Abd elmaboud and Mekheimer [81]. Ellahi et al. [82] constructed the series solutions of MHD Jeffrey fluid flow in eccentric cylinders. Peristaltic motion of fractional bio-fluids is discussed numerically by Tripathi [83]. Nadeem et al. [84] studied the Walter's B fluid in endoscope with peristalsis. Fractional Maxwell fluid flow between coaxial cylinders is discussed by Fetecau et al. [85]. Noreen et al. [86] considered the peristaltic motion of pseudoplastic fluid under the influence of slip and induced magnetic field. Peristaltic flow of second order fluid in presence of induced magnetic field is investigated by Hayat et al. [87]. Yazdanpanh-Ardakani and Niroomand-Oscii [88] proposed a new approach in modeling peristaltic motion of non-Newtonian fluid. Maiti and Misra [89] and Rao and Rao [90] discussed the peristaltic flow of couple stress fluid through porous medium. Hayat et al. [91] considered the Phan-Thein-Tanner fluid flow in a planar channel under peristaltic action. Exact solution to peristaltic transport of power-law fluid in asymmetric channel with compliant walls is obtained by Hayat and Javed [92]. Kalantri et al. [93] explored numerical study of the non-Newtonian fluid through curved channels. Peristaltic motion of fourth grade fluid between porous walls

with suction and injection is analyzed by Hari Prabakaran et al. [94]. Effects of Hall current on pulsatile and peristaltic motion of a particle-fluid suspension is observed by Gad [95]. El Koumy et al. [96] examined the Hall and porous boundaries effects on peristalsis of Maxwell fluid through porous medium with peristalsis. Three dimensional peristaltic flow of Williamson fluid in a rectangular duct is investigated by Ellahi et al. [97]. Nadeem et al. [98] observed the Williamson fluid in a curved channel with compliant walls. Akram et al. [99] obtained the numerical and analytical solutions for Williamson fluid under the influence of induced magnetic field.

There are many applications of heat transfer with peristalsis such as in biomedical sciences and electronic industries etc. Radhakrishnamacharya and Murty [100] studied the non-uniform channel with peristalsis containing viscous fluid. They have given the series solutions in terms of wave number for temperature distribution and heat transfer coefficient by using perturbation technique. Vajravelu et al. [101] analyzed the heat transfer analysis in a vertical porous annular region for viscous fluid between two concentric tubes with peristalsis. Double perturbation method is utilized to obtain the solution about free convection and porosity parameters. In vertical annulus with heat sink/source the problem was deliberated by Mekheimer and Elmaboud [102]. Srinivas and Kothandapani [103] have talked about the peristaltically driven MHD viscous fluid flow with consideration of asymmetry of the channel. Srinivas and Gayathri [104] examined heat transfer effects on peristalsis in vertical asymmetric channel with porous medium. Hayat et al. [105] canvassed the heat transfer effects on MHD viscous fluid flow within an asymmetric channel featuring porous medium with peristalsis. Nadeem and Akbar [106] proposed the mathematical analysis for peristaltic transport of electrically conducting viscous fluid in a channel with heat transfer. Solution was found by using the method called Adomian Decomposition method. Mekheimer et al. [107] revisited the same problem in a channel which was discussed by Vajravelu et al. [101] in tubes. Vasudev et al. [108] examined the simultaneous effects of heat transfer and porous medium on peristaltic transport of viscous fluid in an asymmetric channel. Nadeem and Akram [109] scrutinized consequence of heat transfer on peristalsis with velocity slip condition. Hayat et al. [110] examined the effects of velocity and thermal slips on peristaltic flow with MHD in a channel which is asymmetric. Frictional forces and pressure rise are analyzed with velocity and temperature distributions. An Oldroyd-B fluid



is analyzed under the effects of heat transfer in a channel by Sobh et al. [111]. The channel walls are exhibiting sinusoidal behavior due to the propagation of peristaltic waves. They have obtained series solution by using analytical method called perturbation method for small wave number. Nadeem and Akbar [112, 113] illustrated the heat transfer effects in non-uniform tubes containing Johnson-Segalman and Jeffrey-six constant fluids. A detailed analysis of heat transfer on peristaltically driven fourth grade fluid with effects of induced magnetic field is given by Hayat and Noreen [114]. Ali et al. [115] talked about the influence of curved channel and heat transfer on peristalsis. They have used numerical technique to obtain the solution for temperature distribution whereas stream function is given by analytic technique. Eldabe et al. [116] presented the mixed convection peristaltic flow between two vertical walls. Thermo-diffusion (Soret) and diffusion-thermo (Dufour) effects with temperature dependent viscosity are also interpreted. The mixed convective heat and mass transfer with porous medium through a vertical wavy channel is assessed by Muthuraj and Srinivas [117]. They described two parts of the solution i.e. a mean part and a perturbed part. Third order fluid in a diverging wavy tube with heat transfer is reflected by Nadeem et al. [118]. Nadeem and Akbar [119] inspected radially varying MHD peristaltically driven viscous fluid flow with heat and mass transfer effects in an annulus. Peristaltic flow under the effects of slip and heat transfer is analyzed by Hayat et al. [120]. Srinivas et al. [121] investigated the effects of heat and mass transfer in an asymmetric channel with peristalsis. Srinivas and Muthuraj [122] discussed the MHD mixed convective flow with peristalsis. Effects of chemical reaction and space porosity were also taken into account in a vertical asymmetric channel. Mekheimer et al. [123] considered the simultaneous effects of heat and mass transfer and induced magnetic field effects in peristaltic flow of second grade fluid. Mathematical modelling of unsteady Sisko fluid flow was analyzed by Mekheimer and Elkot [124]. They have considered anisotropically tapered arteries with time-variant overlapping stenosis. Akbar et al. [125] examined the slip and heat transfer effects in flow of third order fluid with peristalsis in an asymmetric channel. Influence of heat transfer on flow of Jeffrey fluid in a vertical porous stratum with peristalsis is mentioned by Vajravelu et al. [126]. Tripathi [127] proposed a mathematical model for swallowing of food bolus via esophagus under the effects of heat transfer. Heat and mass transfer analysis with slip effects in Maxwellian fluid flow under peristaltic action is discussed by Hayat et al. [128]. Nield and Kuznetsov [129]

examined the Cheng-Minkowycz problem for the double-diffusive natural convective boundary layer flow in a porous medium saturated by a nanofluid. Non-Newtonian nanofluid under the heat transfer effects with variable viscosity in two coaxial cylinders and pipe is analyzed by Ellahi et al. [130, 131] respectively. Eldabe et al. [132] discussed the heat and mass transfer in MHD peristaltic flow of a couple stress fluid through a porous medium. Effects of heat and mass transfer on peristaltic flow of a nanofluid between eccentric cylinders are investigated by Nadeem et al. [133]. Peristaltic motion with Soret and Dufour effects is discussed by Hayat et al. [134]. Peristaltic slip flow of viscoelastic fluid with heat and mass transfer in a tube is observed by Sobh [135]. Rao and Rao [136] analyzed the influence of heat transfer on peristaltic transport of couple stress fluid through porous medium. Peristaltically driven viscous fluid flow in a vertical asymmetric channel is studied by Srinivas et al. [137]. They have also considered the wall slip and heat and mass transfer effects. Abd elmaboud et al. [138] revealed the thermal properties of couple stress fluid flow with peristalsis in an asymmetric channel. El-Sayed et al. [139] investigated the effects of chemical reaction and heat and mass transfer through porous medium in vertical peristaltic tube containing non-Newtonian fluid. Shaaban and Abou-Zeid [140] predicted the effects of heat and mass transfer in MHD peristaltic flow between two coaxial cylinders through porous medium. Saravana et al. [141] investigated the peristaltically driven third order fluid in an inclined channel under the influences of slip and heat and mass transfer. Slip effects on MHD peristaltic motion with heat and mass transfer is examined by Hina et al. [142]. Ellahi et al. [143] considered the peristaltic flow in a non-uniform rectangular duct in presence of heat and mass transfer.

Literature survey witnesses that peristaltic flows are also discussed with compliant walls by taking both Newtonian and non-Newtonian fluids in channels/tubes. Mitra and Prasad [144] explored the effects of wall properties on peristalsis. They revealed that the mean flow reversal phenomenon exists at the center and boundaries of the channel. The stability analysis of plane channel flow is examined by Davies and Carpenter [145] between compliant walls. Haroun [146] studied the mean velocity and reversal flow in an asymmetric wavy channel with the compliant wall effects. The peristaltic flow and heat transfer in a channel with flexible walls is analyzed for small wave number by Radhakrishnamacharya and Srinivasulu [147]. The peristaltic flow of micropolar fluid was taken into account by Muthu et al. [148] in a circular

cylindrical tube having flexible walls. Viscous fluid flow with peristalsis is examined by Elnaby and Haroun [149] under the consideration of wall properties. Johnson-Segalman and Jeffrey fluids in a wavy channel with compliant wall properties were investigated by Hayat et al. [150, 151]. Linear Maxwell fluid within a compliant wavy channel was studied by Ali et al. [152] for small amplitude ratio. The effects of wall properties and porous medium in MHD viscous fluid channel flow were revealed by Kothandapani and Srinivas [153]. Srinivas et al. [154] extended the work of Kothandapani and Srinivas [153] for slip effects. Srinivas and Kothandapani [155] have discussed the compliant wall effects on MHD peristaltic flow through a porous space when heat and mass transfer effects are present in the flow analysis. Mustafa et al. [156, 157] obtained the analytical and numerical solutions for the peristaltic flow of nanofluid with slip and heat and mass transfer effects with wall properties. Wall properties effects in peristaltic flow of power-law fluid in an asymmetric peristaltic channel is discussed by Eldabe et al. [158]. Maxwell fluid in an asymmetric channel with wall properties is investigated by Hayat et al. [159]. Hina et al. [160] observed the Johnson-Segalman fluid flow under heat and mass transfer effects in a curved channel with compliant walls.

## Chapter 2

# Peristaltic flow of third-order fluid in a channel with convective boundary conditions

### 2.1 Introduction

This chapter addresses peristaltic flow of third order fluid in an asymmetric channel. Channel walls are subjected to the convective boundary conditions. The channel asymmetry is produced by choosing the peristaltic wave train on the walls to have different amplitudes and phase. Long wavelength approximation and perturbation method give the series solutions for the stream function, temperature and longitudinal pressure gradient. Analysis has been further carried out for pressure rise per wavelength through numerical integration. Several graphs of physical interest are displayed and discussed.

### 2.2 Mathematical formulation and flow equations

Here we formulate the problem for an incompressible third order fluid bounded in a two-dimensional infinite asymmetric channel (see Fig. 2.1). The  $\bar{X}$  and  $\bar{Y}$  axes are selected along and perpendicular to the channel walls respectively. The flow created is due to the imposition

of the following sinusoidal waves:

$$\begin{aligned}\bar{h}_1(\bar{X}, \bar{t}) &= d_1 + a_1 \sin \frac{2\pi}{\lambda}(\bar{X} - c\bar{t}), & \text{upper wall,} \\ \bar{h}_2(\bar{X}, \bar{t}) &= -d_2 - a_2 \sin \left( \frac{2\pi}{\lambda}(\bar{X} - c\bar{t}) + \phi \right), & \text{lower wall.}\end{aligned}\quad (2.1)$$

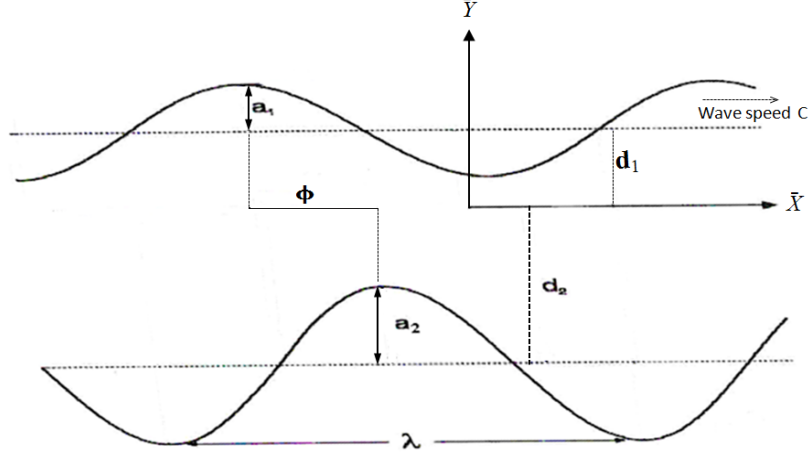


Fig. 2.1. Schematic drawing of the problem

In above expressions  $c$  is the wave speed,  $a_1, a_2$  are the waves amplitudes,  $\lambda$  is the wavelength,  $d_1 + d_2$  is the width of the asymmetric channel, the phase difference  $\phi$  varies in the range  $0 \leq \phi \leq \pi$  ( $\phi = 0$  corresponds to symmetric channel with waves out of phase and  $\phi = \pi$  the waves are in phase) and further  $a_1, a_2, d_1, d_2$  and  $\phi$  satisfy the condition

$$a_1^2 + a_2^2 + 2a_1a_2 \cos \phi \leq (d_1 + d_2)^2. \quad (2.2)$$

For incompressible fluid the continuity equation is

$$\text{div } \bar{\mathbf{V}} = 0. \quad (2.3)$$

The equations of motion and energy in absence of body forces are as follows:

$$\rho \frac{d\bar{\mathbf{V}}}{dt} = -\text{grad } \bar{p} + \text{div } \bar{\mathbf{S}}, \quad (2.4)$$

$$\rho c_p \frac{dT}{d\bar{t}} = k \nabla^2 T + \bar{\boldsymbol{\tau}} \cdot (\text{grad } \bar{\mathbf{V}}), \quad (2.5)$$

in which  $\bar{\mathbf{V}}$  is the velocity,  $\rho$  density of the fluid,  $\frac{d}{d\bar{t}}$  the material time derivative,  $T$  the fluid temperature,  $c_p$  the specific heat,  $k$  the thermal conductivity of the material, the Cauchy stress tensor  $\bar{\boldsymbol{\tau}} = -\bar{p}\bar{\mathbf{I}} + \bar{\mathbf{S}}$ ,  $\bar{p}$  the pressure,  $\bar{\mathbf{S}}$  the extra stress tensor and  $\nabla^2 = \left( \frac{\partial^2}{\partial \bar{X}^2} + \frac{\partial^2}{\partial \bar{Y}^2} \right)$  (The overbar refers to a dimensional quantity).

The exchange of heat with ambient at the walls through Newton's cooling law is given by

$$k \frac{\partial T}{\partial \bar{y}} = -h(T - T_0) \quad \text{at } \bar{y} = \bar{h}_1 \text{ and } \bar{y} = \bar{h}_2, \quad (2.6)$$

where  $h$  is the heat transfer coefficient and  $T_0$  the temperature at the channel walls.

For two-dimensional flow of third order fluid, we have the velocity  $\bar{\mathbf{V}}$  and extra stress tensor  $\bar{\mathbf{S}}$  in the forms:

$$\bar{\mathbf{V}} = (\bar{U}(\bar{X}, \bar{Y}, \bar{t}), \bar{V}(\bar{X}, \bar{Y}, \bar{t}), 0), \quad (2.7)$$

$$\bar{\mathbf{S}} = \mu \bar{\mathbf{A}}_1 + \alpha_1 \bar{\mathbf{A}}_2 + \alpha_2 \bar{\mathbf{A}}_1^2 + \beta_1 \bar{\mathbf{A}}_3 + \beta_2 (\bar{\mathbf{A}}_2 \bar{\mathbf{A}}_1 + \bar{\mathbf{A}}_1 \bar{\mathbf{A}}_2) + \beta_3 (\text{tr } \bar{\mathbf{A}}_1^2) \bar{\mathbf{A}}_1. \quad (2.8)$$

Here  $\mu$  is the coefficient of shear viscosity and  $\alpha_1, \alpha_2, \beta_1, \beta_2, \beta_3$  being the material constants.

The Rivlin-Ericksen tensors are defined by

$$\begin{aligned} \bar{\mathbf{A}}_1 &= (\text{grad } \bar{\mathbf{V}}) + (\text{grad } \bar{\mathbf{V}})^T, \\ \bar{\mathbf{A}}_n &= \frac{d\bar{\mathbf{A}}_{n-1}}{d\bar{t}} + \bar{\mathbf{A}}_{n-1}(\text{grad } \bar{\mathbf{V}}) + (\text{grad } \bar{\mathbf{V}})^T \bar{\mathbf{A}}_{n-1}, \quad n > 1. \end{aligned} \quad (2.9)$$

If  $(\bar{x}, \bar{y})$  and  $(\bar{u}, \bar{v})$  are the coordinates and velocity components in the wave frame  $(\bar{x}, \bar{y})$  then

$$\bar{x} = \bar{X} - c\bar{t}, \quad \bar{y} = \bar{Y}, \quad \bar{u}(\bar{x}, \bar{y}) = \bar{U}(\bar{X}, \bar{Y}, \bar{t}) - c, \quad \bar{v}(\bar{x}, \bar{y}) = \bar{V}(\bar{X}, \bar{Y}, \bar{t}), \quad T(\bar{x}, \bar{y}) = T(\bar{X}, \bar{Y}, \bar{t}). \quad (2.10)$$

Employing these transformations and introducing the following dimensionless variables:

$$\begin{aligned} x &= \frac{2\pi\bar{x}}{\lambda}, \quad y = \frac{\bar{y}}{d_1}, \quad u = \frac{\bar{u}}{c}, \quad v = \frac{\bar{v}}{c}, \quad p = \frac{2\pi d_1^2 \bar{p}}{c\mu\lambda}, \\ h_1 &= \frac{\bar{h}_1}{d_1}, \quad h_2 = \frac{\bar{h}_2}{d_1}, \quad t = \frac{2\pi c\bar{t}}{\lambda}, \quad \mathbf{S} = \frac{d_1}{\mu c} \bar{\mathbf{S}}, \quad \theta = \frac{T - T_0}{T_0}, \end{aligned} \quad (2.11)$$

the extra stress tensor  $\mathbf{S}$  in dimensionless form can be expressed as follows:

$$\mathbf{S} = \mathbf{A}_1 + \lambda_1 \mathbf{A}_2 + \lambda_2 \mathbf{A}_1^2 + \xi_1 \mathbf{A}_3 + \xi_2 (\mathbf{A}_2 \mathbf{A}_1 + \mathbf{A}_1 \mathbf{A}_2) + \xi_3 (\text{tr} \mathbf{A}_1^2) \mathbf{A}_1. \quad (2.12)$$

The velocity components  $u$  and  $v$  in terms of stream function  $\psi$  are

$$u = \frac{\partial \psi}{\partial y}, \quad v = -\delta \frac{\partial \psi}{\partial x}. \quad (2.13)$$

Now Eq. (2.3) is satisfied identically and (2.4) and (2.5) yield

$$\delta \text{Re} \left[ \left( \frac{\partial \psi}{\partial y} \frac{\partial}{\partial x} - \frac{\partial \psi}{\partial x} \frac{\partial}{\partial y} \right) \left( \frac{\partial \psi}{\partial y} \right) \right] + \frac{\partial p}{\partial x} = \delta \frac{\partial S_{xx}}{\partial x} + \frac{\partial S_{xy}}{\partial y}, \quad (2.14)$$

$$-\delta^3 \text{Re} \left[ \left( \frac{\partial \psi}{\partial y} \frac{\partial}{\partial x} - \frac{\partial \psi}{\partial x} \frac{\partial}{\partial y} \right) \left( \frac{\partial \psi}{\partial x} \right) \right] + \frac{\partial p}{\partial y} = \delta^2 \frac{\partial S_{xy}}{\partial x} + \delta \frac{\partial S_{yy}}{\partial y}, \quad (2.15)$$

$$\begin{aligned} \delta \text{Re} \left[ \frac{\partial \psi}{\partial y} \frac{\partial}{\partial x} - \frac{\partial \psi}{\partial x} \frac{\partial}{\partial y} \right] \theta &= \frac{1}{\text{Pr}} \left( \delta^2 \frac{\partial^2}{\partial x^2} + \frac{\partial^2}{\partial y^2} \right) \theta \\ &+ Ec \left[ \delta \frac{\partial^2 \psi}{\partial x \partial y} (S_{xx} - S_{yy}) + \left( \frac{\partial^2 \psi}{\partial y^2} - \delta^2 \frac{\partial^2 \psi}{\partial x^2} \right) S_{xy} \right]. \end{aligned} \quad (2.16)$$

In the above equations, the dimensionless wave number  $\delta$ , the Reynolds number  $\text{Re}$ , the Prandtl number  $\text{Pr}$ , the Eckert number  $Ec$ , the material coefficients  $\lambda_1$ ,  $\lambda_2$ ,  $\xi_1$ ,  $\xi_2$  and  $\xi_3$  are defined respectively by

$$\begin{aligned} \delta &= \frac{2\pi d_1}{\lambda}, \quad \text{Re} = \frac{\rho c d_1}{\mu}, \quad \lambda_1 = \frac{\alpha_1 c}{\mu d_1}, \\ \lambda_2 &= \frac{\alpha_2 c}{\mu d_1}, \quad \xi_1 = \frac{\beta_1 c^2}{\mu d_1^2}, \quad \xi_2 = \frac{\beta_2 c^2}{\mu d_1^2}, \quad \xi_3 = \frac{\beta_3 c^2}{\mu d_1^2}, \\ \text{Pr} &= \frac{\mu c_p}{k}, \quad Ec = \frac{c^2}{T_0 c_p}, \quad Br = \text{Pr} Ec, \end{aligned} \quad (2.17)$$

where  $Br$  is the Brinkman number. Eq. (2.6) gives

$$\frac{\partial \theta}{\partial y} + Bi \theta = 0 \text{ at } y = h_1 \text{ and } y = h_2, \quad (2.18)$$

where  $Bi = h d_1 / k$  is the Biot number.

Here we can see that the components of  $\mathbf{S}$  enters through (2.12) in Eqs. (2.14 – 2.16). Eliminating  $p$  in Eqs. (2.14) and (2.15), we can find the compatibility equation

$$\delta \operatorname{Re} \left[ \left( \frac{\partial \psi}{\partial y} \frac{\partial}{\partial x} - \frac{\partial \psi}{\partial x} \frac{\partial}{\partial y} \right) \nabla^2 \psi \right] = \left[ \left( \frac{\partial^2}{\partial y^2} - \delta^2 \frac{\partial^2}{\partial x^2} \right) S_{xy} \right] + \delta \left[ \frac{\partial^2}{\partial x \partial y} (S_{xx} - S_{yy}) \right], \quad (2.19)$$

where

$$\nabla^2 = \left( \delta^2 \frac{\partial^2}{\partial x^2} + \frac{\partial^2}{\partial y^2} \right),$$

and  $S_{xy}$  is given by

$$S_{xy} = \frac{\partial^2 \psi}{\partial y^2} + 2\Gamma \left( \frac{\partial^2 \psi}{\partial y^2} \right)^3, \quad (2.20)$$

in which  $\Gamma (= \xi_2 + \xi_3)$  is the Deborah number.

In the fixed frame, the instantaneous volume flow rate is given by

$$Q = \int_{\bar{h}_2(\bar{X}, \bar{t})}^{\bar{h}_1(\bar{X}, \bar{t})} \bar{U}(\bar{X}, \bar{Y}, \bar{t}) d\bar{Y}. \quad (2.21)$$

The volume flow rate in wave frame is

$$q = \int_{\bar{h}_2(\bar{x})}^{\bar{h}_1(\bar{x})} \bar{u}(\bar{x}, \bar{y}) d\bar{y}. \quad (2.22)$$

From Eqs. (2.10), (2.21) and (2.22) we can write

$$Q = q + c\bar{h}_1(\bar{x}) - c\bar{h}_2(\bar{x}). \quad (2.23)$$

The time-mean flow over a period  $\Omega (= \lambda/c)$  is defined by [27]:

$$\bar{Q} = \frac{1}{\Omega} \int_0^\Omega Q d\bar{t}. \quad (2.24)$$

Substituting Eq. (2.23) into Eq. (2.24) and then integrating the resulting expression one has

$$\bar{Q} = q + cd_1 + cd_2. \quad (2.25)$$

Defining  $\Theta$  and  $F$  as the dimensionless time-mean flows in the laboratory and wave frames



respectively by

$$\Theta = \frac{\bar{Q}}{cd_1}, \quad F = \frac{q}{cd_1}, \quad (2.26)$$

equation (2.25) becomes

$$\Theta = F + 1 + d, \quad (2.27)$$

with

$$F = \int_{h_2(x)}^{h_1(x)} \frac{\partial \psi}{\partial y} dy = \psi(h_1(x)) - \psi(h_2(x)). \quad (2.28)$$

The dimensionless forms of  $h_i$  ( $i = 1, 2$ ) are

$$h_1(x) = 1 + a \sin(x), \quad h_2(x) = -d - b \sin(x + \phi), \quad (2.29)$$

where  $a = a_1/d_1$ ,  $b = a_2/d_1$ ,  $d = d_2/d_1$  and  $\phi$  satisfies the following relation

$$a^2 + b^2 + 2ab \cos \phi \leq (1 + d)^2. \quad (2.30)$$

The conditions for the dimensionless stream function in wave frame are

$$\begin{aligned} \psi &= \frac{F}{2}, \quad \frac{\partial \psi}{\partial y} = -1, \quad \text{at } y = h_1(x), \\ \psi &= -\frac{F}{2}, \quad \frac{\partial \psi}{\partial y} = -1, \quad \text{at } y = h_2(x). \end{aligned} \quad (2.31)$$

## 2.3 Method of solution

The resulting equation (2.19) is highly non-linear even under the long wavelength and low Reynolds number assumptions [6]. For arbitrary values of parameters involving in this equation, the general solution in closed form seems very difficult. Here the resulting system consists of non-linear differential equation. Attention is hence focused to the perturbation solution for

small Deborah number  $\Gamma$ . For that we expand  $\psi$ ,  $\theta$ ,  $S_{xy}$ ,  $p$  and  $F$  as:

$$\begin{aligned}
\psi &= \psi_0 + \Gamma\psi_1 + \Gamma^2\psi_2 + \dots, \\
\theta &= \theta_0 + \Gamma\theta_1 + \Gamma^2\theta_2 + \dots, \\
S_{xy} &= S_{0xy} + \Gamma S_{1xy} + \Gamma^2 S_{2xy} + \dots, \\
p &= p_0 + \Gamma p_1 + \Gamma^2 p_2 + \dots, \\
F &= F_0 + \Gamma F_1 + \Gamma^2 F_2 + \dots
\end{aligned} \tag{2.32}$$

Substitution of above equations into Eqs. (2.14–2.16), (2.18), (2.19), (2.31) and then collecting the terms of like powers of  $\Gamma$  we have:

### 2.3.1 Zeroth order system and its solution

$$\frac{\partial^4 \psi_0}{\partial y^4} = 0, \tag{2.33}$$

$$\frac{\partial^2 \theta_0}{\partial y^2} + Br \left( \frac{\partial^2 \psi_0}{\partial y^2} \right) S_{0xy} = 0, \tag{2.34}$$

$$\frac{dp_0}{dx} = \frac{\partial^3 \psi_0}{\partial y^3}, \tag{2.35}$$

$$\psi_0 = \frac{F_0}{2}, \quad \frac{\partial \psi_0}{\partial y} = -1, \quad \frac{\partial \theta_0}{\partial y} + Bi\theta_0 = 0, \quad \text{at } y = h_1(x), \tag{2.36}$$

$$\psi_0 = \frac{-F_0}{2}, \quad \frac{\partial \psi_0}{\partial y} = -1, \quad \frac{\partial \theta_0}{\partial y} + Bi\theta_0 = 0, \quad \text{at } y = h_2(x). \tag{2.37}$$

The solutions of the Eqs. (2.33) and (2.34) subject to the boundary conditions (2.36) and (2.37) are

$$\psi_0 = R_1 y^3 + R_2 y^2 + R_3 y + R_4, \tag{2.38}$$

$$\theta_0 = A_1 y^4 + A_2 y^3 + A_3 y^2 + A_4 y + A_5, \tag{2.39}$$

The longitudinal velocity and pressure gradient are given by

$$\begin{aligned} u_0 &= 3R_1y^2 + 2R_2y + R_3, \\ \frac{dp_0}{dx} &= \frac{-12(F_0 + h_1 - h_2)}{(h_1 - h_2)^3}. \end{aligned}$$

The non-dimensional pressure rise per wavelength ( $\Delta P_{\lambda_0}$ ) is given by

$$\Delta P_{\lambda_0} = \int_0^{2\pi} \frac{dp_0}{dx} dx.$$

We note that the solution expressions at this order corresponds to the case of the viscous fluid [27].

### 2.3.2 First order system and its solution

$$\frac{\partial^4 \psi_1}{\partial y^4} = -2 \frac{\partial^2}{\partial y^2} \left[ \left( \frac{\partial^2 \psi_0}{\partial y^2} \right)^3 \right], \quad (2.40)$$

$$\frac{\partial^2 \theta_1}{\partial y^2} + Br \left[ \left( \frac{\partial^2 \psi_0}{\partial y^2} \right) S_{1xy} + \left( \frac{\partial^2 \psi_1}{\partial y^2} \right) S_{0xy} \right] = 0, \quad (2.41)$$

$$\frac{dp_1}{dx} = \frac{\partial^3 \psi_1}{\partial y^3} + 2 \frac{\partial}{\partial y} \left[ \left( \frac{\partial^2 \psi_0}{\partial y^2} \right)^3 \right], \quad (2.42)$$

$$\psi_1 = \frac{F_1}{2}, \quad \frac{\partial \psi_1}{\partial y} = 0, \quad \frac{\partial \theta_1}{\partial y} + Bi\theta_1 = 0, \quad \text{at } y = h_1(x), \quad (2.43)$$

$$\psi_1 = \frac{-F_1}{2}, \quad \frac{\partial \psi_1}{\partial y} = 0, \quad \frac{\partial \theta_1}{\partial y} + Bi\theta_1 = 0, \quad \text{at } y = h_2(x). \quad (2.44)$$

Substituting Eq. (2.38) into Eqs. (2.40) and (2.41), solving the resulting equations and then applying the corresponding boundary conditions we get the solutions for  $\psi_1$ ,  $\theta_1$ ,  $u_1$  and  $dp_1/dx$

in the following forms:

$$\psi_1 = M_1 y^5 + M_2 y^4 + M_3 y^3 + M_4 y^2 + M_5 y + M_6, \quad (2.45)$$

$$\theta_1 = B_1 y^6 + B_2 y^5 + B_3 y^4 + B_4 y^3 + B_5 y^2 + B_6 y + B_7, \quad (2.46)$$

$$u_1 = 5M_1 y^4 + 4M_2 y^3 + 3M_3 y^2 + 2M_4 y + M_5, \quad (2.47)$$

$$\frac{dp_1}{dx} = \frac{-60F_1 + \left(\frac{dp_0}{dx}\right)^3 L_{12} + \left(\frac{dp_0}{dx}\right)^2 R_2 L_{13} + \left(\frac{dp_0}{dx}\right) S_2^2 L_{14}}{5(h_1 - h_2)^3}, \quad (2.48)$$

The pressure rise per wavelength ( $\Delta P_{\lambda_1}$ ) is given by

$$\Delta P_{\lambda_1} = \int_0^{2\pi} \frac{dp_1}{dx} dx.$$

### 2.3.3 Second order system and its solution

$$\frac{\partial^4 \psi_2}{\partial y^4} = -6 \frac{\partial^2}{\partial y^2} \left[ \frac{\partial^2 \psi_1}{\partial y^2} \left( \frac{\partial^2 \psi_0}{\partial y^2} \right)^2 \right], \quad (2.49)$$

$$\frac{\partial^2 \theta_2}{\partial y^2} + Br \left[ \left( \frac{\partial^2 \psi_0}{\partial y^2} \right) S_{2xy} + \left( \frac{\partial^2 \psi_1}{\partial y^2} \right) S_{1xy} + \left( \frac{\partial^2 \psi_2}{\partial y^2} \right) S_{0xy} \right] = 0, \quad (2.50)$$

$$\frac{dp_2}{dx} = \frac{\partial^3 \psi_2}{\partial y^3} + 6 \frac{\partial}{\partial y} \left[ \frac{\partial^2 \psi_1}{\partial y^2} \left( \frac{\partial^2 \psi_0}{\partial y^2} \right)^2 \right], \quad (2.51)$$

$$\psi_2 = \frac{F_2}{2}, \quad \frac{\partial \psi_2}{\partial y} = 0, \quad \frac{\partial \theta_2}{\partial y} + Bi \theta_2 = 0, \quad \text{at } y = h_1(x), \quad (2.52)$$

$$\psi_2 = \frac{-F_2}{2}, \quad \frac{\partial \psi_2}{\partial y} = 0, \quad \frac{\partial \theta_2}{\partial y} + Bi \theta_2 = 0, \quad \text{at } y = h_2(x). \quad (2.53)$$

Employing the same methodology as for the zeroth-order and first-order systems we obtain

$$\psi_2 = N_1 y^7 + N_2 y^6 + N_3 y^5 + N_4 y^4 + N_5 y^3 + N_6 y^2 + N_7 y + N_8, \quad (2.54)$$

$$\theta_2 = C_1 y^8 + C_2 y^7 + C_3 y^6 + C_4 y^5 + C_5 y^4 + C_6 y^3 + C_7 y^2 + C_8 y + C_9, \quad (2.55)$$

$$u_2 = 7N_1 y^6 + 6N_2 y^5 + 5N_3 y^4 + 4N_4 y^3 + 3N_5 y^2 + 2N_6 y + N_7, \quad (2.56)$$

$$\frac{dp_2}{dx} = \frac{-420F_2 + \left(\frac{dp_0}{dx}\right)^2 L_{30} + \left(\frac{dp_0}{dx}\right) S_2 L_{31} + S_2^2 L_{32}}{35(h_1 - h_2)^3}, \quad (2.57)$$

where the values of  $R$ 's,  $A$ 's,  $M$ 's,  $B$ 's,  $N$ 's,  $C$ 's and  $L$ 's in above equations are given as follows:

$$\begin{aligned}
R_1 &= \frac{-2(F_0 + h_1 - h_2)}{(h_1 - h_2)^3}, \\
R_2 &= \frac{3(F_0 + h_1 - h_2)(h_1 + h_2)}{(h_1 - h_2)^3}, \\
R_3 &= \frac{-h_1^3 - 6F_0h_1h_2 - 3h_1^2h_2 + 3h_1h_2^2 + h_2^3}{(h_1 - h_2)^3}, \\
R_4 &= \frac{-(h_1 + h_2)(2h_1h_2(-h_1 + h_2) + F_0(h_1^2 - 4h_1h_2 + h_2^2))}{2(h_1 - h_2)^3}, \\
M_1 &= \frac{-1}{10} \left( \frac{dp_0}{dx} \right)^3, \quad M_2 = - \left( \frac{dp_0}{dx} \right)^2 R_2, \\
M_3 &= \frac{-20F_1 + \left( \frac{dp_0}{dx} \right)^3 L_1 + \left( \frac{dp_0}{dx} \right)^2 R_2 L_2}{10(h_1 - h_2)^3}, \\
M_4 &= \frac{L_3 + \left( \frac{dp_0}{dx} \right)^3 L_4 + \left( \frac{dp_0}{dx} \right)^2 R_2 L_5}{5(h_1 - h_2)^4}, \\
M_5 &= \frac{L_6 + \left( \frac{dp_0}{dx} \right)^2 R_2 L_7 + \left( \frac{dp_0}{dx} \right)^3 L_8}{10(h_1 - h_2)^4}, \\
M_6 &= \frac{L_9 + \left( \frac{dp_0}{dx} \right)^2 R_2 L_{11} + \left( \frac{dp_0}{dx} \right)^3 L_{10}}{10(h_1 - h_2)^4},
\end{aligned}$$

$$\begin{aligned}
L_1 &= (h_1 - h_2)^3(3h_1^2 + 4h_1h_2 + 3h_2^2), \\
L_2 &= 20(h_1 - h_2)^3(h_1 + h_2), \\
L_3 &= 15F_1(h_1^2 - h_2^2), \\
L_4 &= -(h_1 - h_2)^4(h_1 + h_2)(h_1^2 + 3h_1h_2 + h_2^2), \\
L_5 &= 5(h_1 - h_2)^3(h_1 - h_2)(h_1^2 + 4h_1h_2 + h_2^2), \\
L_6 &= -60F_1h_1h_2(h_1 - h_2), \\
L_7 &= 20h_1h_2(h_1 - h_2)^4(h_1 + h_2), \\
L_8 &= (h_1 - h_2)^2[h_1h_2(h_1 - h_2)^2(4h_1^2 + 7h_1h_2 + 4h_2^2), \\
L_9 &= -5F_1(h_1^2 - h_2^2)(h_1^2 - 4h_1h_2 + h_2^2), \\
L_{10} &= -2h_1^2h_2^2(h_1 - h_2)^4(h_1 + h_2)^2, \\
L_{11} &= -10h_1^2h_2^2(h_1 - h_2)^4, \\
L_{12} &= 3(h_1 - h_2)^3(3h_1^2 + 4h_1h_2 + 3h_2^2), \\
L_{13} &= 60(h_1 - h_2)^3(h_1 + h_2), \\
L_{14} &= 120(h_1 - h_2)^3, \\
L_{15} &= (h_1 - h_2)^3[500h_1^4M_1 + 16h_1^3(50h_2M_1 + 21M_2) + 9h_1^2(100h_2^2M_1 + 56h_2M_2 + 21M_3) \\
&\quad + h_2(500h_2^3M_1 + 336h_2^2M_2 + 189h_2M_3 + 70M_4) + h_1(800h_2^3M_1 + 504h_2^2M_2 \\
&\quad + 252h_2M_3 + 70M_4)], \\
L_{16} &= 840(h_1 - h_2)^2[(h_1 - h_2)((3h_1^2 + 4h_1h_2 + 3h_2^2)M_1 + 2(h_1 + h_2)M_2)], \\
L_{17} &= 56(h_1 - h_2)^2[(h_1 - h_2)(40M_1(h_1^3 + h_2^3) + 60h_1h_2M_1(h_1 + h_2) + 27M_2(h_1^2 + h_2^2) \\
&\quad + 36h_1h_2M_1 + 15M_3(h_1 + h_2))],
\end{aligned}$$

$$\begin{aligned}
L_{18} &= 105F_2(h_1^2 - h_2^2), \\
L_{19} &= -84(h_1 - h_2)^3[(h_1 - h_2)(4(h_1^2 + 3h_1h_2 + h_2^2)(5(h_1^2 + h_1h_2 + h_2^2)M_1 + 3(h_1 + h_2)M_2) \\
&\quad + 5(h_1^2 + 4h_1h_2 + h_2^2)M_3 - 2(20h_1^4M_1 + h_1^3(-40h_2M_1 + 18M_2) - 3h_1^2(20h_2^2M_1 \\
&\quad + 6h_2M_2 - 5M_3) - 2h_1(20h_2^3M_1 + 9h_2^2M_2 - 5M_4))], \\
L_{20} &= -(h_1 - h_2)^3[(h_1 - h_2)(200(h_1 + h_2)(2h_1^4 + 6h_1^3h_2 + 5h_1^2h_2^2 + 6h_1h_2^3 + 2h_2^4)M_1 \\
&\quad + 252(h_1^2 + h_1h_2 + h_2^2)(h_1^2 + 3h_1h_2 + h_2^2)M_2 + 126(h_1 + h_2)(h_1^2 + 3h_1h_2 + h_2^2)M_3 \\
&\quad + 35(h_1^2 + 4h_1h_2 + h_2^2)M_4) - 6(100h_1^5M_1 + h_1^4(-300h_2M_1 + 84M_2) \\
&\quad - 3h_1h_2^2(100h_2^2M_1 + 56h_2M_2 + 21M_3) + h_1^3(-4h_2(125h_2M_1 + 42M_2) + 63M_3) \\
&\quad - h_1^2(500h_2^3M_1 + 252h_2^2M_2 + 63h_2M_3 - 35M_4))], \\
L_{21} &= 840(h_1 - h_2)^2[-(h_1 - h_2)^2(2(h_1 + h_2)(h_1^2 + 3h_1h_2 + h_2^2)M_1 + (h_1^2 + 4h_1h_2 + h_2^2)M_2) \\
&\quad + 2(h_1 - h_2)(3(h_1^3M_1 + h_1^2(-h_2M_1 + M_2))], \\
L_{22} &= -210F_2h_1h_2(h_1 - h_2), \\
L_{23} &= 840(h_1 - h_2)^2[h_1h_2(h_1 - h_2)^2((4h_1^2 + 7h_1h_2 + 4h_2^2)M_1 + 2(h_1 + h_2)M_2) \\
&\quad - 2(h_1 - h_2)(2h_1^4M_1 + 3h_1^2h_2M_2 + h_2^3(2h_2M_1 + M_2) + h_1^3(3h_2M_1 + M_2) \\
&\quad + 3h_1h_2(h_2(h_2M_1 + M_2) + M_3))], \\
L_{24} &= 168(h_1 - h_2)^2[h_1h_2(h_1 - h_2)^2(20h_1^3M_1 + 4h_1^2(10h_2M_1 + 3M_2) + h_1(40h_2^2M_1 \\
&\quad + 21h_2M_2 + 5M_3) + h_2(4h_2(5h_2M_1 + 3M_2) + 5M_3)) - (h_1 - h_2)(20h_1^5M_1 \\
&\quad + 4h_1^4(5h_2M_1 + 3M_2) + h_1^3(-20h_2^2M_1 + 18h_2M_2 + 5M_3))], \\
L_{25} &= (h_1 - h_2)^2[h_1h_2(h_1 - h_2)^2(800h_1^4M_1 + 4h_1^3(425h_2M_1 + 126M_2) \\
&\quad + 4h_1^2(500h_2^2M_1 + 252h_2M_2 + 63M_3) + 2h_2(400h_2^3M_1 + 252h_2^2M_2 + 126h_2M_3 + 35M_4) \\
&\quad + h_1(h_2(4h_2(425h_2M_1 + 252M_2) + 441M_3) + 70M_4))], \\
L_{26} &= -35F_2(h_1^2 - h_2^2)(h_1^2 - 4h_1h_2 + h_2^2), \\
L_{27} &= 1680h_1h_2(h_1 - h_2)^2[-h_1h_2(h_1 - h_2)^2(2(h_1 + h_2)M_1 + M_2)], \\
L_{28} &= 56h_1h_2(h_1 - h_2)^2[-h_1h_2(h_1 - h_2)^2(20(3h_1^2 + 4h_1h_2 + 3h_2^2)M_1 + 36(h_1 + h_2)M_2 + 15M_3)], \\
L_{29} &= 2h_1h_2(h_1 - h_2)^2[-h_1h_2(h_1 - h_2)^2(200(h_1 + h_2)(2h_1^2 + h_1h_2 + 2h_2^2)M_1 \\
&\quad + 84(3h_1^2 + 4h_1h_2 + 3h_2^2)M_2 + 126(h_1 + h_2)M_3 + 35M_4)],
\end{aligned}$$

$$\begin{aligned}
L_{30} &= 6(h_1 - h_2)^3[500h_1^4M_1 + 16h_1^3(50h_2M_1 + 21M_2) + 9h_1^2(100h_2^2M_1 \\
&\quad + 56h_2M_2 + 21M_3) + h_2(500h_2^3M_1 + 336h_2^2M_2 + 189h_2M_3 + 70M_4) \\
&\quad + h_1(800h_2^3M_1 + 504h_2^2M_2 + 252h_2M_3 + 70M_4)], \\
L_{31} &= 336(h_1 - h_2)^3[40M_1(h_1^3 + h_2^3) + 60M_1(h_1^2h_2 + h_1h_2^2) \\
&\quad + 9M_2(3h_1^2 + 4h_1h_2 + 3h_2^2) + 15(h_1 + h_2)M_3 + 5M_4], \\
L_{32} &= 5040(h_1 - h_2)^3[(3h_1^2 + 4h_1h_2 + 3h_2^2)M_1 + 2(h_1 + h_2)M_2 + M_3], \\
N_1 &= \frac{-20}{7}M_1 \left( \frac{dp_0}{dx} \right)^2, \\
N_2 &= \frac{-4}{5} \left( \frac{dp_0}{dx} \right) \left( 3M_2 \left( \frac{dp_0}{dx} \right) + 20M_1R_2 \right), \\
N_3 &= \frac{-3}{5} \left( 3M_3 \left( \frac{dp_0}{dx} \right)^2 + 8R_2 \left( 3M_2 \left( \frac{dp_0}{dx} \right) + 5M_1R_2 \right) \right), \\
N_4 &= -M_4 \left( \frac{dp_0}{dx} \right)^2 - 12R_2 \left( M_3 \left( \frac{dp_0}{dx} \right) + 2M_2R_2 \right), \\
N_5 &= \frac{-70F_2 + \left( \frac{dp_0}{dx} \right)^2 L_{15} + R_2^2 L_{16} + \left( \frac{dp_0}{dx} \right) R_2 L_{17}}{35(h_1 - h_2)^3}, \\
N_6 &= \frac{L_{18} + \left( \frac{dp_0}{dx} \right) R_2 L_{19} + \left( \frac{dp_0}{dx} \right)^2 L_{20} + R_2^2 L_{21}}{35(h_1 - h_2)^4}, \\
N_7 &= \frac{L_{22} + \left( \frac{dp_0}{dx} \right) R_2 L_{24} + \left( \frac{dp_0}{dx} \right)^2 L_{25} + R_2^2 L_{23}}{35(h_1 - h_2)^4}, \\
N_8 &= \frac{L_{26} + \left( \frac{dp_0}{dx} \right) R_2 L_{28} + \left( \frac{dp_0}{dx} \right)^2 L_{29} + R_2^2 L_{27}}{70(h_1 - h_2)^4}, \\
A_1 &= -3BrR_1^2, \\
A_2 &= -4BrR_1R_2, \\
A_3 &= -2BrR_2^2, \\
A_4 &= \frac{Br}{Bi}(-3(Bih_1^3 + h_1^2(4 + Bih_2) + h_1h_2(4 + Bih_2) + h_2^2(4 + Bih_2))R_1^2 \\
&\quad - 4(Bih_1^2 + h_1(3 + Bih_2) + h_2(3 + Bih_2))R_1R_2 - 2(2 + Bi(h_1 + h_2))R_2^2), \\
A_5 &= \frac{1}{Bi^2}(Br(-(3Bih_1^3(1 + Bih_2) + h_2^2(4 + Bih_2) + h_1^2(1 + Bih_2)(4 + Bih_2) \\
&\quad + h_1h_2(1 + Bih_2)(4 + Bih_2)R_1^2 - 4(Bih_1^2(1 + Bih_2) + h_2(3 + Bih_2) \\
&\quad + h_1(1 + Bih_2)(3 + Bih_2))R_1R_2 - 2(2 + Bi(h_1 + h_2 + Bih_1h_2))R_2^2)), \\
B_1 &= -\frac{8}{5}BrR_1(5M_1 + 54R_1^3),
\end{aligned}$$



$$\begin{aligned}
B_2 &= -\frac{4}{5}Br(9M_2R_1 + 5M_1R_2 + 216R_1^3R_2), \\
B_3 &= -2Br(3M_3R_1 + 2R_2(M_2 + 36R_1^2R_2)), \\
B_4 &= -4Br(M_4R_1 + M_3R_2 + 16R_1R_2^3), \\
B_5 &= -4BrR_2(M_4 + 4R_2^3), \\
B_6 &= -\frac{1}{5Bi}(2Br(-20h_1^4(6 + Bih_2)M_1R_1 - 18Bih_1^4M_2R_1 - h_1^2(60M_3 + h_2(20h_2 \\
&\quad \times (6 + Bih_2)M_1 + 90M_2 + 18Bih_2M_2 + 15BiM_3) + 10BiM_4)R_1 \\
&\quad - h_1(h_2(2h_2(10h_2(6 + Bih_2)M_1 + 9(5 + Bih_2)M_2) + 15(4 + Bih_2)M_3) \\
&\quad + 10(3 + Bih_2)M_4)R_1 - h_2(h_2(2h_2(10h_2(6 + Bih_2)M_1 + 9(5 + Bih_2)M_2) \\
&\quad + 15(4 + Bih_2)M_3) + 10(3 + Bih_2)M_4)R_1 - 1296h_1^4R_1^4 - 216Bih_1^4h_2R_1^4 \\
&\quad - 216h_1^2h_2^2(6 + Bih_2)R_1^4 - 216h_1h_2^3(6 + Bih_2)R_1^4 - 216h_2^4(6 + Bih_2)R_1^4 \\
&\quad - 4Bih_1^5R_1(5M_1 - 54R_1^3) - h_1^3R_1(120h_2M_1 + 20Bih_2^2M_1 + 90M_2 + 18Bih_2M_2 \\
&\quad + 15BiM_3 + 216h_2(6 + Bih_2)R_1^3 + (-20M_4 - 10(Bih_1^4M_1 + h_1^3((5 + Bih_2)M_1 \\
&\quad + BiM_2) + h_1^2(4M_2 + h_2((5 + Bih_2)M_1 + BiM_2) + BiM_3) + h_1(3M_3 + h_2(4M_2 \\
&\quad + h_2((5 + Bih_2)M_1 + BiM_2) + BiM_3) + BiM_4) + h_2(3M_3 + h_2(4M_2 + h_2((5 + Bih_2)M_1 \\
&\quad + BiM_2) + BiM_3) + BiM_4) - 432(Bih_1^4 + h_1^3(5 + Bih_2) + h_1^2h_2(5 + Bih_2) \\
&\quad + h_1h_2^2(5 + Bih_2) + h_2^3(5 + Bih_2))R_1^3R_2 + 360(Bih_1^3 + h_1^2(4 + Bih_2) \\
&\quad + h_1h_2(4 + Bih_2) + h_2^2(4 + Bih_2))R_1^2R_2^2 - 160(Bih_1^2 + h_1(3 + Bih_2) \\
&\quad + h_2(3 + Bih_2))R_1R_2^3 - 40(2 + (Bi(h_1 + h_2))R_2^4),
\end{aligned}$$

$$\begin{aligned}
B_7 = & -\frac{1}{5Bi^2}(2Br(4Bih_1^5(1+Bih_2)R_1(5M_1+54R_1^3)+h_2R_1(30M_4+h_2(60M_3 \\
& +15h_2(6M_2+BiM_3)+10BiM_4+4Bih_2^3(5M_1+54R_1^3)+6h_2^2(20M_1 \\
& +3BiM_2+216R_1^3))) + 2(10M_4-5h_2(3M_3+h_2(4M_2+h_2((5+Bih_2)M_1 \\
& +BiM_3)+BiM_4)+216h_2^3(5+Bih_2)R_1^3)R_2+360h_2^2(4+Bih_2)R_1^2R_2^2 \\
& +160h_2(3+Bih_2)R_1R_2^3-40(3+Bih_2)R_2^4+h_1^3(1+Bih_2)(R_1(120h_2M_1 \\
& +20Bih_2^2M_1+90M_2+18Bih_2M_2+15BiM_3+216h_2(6+Bih_2)R_1^3) \\
& +2(5(5+Bih_2)M_1+5BiM_2+216(5+Bih_2)R_1^3)R_2+360BiR_1^2R_2^2) \\
& +h_1^2(1+Bih_2)(R_1(60M_3+15h_2(6M_2+BiM_3)+10BiM_4+4Bih_2^3(5M_1+54R_1^3) \\
& +6h_2^2(20M_1+3BiM_2+216R_1^3))+2(5(4M_2+h_2((5+Bih_2)M_1+BiM_2) \\
& +BiM_3)+216h_2(5+Bih_2)R_1^3)R_2+360(4+Bih_2)R_1^2R_2^2+160BiR_1R_2^3) \\
& +h_1(1+Bih_2)(R_1(30M_4+h_2(60M_3+15h_2(6M_2+BiM_3)+10BiM_4 \\
& +4Bih_2^3(5M_1+54R_1^3)+6h_2^2(20M_1+3BiM_2+216R_1^3))) + 2(5(3M_3 \\
& +h_2(4M_2+h_2((5+Bih_2)M_1+BiM_2)+BiM_3)+BiM_4) \\
& +216h_2^2(5+Bih_2)R_1^3)R_2+360h_2(4+Bih_2)R_1^2R_2^2+160(3+Bih_2)R_1R_2^3 \\
& +40BiR_2^4)+2h_1^4(1+Bih_2)(5M_1(2(6+Bih_2)R_1+BiR_2)+9(72R_1^4 \\
& +BiR_1(M_2+12R_1^2(h_2R_1+2R_2))))), \\
C_1 = & -\frac{1}{7}Br(50M_1^2+63N_1R_1+4320M_1R_1^3), \\
C_2 = & -\frac{4}{7}Br(15N_2R_1+864M_2R_1^3+7N_1R_2+20M_1(M_2+72R_1^2R_2)), \\
C_3 = & -\frac{4}{5}Br(6M_2^2+10N_3R_1+432M_3R_1^3+5N_2R_2+864M_2R_1^2R_2 \\
& +10M_1(M_3+48R_1R_2^2)), \\
C_4 = & -\frac{4}{5}Br(5N_3R_2+9M_2(M_3+48R_1R_2^2)+5M_1(M_4+16R_2^3) \\
& +9R_1(N_4+24R_1(M_4R_1+3M_3R_2))),
\end{aligned}$$

$$\begin{aligned}
C_5 &= -Br(3M_3^2 + 4N_4R_2 + 288M_3R_1R_2^2 + 6R_1(N_5 + 48M_4R_1R_2) + 4M_2(M_4 + 16R_2^3)), \\
C_6 &= -4Br(N_6R_1 + R_2(N_5 + 48M_4R_1R_2) + M_3(M_4 + 16R_2^3)), \\
C_7 &= -2Br(M_4^2 + 2N_6R_2 + 32M_4R_2^3), \\
C_8 &= \frac{1}{35Bi}(Br(5Bih_1^7(50M_1^2 + 63N_1R_1 + 4320M_1R_1^3) + 5Bih_2^7(50M_1^2 + 63N_1R_1 + 4320M_1R_1^3) \\
&\quad + 140h_2^2(3M_3^2 + 4M_2M_4 + BiM_3M_4 + 6N_5R_1 + BiN_6R_1 + (4N_4 + BiN_5 + 288M_4R_1^2)R_2 \\
&\quad + 48(6M_3 + BiM_4)R_1R_2^2 + 16(4M_2 + BiM_3)R_2^3) + 140(M_4^2 + 2N_5R_2 + 32M_4R_2^3) \\
&\quad + 70h_2(6M_3(M_4 + 16R_2^3) + Bi(M_4^2 + 2N_6R_2 + 32M_4R_2^3) + 6(N_6R_1 + R_2(N_5 \\
&\quad + 48M_4R_1R_2))) + 20h_2^6(100M_1^2 + 126N_1R_1 + 15BiN_2R_1 + 864BiM_2R_1^3 \\
&\quad + 7BiN_1R_2 + 20M_1(432R_1^3 + Bi(M_2 + 72R_1^2R_2))) + 5h_1^6(50(8 + Bih_2)M_1^2 \\
&\quad + 12BiR_1(5N_2 + 288M_2R_1^2) + 7N_1(9(8 + Bih_2)R_1 + 4BiR_2) + 80M_1(432R_1^3 \\
&\quad + Bi(M_2 + 54h_2R_1^3 + 72R_1^2R_2))) + 28h_2^5(75N_2R_1 + 4320M_2R_1^3 + 35N_1R_2 \\
&\quad + 10M_1(10M_2 + BiM_3 + 720R_1^2R_2 + 48BiR_1R_2^2) + Bi(10N_3R_1 + 432M_3R_1^3 \\
&\quad + 5N_2R_2 + 6M_2(M_2 + 144R_1^2R_2))) + 35h_2^3(4M_2(9M_3 + BiM_4 + 432R_1R_2^2 + 16BiR_2^3) \\
&\quad + Bi(4N_4R_2 + 6R_1(N_5 + 48M_4R_1R_2) + 3M_3(M_3 + 96R_1R_2^2)) + 4(5N_3R_2 \\
&\quad + 5M_1(M_4 + 16R_2^3) + 9R_1(N_4 + 24R_1(M_4R_1 + 3M_3R_2)))) + 28h_2^4(36M_2^2 \\
&\quad + 30(2M_1M_3 + 2N_3R_1 + N_2R_2) + 288(9M_3R_1^3 + 10M_1R_1R_2^2) + 9M_2(576R_1^2R_2 \\
&\quad + Bi(M_3 + 48R_1R_2^2)) + Bi(5N_3R_2 + 5M_1(M_4 + 16R_2^3) + 9R_1(N_4 + 24R_1(M_4R_1 \\
&\quad + 3M_3R_2)))) + h_1^5(5Bih_2^2(50M_1^2 + 63N_1R_1 + 4320M_1R_1^3) + 20h_2(100M_1^2 + 126N_1R_1 \\
&\quad + 15BiN_2R_1 + 864BiM_2R_1^3 + 7BiN_1R_2 + 20M_1(432R_1^3 + Bi(M_2 + 72R_1^2R_2))) \\
&\quad + 28(75N_2R_1 + 4320M_2R_1^3 + 35N_1R_2 + 10M_1(10M_2 + BiM_3 + 720R_1^2R_2 \\
&\quad + 48BiR_1R_2^2) + Bi(10N_3R_1 + 432M_3R_1^3 + 5N_2R_2 + 6M_2(M_2 + 144R_1^2R_2)))) \\
&\quad + h_1^4(5Bih_2^3(50M_1^2 + 63N_1R_1 + 4320M_1R_1^3) + 20h_2^2(100M_1^2 + 126N_1R_1 \\
&\quad + 15BiN_2R_1 + 864BiM_2R_1^3 + 7BiN_1R_2 + 20M_1(432R_1^3 + Bi(M_2 + 72R_1^2R_2))) \\
&\quad + 28h_2(75N_2R_1 + 4320M_2R_1^3 + 35N_1R_2 + 10M_1(10M_2 + BiM_3 + 720R_1^2R_2 \\
&\quad + 48BiR_1R_2^2) + Bi(10N_3R_1 + 432M_3R_1^3 + 5N_2R_2 + 6M_2(M_2 + 144R_1^2R_2)))) \\
&\quad + 28(36M_2^2 + 30(2M_1M_3 + 2N_3R_1 + N_2R_2) + 288(9M_3R_1^3 + 10M_1R_1R_2^2)
\end{aligned}$$

$$\begin{aligned}
& +9R_1(N_4 + 24R_1(M_4R_1 + 3M_3R_2)))) + 9M_2(576R_1^2R_2 + Bi(M_3 + 48R_1R_2^2)) \\
& +Bi(5N_3R_2 + 5M_1(M_4 + 16R_2^3) + h_1^3(5Bi h_2^4(50M_1^2 + 63N_1R_1 + 4320M_1R_1^3) \\
& +20h_2^3(100M_1^2 + 126N_1R_1 + 15BiN_2R_1 + 864BiM_2R_1^3 + 7BiN_1R_2 \\
& +20M_1(432R_1^3 + Bi(M_2 + 72R_1^2R_2))) + 28h_2^2(75N_2R_1 + 4320M_2R_1^3 \\
& +35N_1R_2 + 10M_1(10M_2 + BiM_3 + 720R_1^2R_2 + 48BiR_1R_2^2) + Bi(10N_3R_1 + 432M_3R_1^3 \\
& +5N_2R_2 + 6M_2(M_2 + 144R_1^2R_2))) + 35(4M_2(9M_3 + BiM_4 + 432R_1R_2^2 \\
& +16BiR_2^3) + Bi(4N_4R_2 + 6R_1(N_5 + 48M_4R_1R_2) + 3M_3(M_3 + 96R_1R_2^2)) + 4(5N_3R_2 \\
& +5M_1(M_4 + 16R_2^3) + 9R_1(N_4 + 24R_1(M_4R_1 + 3M_3R_2)))) + 28h_2(36M_2^2 + 30(2M_1M_3 \\
& +2N_3R_1 + N_2R_2) + 288(9M_3R_1^3 + 10M_1R_1R_2^2) + 9M_2(576R_1^2R_2 + Bi(M_3 + 48R_1R_2^2)) \\
& +Bi(5N_3R_2 + 5M_1(M_4 + 16R_2^3) + 9R_1(N_4 + 24R_1(M_4R_1 + 3M_3R_2)))) + h_1^2(5Bi h_2^5(50M_1^2 \\
& +63N_1R_1 + 4320M_1R_1^3) + 140(3M_3^2 + 4M_2M_4 + BiM_3M_4 + 6N_5R_1 + BiN_6R_1 + (4N_4 \\
& +BiN_5 + 288M_4R_1^2)R_2 + 48(6M_3 + BiM_4)R_1R_2^2 + 16(4M_2 + BiM_3)R_2^3) \\
& +20h_2^4(100M_1^2 + 126N_1R_1 + 15BiN_2R_1 + 864BiM_2R_1^3 + 7BiN_1R_2 + 20M_1(432R_1^3 \\
& +Bi(M_2 + 72R_1^2R_2))) + 28h_2^3(75N_2R_1 + 4320M_2R_1^3 + 35N_1R_2 + 10M_1(10M_2 + BiM_3 \\
& +720R_1^2R_2 + 48BiR_1R_2^2) + Bi(10N_3R_1 + 432M_3R_1^3 + 5N_2R_2 + 6M_2(M_2 + 144R_1^2R_2))) \\
& +35h_2(4M_2(9M_3 + BiM_4 + 432R_1R_2^2 + 16BiR_2^3) + Bi(4N_4R_2 + 6R_1(N_5 + 48M_4R_1R_2) \\
& +3M_3(M_3 + 96R_1R_2^2)) + 4(5N_3R_2 + 5M_1(M_4 + 16R_2^3) + 9R_1(N_4 \\
& +24R_1(M_4R_1 + 3M_3R_2)))) + 28h_2^2(36M_2^2 + 30(2M_1M_3 + 2N_3R_1 + N_2R_2) \\
& +288(9M_3R_1^3 + 10M_1R_1R_2^2) + 9M_2(576R_1^2R_2 + Bi(M_3 + 48R_1R_2^2)) + Bi(5N_3R_2 \\
& +5M_1(M_4 + 16R_2^3) + 9R_1(N_4 + 24R_1(M_4R_1 + 3M_3R_2)))) + h_1(5Bi h_2^6(50M_1^2 \\
& +63N_1R_1 + 4320M_1R_1^3) + 140h_2(3M_3^2 + 4M_2M_4 + BiM_3M_4 + 6N_5R_1 + BiN_6R_1 \\
& +(4N_4 + BiN_5 + 288M_4R_1^2)R_2 + 48(6M_3 + BiM_4)R_1R_2^2 + 16(4M_2 + BiM_3)R_2^3) \\
& +70(6M_3(M_4 + 16R_2^3) + Bi(M_4^2 + 2N_6R_2 + 32M_4R_2^3) + 6(N_6R_1 + R_2(N_5 + 48M_4R_1R_2))) \\
& +20h_2^5(100M_1^2 + 126N_1R_1 + 15BiN_2R_1 + 864BiM_2R_1^3 + 7BiN_1R_2 + 20M_1(432R_1^3 \\
& +Bi(M_2 + 72R_1^2R_2))) + 28h_2^4(75N_2R_1 + 4320M_2R_1^3 + 35N_1R_2 \\
& +10M_1(10M_2 + BiM_3 + 720R_1^2R_2 + 48BiR_1R_2^2) + Bi(10N_3R_1 + 432M_3R_1^3 + 5N_2R_2 \\
& +6M_2(M_2 + 144R_1^2R_2))) + 35h_2^2(4M_2(9M_3 + BiM_4 + 432R_1R_2^2 + 16BiR_2^3)
\end{aligned}$$

$$\begin{aligned}
& +Bi(4N_4R_2 + 6R_1(N_5 + 48M_4R_1R_2) + 3M_3(M_3 + 96R_1R_2^2)) + 4(5N_3R_2 + 5M_1(M_4 \\
& + 16R_2^3) + 9R_1(N_4 + 24R_1(M_4R_1 + 3M_3R_2)))) + 28h_2^3(36M_2^2 + 30(2M_1M_3 \\
& + 2N_3R_1 + N_2R_2) + 288(9M_3R_1^3 + 10M_1R_1R_2^2) + 9M_2(576R_1^2R_2 + Bi(M_3 + 48R_1R_2^2)) \\
& + Bi(5N_3R_2 + 5M_1(M_4 + 16R_2^3) + 9R_1(N_4 + 24R_1(M_4R_1 + 3M_3R_2))))), \\
C_9 = & \frac{-1}{35Bi^2}(Br(5Bih_2^7(50M_1^2 + 63N_1R_1 + 4320M_1R_1^3) + 5Bih_1^7(1 + Bih_2)(50M_1^2 + 63N_1R_1 \\
& + 4320M_1R_1^3) + 140h_2^2(3M_3^2 + 4M_2M_4 + BiM_3M_4 + 6N_5R_1 + BiN_6R_1 + (4N_4 + BiN_5 \\
& + 228M_4R_1^2)R_2 + 48(6M_3 + BiM_4)R_1R_2^2 + 16(4M_2 + BiM_3)R_2^3) + 140(M_4^2 + 2N_6R_2 \\
& + 32M_4R_2^3) + 70h_2(6M_3(M_4 + 16R_2^3) + Bi(M_4^2 + 2N_6R_2 + 32M_4R_2^3) + 6(N_6R_1 \\
& + R_2(N_5 + 48M_4R_1R_2))) + 20h_2^6(100M_1^2 + 126N_1R_1 + 15BiN_2R_1 + 864BiM_2R_1^3 \\
& + 7BiN_1R_2 + 20M_1(432R_1^3 + Bi(M_2 + 72R_1^2R_2))) + 5h_1^6(1 + Bih_2)(50(8 + Bih_2)M_1^2 \\
& + 12BiR_1(5N_2 + 288M_2R_1^2) + 7N_1(9(8 + Bih_2)R_1 + 4BiR_2) + 80M_1(432R_1^3 \\
& + Bi(M_2 + 54h_2R_1^3 + 72R_1^2R_2))) + 28h_2^5(75N_2R_1 + 4320M_2R_1^3 + 35N_1R_2 \\
& + 10M_1(10M_2 + BiM_3 + 720R_1^2R_2 + 48BiR_1^2R_2) + Bi(10N_3R_1 + 432M_3R_1^3 \\
& + 5N_2R_2 + 6M_2(M_2 + 144R_1^2R_2))) + 35h_2^3(4M_2(9M_3 + BiM_4 + 432R_1R_2^2 + 16BiR_2^3) \\
& + Bi(4N_4R_2 + 6R_1(N_5 + 48M_4R_1R_2) + 3M_3(M_3 + 96R_1R_2^2) + 4(5N_3R_2 + 5M_1(M_4 + 16R_2^3) \\
& + 9R_1(N_4 + 24R_1(M_4R_1 + 3M_3R_2)))) + 28h_2^4(36M_2^2 + 30(2M_1M_3 + 2N_3R_1 + N_2R_2) \\
& + 288(9M_3R_1^3 + 10M_1R_1R_2^2) + 9M_2(576R_1^2R_2 + Bi(M_3 + 48R_1R_2^2)) + Bi(5N_3R_2 \\
& + 5M_1(M_4 + 16R_2^3) + 9R_1(N_4 + 24R_1(M_4R_1 + 3M_3R_2)))) + h_1^5(1 + Bih_2)(5Bih_2^2(50M_1^2 \\
& + 63N_1R_1 + 4320M_1R_1^3) + 20h_2(100M_1^2 + 126N_1R_1 + 15BiN_2R_1 + 864BiM_2R_1^3 + 7BiN_1R_2 \\
& + 20M_1(432R_1^3 + Bi(M_2 + 72R_1^2R_2))) + 28(75N_2R_1 + 4320M_2R_1^3 + 35N_1R_2 + 10M_1(10M_2 \\
& + BiM_3 + 720R_1^2R_2 + 48BiR_1R_2^2) + Bi(10N_3R_1 + 432M_3R_1^3 + 5N_2R_2 + 6M_2(M_2 + 144R_1^2R_2)))) \\
& + 28(36M_2^2 + 30(2M_1M_3 + 2N_3R_1 + N_2R_2) + 288(9M_3R_1^3 + 10M_1R_1R_2^2) + 9M_2(576R_1^2R_2 \\
& + Bi(M_3 + 48R_1R_2^2)) + Bi(5N_3R_2 + 5M_1(M_4 + 16R_2^3) + 9R_1(N_4 + 24R_1(M_4R_1 + 3M_3R_2)))) \\
& + h_1^3(1 + Bih_2)(5Bih_2^4(50M_1^2 + 63N_1R_1 + 4320M_1R_1^3) + 20h_2^3(100M_1^2 + 126N_1R_1 + 15BiN_2R_1 \\
& + 864BiM_2R_1^3 + 7BiN_1R_2 + 20M_1(432R_1^3 + Bi(M_2 + 72R_1^2R_2))) + 28h_2^2(75N_2R_1 + 4320M_2R_1^3 \\
& + 35N_1R_2 + 10M_1(10M_2 + BiM_3 + 720R_1^2R_2 + 48BiR_1R_2^2) + Bi(10N_3R_1 + 432M_3R_1^3 + 5N_2R_2
\end{aligned}$$

$$\begin{aligned}
& +6M_2(M_2 + 144R_1^2R_2))) + 35(4M_2(9M_3 + BiM_4 + 432R_1R_2^2 + 16BiR_2^2) + Bi(4N_4R_2 \\
& +6R_1(N_5 + 48M_4R_1R_2) + 3M_3(M_3 + 96R_1R_2^2)) + 4(5N_3R_2 + 5M_1(M_4 + 16R_2^3) \\
& +9R_1(N_4 + 24R_1(M_4R_1 + 3M_3R_2)))) + 28h_2(36M_2^2 + 30(2M_1M_3 + 2N_3R_1 \\
& +N_2R_2) + 288(9M_3R_1^3 + 10M_1R_1R_2^2) + 9M_2(576R_1^2R_2 + Bi(M_3 + 48R_1R_2^2)) \\
& +Bi(5N_3R_2 + 5M_1(M_4 + 16R_2^3) + 9R_1(N_4 + 24R_1(M_4R_1 + 3M_3R_2)))) \\
& +h_1^2(1 + Bi h_2)(5Bi h_2^5(50M_1^2 + 63N_1R_1 + 4320M_1R_1^3) + 140(3M_3^2 + 4M_2M_4 \\
& +BiM_3M_4 + 6N_5R_1 + BiN_6R_1 + (4N_4 + BiN_5 + 288M_4R_1^2)R_2 \\
& +48(6M_3 + BiM_4)R_1R_2^2 + 16(4M_2 + BiM_3)R_2^3) + 20h_2^4(100M_1^2 + 126N_1R_1 + 15BiN_2R_1 \\
& +864BiM_2R_1^3 + 7BiN_1R_2 + 20M_1(432R_1^3 + Bi(M_2 + 72R_1^2R_2))) + 28h_2^3(75N_2R_1 \\
& +4320M_2R_1^3 + 35N_1R_2 + 10M_1(10M_2 + BiM_3 + 720R_1^2R_2 + 48BiR_1R_2^2) \\
& +Bi(10N_3R_1 + 432M_3R_1^3 + 5N_2R_2 + 6M_2(M_2 + 144R_1^2R_2))) + 35h_2(4M_2(9M_3 + BiM_4 \\
& +432R_1R_2^2 + 16BiR_2^2) + Bi(4N_4R_2 + 6R_1(N_5 + 48M_4R_1R_2) + 3M_3(M_3 + 96R_1R_2^2)) \\
& +4(5N_3R_2 + 5M_1(M_4 + 16R_2^3) + 9R_1(N_4 + 24R_1(M_4R_1 + 3M_3R_2)))) + 28h_2^2(36M_2^2 \\
& +30(2M_1M_3 + 2N_3R_1 + N_2R_2) + 288(9M_3R_1^3 + 10M_1R_1R_2^2) + 9M_2(576R_1^2R_2 + Bi(M_3 \\
& +48R_1R_2^2)) + Bi(5N_3R_2 + 5M_1(M_4 + 16R_2^3) + 9R_1(N_4 + 24R_1(M_4R_1 + 3M_3R_2)))) \\
& +h_1(1 + Bi h_2)(5Bi h_2^6(50M_1^2 + 63N_1R_1 + 4320M_1R_1^3) + 140h_2(3M_3^2 + 4M_2M_4 \\
& +BiM_3M_4 + 6N_5R_1 + BiN_6R_1 + (4N_4 + BiN_5 + 288M_4R_1^2)R_2 + 48(6M_3 + BiM_4)R_1R_2^2 \\
& +16(4M_2 + BiM_3)R_2^3) + 70(6M_3(M_4 + 16R_2^3) + Bi(M_4^2 + 2N_6R_2 + 32M_4R_2^3) \\
& +6(N_6R_1 + R_2(N_5 + 48M_4R_1R_2))) + 20h_2^5(100M_1^2 + 126N_1R_1 + 15BiN_2R_1 \\
& +864BiM_2R_1^3 + 7BiN_1R_2 + 20M_1(432R_1^3 + Bi(M_2 + 72R_1^2R_2))) + 28h_2^4(75N_2R_1 \\
& +4320M_2R_1^3 + 35N_1R_2 + 10M_1(10M_2 + BiM_3 + 720R_1^2R_2 + 48BiR_1R_2^2) \\
& +Bi(10N_3R_1 + 432M_3R_1^3 + 5N_2R_2 + 6M_2(M_2 + 144R_1^2R_2))) + 35h_2^2(4M_2(9M_3 \\
& +BiM_4 + 432R_1R_2^2 + 16BiR_2^3) + Bi(4N_4R_2 + 6R_1(N_5 + 48M_4R_1R_2) + 3M_3(M_3 \\
& +96R_1R_2^2)) + 4(5N_3R_2 + 5M_1(M_4 + 16R_2^3) + 9R_1(N_4 + 24R_1(M_4R_1 + 3M_3R_2)))) \\
& +28h_2^3(36M_2^2 + 30(2M_1M_3 + 2N_3R_1 + N_2R_2) + 288(9M_3R_1^3 + 10M_1R_1R_2^2) \\
& +9M_2(576R_1^2R_2 + Bi(M_3 + 48R_1R_2^2)) + Bi(5N_3R_2 + 5M_1(M_4 + 16R_2^3) \\
& +9R_1(N_4 + 24R_1(M_4R_1 + 3M_3R_2))))).
\end{aligned}$$

The non-dimensional pressure rise per wavelength ( $\Delta P_{\lambda_2}$ ) is

$$\Delta P_{\lambda_2} = \int_0^{2\pi} \frac{dp_2}{dx} dx.$$

The perturbation expressions of  $\psi$ ,  $\theta$ ,  $\Delta P_\lambda$  and  $dp/dx$  upto  $O(\Gamma^2)$  are denoted by  $\psi^{(2)}$ ,  $\theta^{(2)}$ ,  $\Delta P_\lambda^{(2)}$  and  $dp^{(2)}/dx$  i.e.

$$\begin{aligned} \psi^{(2)} &= \psi_0 + \Gamma\psi_1 + \Gamma^2\psi_2. \\ \theta^{(2)} &= \theta_0 + \Gamma\theta_1 + \Gamma^2\theta_2. \\ \frac{dp^{(2)}}{dx} &= \frac{dp_0}{dx} + \Gamma\frac{dp_1}{dx} + \Gamma^2\frac{dp_2}{dx}. \\ \Delta P_\lambda^{(2)} &= \Delta P_{\lambda_0} + \Gamma\Delta P_{\lambda_1} + \Gamma^2\Delta P_{\lambda_2}. \end{aligned} \tag{2.58}$$

## 2.4 Graphical analysis and discussion

### 2.4.1 Pumping characteristics

In this section our aim is to analyze the behavior of longitudinal pressure gradient and pressure rise per wavelength for embedded flow parameters in the present problem. Note that the definition of pressure rise involves integration of  $dp^{(2)}/dx$ . The arising integral is not solvable analytically. Therefore the involved integral has been computed numerically. The variations of  $dp^{(2)}/dx$  for fixed values of involved parameters are sketched in the Figs. 2.2 and 2.3. The variation of longitudinal pressure gradient ( $dp^{(2)}/dx$ ) per wavelength for various values of the Deborah number  $\Gamma$  can be seen in Fig. 2.2. It is observed that  $dp^{(2)}/dx$  increases by increasing  $\Gamma$  i.e. the longitudinal pressure gradient for a third order fluid ( $\Gamma \neq 0$ ) is greater in magnitude when compared with that of a Newtonian fluid ( $\Gamma = 0$ ). In fact larger  $\Gamma$  physically corresponds to small values of dynamic viscosity. It is also interesting to note that the magnitude of resistance or assistance from the pressure gradient is higher for a third order fluid in comparison to a Newtonian fluid. Fig. 2.3 is plotted to serve the effects of variation of phase difference  $\phi$  on  $dp^{(2)}/dx$ . This Fig. reveals that the longitudinal pressure gradient  $dp^{(2)}/dx$  decreases by increasing the phase difference  $\phi$ . Figs. 2.4-2.6 illustrate the relation between pressure rise per

wavelength  $\Delta p_\lambda^{(2)}$  and flow rate  $\Theta^{(2)}$  for various values of  $\Gamma$ ,  $d$  and  $\phi$ , respectively. It is observed that  $\Delta p_\lambda^{(2)}$  increases by increasing  $\Gamma$  (Fig. 2.4) and it decreases with increasing  $d$  and  $\phi$  (Figs. 2.5 and 2.6). This means that peristalsis has to work against greater pressure rise for a third order fluid when compared to that of a Newtonian fluid. We have calculated the pressure rise required to produce zero average flow rate  $\Delta p_{\lambda(\max)}^{(2)}$  as a function of  $d$  for different values of Deborah number  $\Gamma$  (Fig. 2.7). For a third order fluid ( $\Gamma \neq 0$ ), the value of  $\Delta p_{\lambda(\max)}^{(2)}$  is larger than for a Newtonian fluid ( $\Gamma = 0$ ). Maximum pressure rise decreases with increasing  $d$ .

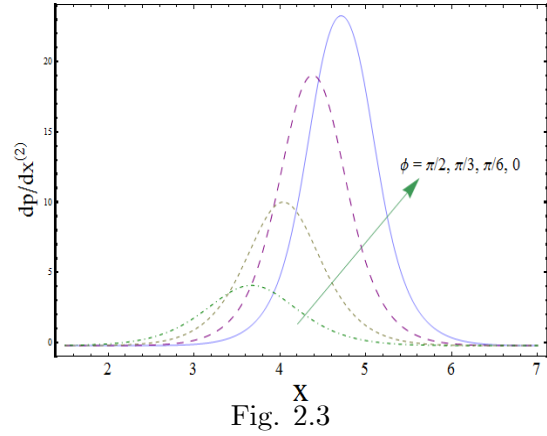
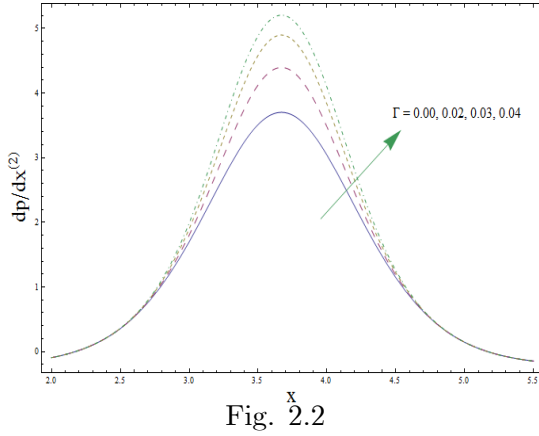


Fig. 2.2: Plot of longitudinal pressure gradient  $dp^{(2)}/dx$  for various values of the Deborah number  $\Gamma$  with  $a = 0.7$ ,  $b = 1.2$ ,  $d = 2$ ,  $\phi = \pi/2$  and  $\Theta = 0.1$ .

Fig. 2.3: Plot of longitudinal pressure gradient  $dp^{(2)}/dx$  for various values of the phase difference  $\phi$  with  $a = 0.7$ ,  $b = 1.2$ ,  $d = 2$ ,  $\Gamma = 0.01$  and  $\Theta = 0.1$ .



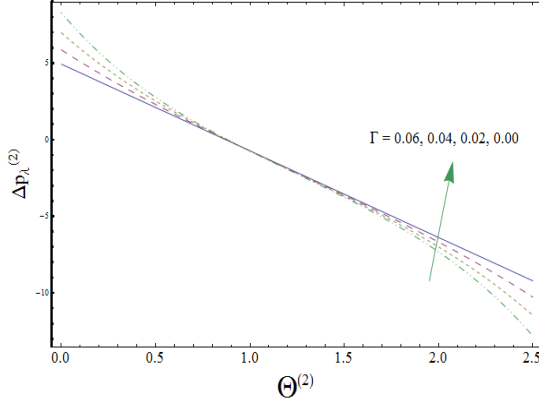


Fig. 2.4

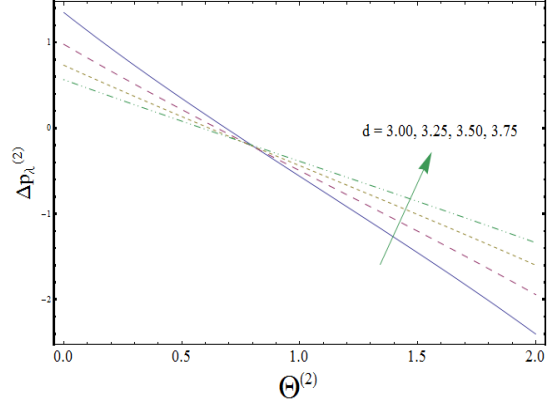


Fig. 2.5

Fig. 2.4: Plot of pressure rise per wavelength  $\Delta p_\lambda^{(2)}$  versus flow rate  $\Theta^{(2)}$  for various values of the Deborah number  $\Gamma$  with  $a = 0.7$ ,  $b = 1.2$ ,  $d = 2$  and  $\phi = \pi/2$ .

Fig. 2.5: Plot of pressure rise per wavelength  $\Delta p_\lambda^{(2)}$  versus flow rate  $\Theta^{(2)}$  for various values of the channel width  $d$  with  $a = 0.7$ ,  $b = 1.2$ ,  $\Gamma = 0.1$  and  $\phi = \pi/2$ .

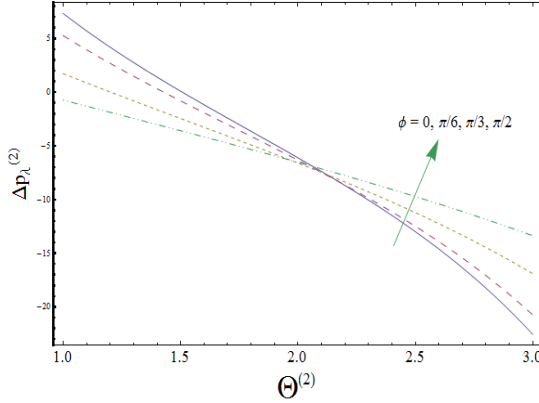


Fig. 2.6

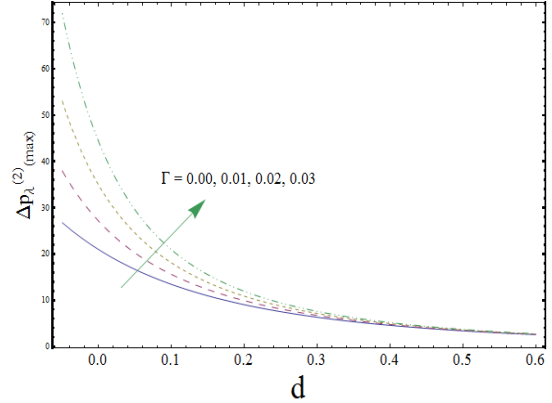


Fig. 2.7

Fig. 2.6: Plot of pressure rise per wavelength  $\Delta p_\lambda^{(2)}$  versus flow rate  $\Theta^{(2)}$  for various values of the phase difference  $\phi$  with  $a = 0.7$ ,  $b = 1.2$ ,  $d = 2$  and  $\Gamma = 0.01$ .

Fig. 2.7: Plot of maximum pressure rise per wavelength  $\Delta p_{\lambda(\max)}^{(2)}$  for various values of the Deborah number  $\Gamma$  with channel width  $d$  when  $a = 0.3$ ,  $b = 0.2$ ,  $\phi = \pi/2$  and  $\Theta = -0.001$ .

### 2.4.2 Velocity and temperature profiles

In this subsection the effects of various emerging parameters on the velocity  $u$  and temperature profile  $\theta^{(2)}$  are discussed. Fig. 2.8 displays the effects of  $\Gamma$  on the longitudinal velocity  $u$ . It shows that an increase in  $\Gamma$  causes a decrease in the magnitude of  $u$  at the boundaries of channel. However the magnitude of  $u$  increases by increasing  $\Gamma$  at the center of channel. Physically this corresponds to the situation when fluid offers less resistance in terms of small viscous effects. The selected values in this Fig. for the Deborah number are taken less than unity because we have developed the perturbation solution. The Deborah number is treated here as a perturbation quantity. Figs. 2.9 and 2.11 show an increase in the fluid temperature with maximum value along the centerline and minimum at the walls due to convective condition. It is noteworthy that the fluid temperature generally increases with increasing values of the Deborah number  $\Gamma$  and the Brinkman number  $Br$ . Actually Brinkman number  $Br$  involves the viscous dissipation effects which are due to the energy production and thus temperature increases. Fig. 2.10 illustrates the effects of Biot number  $Bi$  on temperature profile  $\theta^{(2)}$ . This Fig. reveals that by increasing the value of Biot number  $Bi$  the temperature profile  $\theta^{(2)}$  increases at the lower wall of the channel while it has the opposite behavior at the upper wall of channel. Here we have considered the Biot number  $Bi$  much larger than one due to non-uniformity of the temperature fields within the fluid. However problems involving small  $Bi$  are thermally simple due to the uniform temperature fields inside the fluid.

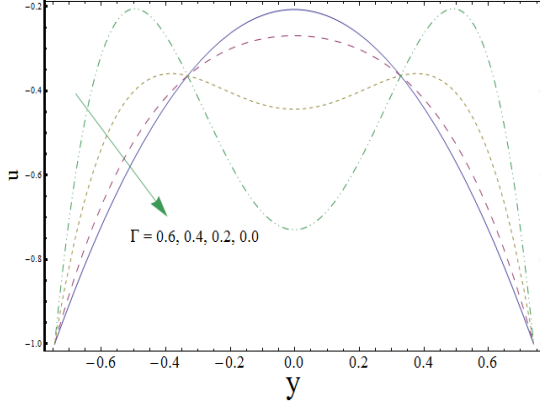


Fig. 2.8

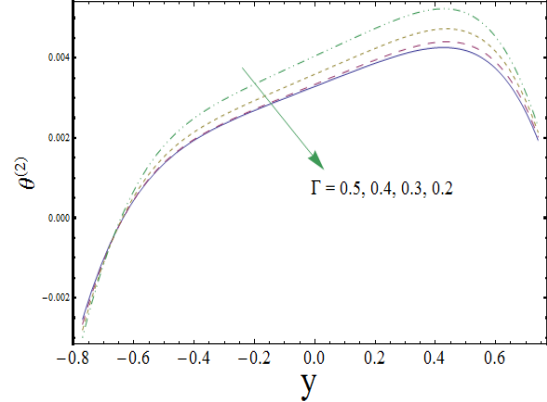


Fig. 2.9

Fig. 2.8.:Plot of longitudinal velocity  $u$  for various values of Deborah number  $\Gamma$  with  $a = 0.3$ ,  $b = 0.6$ ,  $d = 0.9$ ,  $\phi = \pi/4$ ,  $\Theta = 1.2$ ,  $x = -\pi/3$  and  $dp^{(2)}/dx = 1$ .

Fig. 2.9: Plot of the temperature  $\theta^{(2)}$  for various values of the Deborah number  $\Gamma$  with  $a = 0.3$ ,  $b = 0.5$ ,  $d = 0.9$ ,  $\phi = \pi/4$ ,  $\Theta = 0.5$ ,  $x = -\pi/3$ ,  $dp^{(2)}/dx = 1$ ,  $Br = 1$  and  $Bi = 10$ .

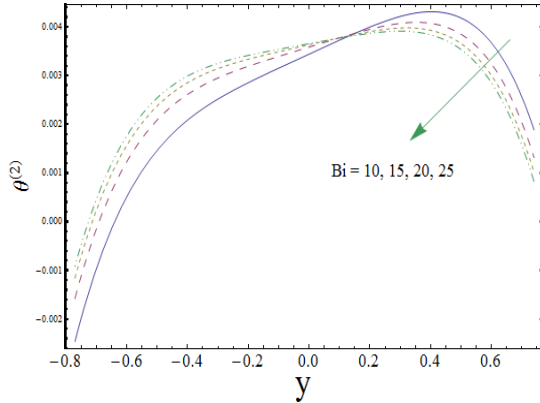


Fig. 2.10

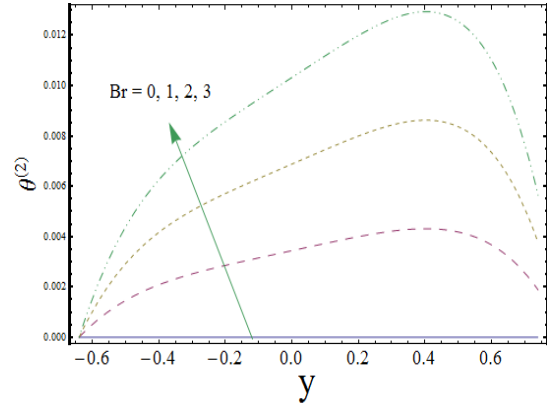


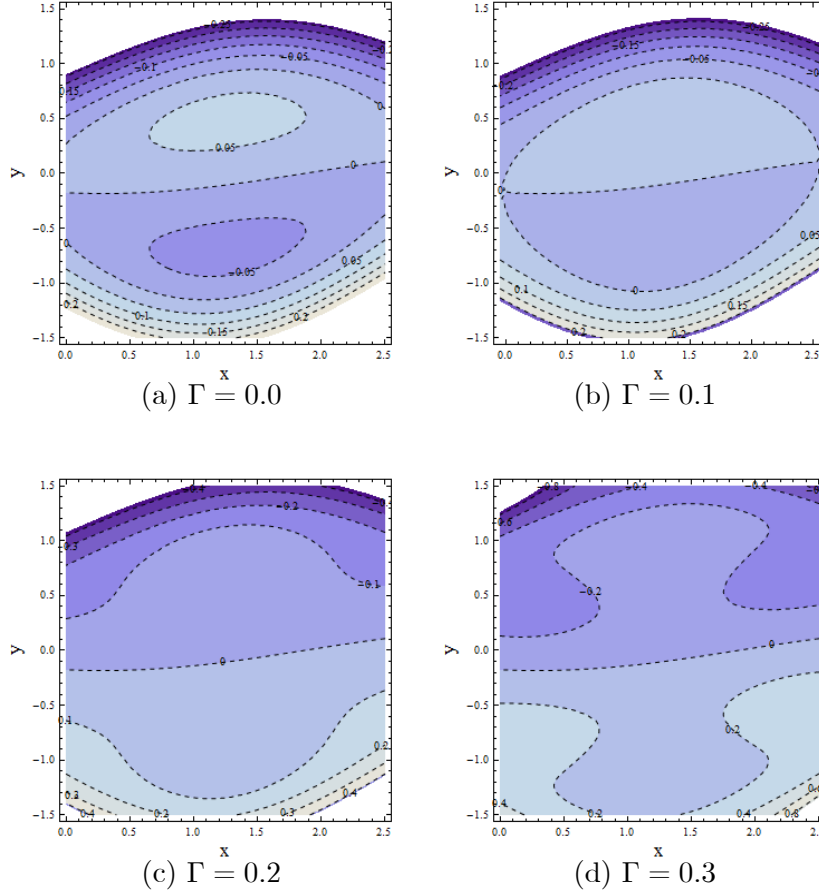
Fig. 2.11

Fig. 2.10: Plot of the temperature  $\theta^{(2)}$  for various values of the Biot number  $Bi$  with  $a = 0.3$ ,  $b = 0.5$ ,  $d = 0.9$ ,  $\phi = \pi/4$ ,  $\Theta = 0.5$ ,  $x = -\pi/3$ ,  $dp^{(2)}/dx = 1$ ,  $Br = 1$  and  $\Gamma = 0.1$ .

Fig. 2.11: Plot of the temperature  $\theta^{(2)}$  for various values of the Brinkman number  $Br$  with  $a = 0.3$ ,  $b = 0.5$ ,  $d = 0.9$ ,  $\phi = \pi/4$ ,  $\Theta = 0.5$ ,  $x = -\pi/3$ ,  $dp^{(2)}/dx = 1$ ,  $Bi = 10$  and  $\Gamma = 0.1$ .

### 2.4.3 Trapping

In general the shape of streamlines is similar to that of a boundary wall in the wave frame. However, some of the streamlines split and enclose a bolus under certain conditions and this bolus moves as a whole with the wave. This phenomenon is known as trapping. Effect of  $\Gamma$  on trapping is illustrated in Fig. 2.12. It is observed that the size of trapped bolus decreases with increasing  $\Gamma$  and disappears for  $\Gamma = 0.2$  when we have considered the negative flux. The streamlines for different  $\phi$  are plotted in Fig. 2.13. It is observed that the bolus appears at the center region for  $\phi = 0$  and it moves towards left and decreases in size as  $\phi$  increases and disappears for  $\phi = \pi$ .



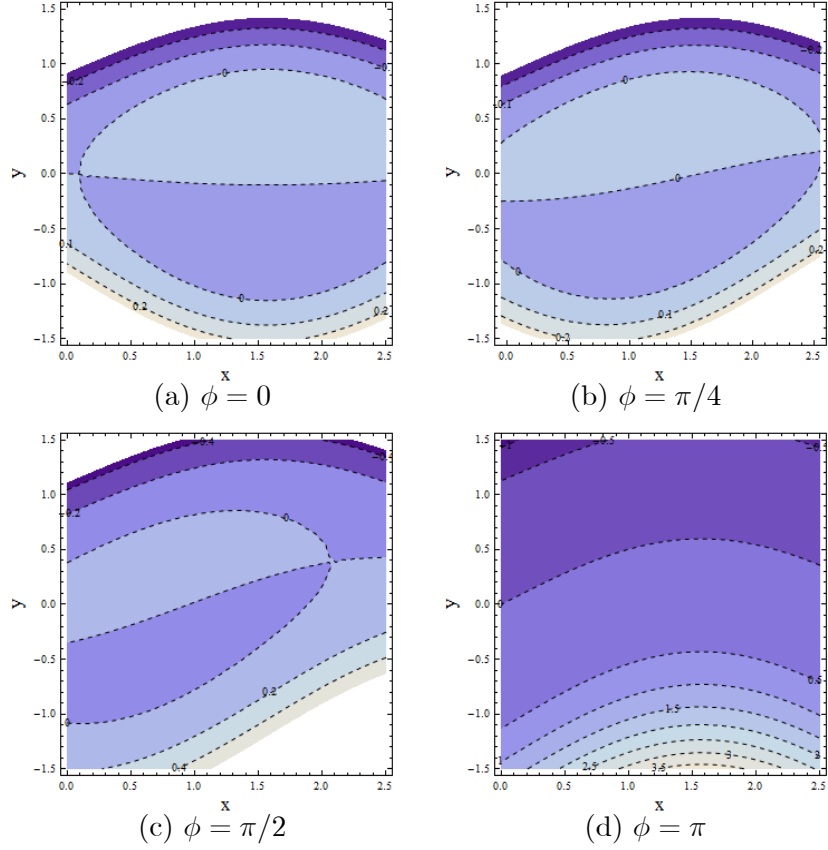


Fig. 2.13: Streamlines for  $a = 0.5$ ,  $b = 0.7$ ,  $d = 1$ ,  $dp^{(2)}/dx = 1$ ,  $\Theta = 1.28$ ,  $\Gamma = 0.01$  with different  $\phi$ .

## 2.5 Closing remarks

In this chapter the regular perturbation method is employed to investigate the peristaltic flow of third order fluid in an asymmetric channel with convective conditions at the channel walls. The study reveals that a combined increase in Biot number, Brinkman number and non-Newtonian parameter enhances the thermal stability of the flow. The results for viscous fluid can be deduced as special case of present problem when  $\Gamma = 0$ . A comparative study of present results for zero Deborah number in equation of motion is with complete agreement to the case of viscous fluid (see ref. [27]).

## Chapter 3

# Simultaneous effects of convective conditions and nanoparticles on peristaltic motion

### 3.1 Introduction

This chapter deals with the peristaltic transport of viscous nanofluid in an asymmetric channel. The channel walls satisfy the convective conditions. The effects of Brownian motion and thermophoresis parameters are taken into account. The relevant flow analysis is first modeled and then computed for the series solutions of temperature and concentration fields. Closed form expression of stream function is constructed. Plots are prepared for a parametric study reflecting the effects of Brownian motion, thermophoresis, Prandtl, Eckert and Biot numbers.

### 3.2 Constitutive equations

The balances of mass, momentum, temperature and nanoparticle volume fraction are given by [129]:

$$\text{div } \bar{\mathbf{V}} = 0, \quad (3.1)$$

$$\frac{d\bar{\mathbf{V}}}{d\bar{t}} = -\frac{1}{\rho_f} \nabla \bar{P} + \nu \nabla^2 \bar{\mathbf{V}}, \quad (3.2)$$

$$\frac{d\bar{T}}{d\bar{t}} = \alpha^* \nabla^2 \bar{T} + \frac{\nu}{c_p} (\bar{\boldsymbol{\tau}} \cdot \bar{\mathbf{L}}) + \tau^* [D_B \nabla \bar{C} \nabla \bar{T} + (D_{\bar{T}}/\bar{T}_m) \nabla \bar{T} \nabla \bar{T}], \quad (3.3)$$

$$\frac{d\bar{C}}{d\bar{t}} = D_B \nabla^2 \bar{C} + (D_{\bar{T}}/\bar{T}_m) \nabla^2 \bar{T}. \quad (3.4)$$

Here  $\bar{\mathbf{V}}$  is the velocity field,  $\bar{T}$  is the fluid temperature,  $\bar{C}$  the nanoparticle concentration,  $d/d\bar{t}$  the material time derivative,  $\nu$  the kinematic viscosity,  $\bar{P}$  the pressure,  $\rho_f$  the density of an incompressible fluid,  $\rho_p$  the density of nanoparticles,  $\alpha^*$  the thermal diffusivity,  $D_B$  the Brownian motion coefficient,  $D_{\bar{T}}$  the thermophoretic diffusion coefficient,  $\tau^* = (\rho c)_p/(\rho c)_f$  the ratio of effective heat capacity of the nanoparticle material to heat capacity of the fluid and  $\bar{T}_m$  the mean temperature.

### 3.3 Mathematical modeling

Let us consider the peristaltic motion of viscous nanofluid in an asymmetric channel. We take  $(\bar{X}, \bar{Y})$  as the Cartesian coordinates with  $\bar{X}$  being measured in the direction of wave propagation and  $\bar{Y}$  in the direction normal to the  $\bar{X}$ -axis. Let  $\bar{Y} = \bar{h}_1$  and  $\bar{Y} = \bar{h}_2$  be the upper and lower boundaries of the channel respectively (see Fig. 2.1). The motion is induced by sinusoidal wave trains propagating with a constant speed  $c$  along the channel walls. These are defined by

$$\bar{h}_1(\bar{X}, \bar{t}) = d_1 + a_1 \cos \left[ \frac{2\pi}{\lambda} (\bar{X} - c\bar{t}) \right], \quad \text{upper wall}, \quad (3.5)$$

$$\bar{h}_2(\bar{X}, \bar{t}) = -d_2 - a_2 \cos \left[ \frac{2\pi}{\lambda} (\bar{X} - c\bar{t}) + \phi \right], \quad \text{lower wall}, \quad (3.6)$$

where  $a_1, a_2$  are the waves amplitudes,  $\lambda$  is the wavelength,  $d_1 + d_2$  is the width of the asymmetric channel and the phase difference  $\phi$  varies in the range  $0 \leq \phi \leq \pi$  ( $\phi = 0$  corresponds to symmetric channel with waves out of phase and for  $\phi = \pi$  the waves are in phase). Further

$a_1, a_2, d_1, d_2$  and  $\phi$  satisfy the condition

$$a_1^2 + a_2^2 + 2a_1a_2 \cos \phi \leq (d_1 + d_2)^2. \quad (3.7)$$

Considering a wave frame  $(\bar{x}, \bar{y})$  that moves with a velocity  $c$  away from the fixed frame  $(\bar{X}, \bar{Y})$ , we write

$$\begin{aligned} \bar{x} &= \bar{X} - c\bar{t}, \quad \bar{y} = \bar{Y}, \quad \bar{u}(\bar{x}, \bar{y}) = \bar{U}(\bar{X}, \bar{Y}, \bar{t}) - c, \quad \bar{v}(\bar{x}, \bar{y}) = \bar{V}(\bar{X}, \bar{Y}, \bar{t}), \\ \bar{T}(\bar{x}, \bar{y}) &= \bar{T}(\bar{X}, \bar{Y}, \bar{t}), \quad \bar{C}(\bar{x}, \bar{y}) = \bar{C}(\bar{X}, \bar{Y}, \bar{t}), \quad \bar{p}(\bar{x}, \bar{y}) = \bar{P}(\bar{X}, \bar{Y}, \bar{t}), \end{aligned} \quad (3.8)$$

in which  $(\bar{u}, \bar{v})$  and  $(\bar{U}, \bar{V})$  are the velocity components in the wave and the fixed frames respectively,  $\bar{p}$  and  $\bar{P}$  stand for pressure in the wave and fixed frames.

The exchange of heat with ambient at the walls through Newton's cooling law is given by

$$k \frac{\partial \bar{T}}{\partial \bar{y}} = -h(\bar{T} - T_0) \quad \text{at} \quad \bar{y} = \bar{h}_1, \quad (3.9)$$

$$k \frac{\partial \bar{T}}{\partial \bar{y}} = -h(T_1 - \bar{T}) \quad \text{at} \quad \bar{y} = \bar{h}_2, \quad (3.10)$$

where  $h$  is the heat transfer coefficient and  $T_0$  and  $T_1$  are the ambient temperatures at the upper and lower channel walls respectively.

The relevant flow equations in wave frame can be expressed as

$$\frac{\partial \bar{u}}{\partial \bar{x}} + \frac{\partial \bar{v}}{\partial \bar{y}} = 0, \quad (3.11)$$

$$\bar{u} \frac{\partial \bar{u}}{\partial \bar{x}} + \bar{v} \frac{\partial \bar{u}}{\partial \bar{y}} = -\frac{1}{\rho_f} \frac{\partial \bar{p}}{\partial \bar{x}} + \nu \left( \frac{\partial^2 \bar{u}}{\partial \bar{x}^2} + \frac{\partial^2 \bar{u}}{\partial \bar{y}^2} \right), \quad (3.12)$$

$$\bar{u} \frac{\partial \bar{v}}{\partial \bar{x}} + \bar{v} \frac{\partial \bar{v}}{\partial \bar{y}} = -\frac{1}{\rho_f} \frac{\partial \bar{p}}{\partial \bar{y}} + \nu \left( \frac{\partial^2 \bar{v}}{\partial \bar{x}^2} + \frac{\partial^2 \bar{v}}{\partial \bar{y}^2} \right), \quad (3.13)$$

$$\begin{aligned} \bar{u} \frac{\partial \bar{T}}{\partial \bar{x}} + \bar{v} \frac{\partial \bar{T}}{\partial \bar{y}} &= \alpha^* \left( \frac{\partial^2 \bar{T}}{\partial \bar{x}^2} + \frac{\partial^2 \bar{T}}{\partial \bar{y}^2} \right) + \frac{\nu}{c_p} \left[ 4 \left( \frac{\partial \bar{u}}{\partial \bar{x}} \right)^2 + \left( \frac{\partial \bar{u}}{\partial \bar{y}} + \frac{\partial \bar{v}}{\partial \bar{x}} \right)^2 \right] \\ &+ \tau^* \left[ D_B \left( \frac{\partial \bar{C}}{\partial \bar{x}} \frac{\partial \bar{T}}{\partial \bar{x}} + \frac{\partial \bar{C}}{\partial \bar{y}} \frac{\partial \bar{T}}{\partial \bar{y}} \right) + \frac{D_{\bar{T}}}{\bar{T}_m} \left\{ \left( \frac{\partial \bar{T}}{\partial \bar{x}} \right)^2 + \left( \frac{\partial \bar{T}}{\partial \bar{y}} \right)^2 \right\} \right], \end{aligned} \quad (3.14)$$

$$\bar{u} \frac{\partial \bar{C}}{\partial \bar{x}} + \bar{v} \frac{\partial \bar{C}}{\partial \bar{y}} = D_B \left( \frac{\partial^2 \bar{C}}{\partial \bar{x}^2} + \frac{\partial^2 \bar{C}}{\partial \bar{y}^2} \right) + \frac{D_{\bar{T}}}{\bar{T}_m} \left( \frac{\partial^2 \bar{T}}{\partial \bar{x}^2} + \frac{\partial^2 \bar{T}}{\partial \bar{y}^2} \right). \quad (3.15)$$



Defining dimensionless variables, Reynolds number (Re), Prandtl number (Pr), Eckert number ( $Ec$ ), Brownian motion parameter ( $Nb$ ), the thermophoresis parameter ( $Nt$ ), Schmidt number ( $Sc$ ) and Biot number ( $Bi$ ) through the following variables

$$\begin{aligned} x &= \frac{\bar{x}}{\lambda}, \quad y = \frac{\bar{y}}{d_1}, \quad u = \frac{\bar{u}}{c}, \quad v = \frac{\bar{v}}{c}, \quad p = \frac{d_1^2 \bar{p}}{c \lambda \mu}, \quad \delta = \frac{d_1}{\lambda}, \\ h_1 &= \frac{\bar{h}_1}{d_1}, \quad h_2 = \frac{\bar{h}_2}{d_1}, \quad t = \frac{c \bar{t}}{\lambda}, \quad \theta = \frac{\bar{T} - T_0}{T_1 - T_0}, \quad \sigma = \frac{\bar{C} - C_0}{C_1 - C_0}, \\ \text{Re} &= \frac{\rho c d_1}{\mu}, \quad \text{Pr} = \frac{\nu}{\alpha^*}, \quad Ec = \frac{c^2}{c_f (T_1 - T_0)}, \quad Nb = \frac{\tau^* D_B (C_1 - C_0)}{\nu}, \\ Nt &= \frac{\tau^* D_{\bar{T}} (T_1 - T_0)}{\bar{T}_m \nu}, \quad Sc = \frac{\nu}{D_B}, \quad Bi = \frac{h d_1}{k}, \end{aligned} \quad (3.16)$$

the governing Eqs. (3.11 – 3.15) can be put into the forms

$$\delta \frac{\partial u}{\partial x} + \frac{\partial v}{\partial y} = 0, \quad (3.17)$$

$$\text{Re} \left( \delta u \frac{\partial}{\partial x} + v \frac{\partial}{\partial y} \right) u = -\frac{\partial p}{\partial x} + \delta^2 \frac{\partial^2 u}{\partial x^2} + \frac{\partial^2 u}{\partial y^2}, \quad (3.18)$$

$$\text{Re} \delta \left( \delta u \frac{\partial}{\partial x} + v \frac{\partial}{\partial y} \right) v = -\frac{\partial p}{\partial y} + \delta \left( \delta^2 \frac{\partial^2 v}{\partial x^2} + \frac{\partial^2 v}{\partial y^2} \right), \quad (3.19)$$

$$\begin{aligned} \text{Re} \left( \delta u \frac{\partial}{\partial x} + v \frac{\partial}{\partial y} \right) \theta &= \frac{1}{\text{Pr}} \left( \delta^2 \frac{\partial^2 \theta}{\partial x^2} + \frac{\partial^2 \theta}{\partial y^2} \right) + Ec \left[ 4\delta^2 \left( \frac{\partial u}{\partial x} \right)^2 + \left( \frac{\partial u}{\partial y} + \delta^2 \frac{\partial v}{\partial x} \right)^2 \right] \\ &+ Nb \left( \delta^2 \frac{\partial \sigma}{\partial x} \frac{\partial \theta}{\partial x} + \frac{\partial \sigma}{\partial y} \frac{\partial \theta}{\partial y} \right) + Nt \left[ \delta^2 \left( \frac{\partial \theta}{\partial x} \right)^2 + \left( \frac{\partial \theta}{\partial y} \right)^2 \right], \end{aligned} \quad (3.20)$$

$$\text{Re} Sc \left( \delta u \frac{\partial}{\partial x} + v \frac{\partial}{\partial y} \right) \sigma = \delta^2 \frac{\partial^2 \sigma}{\partial x^2} + \frac{\partial^2 \sigma}{\partial y^2} + \frac{Nt}{Nb} \left( \delta^2 \frac{\partial^2 \theta}{\partial x^2} + \frac{\partial^2 \theta}{\partial y^2} \right). \quad (3.21)$$

Defining the velocity components  $u$  and  $v$  in terms of the stream function  $\psi$  by

$$u = \psi_y, \quad v = -\delta \psi_x. \quad (3.22)$$

In the limit  $\text{Re} \rightarrow 0$ , the inertialess flow corresponds to Poiseuille-like longitudinal velocity profile. The pressure gradient depends upon  $x$  and  $t$  only in laboratory frame. It does not depend on  $y$ . Such features can be expected because there is no streamline curvature to produce transverse pressure gradient when  $\delta = 0$ . The assumptions of long wavelength and small Reynolds number give  $\delta = 0$  and  $\text{Re} = 0$ . It should be pointed out that the theory of long

wavelength and zero Reynolds number remains applicable for case of chyme transport in small intestine [47]. In this case  $c = 2$  cm/min,  $a = 1.25$  cm and  $\lambda = 8.01$  cm. Here half width of intestine is small in comparison to wavelength i.e.  $a/\lambda = 0.156$ . It is also declared by Lew et al. [10] that Reynolds number in small intestine was small. Further, the situation of intrauterine fluid flow due to myomaterial contractions is a peristaltic type fluid motion in a cavity. The sagittal cross section of the uterus reveals a narrow channel enclosed by two fairly parallel walls [54]. The  $1 - 3$  mm width of this channel is very small compared with its 50 mm length [52], defining an opening angle from cervix to fundus of about 0.04 rad. Analysis of dynamics parameters of the uterus revealed frequency, wavelength, amplitude and velocity of the fluid-wall interface during a typical contractile wave were found to be  $0.01 - 0.057$  Hz,  $10 - 30$  mm,  $0.05 - 0.2$  mm and  $0.5 - 1.9$  mm/s respectively. Therefore adopting low Reynolds number and long wavelength analysis [6] we have

$$\frac{\partial p}{\partial x} = \frac{\partial^3 \psi}{\partial y^3}, \quad (3.23)$$

$$\frac{\partial p}{\partial y} = 0, \quad (3.24)$$

$$\frac{1}{Pr} \frac{\partial^2 \theta}{\partial y^2} + Ec \left( \frac{\partial^2 \psi}{\partial y^2} \right)^2 + Nb \left( \frac{\partial \sigma}{\partial y} \frac{\partial \theta}{\partial y} \right) + Nt \left( \frac{\partial \theta}{\partial y} \right)^2 = 0, \quad (3.25)$$

$$\frac{\partial^2 \sigma}{\partial y^2} + \frac{Nt}{Nb} \frac{\partial^2 \theta}{\partial y^2} = 0, \quad (3.26)$$

where continuity equation is identically satisfied and the above equations indicate that  $p \neq p(y)$ .

Defining  $\Theta$  and  $F$  as the dimensionless time-mean flows in the laboratory and wave frames respectively we have

$$\Theta = F + 1 + d, \quad (3.27)$$

$$F = \int_{h_2}^{h_1} \frac{\partial \psi}{\partial y} dy. \quad (3.28)$$

Keeping in view the physical constraints of the problem, the boundary conditions in the fixed

frame may be expressed mathematically as follows

$$\bar{U} = 0, \text{ at } \bar{Y} = \bar{h}_1 \text{ and } \bar{Y} = \bar{h}_2, \quad (3.29)$$

$$\bar{C} = C_0 \text{ at } \bar{Y} = \bar{h}_1, \quad (3.30)$$

$$\bar{C} = C_1 \text{ at } \bar{Y} = \bar{h}_2. \quad (3.31)$$

Writing the above conditions through Eq. (3.8), the dimensionless boundary conditions are

$$\psi = -1, \text{ at } y = h_1 \text{ and } y = h_2, \quad (3.32)$$

$$\psi = F/2, \sigma = 0 \text{ at } y = h_1, \quad (3.33)$$

$$\psi = -F/2, \sigma = 1 \text{ at } y = h_2. \quad (3.34)$$

Also Eqs. (3.9) and (3.10) give

$$\frac{\partial \theta}{\partial y} + Bi\theta = 0 \text{ at } y = h_1, \quad (3.35)$$

$$\frac{\partial \theta}{\partial y} + Bi(1 - \theta) = 0 \text{ at } y = h_2. \quad (3.36)$$

The dimensionless forms of  $h_i$ 's ( $i = 1, 2$ ) are

$$h_1(x) = 1 + a \cos(2\pi x), \quad h_2(x) = -d - b \cos(2\pi x + \phi), \quad (3.37)$$

where  $a = a_1/d_1$ ,  $b = a_2/d_1$ ,  $d = d_2/d_1$  and  $\phi$  satisfy the following relation

$$a^2 + b^2 + 2ab \cos \phi \leq (1 + d)^2.$$

The pressure rise per wavelength ( $\Delta P_\lambda$ ) is

$$\Delta P_\lambda = \int_0^1 \frac{dp}{dx} dx. \quad (3.38)$$

### 3.4 Solution procedure

The computations of Eqs. (3.25) and (3.26) are made through homotopy perturbation method (HPM). For that we write

$$H(q, \theta) = (1 - q) [L(\theta) + Ec\psi_{yy}^2 - L(\theta_0)] + q \left[ L(\theta) + Nb \left( \frac{\partial \sigma}{\partial y} \frac{\partial \theta}{\partial y} \right) + Nt \left( \frac{\partial \theta}{\partial y} \right)^2 \right] \quad (3.39)$$

$$H(q, \sigma) = (1 - q) [L(\sigma) - L(\sigma_0)] + q \left[ L(\sigma) + \frac{Nt}{Nb} \left( \frac{\partial^2 \theta}{\partial y^2} \right) \right], \quad (3.40)$$

where we have taken  $L = \frac{\partial^2}{\partial y^2}$  as the linear operator and  $\psi(y)$  is computed by using Eq. (3.23) and boundary conditions (3.32 – 3.34). Exact solution for  $\psi$  is

$$\psi(y) = -\frac{(h_1 + h_2 - 2y)}{2(h_1 - h_2)^3} \left[ \begin{array}{c} -2(h_1 - h_2)(h_1 - y)(h_2 - y) \\ + F(h_1^2 - 4h_1h_2 + h_2^2 + 2(h_1 + h_2)y - 2y^2) \end{array} \right]. \quad (3.41)$$

We define initial guesses as

$$\begin{aligned} \theta_0(y) &= 1 + \frac{Bi(h_2 - y) - 1}{Bi(h_1 - h_2) + 2} + \frac{3EcPr(F + h_1 - h_2)^2}{4(h_1 - h_2)^3} \\ &\quad \times \left[ \frac{8 + Bi(h_1 - h_2)}{Bi} - \frac{(h_1 - h_2 - 2y)^4}{(h_1 - h_2)^3} \right], \end{aligned} \quad (3.42)$$

$$\sigma_0(y) = \frac{h_1 - y}{h_1 - h_2}. \quad (3.43)$$

Let us write

$$\theta(y, q) = \theta_0 + q\theta_1 + q^2\theta_2 + \dots, \quad (3.44)$$

$$\sigma(y, q) = \sigma_0 + q\sigma_1 + q^2\sigma_2 + \dots \quad (3.45)$$

The solutions of temperature and nanoparticle concentration (for  $q = 1$ ) are constructed as follows:

$$\theta(y) = A_1y^8 + A_2y^7 + A_3y^6 + A_4y^5 + A_5y^4 + A_6y^3 + A_7y^2 + A_8y + A_9, \quad (3.46)$$

$$\sigma(y) = B_1y^4 + B_2y^3 + B_3y^2 + B_4y + B_5, \quad (3.47)$$

where

$$\begin{aligned}
A_1 &= \frac{-288pEc^2(F+h_1-h_2)^4NtPr^2}{7(h_1-h_2)^{12}}, \\
A_2 &= -4(h_1+h_2)A_1, \\
A_3 &= 7(h_1+h_2)^2A_1, \\
A_4 &= \frac{12pEcPr(F+h_1-h_2)^2}{5(2+Bi(h_1-h_2))(h_1-h_2)^{12}} \left[ (h_1-h_2)^5 \{ (2+Bi(h_1-h_2))Nb \right. \\
&\quad \left. + 2Bi(h_2-h_1)Nt \} + 120Ec(2+Bi(h_1-h_2))(F+h_1-h_2)^2 \right. \\
&\quad \left. \times (h_1+h_2)^3NtPr \right], \\
A_5 &= \frac{6EcPr(F+h_1-h_2)^2}{(h_1-h_2)^{12}} \left[ -2(h_1-h_2)^6 - (1/(2+Bi(h_1-h_2))) \right. \\
&\quad \times \{ (h_1-h_2)^5(h_1+h_2)((2+Bi(h_1-h_2))Nb + 2Bi(-h_1+h_2)Nt)p \} \\
&\quad \left. - 30pEcNtPr(F+h_1-h_2)^2(h_1+h_2)^4 \right], \\
A_6 &= \frac{6EcPr(F+h_1-h_2)^2}{(h_1-h_2)^{12}} \left[ 4(h_1-h_2)^6(h_1+h_2) + (1/(2+Bi(h_1-h_2))) \right. \\
&\quad \times \{ (h_1-h_2)^5(h_1+h_2)^2((2+Bi(h_1-h_2))Nb + 2Bi(-h_1+h_2)Nt)p \} \\
&\quad \left. + 12pEcNtPr(F+h_1-h_2)^2(h_1+h_2)^5 \right], \\
A_7 &= \frac{1}{2(h_1-h_2)^{12}} \left[ 36EcPr(F+h_1-h_2)^2(h_1-h_2)^6(h_1+h_2)^2 \right. \\
&\quad \left. + (p/(2+Bi(h_1-h_2))^2) \{ -Bi(h_1-h_2)^6 + 6EcPr(2+Bi(h_1-h_2)) \right. \\
&\quad \times (F+h_1-h_2)^2(h_1+h_2)^3 \} \{ (h_1-h_2)^5((2+Bi(h_1-h_2))Nb \\
&\quad \left. + Bi(-h_1+h_2)Nt) + 6EcNtPr(2+Bi(h_1-h_2))(F+h_1-h_2)^2(h_1+h_2)^3 \} \right], \\
A_8 &= \frac{-Bi}{2+Bi(h_1-h_2)} + \frac{6EcPr(F+h_1-h_2)^2(h_1+h_2)^3}{(h_1-h_2)^6} \\
&\quad + \frac{p}{70(2+Bi(h_1-h_2))^2(h_1-h_2)^{12}} \left[ 240EcPr(F+h_1-h_2)^2 \right. \\
&\quad \times \{ 7h_1h_2(h_1-h_2)^5(h_1^2+h_2^2)Nb + 3EcNtPr(F+h_1-h_2)^2(h_1+h_2)^7 \} \\
&\quad \left. + Bi^2(h_1-h_2)^2 \{ 35(Nt-Nb)((h_1^{11}+h_2^{11}) - 9h_1h_2(h_1^9+h_2^9)) \} \right]
\end{aligned}$$

$$\begin{aligned}
& +35h_1^2h_2^2(h_1^7+h_2^7)-75h_1^3h_2^3(h_1^5+h_2^5)+90h_1^4h_2^4(h_1^3+h_2^3) \\
& -42h_1^5h_2^5(h_1+h_2)+42Ec(h_1-h_2)^5(F+h_1-h_2)^2((h_1^4 \\
& +16h_1h_2(h_1^2+h_2^2)+6h_1^2h_2^2)Nb-20h_1h_2(h_1^2+h_2^2)Nt)\Pr \\
& +360Ec^2Pr^2Nt(h_1-h_2)(h_1+h_2)^7(F+h_1-h_2)^4\}]\,, \\
A_9 = & 1+\frac{-1+Bi h_2}{2+Bi(h_1-h_2)}-L(8+(h_1+h_2)^4+Bi(h_1-h_2)^3) \\
& +(p/(70Bi(2+Bi(h_1-h_2))^2(h_1-h_2)^{12})[-70Bi(h_1-h_2)^{12}Nb \\
& +84BiEc(h_1-h_2)^5(F+h_1-h_2)^2(h_1^5-5h_1^4h_2-5h_1h_2^4+h_2^5)Nb\Pr \\
& +720Ec^2(h_1-h_2)^7(F+h_1-h_2)^4NtPr^2+720BiEc^2(F+h_1-h_2)^4 \\
& \times((h_1^8+h_2^8)-9h_1h_2(h_1^6+h_2^6)+28h_1^2h_2^2(h_1^4+h_2^4)-63h_1^3h_2^3(h_1^2+h_2^2) \\
& +70h_1^4h_2^4)NtPr^2-Bi^3h_1h_2(h_1-h_2)^2\{-35(Nb-Nt)(h_1-h_2)^{10} \\
& +42Ec(h_1-h_2)^5(F+h_1-h_2)^2(h_1+h_2)(h_1^2+h_2^2)(Nb-2Nt)\Pr \\
& +180Ec^2(F+h_1-h_2)^4(h_1^2+h_2^2)(h_1^4+6h_1^2h_2^2+h_2^4)NtPr^2\} \\
& +Bi^2(h_1-h_2)\{-35Nb((h_1^{12}+h_2^{12})-14h_1h_2(h_1^{10}+h_2^{10})+86h_1^2h_2^2(h_1^8+h_2^8) \\
& -310h_1^3h_2^3(h_1^6+h_2^6)+735h_1^4h_2^4(h_1^4+h_2^4)-1212h_1^5h_2^5(h_1^2+h_2^2)+1428h_1^6h_2^6) \\
& +35Nt(h_1-h_2)^{12}+42Ec(h_1-h_2)^5(F+h_1-h_2)^2(h_1+h_2) \\
& \times((Nb-2Nt)(h_1^4+6h_1^2h_2^2+h_2^4)+4h_1h_2(-2Nb+3Nt) \\
& \times(h_1^2+h_2^2))\Pr+180Ec^2(F+h_1-h_2)^4(h_1^8-12h_1^7h_2+28h_1^6h_2^2-84h_1^5h_2^3 \\
& +70h_1^4h_2^4-84h_1^3h_2^5+28h_1^2h_2^6-12h_1h_2^7+h_2^8)NtPr^2\}]\,,
\end{aligned}$$

$$\begin{aligned}
L &= -\frac{3Ec\Pr(F+h_1-h_2)^2}{4(h_1-h_2)^6}, \\
B_1 &= \frac{12pEcNt\Pr(F+h_1-h_2)^2}{Nb(h_1-h_2)^6}, \\
B_2 &= 2(h_1+h_2)B_1, \\
B_3 &= \frac{3}{2}(h_1+h_2)^2B_1, \\
B_4 &= \frac{-1}{(h_1-h_2)}+\frac{1}{2}(h_1+h_2)^3B_1, \\
B_5 &= \frac{h_2}{(h_1-h_2)}+\frac{h_1h_2}{2}(h_1^2+h_2^2)B_1,
\end{aligned}$$

### 3.5 Results and discussion

In this section, the effects of various emerging parameters on the temperature  $\theta$ , nanoparticle volume fraction  $\phi$  and heat transfer coefficient at the upper wall are discussed in detail. Figs. 3.1 and 3.2 show the effects of Eckert number  $Ec$  and Prandtl number  $Pr$  on temperature profile  $\theta$  respectively. These Figs. depict that the temperature  $\theta$  increases with an increase in Eckert and Prandtl numbers due to the strong viscous dissipation effects. Also  $Ec = 0$  corresponds to the situation in which viscous dissipation effects are absent. Effect of Brownian motion parameter  $Nb$  and thermophoresis parameter  $Nt$  on temperature profile  $\theta$  is illustrated in Fig. 3.3. It is observed from this Fig. that the temperature  $\theta$  increases when  $Nb$  and  $Nt$  are increased. As the Brownian motion and thermophoretic effects strengthen, this corresponds to the effective movement of nanoparticles from the wall to the fluid which results in the significant increase of temperature  $\theta$ . The temperature profile  $\theta$  decreases with an increase in the Biot number  $Bi$  because of the non-uniform temperature distribution in the fluid (see Fig. 3.4). Effects of Eckert number ( $Ec$ ) and Prandtl number ( $Pr$ ) on nanoparticle volume fraction field  $\phi$  are seen in the Figs. 3.5 and 3.6. The nanoparticles volume fraction field  $\phi$  is found to decrease when the effects of Eckert and Prandtl numbers intensify. However the nanoparticle volume fraction field  $\phi$  increases with an increase in Brownian motion parameter  $Nb$ . On the other hand  $\phi$  decreases when we intensify the thermophoresis parameter  $Nt$  (see Figs. 3.7 and 3.8). The behaviors of parameters on the heat transfer coefficient at the upper wall have been observed in the Figs. 3.9-3.12. The heat transfer coefficient is denoted by  $Z(x) = (h_1)_x \theta_y(h_1)$  which actually defines the rate of heat transfer or heat flux at the upper wall. The heat transfer coefficient  $Z(x)$  increases when the values of Biot number  $Bi$  are set to be increased (see Fig. 3.9). According to Fig. 3.10 the heat transfer coefficient  $Z(x)$  increases by increasing the values of Brownian motion parameter  $Nb$  and thermophoresis variable  $Nt$ . As a consequence the nanoparticle enhances the heat transfer rate. Further it is noted that increasing the values of Prandtl number  $Pr$ , the heat transfer coefficient  $Z(x)$  is increased (see Fig. 3.11). It is important to note that in all these Figs. the viscous dissipation effects are significantly large ( $Ec = 1.0$ ) which enhances the heat transfer rate. Fig. 3.12 shows the effects of Eckert number  $Ec$  on heat transfer coefficient  $Z(x)$ . This Fig. depicts that the heat transfer coefficient  $Z(x)$  is much larger for higher values of the Eckert number ( $Ec > 1$ ) when compared with the case

of no viscous dissipation ( $Ec = 0.01$ ). Fig. 3.13 is plotted to see the effects of channel width  $d$  on trapping. For this Fig.  $d = 0.6$  (panels (a) and (b)),  $d = 0.7$  (panels (c) and (d)),  $d = 1.3$  (panels (e) and (f)) and the other parameters are  $a = 0.5$ ,  $b = 0.7$  and  $\Theta = 1.2$ . It is observed from this Fig. that size of the trapping bolus decreases by increasing the value of channel width  $d$ . The left panel shows the trapping for phase difference  $\phi = 0$  and right panel for  $\phi = \pi/2$ . A comparative study of these panels reveals that the trapping bolus is symmetric with respect to the channel for  $\phi = 0$ . On the other hand for  $\phi = \pi/2$  the trapping bolus shifts towards left because of the asymmetry of channel. Fig. 3.14 depicts the effects of flow rate  $\Theta$  on trapping. This Fig. shows that the trapping bolus increases in size when we increase the values of flow rate  $\Theta$ . In this Fig.  $\Theta = 0.9$  (panels (a) and (b)),  $\Theta = 1.2$  (panels (c) and (d)),  $\Theta = 1.8$  (panels (e) and (f)) and other parameters are  $a = 0.5$ ,  $b = 0.7$  and  $d = 1.2$ . Also the trapping bolus shifts towards left in an asymmetric case (right panel) when compared with the symmetric case (left panel).

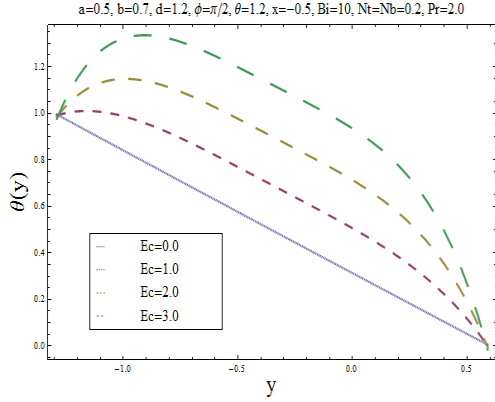


Fig. 3.1

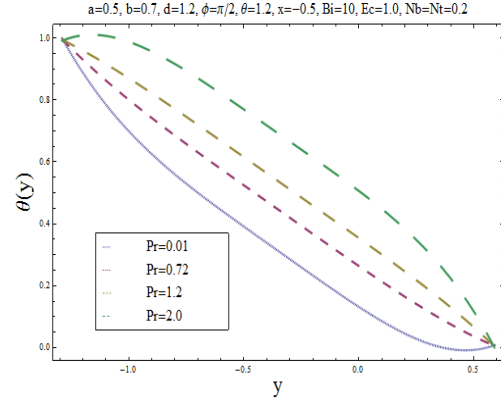


Fig. 3.2

Fig. 3.1: Temperature profile  $\theta(y)$  for  $Ec$ .

Fig. 3.2: Temperature profile  $\theta(y)$  for  $Pr$ .



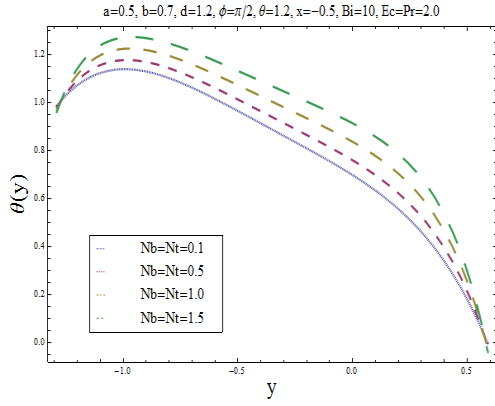


Fig. 3.3

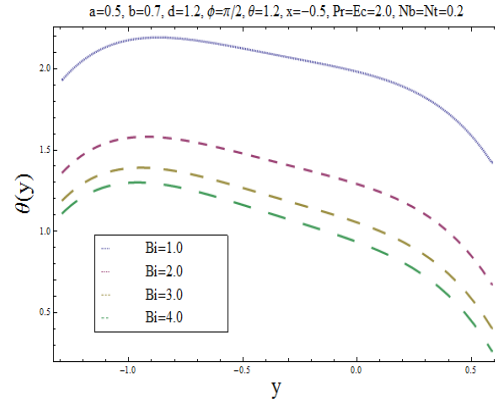


Fig. 3.4

Fig. 3.3: Temperature profile  $\theta(y)$  for  $Nb$  and  $Nt$ .

Fig. 3.4: Temperature profile  $\theta(y)$  for  $Bi$ .

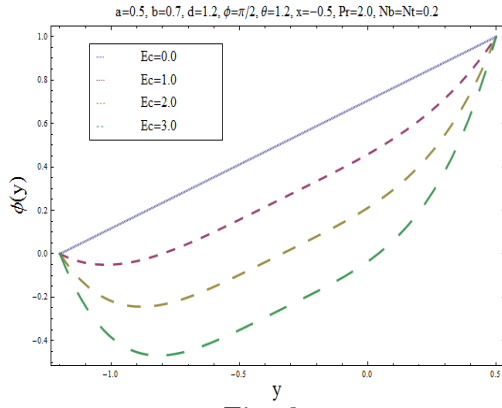


Fig. 3.5

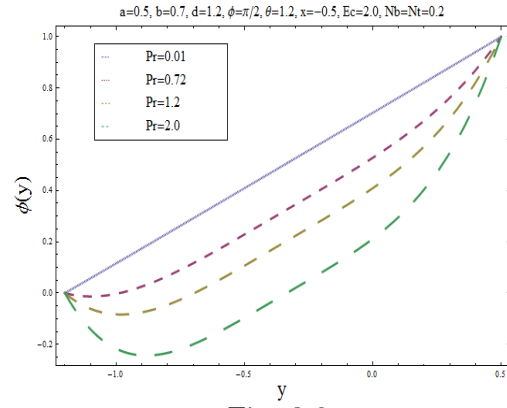


Fig. 3.6

Fig. 3.5: Nanoparticle volume fraction  $\phi(y)$  for  $Ec$ .

Fig. 3.6: Nanoparticle volume fraction  $\phi(y)$  for  $Pr$ .

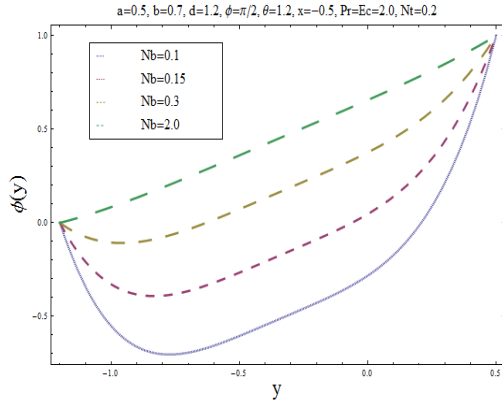


Fig. 3.7

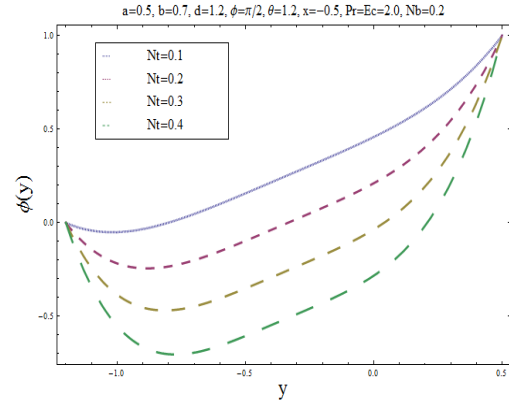


Fig. 3.8

Fig. 3.7: Nanoparticle volume fraction  $\phi(y)$  for  $Nb$ .

Fig. 3.8: Nanoparticle volume fraction  $\phi(y)$  for  $Nt$ .

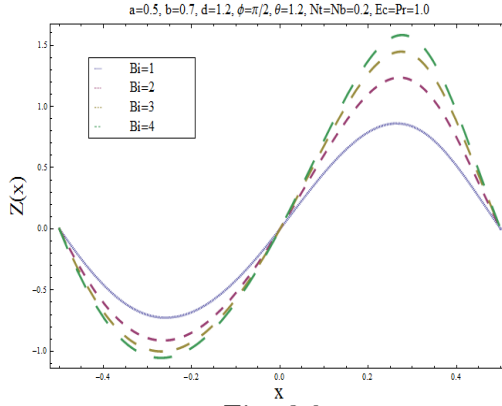


Fig. 3.9

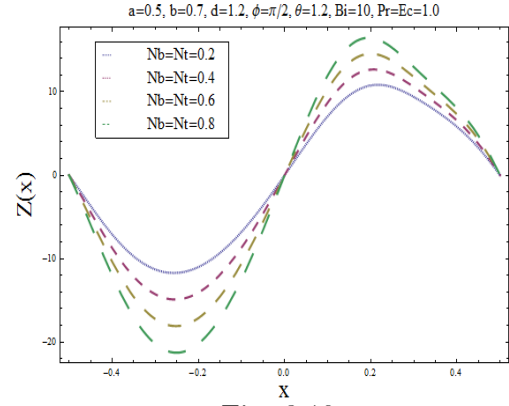


Fig. 3.10

Fig. 3.9: Heat transfer coefficient  $Z(x)$  for  $Bi$ .

Fig. 3.10: Heat transfer coefficient  $Z(x)$  for  $Nb$  and  $Nt$ .

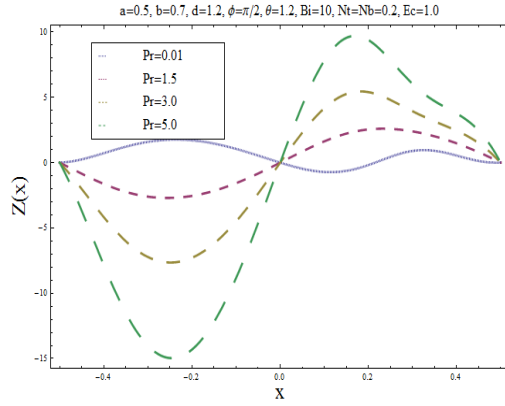


Fig. 3.11

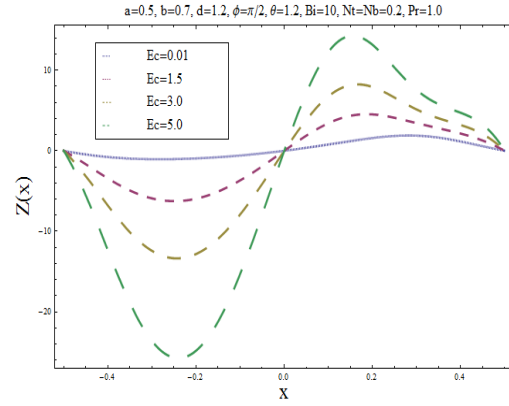


Fig. 3.12

Fig. 3.11: Heat transfer coefficient  $Z(x)$  for  $Pr$ .

Fig. 3.12: Heat transfer coefficient  $Z(x)$  for  $Ec$ .

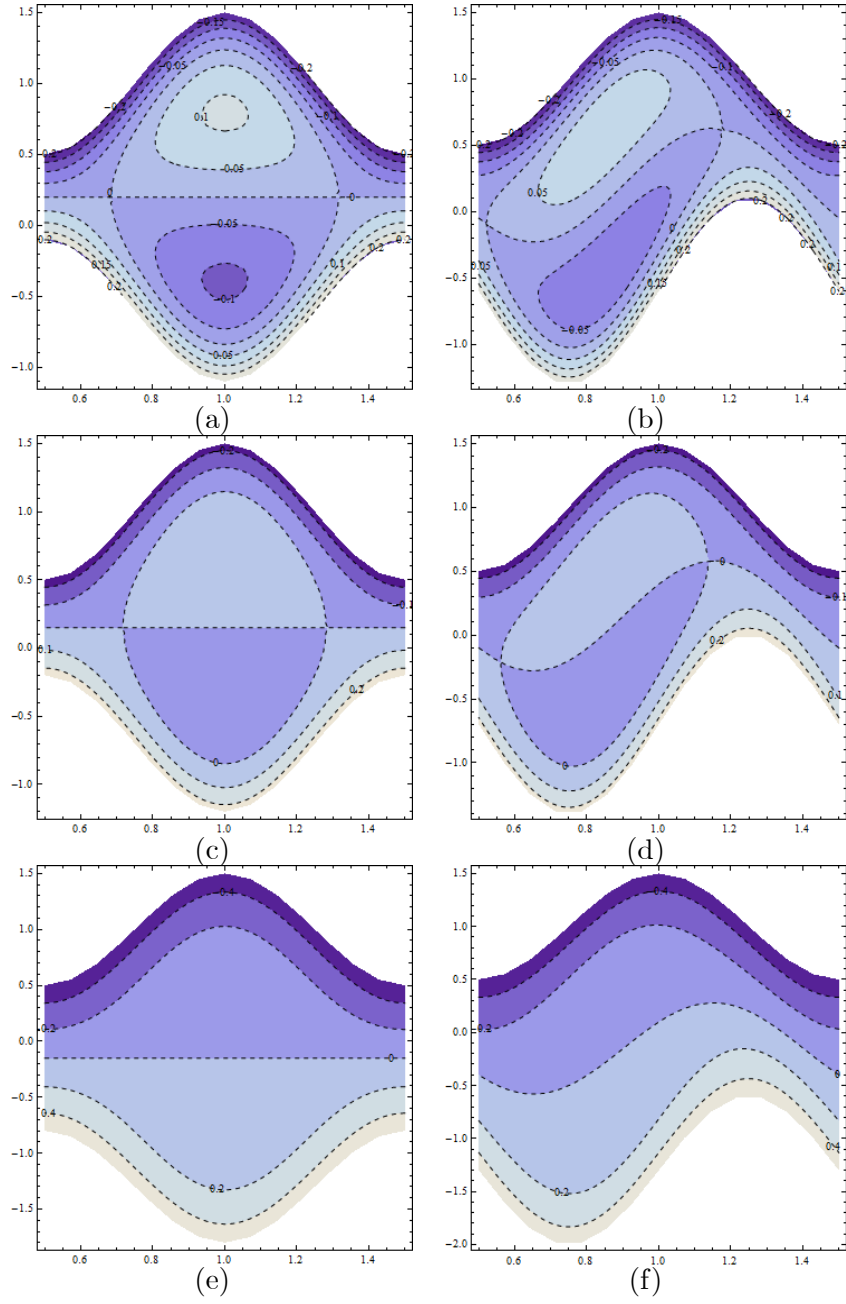


Fig. 3.13: Streamlines for different values of  $d$  (panels (a), (c) and (e) for  $\phi = 0$  and panels (b), (d) and (f) for  $\phi = \pi/2$ ).

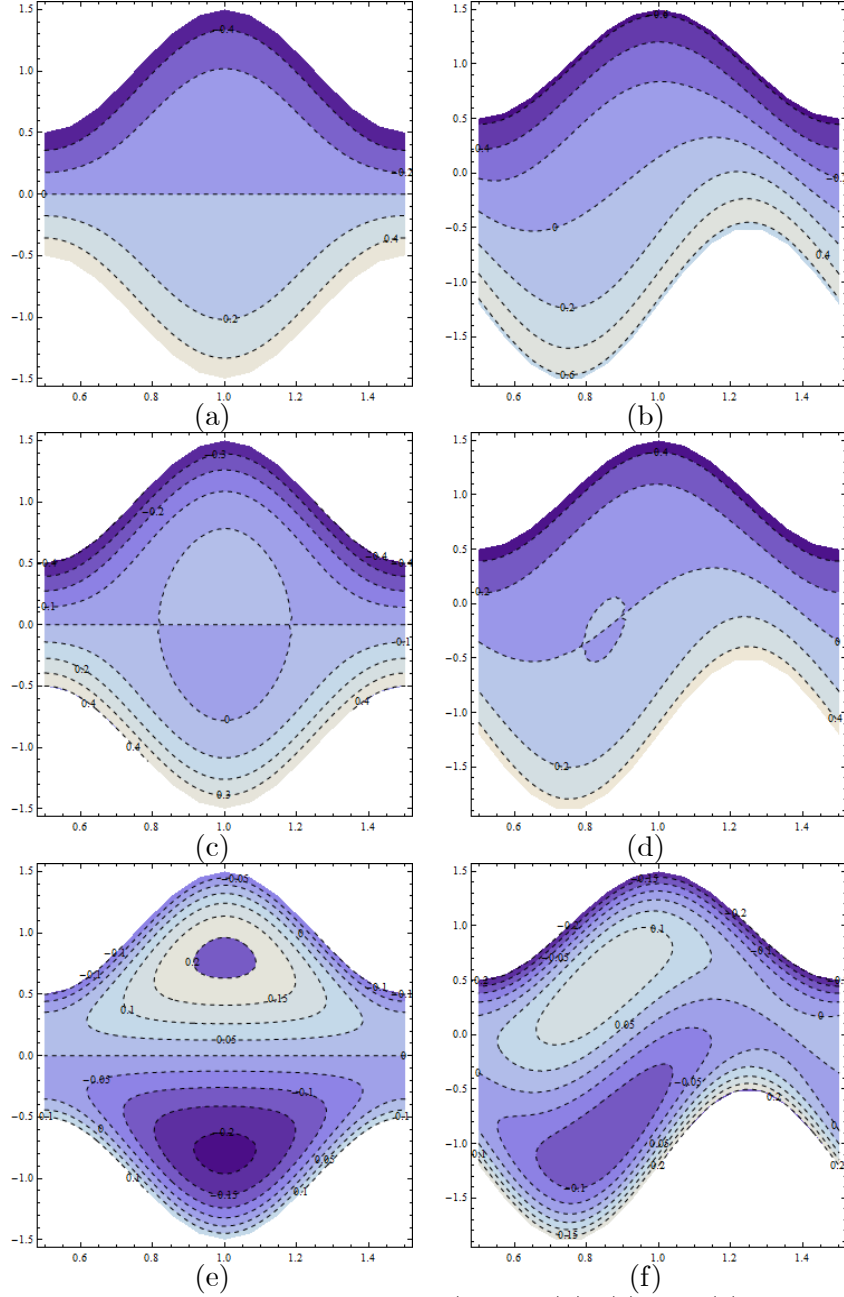


Fig. 3.14: Streamlines for different values of  $\Theta$  (panels (a), (c) and (e) for  $\phi = 0$  and panels (b), (d) and (f) for  $\phi = \pi/2$ ).

### 3.6 Main points

This chapter addresses the effects of nanoparticles and convective conditions on peristaltic motion in an asymmetric channel. Viscous dissipation effects are also considered. The conducted

study leads to the following observations:

- The temperature increases while nanoparticle volume fraction decreases when there is increase in Eckert and Prandtl numbers.
- By increasing the value of Brownian motion and thermophoresis parameter, the temperature profile increases.
- Temperature is a decreasing function of Biot number.
- Nanoparticle volume fraction field increases with an increase in Brownian motion parameter and it decreases by increasing thermophoresis parameter.
- Heat transfer coefficient increases when there is increase in the Biot, Brownian motion, thermophoresis, Prandtl and Eckert parameters.
- Trapping decreases with an increase in channel width while it increases by increasing the flow rate.

## Chapter 4

# Soret and Dufour effects in peristaltic transport of physiological fluids with chemical reaction: A mathematical analysis

### 4.1 Introduction

The peristaltically driven Casson fluid flow in an asymmetric channel with convective conditions is investigated in this chapter. The Soret and Dufour effects are studied in the presence of chemical reaction. The relevant flow analysis is modelled for Casson fluid in a wave frame. Computations of solutions are made for the velocity, temperature and concentration fields. Here two yield planes exist because of channel asymmetry. These planes are described in terms of the core width by working on the transcendental equation. Closed form expression of stream function is constructed. Plots are prepared for a parametric study reflecting the effects of Casson fluid parameter, chemical reaction parameter, Prandtl, Schmidt, Soret, Dufour and Biot numbers.

## 4.2 Governing equation

The constitutive equation corresponding to the flow of a Casson fluid is given by

$$\bar{\tau}^{\frac{1}{2}} = \bar{\tau}_y^{\frac{1}{2}} + \left| -\mu_\infty \frac{\partial \bar{U}}{\partial \bar{Y}} \right|^{\frac{1}{2}} \quad \text{if } \bar{\tau} \geq \bar{\tau}_y, \quad (4.1)$$

$$\frac{\partial \bar{U}}{\partial \bar{Y}} = 0 \quad \text{if } \bar{\tau} \leq \bar{\tau}_y, \quad (4.2)$$

where  $\mu_\infty$  is the viscosity at high shear rate and  $\bar{\tau}_y$  is the yield stress. It is interesting to note that when shear stress is less than the yield stress, the velocity gradient vanishes (see relation (4.2)). As a consequence whenever  $\bar{\tau} \leq \bar{\tau}_y$ , plug flow sets in. These relations between  $\frac{\partial \bar{U}}{\partial \bar{Y}}$  and  $\bar{\tau}$  are applicable for positive values of  $\bar{\tau}$  and negative values of  $\frac{\partial \bar{U}}{\partial \bar{Y}}$ . For more general situation, the equivalent form of these relations where  $\bar{\tau}$  and  $\frac{\partial \bar{U}}{\partial \bar{Y}}$  can change the sign may be written as

$$\mu_\infty \frac{\partial \bar{U}}{\partial \bar{Y}} = - \left( 1 + \frac{\bar{\tau}_y}{|\bar{\tau}|} - 2 \frac{\bar{\tau}_y^{\frac{1}{2}}}{|\bar{\tau}|^{1/2}} \right) \bar{\tau} \quad \text{if } \bar{\tau} \geq \bar{\tau}_y, \quad (4.3)$$

$$\frac{\partial \bar{U}}{\partial \bar{Y}} = 0 \quad \text{if } \bar{\tau} \leq \bar{\tau}_y. \quad (4.4)$$

## 4.3 Problem formulation

Consider the peristaltic motion of a non-Newtonian fluid, modelled as a Casson fluid in the two dimensional asymmetric channel by taking  $(\bar{X}, \bar{Y})$  as the Cartesian coordinates with  $\bar{X}$  being measured in the direction of wave propagation and  $\bar{Y}$  in the direction normal to the  $\bar{X}$ -axis. The motion is induced due to the propagation of sinusoidal wave trains with a constant speed  $c$  along the channel walls. Let  $\bar{Y} = \bar{h}_1$  and  $\bar{Y} = \bar{h}_2$  be the upper and lower boundaries of the channel respectively (see Fig. 2.1). Then

$$\bar{h}_1(\bar{X}, \bar{t}) = d_1 + a_1 \cos \left[ \frac{2\pi}{\lambda} (\bar{X} - c\bar{t}) \right], \quad \text{upper wall}, \quad (4.5)$$

$$\bar{h}_2(\bar{X}, \bar{t}) = -d_2 - a_2 \cos \left[ \frac{2\pi}{\lambda} (\bar{X} - c\bar{t}) + \phi \right], \quad \text{lower wall}, \quad (4.6)$$



where  $a_1, a_2$  are the waves amplitudes,  $\lambda$  is the wavelength,  $d_1 + d_2$  is the width of the asymmetric channel and the phase difference  $\phi$  varies in the range  $0 \leq \phi \leq \pi$ . Here  $\phi = 0$  corresponds to symmetric channel with waves out of phase and  $\phi = \pi$  the waves are in phase. Further  $a_1, a_2, d_1, d_2$  and  $\phi$  satisfy the condition

$$a_1^2 + a_2^2 + 2a_1a_2 \cos \phi \leq (d_1 + d_2)^2. \quad (4.7)$$

From Eqs. (4.3) and (4.4) there is no doubt that such type of flows are three phase in nature when asymmetric channel is considered. Here the plug flow region is the central core region. If the plug flow region is represented by  $\bar{\kappa}_1 \leq \bar{Y} \leq \bar{\kappa}_2$  where  $\bar{h}_2 \leq \bar{\kappa}_1, \bar{\kappa}_2 \leq \bar{h}_1$  and the two shear flow regions by  $\bar{h}_2 \leq \bar{Y} \leq \bar{\kappa}_1$  and  $\bar{\kappa}_2 \leq \bar{Y} \leq \bar{h}_1$ , then in these regions the Casson fluid's constitutive equations (4.3) and (4.4) can be written as

$$\mu_\infty \frac{\partial \bar{U}}{\partial \bar{Y}} = -\bar{\tau} + \bar{\tau}_y - 2\bar{\tau}_y^{1/2} |\bar{\tau}|^{1/2} \quad \text{if } \bar{h}_2 \leq \bar{Y} \leq \bar{\kappa}_1, \quad (4.8)$$

$$\frac{\partial \bar{U}}{\partial \bar{Y}} = 0 \quad \text{if } \bar{\kappa}_1 \leq \bar{Y} \leq \bar{\kappa}_2, \quad (4.9)$$

$$\mu_\infty \frac{\partial \bar{U}}{\partial \bar{Y}} = -\left(\bar{\tau} + \bar{\tau}_y - 2\bar{\tau}_y^{1/2} |\bar{\tau}|^{1/2}\right) \quad \text{if } \bar{\kappa}_2 \leq \bar{Y} \leq \bar{h}_1, \quad (4.10)$$

in which the two yield plane locations, namely  $\bar{Y} = \bar{\kappa}_1$  and  $\bar{Y} = \bar{\kappa}_2$ , are to be discovered as part of solution to the problem under consideration.

The flow is steady in wave frame, if pressure difference between the ends of the channel is constant and channel length is finite (equal to an integral number of wavelength) as given by Shapiro et al. [6]. We presume that these conditions are best fitted to our problem in wave frame then Galilean transformations between the moving  $o(x, y)$  and fixed frames  $O(X, Y, t)$  are given by

$$\begin{aligned} \bar{x} &= \bar{X} - c\bar{t}, \quad \bar{y} = \bar{Y}, \quad \bar{u}(\bar{x}, \bar{y}) = \bar{U}(\bar{X}, \bar{Y}, \bar{t}) - c, \quad \bar{v}(\bar{x}, \bar{y}) = \bar{V}(\bar{X}, \bar{Y}, \bar{t}), \\ \bar{T}(\bar{x}, \bar{y}) &= \bar{T}(\bar{X}, \bar{Y}, \bar{t}), \quad \bar{C}(\bar{x}, \bar{y}) = \bar{C}(\bar{X}, \bar{Y}, \bar{t}), \quad \bar{p}(\bar{x}, \bar{y}) = \bar{P}(\bar{X}, \bar{Y}, \bar{t}), \end{aligned} \quad (4.11)$$

in which  $(\bar{u}, \bar{v})$  and  $(\bar{U}, \bar{V})$  are the velocity components in the wave and the fixed frames respectively and  $\bar{p}$  and  $\bar{P}$  stand for pressure in the wave and fixed frames. Also  $\bar{T}$  and  $\bar{C}$  are the

temperature and concentration of the fluid in dimensional form.

Defining dimensionless variables, wave number ( $\delta$ ), temperature ( $\theta$ ), concentration ( $\sigma$ ), Prandtl number ( $Pr$ ), Dufour number ( $Du$ ), Schmidt number ( $Sc$ ), Soret number ( $Sr$ ) and chemical reaction parameter ( $\gamma$ ) by

$$\begin{aligned} x &= \frac{\bar{x}}{\lambda}, \quad y = \frac{\bar{y}}{d_1}, \quad u = \frac{\bar{u}}{c}, \quad v = \frac{\bar{v}}{c\delta}, \quad p = \frac{d_1^2 \bar{p}}{c\lambda\mu_\infty}, \quad \delta = \frac{d_1}{\lambda}, \quad \tau = \frac{\bar{\tau}d_1}{\mu_\infty c}, \\ h_1 &= \frac{\bar{h}_1}{d_1}, \quad h_2 = \frac{\bar{h}_2}{d_1}, \quad t = \frac{c\bar{t}}{\lambda}, \quad \theta = \frac{\bar{T} - T_a}{T_a}, \quad \sigma = \frac{\bar{C} - C_0}{C_1 - C_0}, \quad \tau_y = \frac{\bar{\tau}_y d_1}{\mu_\infty c}, \\ d &= \frac{d_2}{d_1}, \quad a = \frac{a_1}{d_1}, \quad b = \frac{b_1}{d_1}, \quad \bar{\kappa}_1 = \frac{\kappa_1}{d_1}, \quad \bar{\kappa}_2 = \frac{\kappa_2}{d_1}, \quad Pr = \frac{\mu c_p}{k}, \quad Sc = \frac{\nu}{D}, \\ Du &= \frac{Dk_T(C_1 - C_0)}{\mu c_p C_s T_a}, \quad Sr = \frac{Dk_T}{\nu(C_1 - C_0)}, \quad \gamma = \frac{k_1 d_1^2}{\nu}, \quad \gamma^* = \frac{k_1 d_1^2 C_0}{\nu(C_1 - C_0)}, \end{aligned} \quad (4.12)$$

the relevant dimensionless flow equations under long wavelength along with low Reynolds number assumptions can be expressed as

$$-\frac{\partial p}{\partial x} - \frac{\partial \tau}{\partial y} = 0, \quad (4.13)$$

$$\frac{\partial p}{\partial y} = 0, \quad (4.14)$$

$$\frac{1}{Pr} \frac{\partial^2 \theta}{\partial y^2} + Du \frac{\partial^2 \sigma}{\partial y^2} = 0, \quad (4.15)$$

$$\frac{1}{Sc} \frac{\partial^2 \sigma}{\partial y^2} + Sr \frac{\partial^2 \theta}{\partial y^2} - \gamma \sigma - \gamma^* = 0. \quad (4.16)$$

Eq. (4.14) indicates that  $p \neq p(y)$ .

The Casson's fluid constitutive equation in dimensionless form is expressed by

$$\frac{\partial u}{\partial y} = -\tau + \tau_y - 2\tau_y^{1/2} |\tau|^{1/2} \quad \text{if } h_2 \leq y \leq \kappa_1, \quad (4.17)$$

$$\frac{\partial u}{\partial y} = 0 \quad \text{if } \kappa_1 \leq y \leq \kappa_2, \quad (4.18)$$

$$\frac{\partial u}{\partial y} = -\left(\tau + \tau_y - 2\tau_y^{1/2} |\tau|^{1/2}\right) \quad \text{if } \kappa_2 \leq y \leq h_1, \quad (4.19)$$

whereas the non-dimensional form of the peristaltic walls are given by

$$y = h_1 = 1 + a \cos(2\pi x), \quad (4.20)$$

$$y = h_2 = -d - b \cos(2\pi x + \phi). \quad (4.21)$$

In fixed frame of reference, the instantaneous volume flow rate is given by

$$Q = \int_{\bar{h}_2(\bar{X}, \bar{t})}^{\bar{h}_1(\bar{X}, \bar{t})} \bar{U}(\bar{X}, \bar{Y}, \bar{t}) d\bar{Y}, \quad (4.22)$$

whereas in wave frame of reference, it is given by

$$q = \int_{h_2(\bar{x})}^{h_1(\bar{x})} \bar{u}(\bar{x}, \bar{y}) d\bar{y}. \quad (4.23)$$

From Eqs. (4.11), (4.22) and (4.23) we can write

$$Q = q + c\bar{h}_1(\bar{x}) - c\bar{h}_2(\bar{x}). \quad (4.24)$$

The time-mean flow over a period  $\Omega$  is defined as

$$\bar{Q} = \frac{1}{\Omega} \int_0^{\Omega} Q d\bar{t} = q + cd_1 + cd_2. \quad (4.25)$$

Defining  $\Theta$  and  $F$  as the dimensionless time-mean flows in the fixed and wave frames respectively by

$$\Theta = \frac{\bar{Q}}{cd_1}, \quad F = \frac{q}{cd_1}, \quad (4.26)$$

we have

$$\Theta = F + 1 + d, \quad (4.27)$$

$$F = \int_{h_2(x)}^{h_1(x)} u(y) dy. \quad (4.28)$$

Keeping in view the physical constraints of the problem, the boundary conditions in the fixed frame may be expressed mathematically as follows:

$$\bar{U}(\bar{Y} = \bar{h}_1) = 0 = \bar{U}(\bar{Y} = \bar{h}_2), \quad (4.29)$$

$$-\bar{\tau}(\bar{Y} = \bar{\kappa}_1) = \bar{\tau}_y = \bar{\tau}(\bar{Y} = \bar{\kappa}_2), \quad (4.30)$$

$$\bar{U}(\bar{Y} = \bar{\kappa}_1) = \bar{U}_p = \bar{U}(\bar{Y} = \bar{\kappa}_2), \quad (4.31)$$

$$k \frac{\partial \bar{T}}{\partial \bar{Y}} = -\eta_1(\bar{T} - T_a), \quad \bar{C} = C_1 \text{ at } \bar{Y} = \bar{h}_1, \quad (4.32)$$

$$k \frac{\partial \bar{T}}{\partial \bar{Y}} = -\eta_2(T_a - \bar{T}), \quad \bar{C} = C_0 \text{ at } \bar{Y} = \bar{h}_2. \quad (4.33)$$

Writing the above conditions through Eqs. (4.11) and (4.12), the dimensionless boundary conditions are

$$u(y = h_1) = -1 = u(y = h_2), \quad (4.34)$$

$$-\tau(y = \kappa_1) = \tau_y = \tau(y = \kappa_2), \quad (4.35)$$

$$u(y = \kappa_1) = u_p = u(y = \kappa_2), \quad (4.36)$$

$$\frac{\partial \theta}{\partial y} + Bi_1 \theta = 0, \quad \sigma = 1 \text{ at } y = h_1, \quad (4.37)$$

$$\frac{\partial \theta}{\partial y} - Bi_2 \theta = 0, \quad \sigma = 0 \text{ at } y = h_2, \quad (4.38)$$

where  $Bi_1 = \eta_1 d_1 / k$  and  $Bi_2 = \eta_2 d_1 / k$  are the Biot numbers at the upper and lower walls of channel respectively.

## 4.4 Solution methodology

The solution of Eq. (4.13) through (4.35) is given by

$$\tau = -\frac{dp}{dx}(y - \Lambda), \quad (4.39)$$

where

$$\Lambda = \left( \frac{\kappa_1 + \kappa_2}{2} \right). \quad (4.40)$$

Using Eqs. (4.35) and (4.39), we obtain

$$\frac{\kappa_2 - \kappa_1}{2} = \beta, \quad (4.41)$$

where

$$\beta = \tau_y / \left(-\frac{dp}{dx}\right) \quad (4.42)$$

represents the half width of plug flow region.

Replacing the expression for  $\tau$  from Eq. (4.39) in the constitutive equations (4.17 – 4.19) and integrating with the help of distribution in different regions as

$$u(y) = u^-(y) = -1 - \frac{dp}{dx} \left\{ (\Lambda + \beta)(y - h_2) - \frac{1}{2}(y^2 - h_2^2) + \frac{4}{3}\sqrt{\beta}[(\Lambda - y)^{3/2} - (\Lambda - h_2)^{3/2}] \right\} \quad \text{for } h_2 \leq y \leq \kappa_1, \quad (4.43)$$

$$u(y) = u_p = \text{constant} \quad \text{for } \kappa_1 \leq y \leq \kappa_2, \quad (4.44)$$

$$u(y) = u^+(y) = -1 - \frac{dp}{dx} \left\{ \frac{1}{2}(h_1^2 - y^2) + (\beta - \Lambda)(h_1 - y) - \frac{4}{3}\sqrt{\beta}[(h_1 - \Lambda)^{3/2} - (y - \Lambda)^{3/2}] \right\} \quad \text{for } \kappa_2 \leq y \leq h_1, \quad (4.45)$$

where  $u^-$  and  $u^+$  are the velocities in respective shear flow regions  $h_2 \leq y \leq \kappa_1$  and  $\kappa_2 \leq y \leq h_1$  and  $u_p$  shows the velocity in plug flow region  $\kappa_1 \leq y \leq \kappa_2$  which can be determined from Eq. (4.36). Here  $\beta \rightarrow 0$  corresponds to the Newtonian fluid and  $a = b$ ,  $d = 1$  and  $\phi = 0$ , the expression for longitudinal velocity are in good agreement with the expression obtained by Shapiro et al.[6] in symmetric channel case.

The relation for velocity profile at  $y = \kappa_1$  and  $y = \kappa_2$  after using the continuity condition (4.36) is given by

$$\begin{aligned} & -3h_1^2 + 3h_2^2 - 8\sqrt{\beta}\Lambda\sqrt{h_1 - \Lambda} + 8h_2\sqrt{\Lambda - h_2} - 8\sqrt{\beta}\Lambda\sqrt{\Lambda - h_2} \\ & -6h_2(\beta + \Lambda) + h_1(-6\beta + 8\sqrt{\beta}\sqrt{h_1 - \Lambda} + 6\Lambda) + 8\sqrt{\beta}\Lambda\sqrt{\Lambda - \kappa_1} - 8\sqrt{\beta}\kappa_1\sqrt{\Lambda - \kappa_1} \\ & + 8\sqrt{\beta}\Lambda\sqrt{\kappa_2 - \Lambda} - 8\sqrt{\beta}\kappa_2\sqrt{\kappa_2 - \Lambda} + 3((2(\beta + \Lambda) - \kappa_1)\kappa_1 + 2(\beta - \Lambda)\kappa_2 + \kappa_2^2) = 0. \end{aligned} \quad (4.46)$$

A system of equations in two unknowns  $\kappa_1$  and  $\kappa_2$  is demonstrated from relations (4.41) and (4.46). From these equations and with the help of the relation  $\Lambda = \left(\frac{\kappa_1 + \kappa_2}{2}\right)$ , we can get the values of  $\kappa_1$  and  $\kappa_2$ .

The transverse velocity component  $v$  can be calculated from the continuity equation through

$$\frac{\partial v}{\partial y} = -\frac{\partial u}{\partial x}. \quad (4.47)$$

Defining the stream function as

$$d\psi = udy - vdx, \quad (4.48)$$

and using the conditions  $\psi = \frac{F}{2}$  at  $y = h_1$  and  $\psi = -\frac{F}{2}$  at  $y = h_2$ , the stream function is obtained in the three regions as given below.

$$\begin{aligned} \psi(y) = \psi^-(y) = & -y - \frac{dp}{dx} \left\{ (\Lambda + \beta) \left( \frac{y^2}{2} - h_2 y \right) - \frac{1}{2} \left( \frac{y^3}{3} - h_2^2 y \right) \right. \\ & \left. - \frac{4}{3} \sqrt{\beta} \left[ \frac{2}{5} (\Lambda - y)^{5/2} + (\Lambda - h_2)^{3/2} y \right] \right\} + C_1 \quad \text{for } h_2 \leq y \leq \kappa_1, \end{aligned} \quad (4.49)$$

$$\psi(y) = \psi_p = u_p y + C_p \quad \text{for } \kappa_1 \leq y \leq \kappa_2, \quad (4.50)$$

$$\begin{aligned} \psi(y) = \psi^+(y) = & -y - \frac{dp}{dx} \left\{ \frac{1}{2} (h_1^2 y - \frac{y^3}{3}) + (\beta - \Lambda) (h_1 y - \frac{y^2}{2}) \right. \\ & \left. - \frac{4}{3} \sqrt{\beta} \left[ (h_1 - \Lambda)^{3/2} y - \frac{2}{5} (y - \Lambda)^{5/2} \right] \right\} + C_2 \quad \text{for } \kappa_2 \leq y \leq h_1, \end{aligned} \quad (4.51)$$

where

$$C_1 = \frac{-F}{2} + h_2 + \frac{dp}{dx} \left\{ \frac{-\Lambda h_2^2}{2} + \frac{h_2^3}{3} - \frac{\beta h_2^2}{2} - \frac{4}{15} \sqrt{\beta} (\Lambda - h_2)^{3/2} (2\Lambda + 3h_2) \right\}, \quad (4.52)$$

$$\begin{aligned} C_p = & \frac{-F}{2} + h_2 - \frac{dp}{dx} \left\{ (\Lambda + \beta) \left( \frac{h_2^2 - \kappa_1^2}{2} \right) + \frac{1}{3} (\kappa_1^3 - h_2^3) \right. \\ & \left. - \frac{4}{15} \sqrt{\beta} [(\Lambda - \kappa_1)^{3/2} (2\Lambda + 3h_2) - (\Lambda - h_2)^{3/2} (2\Lambda + 3h_2)] \right\}, \end{aligned} \quad (4.53)$$

$$C_2 = \frac{F}{2} + h_1 + \frac{dp}{dx} \left\{ \frac{h_1^3}{3} + (\beta - \Lambda) \frac{h_1^2}{2} - \frac{4}{15} \sqrt{\beta} (h_1 - \Lambda)^{3/2} (3h_1 + 2\Lambda) \right\}. \quad (4.54)$$

For symmetric channel case, the expression for  $\psi$  matches to that found by Mernone et al. [56].

As  $\beta \rightarrow 0$  (Newtonian case) we have  $\kappa_1 = \kappa_2 = \frac{h_1 + h_2}{2}$  and in this case the stream function

agrees with the expression given by Mishra and Rao [27], when  $\beta = 0$  and  $a = b$ ,  $d = 1$ ,  $\phi = 0$  (i.e. the flow of Newtonian fluid in symmetric channel case) the stream function corresponds to that of Shapiro et al. [6].

The pressure gradient is obtained by using Eq. (4.28) as follows:

$$\frac{dp}{dx} = -\frac{(F + h_1 - h_2)}{g(x)}, \quad (4.55)$$

where

$$\begin{aligned} g(x) = & \frac{1}{3}(h_1^3 - h_2^3 + \kappa_1^3 - \kappa_2^3) + \frac{\Lambda}{2}(h_2^2 - h_1^2 + \kappa_2^2 - \kappa_1^2) + \frac{\beta}{2}(h_1^2 + h_2^2 - \kappa_1^2 - \kappa_2^2) \\ & - \frac{4}{15}\sqrt{\beta}[(\Lambda - \kappa_1)^{3/2}(2\Lambda + 3\kappa_1) - (\Lambda - h_2)^{3/2}(2\Lambda + 3h_2) \\ & + (h_1 - \Lambda)^{3/2}(3h_1 + 2\Lambda) - (\kappa_2 - \Lambda)^{3/2}(2\Lambda + 3\kappa_2)]. \end{aligned} \quad (4.56)$$

The pressure rise per wavelength ( $\Delta P_\lambda$ ) is

$$\Delta P_\lambda = \int_0^\lambda \frac{dp}{dx} dx. \quad (4.57)$$

The solutions of Eqs. (4.15) and (4.16) corresponding to boundary conditions (4.37) and (4.38) are given by

$$\begin{aligned} \theta(y) = & \frac{1}{(A_2 A_4 \gamma)} [Du \Pr \csc h A_3 \{ \gamma (A_1 (-1 + Bi_1(y - h_2)) + A_1 (1 + Bi_2(y - h_2)) \cosh A_3 \\ & + A_2 (Bi_1(1 + Bi_2(y - h_2)) \sinh A_3 + A_4 \sinh(\frac{(h_2 - y)A_1}{A_2}))) \\ & + (A_1 (-2 + Bi_1(y - h_1) - Bi_2(y - h_2)) + A_1 (2 - Bi_1(y - h_1) + Bi_2(y - h_2)) \cosh A_3 \\ & + A_2 A_4 (\sinh A_3 - \sinh(\frac{(h_1 - y)A_1}{A_2}) + \sinh(\frac{(h_2 - y)A_1}{A_2}))) \gamma^* \}], \end{aligned} \quad (4.58)$$

$$\begin{aligned} \sigma(y) = & -\frac{1}{\gamma} [\csc h A_3 \{ \gamma \sinh(\frac{(h_2 - y)A_1}{A_2}) \\ & + (\sinh A_3 - \sinh(\frac{(h_1 - y)A_1}{A_2}) + \sinh(\frac{(h_2 - y)A_1}{A_2})) \gamma^* \}], \end{aligned} \quad (4.59)$$

where

$$\begin{aligned} A_1 &= \sqrt{\gamma Sc}, \quad A_2 = \sqrt{1 - Du \Pr Sc Sr}, \\ A_3 &= \frac{(h_1 - h_2)A_1}{A_2}, \quad A_4 = Bi_1 + Bi_2 + Bi_1 Bi_2 (h_1 - h_2). \end{aligned}$$

## 4.5 Discussion

### 4.5.1 Yield plane locations

The solid-like behavior of the fluid (i.e. a plug core) is perceived under the yield stress effects in a region in which the yield stress is greater than the magnitude of shear stress. A yield point is defined as a point where the yield value is equal to the magnitude of actual shear stress and yield plane is the locus of all yield points. The positions of two yield planes are deliberated from the perspective of asymmetry of channel walls. The width of core region is determined by these two yield planes. It is interpreted from Eq. (4.42) that the width  $2\beta$  of the plug flow region is dependent on shear stress  $\tau_y$ . However the pressure gradient does not depend on the channel asymmetry. Location of the first yield plane  $\kappa_1$  with inflicted phase angle  $\phi$  on the lower channel wall is shown in Table 4.1. By using the relation (4.41) and Table 4.1, the location for second yield plane  $\kappa_2$  can be computed. It is remarkable that the yield plane ( $\lambda_1$ ) moves in the direction near to upper channel wall as  $\phi$  increases for fixed value of  $\tau_y$  and the width of plug region increases with an increase in  $\tau_y$ . We can see that these results are in an excellent agreement with the results obtained by Rani and Sarojamma [58].



$\phi$	$\tau_y$					
	0.0	0.05	0.1	0.15	2.0	2.5
0	0.000	-0.05	-0.100	-0.150	-2.00	-0.250
$\pi/6$	0.033	-0.016	-0.066	-0.116	-0.166	-0.216
$\pi/3$	0.125	0.075	0.025	-0.025	-0.075	-0.125
$\pi/2$	0.250	0.200	0.150	0.100	0.050	0.000
$2\pi/3$	0.376	0.325	0.275	0.225	0.175	0.125
$5\pi/6$	0.466	0.416	0.366	0.316	0.266	0.216
$\pi$	0.500	0.450	0.4	0.350	0.300	0.250

**Table 4.1.** Variation in yield plane location  $\kappa_1$  with  $\phi$  when the amplitudes are same ( $a = b = 0.5$ ,  $d = 1$ ) for various values of  $\tau_y$ .

#### 4.5.2 Pumping characteristics

In this subsection our aim is to analyze the pressure gradient  $dp/dx$  and pressure rise per wavelength  $\Delta p_\lambda$  for different embedding parameters in the present problem. Fig. 4.1 is plotted to serve the effects of Casson fluid parameter  $\beta$  on pressure gradient  $dp/dx$ . It is anticipated that the pressure gradient increases at the center of the channel while it decreases near the walls with an increase in Casson fluid parameter  $\beta$ . It is interesting to note that the assistance or resistance from pressure gradient for a Casson fluid ( $\beta \neq 0$ ) is higher when compared to a Newtonian fluid ( $\beta = 0$ ). Fig. 4.2 depicts the variation in pressure gradient  $dp/dx$  for different values of phase difference  $\phi$ . We observe that by increasing the values of the phase difference  $\phi$  the pressure gradient  $dp/dx$  decreases. The effects of various values of flow rate  $\Theta$  on pressure gradient  $dp/dx$  are shown in Fig. 4.3. It is observed that pressure gradient increases when flow rate  $\Theta$  increases. Fig. 4.4 shows the variation in pressure rise per wavelength  $\Delta p_\lambda$  against flow rate  $\Theta$  for various values of Casson fluid parameter  $\beta$ . For such purpose, the numerical integration has been carried out in Eq. (4.57) using "MATHEMATICA". It is seen that by increasing the value of  $\beta$  the pressure rise increases in the peristaltic pumping region and it decreases in the copumping region when  $\beta$  is increased. This means peristalsis works against greater pressure rise for a Casson fluid ( $\beta \neq 0$ ) when compared to a Newtonian fluid ( $\beta = 0$ ). The opposite behavior is observed for different values of phase difference  $\phi$  in Fig. 4.5. That

is pressure rise per wavelength  $\Delta p_\lambda$  decreases in peristaltic pumping region and it increases in copumping region when phase difference  $\phi$  is increased. Figs. 4.6 and 4.7 are plotted to see the effects of upper and lower wave amplitudes  $a$  and  $b$  on pressure rise per wavelength  $\Delta p_\lambda$  respectively. These Figs. show that pressure rise increases in the peristaltic pumping region with an increase in upper wave amplitude  $a$  as well as lower wave amplitude  $b$ . However it has opposite behavior in the copumping region.

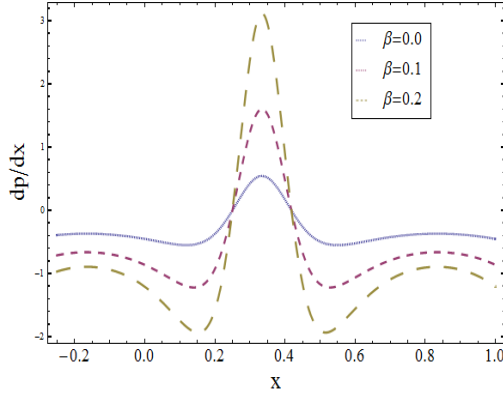


Fig. 4.1

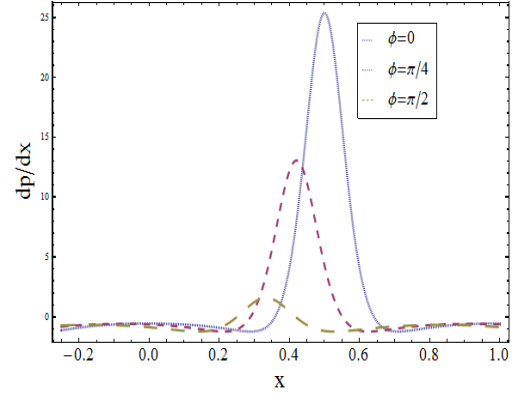


Fig. 4.2

Fig. 4.1: Variation in  $dp/dx$  for  $\beta$  when  $a = 0.7$ ,  $b = 1.2$ ,  $d = 2$ ,  $\phi = \pi/2$ ,  $\Theta = 1.2$ .

Fig. 4.2: Variation in  $dp/dx$  for  $\phi$  when  $a = 0.7$ ,  $b = 1.2$ ,  $d = 2$ ,  $\beta = 0.1$ ,  $\Theta = 1.2$ .

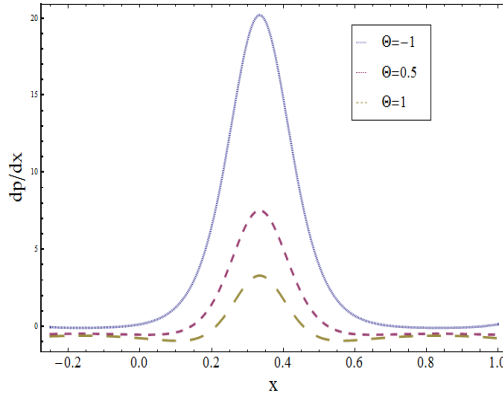


Fig. 4.3

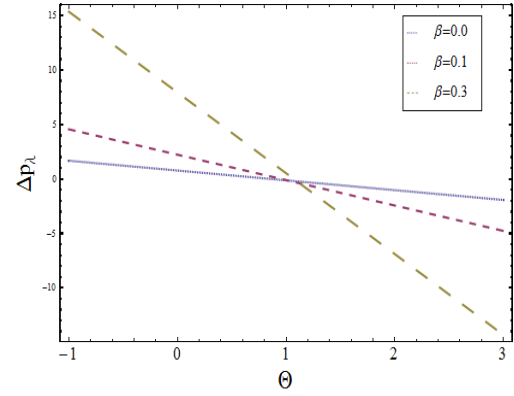


Fig. 4.4

Fig. 4.3: Variation in  $dp/dx$  for  $\Theta$  when  $a = 0.7$ ,  $b = 1.2$ ,  $d = 2$ ,  $\phi = \pi/2$ ,  $\beta = 0.2$ .

Fig. 4.4: Variation in  $\Delta p_\lambda$  versus  $\Theta$  for  $\beta$  when  $a = 0.7$ ,  $b = 1.2$ ,  $d = 2$ ,  $\phi = \pi/2$ .

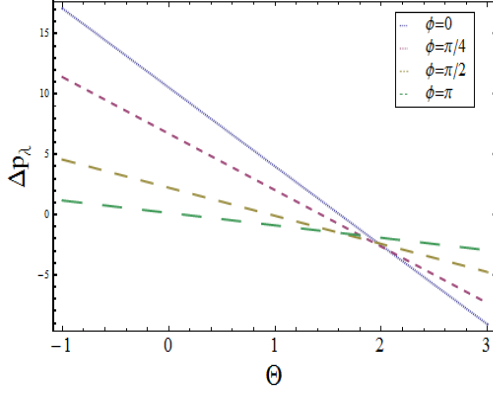


Fig. 4.5

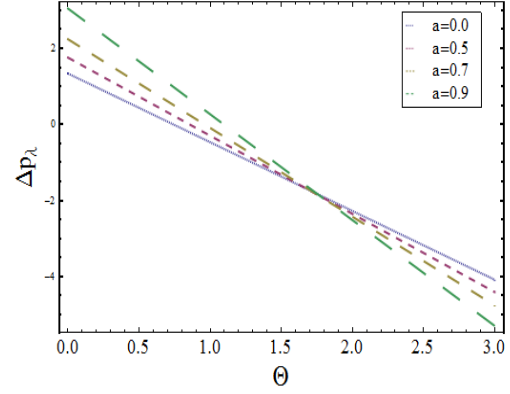


Fig. 4.6

Fig. 4.5: Variation in  $\Delta p_\lambda$  versus  $\Theta$  for  $\phi$  when  $a = 0.7$ ,  $b = 1.2$ ,  $d = 2$ ,  $\beta = 0.1$ .

Fig. 4.6: Variation in  $\Delta p_\lambda$  versus  $\Theta$  for  $a$  when  $b = 1.2$ ,  $d = 2$ ,  $\phi = \pi/2$ ,  $\beta = 0.1$ .

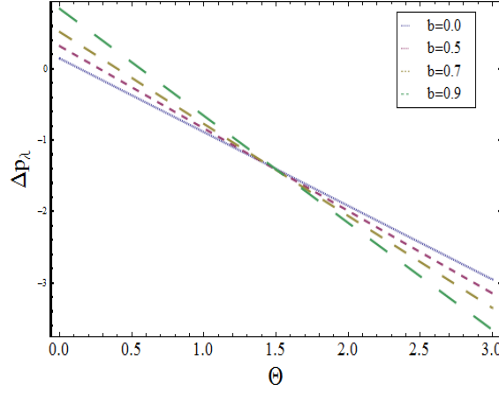


Fig. 4.7

Fig. 4.7: Variation in  $\Delta p_\lambda$  versus  $\Theta$  for  $b$  when  $a = 0.5$ ,  $d = 2$ ,  $\phi = \pi/2$ ,  $\beta = 0.1$ .

### 4.5.3 Velocity distribution

The variations of axial velocity in symmetric ( $a = b = 0.5$ ,  $d = 1$ ,  $\phi = 0$ ) and asymmetric ( $a = 0.5$ ,  $b = 1.2$ ,  $d = 1.2$ ,  $\phi = \pi/4$ ) channels are shown in the Figs. 4.8 (a) and 4.8 (b) respectively. The velocity in a symmetric channel is seen to be symmetric while the profiles are skewed towards lower boundary in an asymmetric channel. Also it is noticed that the

magnitude of the velocity reduces as yield stress is increased and plug flow dominates over the cross-section.

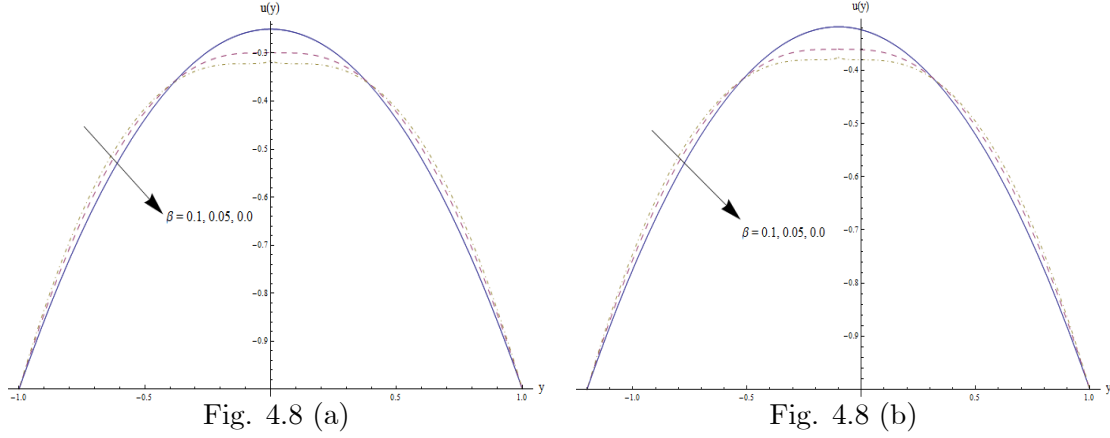


Fig. 4.8 (a): Longitudinal velocity  $u(y)$  for  $\beta$  when  $a = 0.5$ ,  $b = 0.5$ ,  $d = 1$ ,  $\phi = 0$ ,  $x = 0.25$  and  $\Theta = 1$ .

Fig. 4.8 (b): Longitudinal velocity  $u(y)$  for  $\beta$  when  $a = 0.5$ ,  $b = 1.2$ ,  $d = 1.2$ ,  $\phi = 0$ ,  $x = 0.25$  and  $\Theta = 1$ .

#### 4.5.4 Temperature profile

This subsection deals with the effects of various emerging parameters on temperature field  $\theta(y)$ . It is noteworthy that the temperature profile  $\theta(y)$  increases when there is an increase in the Prandtl Pr and Schmidt numbers  $Sc$  (see Figs. 4.9 and 4.10). Effects of chemical reaction parameter  $\gamma$  on temperature profile  $\theta(y)$  are shown in Fig. 4.11. It is observed that by increasing the chemical reaction parameter  $\gamma$  the temperature profile increases. Here we have considered  $\gamma > 0$  which represents the destructive chemical reaction process. In Figs. 4.12 and 4.13, the effects of the Biot numbers  $Bi_1$  and  $Bi_2$  on temperature profile  $\theta(y)$  are observed. We see that by increasing the values of  $Bi_1$  the temperature decreases near the upper wall while it has no significant effect near the lower wall of channel. Also temperature decreases near the lower wall of the channel when there is an increase in  $Bi_2$  while it has no effect near the upper wall of channel. Here we have considered the non-uniform temperature fields within the fluid (i.e., Biot numbers are much greater than 1) because problems involving small Biot numbers are thermally

simple due to the uniform temperature fields within the material. Effects of Soret and Dufour on temperature profile  $\theta(y)$  are depicted in Figs. 4.14 and 4.15. We illustrate that by increasing the value of Soret number  $Sr$  the temperature profile gradually decreases (see Fig. 4.14) while it increases with an increase in Dufour number  $Du$  (see Fig. 4.15). Physically we can observe that the diffusion-thermo or Dufour effect describes the heat flux created when a chemical system is under a concentration gradient. These effects depend upon thermal diffusion which is generally very small but can be sometimes significant when the participating species are of widely differing molecular weights. Mass diffusion occurs if the species are initially distributed unevenly i.e., when a concentration gradient exists. A temperature gradient can also work as a driving force for mass diffusion called thermo-diffusion or Soret effects. Therefore the higher the temperature gradient, the larger the Soret effects.

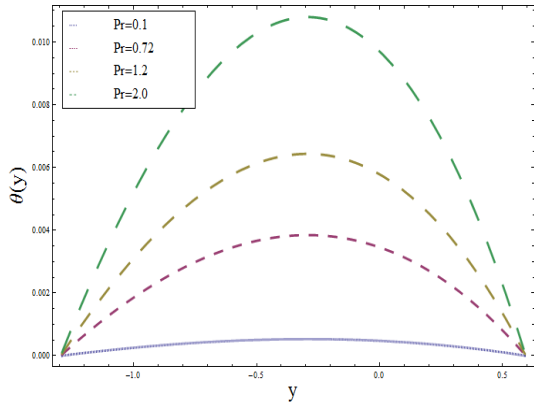


Fig. 4.9

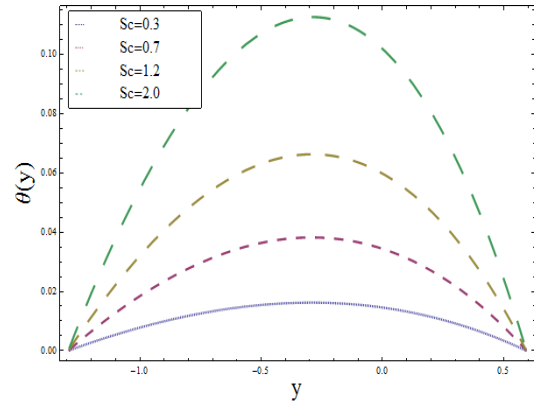


Fig. 4.10

Fig. 4.9: Temperature profile  $\theta(y)$  for various values of  $Pr$  when  $a = 0.5$ ,  $b = 0.7$ ,  $d = 1.2$ ,

$$\phi = \pi/2, \Theta = 1.2, x = -0.5, Bi_1 = 8, Bi_2 = 10, Sc = Sr = Du = \gamma = 0.2.$$

Fig. 4.10: Temperature profile  $\theta(y)$  for various values of  $Sc$  when  $a = 0.5$ ,  $b = 0.7$ ,  $d = 1.2$ ,

$$\phi = \pi/2, \Theta = 1.2, x = -0.5, Bi_1 = 8, Bi_2 = 10, Pr = 2.0, Sr = Du = \gamma = 0.2.$$

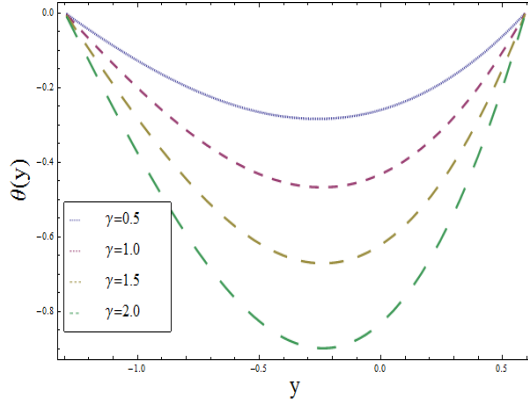


Fig. 4.11

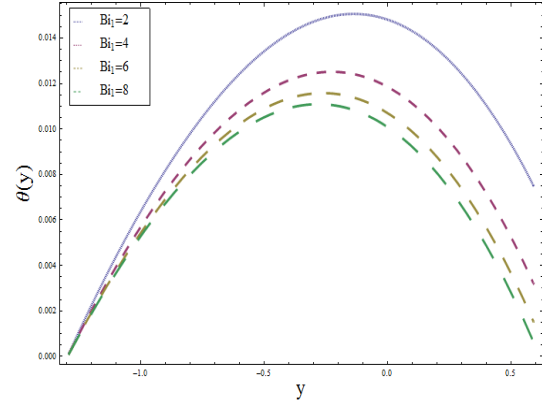


Fig. 4.12

Fig. 4.11: Temperature profile  $\theta(y)$  for various values of  $\gamma$  when  $a = 0.5$ ,  $b = 0.7$ ,  $d = 1.2$ ,  $\phi = \pi/2$ ,  $\Theta = 1.2$ ,  $x = -0.5$ ,  $Bi_1 = 8$ ,  $Bi_2 = 10$ ,  $Pr = 2.0$ ,  $Sc = Sr = Du = \gamma = 0.2$ .

Fig. 4.12: Temperature profile  $\theta(y)$  for various values of  $Bi_1$  when  $a = 0.5$ ,  $b = 0.7$ ,  $d = 1.2$ ,  $\phi = \pi/2$ ,  $\Theta = 1.2$ ,  $x = -0.5$ ,  $Bi_2 = 10$ ,  $Pr = 2.0$ ,  $Sc = Sr = Du = \gamma = 0.2$ .

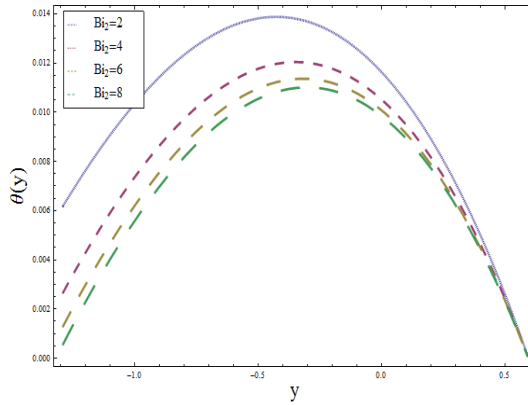


Fig. 4.13

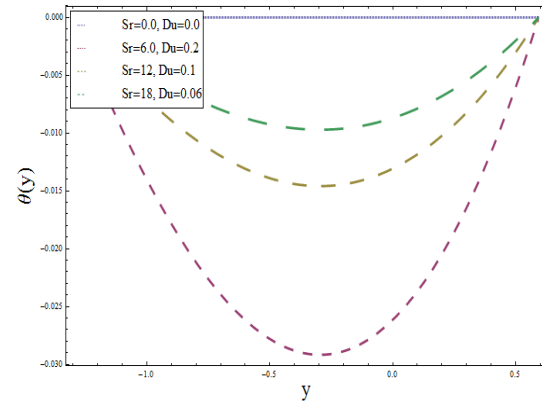


Fig. 4.14

Fig. 4.13: Temperature profile  $\theta(y)$  for various values of  $Bi_2$  when  $a = 0.5$ ,  $b = 0.7$ ,  $d = 1.2$ ,  $\phi = \pi/2$ ,  $\Theta = 1.2$ ,  $x = -0.5$ ,  $Bi_1 = 10$ ,  $Pr = 2.0$ ,  $Sc = Sr = Du = \gamma = 0.2$ .

Fig. 4.14: Temperature profile  $\theta(y)$  for various values of  $Sr$  when  $a = 0.5$ ,  $b = 0.7$ ,  $d = 1.2$ ,  $\phi = \pi/2$ ,  $\Theta = 1.2$ ,  $x = -0.5$ ,  $Bi_1 = 8$ ,  $Bi_2 = 10$ ,  $Pr = 2.0$ ,  $Sc = Du = \gamma = 0.2$ .

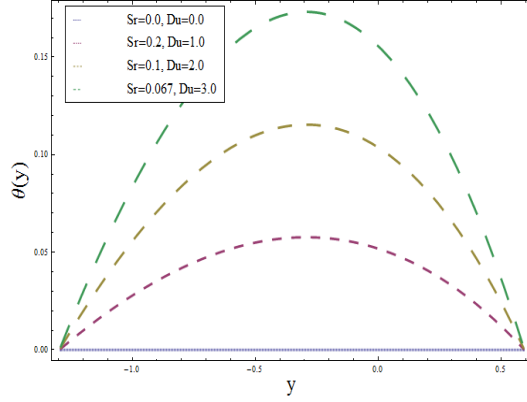


Fig. 4.15

Fig. 4.15: Temperature profile  $\theta(y)$  for various values of  $Du$  when  $a = 0.5$ ,  $b = 0.7$ ,  $d = 1.2$ ,

$\phi = \pi/2$ ,  $\Theta = 1.2$ ,  $x = -0.5$ ,  $Bi_1 = 8$ ,  $Bi_2 = 10$ ,  $Pr = 2.0$ ,  $Sc = Sr = \gamma = 0.2$ .

#### 4.5.5 Concentration profile

This subsection deals with the variation in the concentration profile  $\sigma(y)$  for different values of embedding parameters in the problem. Here it is noted that by increasing the values of Prandtl number  $Pr$ , chemical reaction parameter  $\gamma$ , Soret  $Sr$  and Dufour  $Du$  numbers and Schmidt number  $Sc$  concentration profile  $\sigma(y)$  decreases (see Figs. 4.16-4.20). Schmidt number  $Sc$  is a dimensionless number defined as the ratio of momentum diffusivity (viscosity) and mass diffusivity and it is used to characterize fluid flows in which there are simultaneous momentum and mass diffusion convection processes. The effect of chemical reaction parameter  $\gamma$  is very important in concentration field  $\sigma(y)$ . Chemical reaction increases the rate of interfacial mass transfer. Reaction reduces the local concentration, thus increases its concentration gradient and its flux when we have constructive chemical reaction. In our problem we have considered  $\gamma > 0$  which corresponds to the destructive chemical reaction.

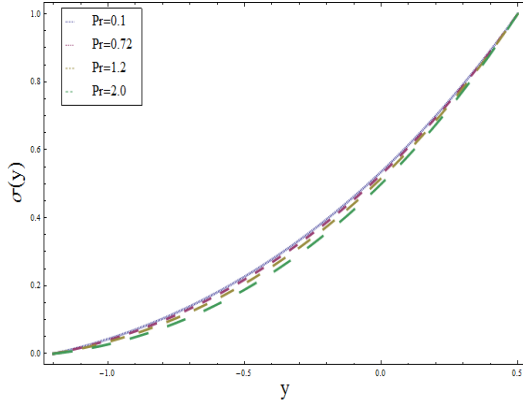


Fig. 4.16

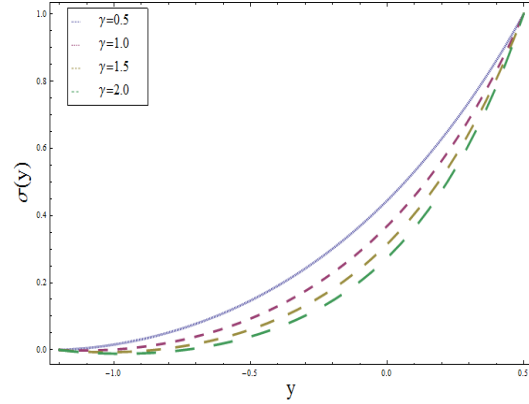


Fig. 4.17

Fig. 4.16: Concentration profile  $\sigma(y)$  for various values of  $Pr$  when  $a = 0.5$ ,  $b = 0.7$ ,  $d = 1.2$ ,  $\phi = \pi/2$ ,  $\Theta = 1.2$ ,  $x = -0.5$ ,  $Sc = 2.0$ ,  $Sr = Du = \gamma = 0.2$ .

Fig. 4.17: Concentration profile  $\sigma(y)$  for various values of  $\gamma$  when  $a = 0.5$ ,  $b = 0.7$ ,  $d = 1.2$ ,  $\phi = \pi/2$ ,  $\Theta = 1.2$ ,  $x = -0.5$ ,  $Pr = Sc = 2.0$ ,  $Sr = Du = 0.2$ .

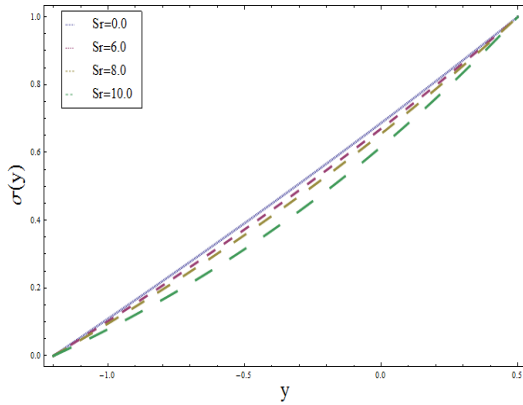


Fig. 4.18

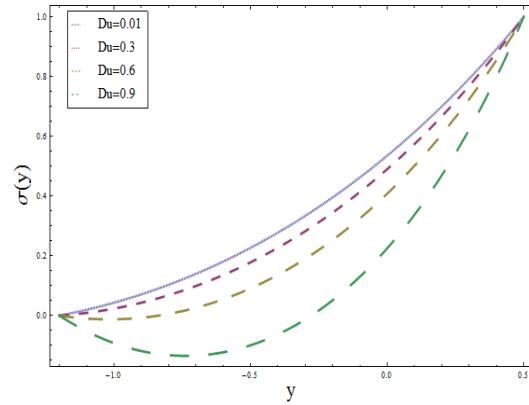


Fig. 4.19

Fig. 4.18: Concentration profile  $\sigma(y)$  for various values of  $Sr$  when  $a = 0.5$ ,  $b = 0.7$ ,  $d = 1.2$ ,  $\phi = \pi/2$ ,  $\Theta = 1.2$ ,  $x = -0.5$ ,  $Pr = Sc = 2.0$ ,  $\gamma = Du = 0.2$ .

Fig. 4.19: Concentration profile  $\sigma(y)$  for various values of  $Du$  when  $a = 0.5$ ,  $b = 0.7$ ,  $d = 1.2$ ,  $\phi = \pi/2$ ,  $\Theta = 1.2$ ,  $x = -0.5$ ,  $Pr = Sc = 2.0$ ,  $\gamma = Sr = 0.2$ .



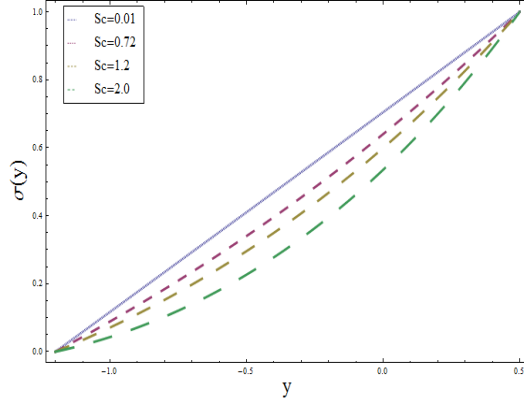


Fig. 4.20

Fig. 4.20: Concentration profile  $\sigma(y)$  for various values of  $Sc$  when  $a = 0.5$ ,  $b = 0.7$ ,  $d = 1.2$ ,

$$\phi = \pi/2, \Theta = 1.2, x = -0.5, \text{Pr} = 2.0, \gamma = \text{Sr} = \text{Du} = 0.2.$$

#### 4.5.6 Streamlines and trapping

The shape of the streamlines is generally the same as that of the walls in the wave frame of reference. However some of the streamlines split and enclose a bolus under certain conditions which moves as a whole with the wave. This is known as trapping. Figs. 4.21 and 4.22 are sketched to see the effects of Casson fluid parameter  $\beta$  and volume flow rate  $\Theta$  on trapping. The panels on left side show the trapping phenomenon for the case of symmetric channel ( $a = b = 0.5$ ,  $d = 1$ ,  $\phi = 0$ ) and the panels on right side show the trapping for the case of asymmetric channel ( $a = 0.5$ ,  $b = 0.7$ ,  $d = 1.2$ ,  $\phi = \pi/4$ ). From Fig. 4.21 it is revealed that trapped bolus exists and decreases in size when there is an increase in the Casson fluid parameter  $\beta$ . In this Fig.  $\beta = 0.0$  (panels (a) and (b)),  $\beta = 0.2$  (panels (c) and (d)) and  $\beta = 0.3$  (panels (e) and (f)). Fig. 4.22 shows that the trapped bolus increases by increasing the value of volume flow rate  $\Theta$ . For this Fig.  $\Theta = 1.2$  (panels (a) and (b)),  $\Theta = 1.5$  (panels (c) and (d)) and  $\Theta = 1.7$  (panels (e) and (f)). A comparative study of these panels reveals that the trapped bolus is symmetric with respect to the channel for  $\phi = 0$  (left panel). On the other hand for  $\phi = \pi/4$  the trapped bolus shifts towards left (lower wall) because of the asymmetry of channel (right panel).

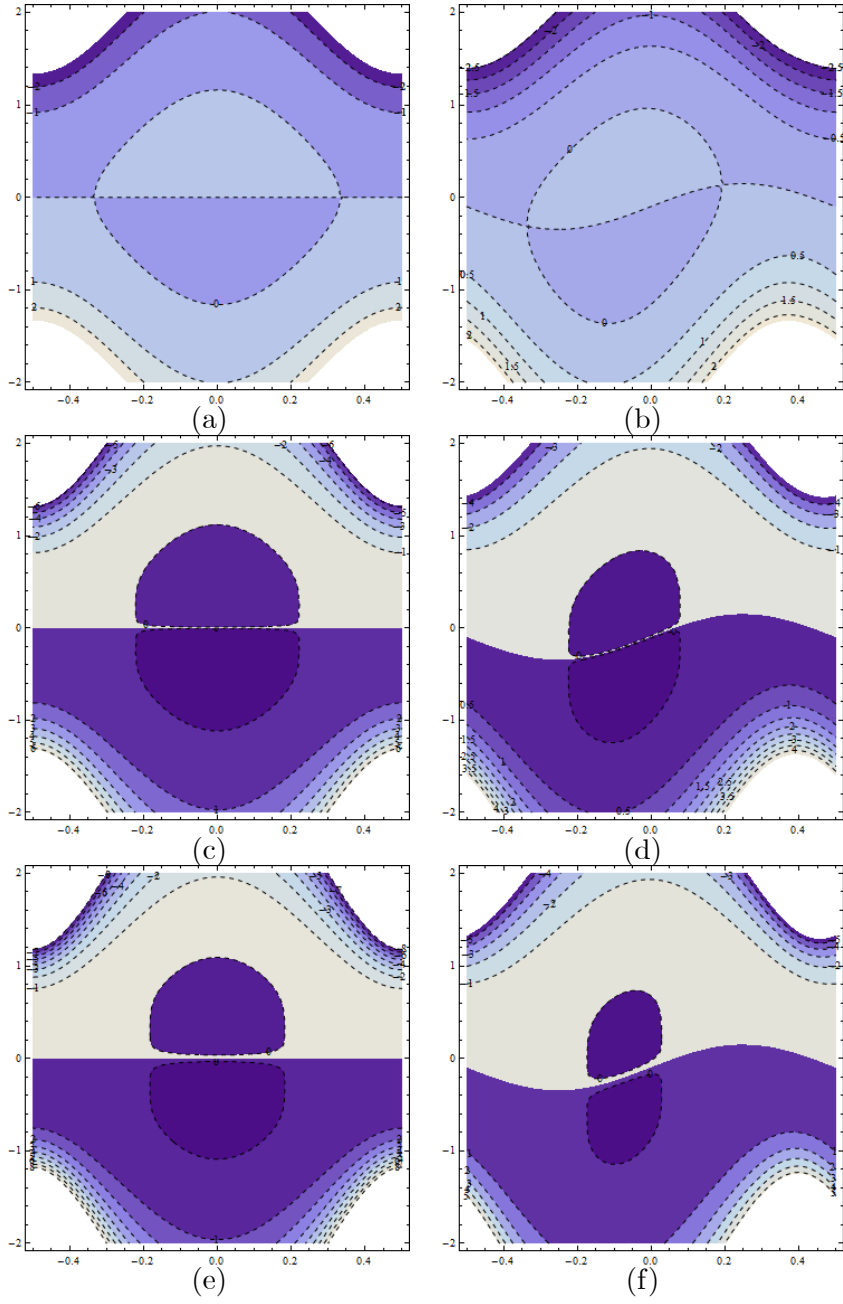


Fig. 4.21: Streamlines for different values of  $\beta$  (panels (a), (c) and (e) for  $\phi = 0$  and panels (b), (d) and (f) for  $\phi = \pi/4$ ).

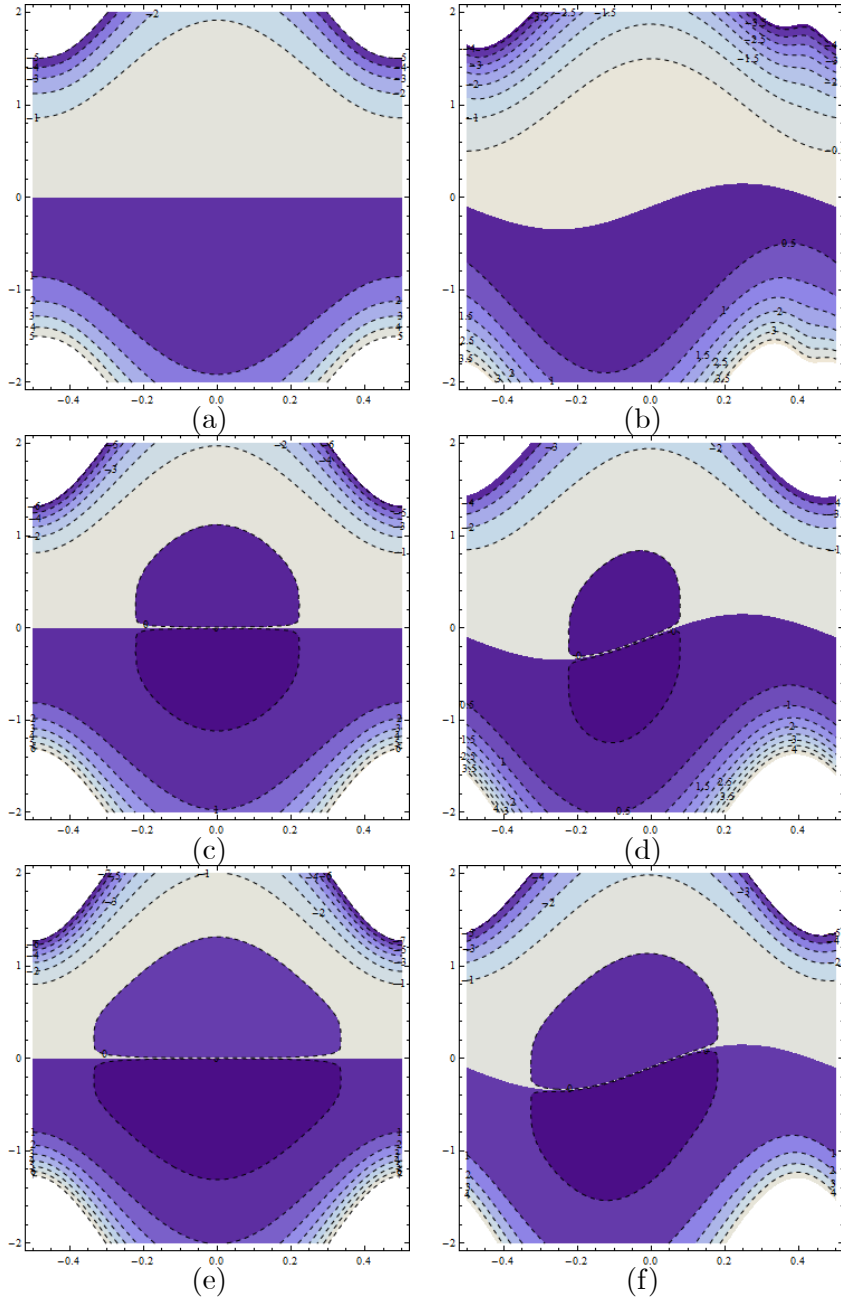


Fig. 4.22: Streamlines for different values of  $\Theta$  (panels (a), (c) and (e) for  $\phi = 0$  and panels (b), (d) and (f) for  $\phi = \pi/4$ ).

## 4.6 Conclusions

This chapter addresses the Soret and Dufour effects in Casson fluid flow in an asymmetric channel with peristalsis and convective conditions. The presented study leads to the following observations:

- Due to asymmetry in the channel, the yield stress  $\tau_y$  of the fluid tends to form two yield planes in the plug core region. The yield planes are found to be located symmetrically when channel is symmetric and they are skewed towards the boundary wall with higher amplitude (or phase difference) in an asymmetric channel.
- The magnitude of the pressure gradient  $dp/dx$  increases by increasing the values of Casson fluid parameter ( $\beta$ ). Also assistance or resistance from pressure gradient for a Casson fluid ( $\beta \neq 0$ ) is higher than that of a Newtonian fluid ( $\beta = 0$ ).
- Pressure rise per wavelength  $\Delta p_\lambda$  increases in peristaltic pumping region and it decreases in copumping region when there is an increase in the Casson fluid parameter ( $\beta$ ).
- By increasing the values of Casson fluid parameter  $\beta$  the magnitude of velocity increases at the center of the channel and it decreases near the channel walls. The velocity in a symmetric channel ( $\phi = 0$ ) is seen to be symmetric while the profiles are skewed towards lower boundary in an asymmetric channel ( $\phi = \pi/4$ ).
- The magnitude of the velocity  $u(y)$  lessens and plug flow dominates over the cross-section when  $\beta$  increases.
- By increasing the values of Prandtl ( $Pr$ ), Schmidt ( $Sc$ ) and Soret ( $Sr$ ) numbers, temperature profile  $\theta(y)$  increases. On the other hand temperature profile  $\theta(y)$  decreases when Biot numbers ( $Bi_1, Bi_2$ ), chemical reaction parameter ( $\gamma$ ) and Dufour number ( $Du$ ) are increased.
- Concentration profile  $\sigma(y)$  is a decreasing function of Prandtl ( $Pr$ ), Soret ( $Sr$ ), Dufour ( $Du$ ), Schmidt ( $Sc$ ) and chemical reaction ( $\gamma$ ) parameters.
- Trapping decreases with an increase in Casson fluid parameter  $\beta$  while it increases by increasing the volume flow rate  $\Theta$ .

## Chapter 5

# Exact solution for peristaltic flow of couple stress fluid in an asymmetric channel with convective conditions

### 5.1 Introduction

This chapter explores the heat transfer effects in peristaltic flow of couple stress fluid. An incompressible fluid is considered in a channel with convective boundary conditions. This study is motivated towards investigating the physiological flow through particle size effect. Long wavelength and low Reynolds number approach is adopted. Effects of various physical parameters reflecting couple stress parameter and Brinkman and Biot numbers on the velocity profile, streamlines pattern, temperature profile, pumping action and trapping are studied. Computational results are presented in graphical form.

### 5.2 Mathematical modeling and analysis

Let us consider the peristaltic motion of couple stress fluid in an asymmetric channel. We take  $(\bar{X}, \bar{Y})$  as the Cartesian coordinates with  $\bar{X}$  being measured in the direction of wave propagation and  $\bar{Y}$  in the direction normal to the  $\bar{X}$ -axis. Let  $\bar{Y} = \bar{h}_1$  and  $\bar{Y} = \bar{h}_2$  be the upper and lower boundaries of the channel respectively (see Fig. 2.1). The motion is induced by sinusoidal wave

trains propagating with a constant speed  $c$  along the channel walls. These are

$$\begin{aligned}\bar{h}_1(\bar{X}, \bar{t}) &= d_1 + a_1 \cos \left[ \frac{2\pi}{\lambda} (\bar{X} - c\bar{t}) \right], & \text{upper wall,} \\ \bar{h}_2(\bar{X}, \bar{t}) &= -d_2 - a_2 \cos \left[ \frac{2\pi}{\lambda} (\bar{X} - c\bar{t}) + \phi \right], & \text{lower wall,}\end{aligned}\quad (5.1)$$

where  $a_1, a_2$  are the waves amplitudes,  $\lambda$  is the wavelength,  $d_1 + d_2$  is the width of the asymmetric channel and the phase difference  $\phi$  varies in the range  $0 \leq \phi \leq \pi$  ( $\phi = 0$  corresponds to symmetric channel with waves out of phase and  $\phi = \pi$  the waves are in phase). Further  $a_1, a_2, d_1, d_2$  and  $\phi$  satisfy the condition

$$a_1^2 + a_2^2 + 2a_1a_2 \cos \phi \leq (d_1 + d_2)^2. \quad (5.2)$$

The relevant equations in the absence of body moment and body couple can be put as follows:

$$\frac{\partial \bar{U}}{\partial \bar{X}} + \frac{\partial \bar{V}}{\partial \bar{Y}} = 0, \quad (5.3)$$

$$\rho \left( \frac{\partial}{\partial \bar{t}} + \bar{U} \frac{\partial}{\partial \bar{X}} + \bar{V} \frac{\partial}{\partial \bar{Y}} \right) \bar{U} = -\frac{\partial \bar{P}}{\partial \bar{X}} + \mu \nabla_1^2 \bar{U} - \eta^* \nabla_1^4 \bar{U}, \quad (5.4)$$

$$\rho \left( \frac{\partial}{\partial \bar{t}} + \bar{U} \frac{\partial}{\partial \bar{X}} + \bar{V} \frac{\partial}{\partial \bar{Y}} \right) \bar{V} = -\frac{\partial \bar{P}}{\partial \bar{Y}} + \mu \nabla_1^2 \bar{V} - \eta^* \nabla_1^4 \bar{V}, \quad (5.5)$$

$$\begin{aligned}\rho c_p \left( \frac{\partial}{\partial \bar{t}} + \bar{U} \frac{\partial}{\partial \bar{X}} + \bar{V} \frac{\partial}{\partial \bar{Y}} \right) T &= k \nabla_1^2 T + \mu \left[ 2 \left( \frac{\partial \bar{U}}{\partial \bar{X}} \right)^2 + 2 \left( \frac{\partial \bar{V}}{\partial \bar{Y}} \right)^2 + \left( \frac{\partial \bar{U}}{\partial \bar{Y}} + \frac{\partial \bar{V}}{\partial \bar{X}} \right)^2 \right] \\ &+ \eta^* \left[ \left( \frac{\partial^2 \bar{V}}{\partial \bar{X}^2} + \frac{\partial^2 \bar{V}}{\partial \bar{Y}^2} \right)^2 + \left( \frac{\partial^2 \bar{U}}{\partial \bar{X}^2} + \frac{\partial^2 \bar{U}}{\partial \bar{Y}^2} \right)^2 \right],\end{aligned} \quad (5.6)$$

where  $\rho$  is the fluid density,  $\bar{t}$  the time,  $\bar{U}$  and  $\bar{V}$  are the velocity components,  $\mu$  the dynamic viscosity,  $\bar{P}$  the pressure,  $\eta^*$  the couple stress parameter,  $T$  the fluid temperature,  $c_p$  the specific heat,  $k$  the thermal conductivity of the material,  $\nabla_1^2 = \left( \frac{\partial^2}{\partial \bar{X}^2} + \frac{\partial^2}{\partial \bar{Y}^2} \right)$  and  $\nabla_1^4 = \nabla_1^2 \nabla_1^2$ . Note that the overbar just refers to a dimensional quantity.

Considering a wave frame  $(\bar{x}, \bar{y})$  that moves with a velocity  $c$  away from the fixed frame

$(\bar{X}, \bar{Y})$ , we write

$$\begin{aligned}\bar{x} &= \bar{X} - c\bar{t}, \quad \bar{y} = \bar{Y}, \quad \bar{u}(\bar{x}, \bar{y}) = \bar{U}(\bar{X}, \bar{Y}, \bar{t}) - c, \\ \bar{v}(\bar{x}, \bar{y}) &= \bar{V}(\bar{X}, \bar{Y}, \bar{t}), \quad T(\bar{x}, \bar{y}) = T(\bar{X}, \bar{Y}, \bar{t}), \quad \bar{p}(\bar{x}, \bar{y}) = \bar{P}(\bar{X}, \bar{Y}, \bar{t}),\end{aligned}\tag{5.7}$$

in which  $(\bar{u}, \bar{v})$  and  $(\bar{U}, \bar{V})$  are the velocity components in the wave and the fixed frames respectively,  $p$  and  $P$  denote the pressure in wave and fixed frames of reference.

The exchange of heat with ambient at the walls through Newton's cooling law is given by

$$k \frac{\partial T}{\partial \bar{y}} = -\eta_1(T - T_a) \quad \text{at} \quad \bar{y} = \bar{h}_1,\tag{5.8}$$

$$k \frac{\partial T}{\partial \bar{y}} = -\eta_2(T_a - T) \quad \text{at} \quad \bar{y} = \bar{h}_2,\tag{5.9}$$

where  $\eta_1$  ( $\eta_2$ ) is the heat transfer coefficient at the upper (lower) channel wall and  $T_a$  is the ambient temperature.

The relevant flow equations can be expressed as follows

$$\frac{\partial \bar{u}}{\partial \bar{x}} + \frac{\partial \bar{v}}{\partial \bar{y}} = 0,\tag{5.10}$$

$$\rho \left( \bar{u} \frac{\partial}{\partial \bar{x}} + \bar{v} \frac{\partial}{\partial \bar{y}} \right) \bar{u} = -\frac{\partial \bar{p}}{\partial \bar{x}} + \mu \nabla^2 \bar{u} - \eta^* \nabla^4 \bar{u},\tag{5.11}$$

$$\rho \left( \bar{u} \frac{\partial}{\partial \bar{x}} + \bar{v} \frac{\partial}{\partial \bar{y}} \right) \bar{v} = -\frac{\partial \bar{p}}{\partial \bar{y}} + \mu \nabla^2 \bar{v} - \eta^* \nabla^4 \bar{v},\tag{5.12}$$

$$\begin{aligned}\rho c_p \left( \bar{u} \frac{\partial}{\partial \bar{x}} + \bar{v} \frac{\partial}{\partial \bar{y}} \right) T &= k \nabla^2 T + \mu \left[ 2 \left( \frac{\partial \bar{u}}{\partial \bar{x}} \right)^2 + 2 \left( \frac{\partial \bar{v}}{\partial \bar{y}} \right)^2 + \left( \frac{\partial \bar{u}}{\partial \bar{y}} + \frac{\partial \bar{v}}{\partial \bar{x}} \right)^2 \right] \\ &+ \eta^* \left[ \left( \frac{\partial^2 \bar{v}}{\partial \bar{x}^2} + \frac{\partial^2 \bar{v}}{\partial \bar{y}^2} \right)^2 + \left( \frac{\partial^2 \bar{u}}{\partial \bar{x}^2} + \frac{\partial^2 \bar{u}}{\partial \bar{y}^2} \right)^2 \right],\end{aligned}\tag{5.13}$$

where  $\nabla^2 = \left( \frac{\partial^2}{\partial \bar{x}^2} + \frac{\partial^2}{\partial \bar{y}^2} \right)$  and  $\nabla^4 = \nabla^2 \nabla^2$ .

The non-dimensional variables, Reynolds number (Re), Prandtl number (Pr), Eckert number ( $Ec$ ), Brinkman number ( $Br$ ) and Biot numbers ( $Bi_1$ ,  $Bi_2$ ) are represented by the following

definitions:

$$\begin{aligned}
x &= \frac{\bar{x}}{\lambda}, \quad y = \frac{\bar{y}}{d_1}, \quad u = \frac{\bar{u}}{c}, \quad v = \frac{\bar{v}}{c\delta}, \quad p = \frac{d_1^2 \bar{p}}{c\lambda\mu}, \quad \delta = \frac{d_1}{\lambda}, \\
h_1 &= \frac{\bar{h}_1}{d_1}, \quad h_2 = \frac{\bar{h}_2}{d_1}, \quad t = \frac{c\bar{t}}{\lambda}, \quad \theta = \frac{T - T_a}{T_a}, \quad \eta = \frac{\eta^*}{\mu d_1^2}, \\
\text{Re} &= \frac{\rho c d_1}{\mu}, \quad \text{Pr} = \frac{\rho c_p \nu}{k}, \quad Ec = \frac{c^2}{c_p T_a}, \quad Br = \text{Pr} Ec, \\
Bi_1 &= \frac{\eta_1 d_1}{k}, \quad Bi_2 = \frac{\eta_2 d_1}{k}.
\end{aligned} \tag{5.14}$$

The governing Eqs. (5.10 – 5.13) can be written as

$$\frac{\partial u}{\partial x} + \frac{\partial v}{\partial y} = 0, \tag{5.15}$$

$$\text{Re} \delta \left( u \frac{\partial}{\partial x} + v \frac{\partial}{\partial y} \right) u = -\frac{\partial p}{\partial x} + \nabla^2 u - \eta \nabla^4 u, \tag{5.16}$$

$$\text{Re} \delta^3 \left( u \frac{\partial}{\partial x} + v \frac{\partial}{\partial y} \right) v = -\frac{\partial p}{\partial y} + \delta^2 \nabla^2 v - \delta^2 \eta \nabla^4 v, \tag{5.17}$$

$$\begin{aligned}
\text{Pr Re} \delta \left( u \frac{\partial}{\partial x} + v \frac{\partial}{\partial y} \right) \theta &= \nabla^2 \theta + Br \left[ 2\delta^2 \left( \frac{\partial u}{\partial x} \right)^2 + 2\delta^2 \left( \frac{\partial v}{\partial y} \right)^2 + \left( \frac{\partial u}{\partial y} + \delta^2 \frac{\partial v}{\partial x} \right)^2 \right] \\
&+ \eta Br \left[ \delta^2 \left( \delta^2 \frac{\partial^2 v}{\partial x^2} + \frac{\partial^2 v}{\partial y^2} \right)^2 + \left( \delta^2 \frac{\partial^2 u}{\partial x^2} + \frac{\partial^2 u}{\partial y^2} \right)^2 \right],
\end{aligned} \tag{5.18}$$

where  $\nabla^2 = \left( \delta^2 \frac{\partial^2}{\partial x^2} + \frac{\partial^2}{\partial y^2} \right)$ . Equations (5.8) and (5.9) give

$$\frac{\partial \theta}{\partial y} + Bi_1 \theta = 0 \text{ at } y = h_1, \tag{5.19}$$

$$\frac{\partial \theta}{\partial y} - Bi_2 \theta = 0 \text{ at } y = h_2. \tag{5.20}$$

By long wavelength and low Reynolds number assumptions [6] we have

$$\frac{\partial p}{\partial x} - \frac{\partial^2 u}{\partial y^2} + \eta \frac{\partial^4 u}{\partial y^4} = 0, \tag{5.21}$$

$$\frac{\partial p}{\partial y} = 0, \tag{5.22}$$

$$\frac{\partial^2 \theta}{\partial y^2} + Br \left( \frac{\partial u}{\partial y} \right)^2 + \eta Br \left( \frac{\partial^2 u}{\partial y^2} \right)^2 = 0, \tag{5.23}$$



where continuity equation is identically satisfied. The above equations indicate that  $p \neq p(y)$ .

Keeping in view the physical constraints of the problem, the boundary conditions in the fixed frame may be expressed mathematically as follows:

$$\bar{U} = 0, \quad \bar{U}_{\bar{Y}\bar{Y}} = 0 \text{ at } \bar{Y} = \bar{h}_1 \text{ and } \bar{Y} = \bar{h}_2, \quad (5.24)$$

The non-dimensional boundary conditions in wave frame are

$$u = -1, \quad u_{yy} = 0 \text{ at } y = h_1 \text{ and } y = h_2. \quad (5.25)$$

The closed form solutions of Eqs. (5.21) and (5.23) satisfying the boundary conditions (5.19), (5.20) and (5.25) are found in the forms

$$u(y) = \frac{1}{2} \left[ -2 + \frac{dp}{dx} (h_1 - y)(h_2 - y) + 2\eta \frac{dp}{dx} - 2\eta \frac{dp}{dx} \cosh \left( \frac{h_1 + h_2}{2\sqrt{\eta}} \right) \sec h \left( \frac{h_1 - h_2}{2\sqrt{\eta}} \right) \right], \quad (5.26)$$

$$\theta(y) = Br \left( \frac{dp}{dx} \right)^2 [A_1 y^4 + A_2 y^3 + A_3 y^2 + A_4(y)y + A_5(y)], \quad (5.27)$$

where

$$\begin{aligned}
A_1 &= \frac{-1}{12}, \quad A_2 = \frac{(h_1 + h_2)}{6}, \quad A_3 = -\frac{(h_1 + h_2)^2 + 4\eta}{8}, \\
A_4(y) &= \frac{1}{[24(Bi_1 + Bi_2 + Bi_1 Bi_2(h_1 - h_2))(1 + \cosh(\frac{h_1 - h_2}{\sqrt{\eta}}))]} \\
&\times [2Bi_1(3h_1^2 h_2 + h_2^3 + 12h_1 \eta) + Bi_2(Bi_1(h_1^4 - h_2^4) \\
&- 2h_1 h_2^2(-3 + Bi_1 h_2) + 2h_1^3(1 + Bi_1 h_2) + 12Bi_1 h_1^2 \eta \\
&- 12h_2(-2 + Bi_1 h_2)\eta) + \{2Bi_1(3h_1^2 h_2 + h_2^3 + 12h_1 \eta) \\
&+ Bi_2(Bi_1(h_1^4 - h_2^4) - 2h_1 h_2^2(-3 + Bi_1 h_2) + 2h_1^3(1 + Bi_1 h_2) \\
&+ 12Bi_1 h_1^2 \eta - 12h_2(-2 + Bi_1 h_2)\eta)\} \cosh(\frac{h_1 - h_2}{\sqrt{\eta}}) \\
&+ 24\eta^{3/2}\{(-Bi_1 + Bi_2) \sinh(\frac{h_1 - h_2}{\sqrt{\eta}}) \\
&- 2(Bi_1 + Bi_2 + Bi_1 Bi_2(h_1 - h_2)) \left( \sinh(\frac{h_1 - y}{\sqrt{\eta}}) + \sinh(\frac{h_2 - y}{\sqrt{\eta}}) \right) \} \Big], \\
A_5(y) &= \frac{1}{[24(Bi_1 + Bi_2 + Bi_1 Bi_2(h_1 - h_2))(1 + \cosh(\frac{h_1 - h_2}{\sqrt{\eta}}))]} \\
&\times [h_2^3(-2 + Bi_2 h_2) + h_1^4(Bi_1(1 - Bi_2 h_2)) + h_1^3(2 - 2Bi_2 h_2 + Bi_1 h_2(-4 + Bi_2 h_2)) \\
&- 12h_2(-2 + Bi_2 h_2)\eta + 48(Bi_1 + Bi_2 - Bi_1 Bi_2 h_2)\eta^2 + h_1^2(h_2(-6 + 3Bi_2 h_2 \\
&+ Bi_1 h_2(3 - Bi_2 h_2)) - 12Bi_1(1 + Bi_2 h_2)\eta) + h_1(-2(Bi_1 + 2Bi_2)h_2^3 \\
&+ Bi_1 Bi_2 h_2^4 + 24\eta(-1 + 2Bi_1 Bi_2 \eta) + 6h_2^2(1 + 2Bi_1 Bi_2 \eta)) + \{h_2^3(-2 + Bi_2 h_2) \\
&+ h_1^4(Bi_1 - Bi_1 Bi_2 h_2) + h_1^3(2 - 2Bi_2 h_2 + Bi_1 h_2(-4 + Bi_2 h_2)) - 12h_2(-2 + Bi_2 h_2)\eta \\
&+ 60(Bi_1 + Bi_2 - Bi_1 Bi_2 h_2)\eta^2 + h_1^2(h_2(-6 + 3Bi_2 h_2 + Bi_1 h_2(3 - Bi_2 h_2)) \\
&- 12Bi_1(1 + Bi_2 h_2)\eta) + h_1(-2(Bi_1 + 2Bi_2)h_2^3 + Bi_1 Bi_2 h_2^4 + 6h_2^2(1 + 2Bi_1 Bi_2 \eta) \\
&+ 12\eta(-2 + 5Bi_1 Bi_2 \eta))\} \cosh(\frac{h_1 - h_2}{\sqrt{\eta}}) + 12\eta^{3/2}\{-(Bi_1 + Bi_2 + Bi_1 Bi_2(h_1 - h_2)) \\
&\times \sqrt{\eta} \cosh(\frac{h_1 + h_2 - 2y}{\sqrt{\eta}}) - 2(-2 - Bi_1 h_2 + Bi_2(h_1 + Bi_1(h_1 - h_2)^2)) \sinh(\frac{h_1 - h_2}{\sqrt{\eta}}) \\
&+ 2(Bi_1 + Bi_2 + Bi_1 Bi_2(h_1 - h_2)) \left( -2\sqrt{\eta}(\cosh(\frac{h_1 - y}{\sqrt{\eta}}) + \cosh(\frac{h_2 - y}{\sqrt{\eta}})) \right. \\
&\left. + (h_1 + h_2)(\sinh(\frac{h_1 - y}{\sqrt{\eta}}) + \sinh(\frac{h_2 - y}{\sqrt{\eta}})) \right) \} \Big].
\end{aligned}$$

Defining  $\Theta$  and  $F$  as the dimensionless time-mean flows in the laboratory and wave frames

respectively we have

$$\Theta = F + 1 + d, \quad (5.28)$$

$$F = \int_{h_2}^{h_1} u(y) dy. \quad (5.29)$$

Substituting Eq. (5.26) into Eq. (5.29) and performing the integration, we find that

$$F = -\frac{1}{12}(h_1 - h_2) \left( 12 + \frac{dp}{dx} ((h_1 - h_2)^2 - 12\eta) \right) - 2\eta^{3/2} \frac{dp}{dx} \tanh \left( \frac{h_1 - h_2}{2\sqrt{\eta}} \right). \quad (5.30)$$

The pressure gradient obtained from Eq. (5.30) can be expressed as

$$\frac{dp}{dx} = \frac{(F + h_1 - h_2)}{\left[ \frac{1}{12}(h_2 - h_1) ((h_1 - h_2)^2 - 12\eta) - 2\eta^{3/2} \tanh \left( \frac{h_1 - h_2}{2\sqrt{\eta}} \right) \right]}. \quad (5.31)$$

The dimensionless forms of  $h_i$  ( $i = 1, 2$ ) are

$$h_1(x) = 1 + a \cos(2\pi x), \quad h_2(x) = -d - b \cos(2\pi x + \phi), \quad (5.32)$$

where  $a = a_1/d_1$ ,  $b = a_2/d_1$ ,  $d = d_2/d_1$  and  $\phi$  satisfy the following relation

$$a^2 + b^2 + 2ab \cos \phi \leq (1 + d)^2.$$

The pressure rise per wavelength ( $\Delta P_\lambda$ ) is given by

$$\Delta P_\lambda = \int_0^1 \frac{dp}{dx} dx. \quad (5.33)$$

## 5.3 Results and discussion

### 5.3.1 Pumping characteristics

In this subsection, we discuss the effects of pertinent parameters on pumping characteristics. Figs. 5.1 and 5.2 are plotted to see the effects of couple stress parameter  $\eta$  and flow rate  $\Theta$  on pressure gradient respectively. These Figs. show that pressure gradient decreases with an

increase in couple stress parameter  $\eta$  and pressure gradient increases by increasing flow rate  $\Theta$ . Figs. 5.3 – 5.7 depict the effects of different parameters on pressure rise per wavelength  $\Delta p_\lambda$  versus flow rate  $\Theta$ . Note that the definition of pressure rise per wavelength  $\Delta p_\lambda$  involves integration of  $dp/dx$  (see Eq. (5.33)). The arising integral is not solvable analytically. Therefore the involved integral has been computed numerically by using "Mathematica". Figs. 5.3 – 5.5 reveal that pumping increases in the peristaltic pumping region ( $\Delta p_\lambda > 0$ ,  $\Theta > 0$ ) while it decreases in augmented pumping region ( $\Delta p_\lambda < 0$ ,  $\Theta > 0$ ) with an increase in couple stress parameter  $\eta$ , upper wave amplitude  $a$  and lower wave amplitude  $b$  respectively. Figs. 5.6 and 5.7 show the effects of channel width  $d$  and phase difference  $\phi$  on the pressure rise per wavelength  $\Delta p_\lambda$ . These Figs. depict that pumping decreases in peristaltic pumping region ( $\Delta p_\lambda > 0$ ,  $\Theta > 0$ ) while it increases in augmented pumping region ( $\Delta p_\lambda < 0$ ,  $\Theta > 0$ ) with an increase in  $d$  and  $\phi$ .

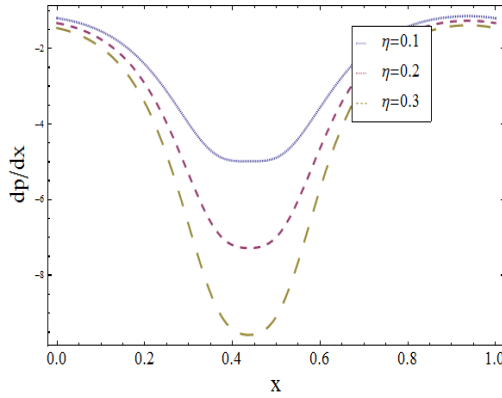


Fig. 5.1

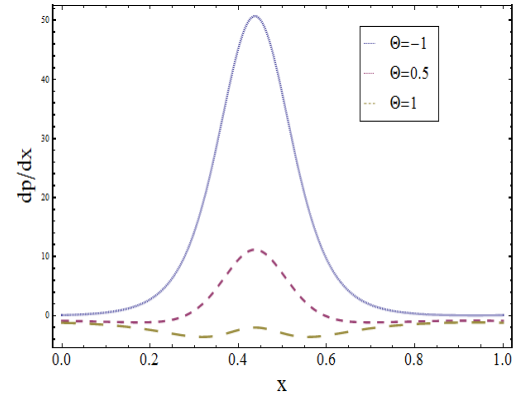


Fig. 5.2

Fig. 5.1: Plot of  $dp/dx$  for  $\eta$  with  $a = 0.5$ ,  $b = 0.5$ ,  $d = 1$ ,  $\phi = \pi/4$ ,  $\Theta = 1.2$ .

Fig. 5.2: Plot of  $dp/dx$  for  $\Theta$  with  $a = 0.5$ ,  $b = 0.5$ ,  $d = 1$ ,  $\phi = \pi/4$ ,  $\eta = 0.2$ .

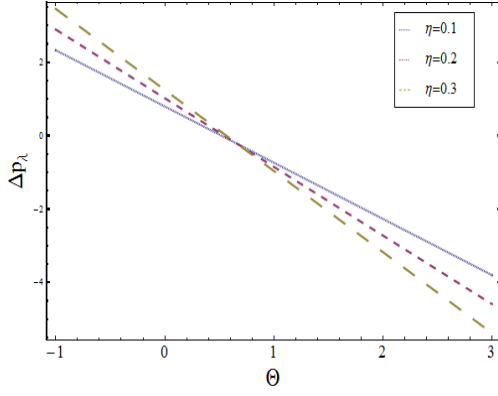


Fig. 5.3

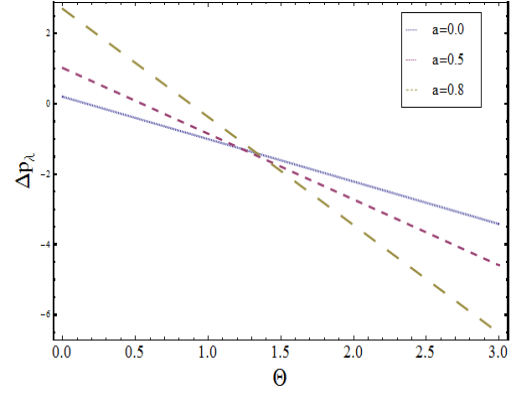


Fig. 5.4

Fig. 5.3: Plot of  $\Delta p_\lambda$  versus  $\Theta$  for various values of  $\eta$  with  $a = 0.5$ ,  $b = 0.5$ ,  $d = 1.5$ ,  $\phi = \pi/4$ .

Fig. 5.4: Plot of  $\Delta p_\lambda$  versus  $\Theta$  for various values of  $a$  with  $\eta = 0.2$ ,  $b = 0.5$ ,  $d = 1.5$ ,  $\phi = \pi/4$ .

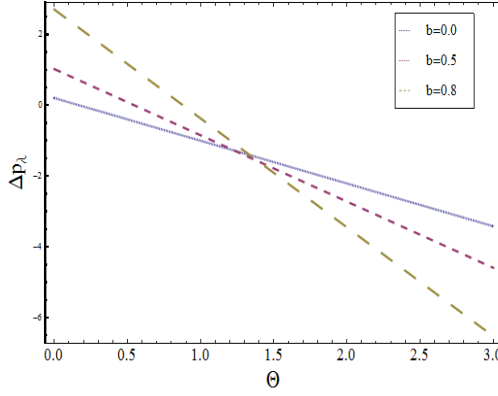


Fig. 5.5

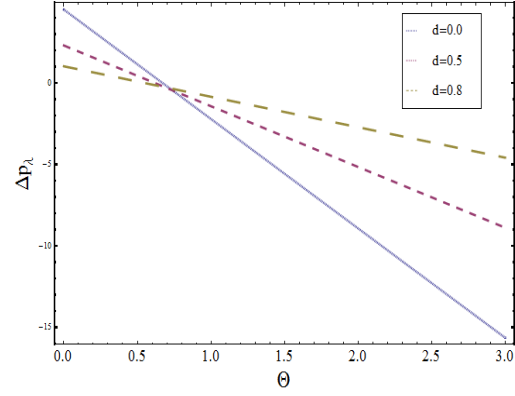


Fig. 5.6

Fig. 5.5: Plot of  $\Delta p_\lambda$  versus  $\Theta$  for various values of  $b$  with  $a = 0.5$ ,  $\eta = 0.2$ ,  $d = 1.5$ ,  $\phi = \pi/4$ .

Fig. 5.6: Plot of  $\Delta p_\lambda$  versus  $\Theta$  for various values of  $d$  with  $a = 0.5$ ,  $b = 0.5$ ,  $\eta = 0.2$ ,  $\phi = \pi/4$ .

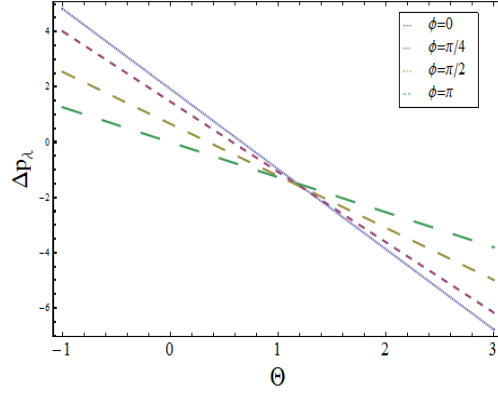


Fig. 5.7

Fig. 5.7: Plot of  $\Delta p_\lambda$  versus  $\Theta$  for various values of  $\phi$  with  $a = 0.5$ ,  $b = 0.5$ ,  $d = 1.5$ ,  $\eta = 0.4$ .

### 5.3.2 Velocity behavior

In this subsection, we discuss the behavior of velocity profile  $u(y)$  for different values of emerging parameters. Fig. 5.8 shows that the axial velocity  $u(y)$  increases at the center of channel by increasing couple stress parameter  $\eta$ . However the axial velocity  $u(y)$  decreases near the channel walls with an increase in the couple stress parameter  $\eta$ . It is worth mentioning that magnitude of axial velocity  $u(y)$  is larger for couple stress fluid when compared to the Newtonian case ( $\eta \rightarrow 0$ ). Effect of various values of the flow rate  $\Theta$  is shown in Fig. 5.9. It is important to note that the axial velocity  $u(y)$  increases with an increase in the flow rate  $\Theta$ .

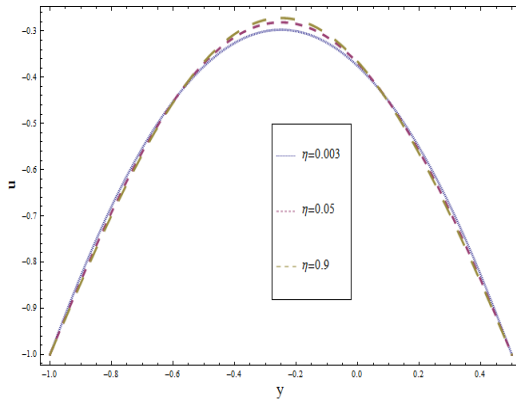


Fig. 5.8

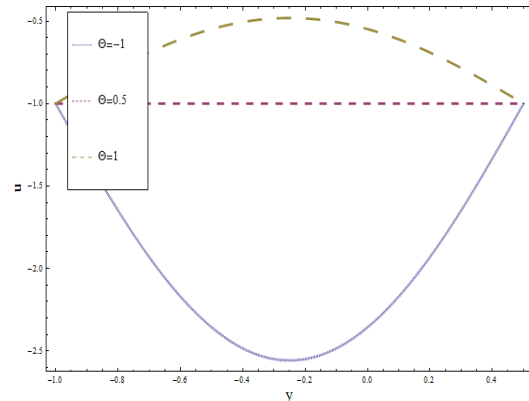


Fig. 5.9

Fig. 5.8: Plot of axial velocity  $u$  for  $\eta$  with  $a = 0.5$ ,  $b = 0.5$ ,  $d = 1$ ,  $\phi = \pi/2$ ,  $\Theta = 1.2$ ,  
 $x = -0.5$ .

Fig. 5.9: Plot of axial velocity  $u$  for  $\Theta$  with  $a = 0.5$ ,  $b = 0.5$ ,  $d = 1$ ,  $\phi = \pi/2$ ,  $\eta = 0.3$ ,  
 $x = -0.5$ .

### 5.3.3 Temperature profile

The effects of various parameters on temperature profile  $\theta(y)$  are analyzed in this subsection. Figs. 5.10 and 5.11 reveal that temperature profile  $\theta(y)$  increases by increasing the values of couple stress parameter  $\eta$  and Brinkman number  $Br$ . Since Brinkman number is the product of Prandtl  $Pr$  and Eckert  $Ec$  number and Eckert number  $Ec$  involves the viscous dissipation effects which are due to the energy production. That is why the temperature increases in view of viscous dissipation. By increasing the values of Biot number  $Bi_1$  the temperature profile  $\theta(y)$  decreases near the upper wall while it has no significant effect near the lower wall of the channel. On the other hand, the temperature profile  $\theta(y)$  decreases near lower wall for increasing values of  $Bi_2$  while it has no significant effect near the upper wall of the channel (see Figs. 5.12 and 5.13). Here we have considered the Biot numbers much larger than unity. This is because of non-uniformity of the temperature fields within the fluid. The present analysis of convective conditions reduces to the results for the prescribed surface temperature for high Biot numbers (i.e.  $Bi_1 \rightarrow \infty$  and  $Bi_2 \rightarrow \infty$ ) [136].

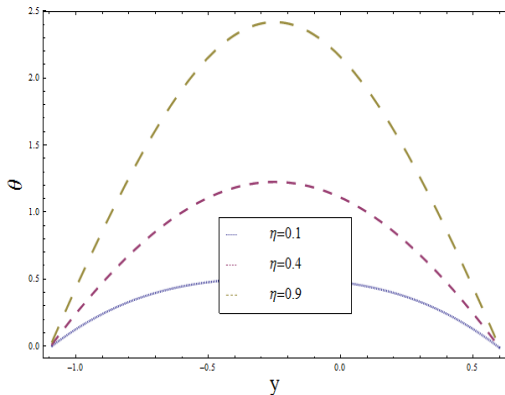


Fig. 5.10

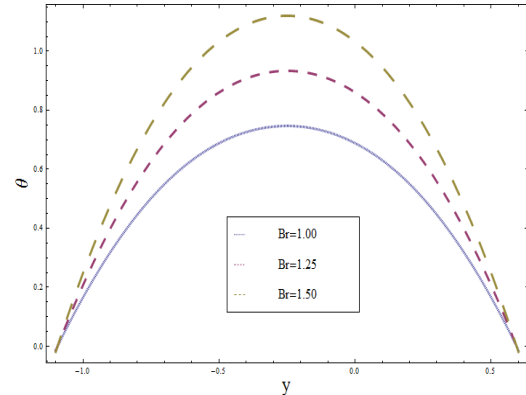


Fig. 5.11

Fig. 5.10: Plot of the temperature profile  $\theta$  for  $\eta$  with  $a = 0.5$ ,  $b = 0.5$ ,  $d = 1$ ,  $\phi = \pi/2$ ,

$$\Theta = 1.2, x = -0.5, Bi_1 = 8, Bi_2 = 10, Br = 1.$$

Fig. 5.11: Plot of the temperature profile  $\theta$  for  $Br$  with  $a = 0.5$ ,  $b = 0.5$ ,  $d = 1$ ,  $\phi = \pi/2$ ,

$$\Theta = 1.2, x = -0.5, Bi_1 = 8, Bi_2 = 10, \eta = 0.2.$$

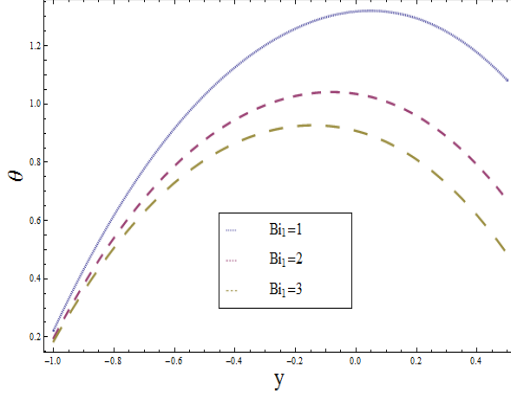


Fig. 5.12

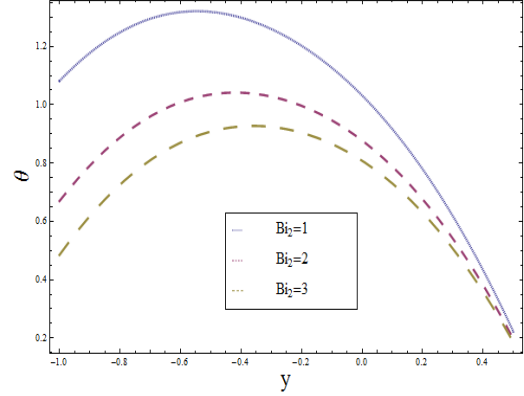


Fig. 5.13

Fig. 5.12: Plot of the temperature profile  $\theta$  for  $Bi_1$  with  $a = 0.5$ ,  $b = 0.5$ ,  $d = 1$ ,  $\phi = \pi/2$ ,

$$\Theta = 1.2, x = -0.5, \eta = 0.2, Bi_2 = 10, Br = 1.$$

Fig. 5.13: Plot of the temperature profile  $\theta$  for  $Bi_2$  with  $a = 0.5$ ,  $b = 0.5$ ,  $d = 1$ ,  $\phi = \pi/2$ ,

$$\Theta = 1.2, x = -0.5, \eta = 0.2, Bi_1 = 10, Br = 1.$$

### 5.3.4 Trapping

The shape of streamlines is similar to that of a boundary wall in the wave frame as the walls are stationary in general. However, some of the streamlines split and enclose a bolus under certain conditions and this bolus moves as a whole with the wave. This phenomenon is known as trapping. In this subsection we check the effects of different parameters on trapping. Thus Figs. 5.14 – 5.16 are plotted to see the effects of couple stress parameter  $\eta$ , the flow rate  $\Theta$  and the channel width  $d$ . These Figs. indicate that the size of trapped bolus decreases with an increase in couple stress parameter  $\eta$  and channel width  $d$  (see Figs. 5.14 and 5.16). The number of streamlines reduce when the channel width  $d$  increases and consequently the trapping reduces. Further the size of the trapped bolus increases when flow rate  $\Theta$  is increased (see Fig. 5.15). It is also interesting to note that for negative flow rate  $\Theta$  the trapping does not exist.



However trapping only exists for positive values of flow rate  $\Theta$ .

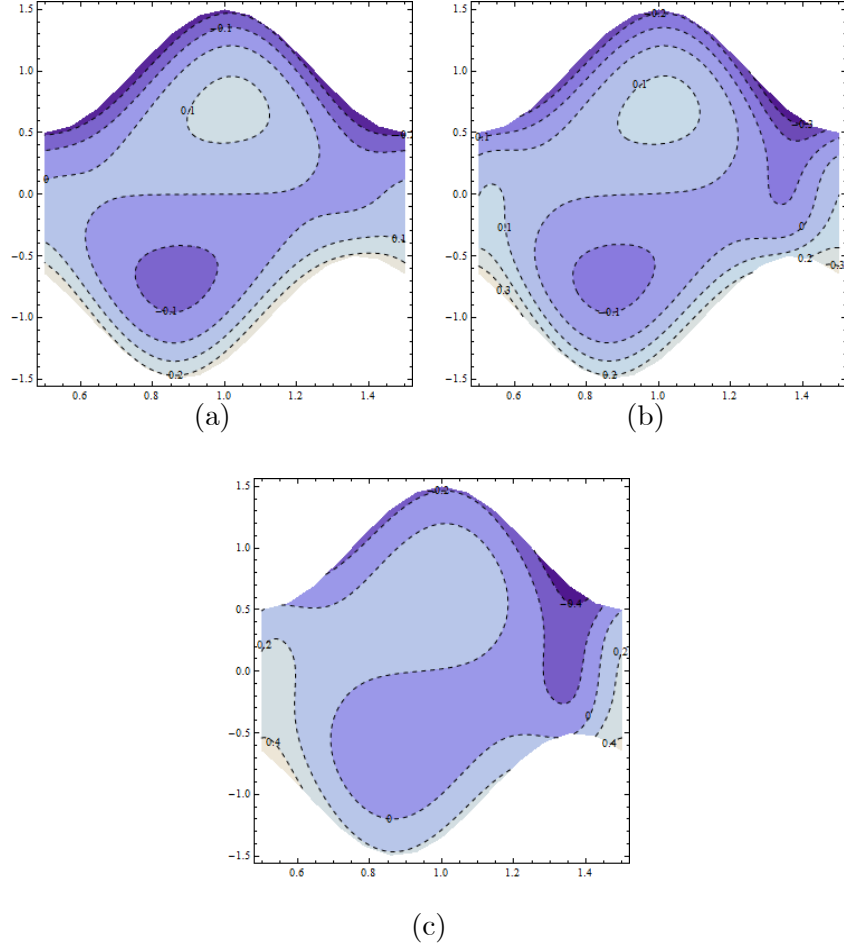


Fig. 5.14: Streamline pattern for  $a = 0.5$ ,  $b = 0.5$ ,  $d = 1$ ,  $\phi = \pi/4$ ,  $\Theta = 1.5$  with different  $\eta$  (a)  $\eta = 0.1$ , (b)  $\eta = 0.2$ , (c)  $\eta = 0.3$ .

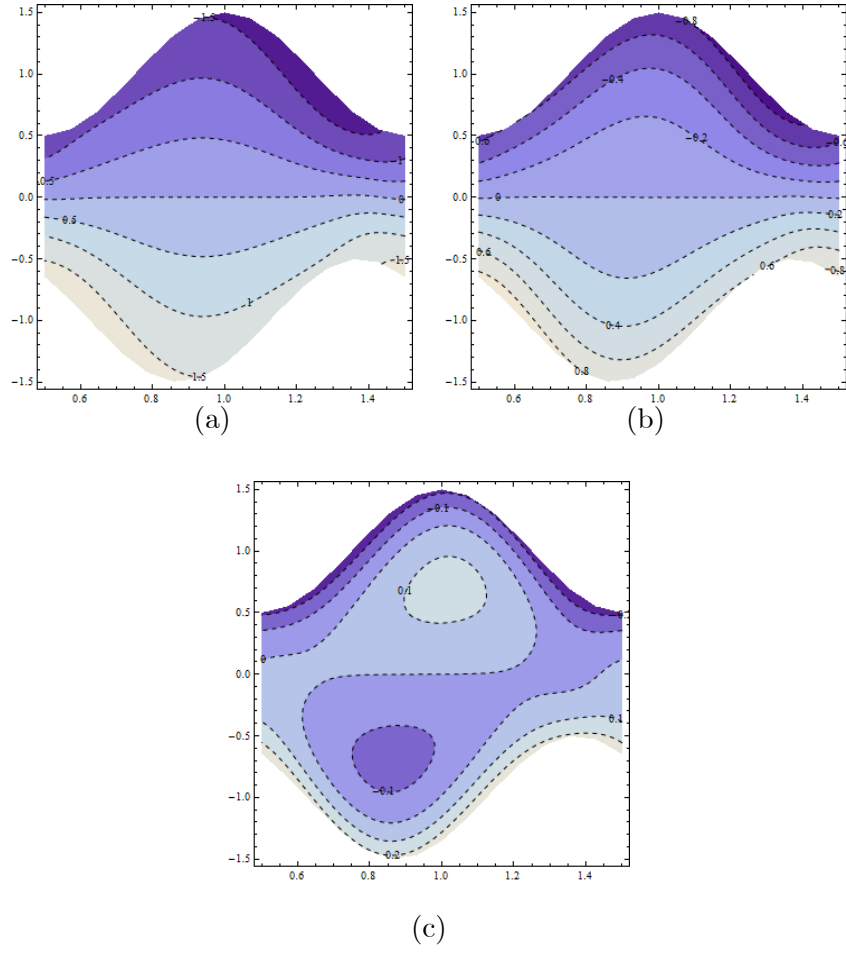


Fig. 5.15: Streamline pattern for  $a = 0.5$ ,  $b = 0.5$ ,  $d = 1$ ,  $\phi = \pi/4$ ,  $\eta = 0.1$  with different  $\Theta$  (a)  $\Theta = -1$ , (b)  $\Theta = 0.5$ , (c)  $\Theta = 1.5$ .

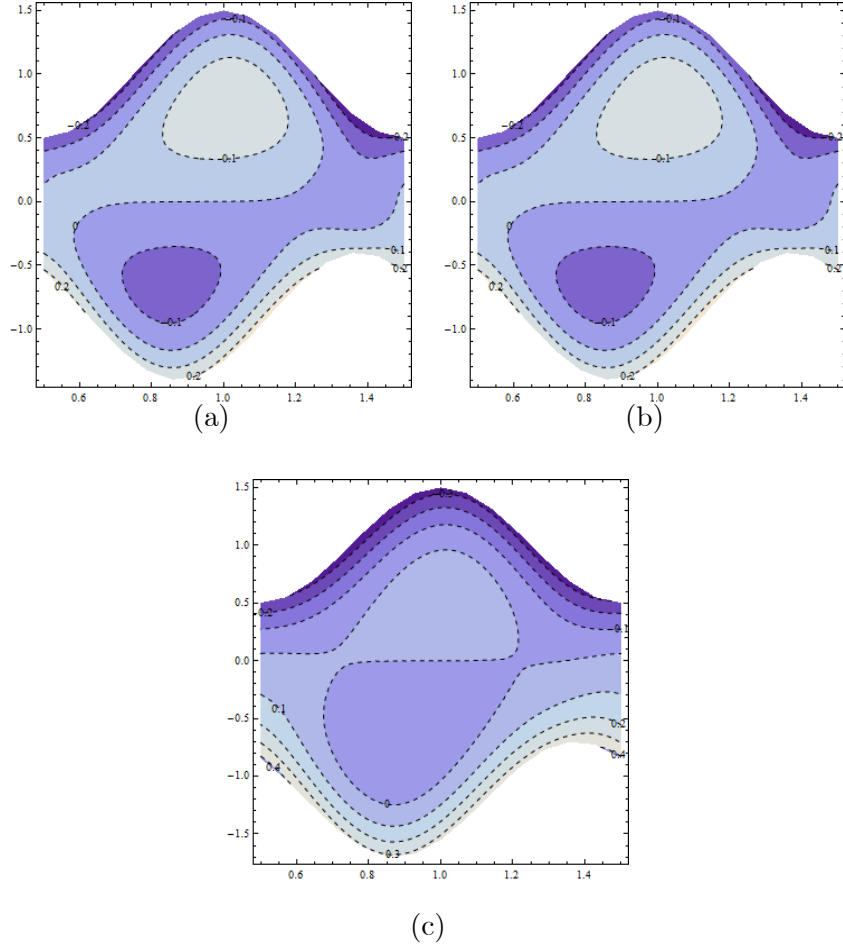


Fig. 5.16: Streamline pattern for  $a = 0.5$ ,  $b = 0.5$ ,  $\eta = 0.1$ ,  $\phi = \pi/4$ ,  $\Theta = 1.5$  with different  $d$   
(a)  $d = 0.7$ , (b)  $d = 0.9$ , (c)  $d = 1.2$ .

### 5.3.5 Closing remarks

Peristaltic flow of couple stress fluid in an asymmetric channel with convective boundary conditions at the channel walls is investigated in this chapter. Here we have the following observations:

- The peristaltic pumping decreases with an increase in couple stress parameter  $\eta$ . Such fact is due to the consideration of body couples and body moments within the fluid.
- The longitudinal pressure gradient  $dp/dx$  decreases by increasing the couple stress para-

meter  $\eta$  in the narrow part of the channel while in the wider part of the channel there is no effective difference.

- The axial velocity  $u(y)$  increases in the narrow part of the channel while it shows opposite behavior in the wider part of the channel when couple stress parameter  $\eta$  increases.
- Impact of couple stress parameter  $\eta$  and Brinkman number  $Br$  on the temperature is similar qualitatively.
- The Biot and Brinkman numbers on temperature have opposite effects.
- The results for the prescribed surface temperature are deduced as a special case of the present analysis when  $Bi_1 \rightarrow \infty$  and  $Bi_2 \rightarrow \infty$  [136].

## Chapter 6

# Peristaltic flow of Johnson-Segalman fluid in an asymmetric channel with convective boundary conditions

### 6.1 Introduction

This chapter is concerned with the peristaltic transport of Johnson-Segalman fluid in an asymmetric channel with convective boundary conditions. Mathematical modelling is based upon the conservation laws of mass, linear momentum and energy. Resulting equations have been solved after using long wavelength and low Reynolds number considerations. Results for the axial pressure gradient, velocity and temperature profiles are obtained for small Weissenberg number. Expressions of the pressure gradient, velocity and temperature are analyzed for various embedded parameters. Pumping and trapping phenomena are also explored.

### 6.2 Flow equations

The constitutive equations of Johnson-Segalman fluid are [42]

$$\bar{\sigma} = -\bar{p}\bar{\mathbf{I}} + \bar{\tau}, \quad \bar{\tau} = 2\mu\bar{\mathbf{D}} + \bar{\mathbf{S}}, \quad (6.1)$$

$$\bar{\mathbf{S}} + m_1 \left[ \frac{d\bar{\mathbf{S}}}{dt} + \bar{\mathbf{S}} (\bar{\mathbf{W}} - e\bar{\mathbf{D}}) + (\bar{\mathbf{W}} - e\bar{\mathbf{D}})^* \bar{\mathbf{S}} \right] = 2\xi\bar{\mathbf{D}}, \quad (6.2)$$

in which  $\bar{\boldsymbol{\sigma}}$  is the Cauchy stress tensor,  $\bar{p}$  the pressure,  $\bar{\mathbf{I}}$  the unit tensor,  $\bar{\boldsymbol{\tau}}$  the extra stress tensor,  $\mu$  the dynamic viscosity,  $\xi$  the elastic shear modulus,  $m_1$  the relaxation time and  $e$  the slip parameter. Here  $\bar{\mathbf{D}}$  and  $\bar{\mathbf{W}}$  are the symmetric and skew-symmetric parts of the velocity gradient ( $\bar{\mathbf{L}} = \text{grad } \bar{\mathbf{V}}$ ), respectively. These are given by

$$\bar{\mathbf{D}} = \frac{1}{2}(\bar{\mathbf{L}} + \bar{\mathbf{L}}^*), \quad \bar{\mathbf{W}} = \frac{1}{2}(\bar{\mathbf{L}} - \bar{\mathbf{L}}^*). \quad (6.3)$$

We note that, for  $e = 1$  and  $\mu = 0$ , the model (2) reduces to Maxwell model. Further, when  $m_1 = 0$  the model recovers viscous fluid and asterisk (\*) denotes the matrix transpose.

The equations of continuity, momentum and energy are

$$\text{div } \bar{\mathbf{V}} = 0, \quad (6.4)$$

$$\rho \frac{d\bar{\mathbf{V}}}{d\bar{t}} = \text{div } \bar{\boldsymbol{\sigma}}, \quad (6.5)$$

$$\rho c_p \frac{dT}{d\bar{t}} = k \nabla^2 T + \bar{\boldsymbol{\tau}} \cdot (\text{grad } \bar{\mathbf{V}}), \quad (6.6)$$

where  $\rho$  is the fluid density,  $\bar{t}$  the time,  $\bar{\mathbf{V}}$  the velocity,  $T$  the fluid temperature,  $c_p$  the specific heat,  $k$  the thermal conductivity of the material and  $\nabla^2 = \left( \frac{\partial^2}{\partial \bar{X}^2} + \frac{\partial^2}{\partial \bar{Y}^2} \right)$ . Note that the over bar just refers to a dimensional quantity.

### 6.3 Problem statement

We investigate the flow of peristaltically driven incompressible Johnson-Segalman fluid in an asymmetric channel (see Fig. 2.1). The  $\bar{X}$  and  $\bar{Y}$  axes are selected along and perpendicular to the channel walls respectively. The flow is caused by waves propagating along the channel walls. The channel walls for heat transfer satisfy the convective conditions. The geometry of the walls is put into the forms given below:

$$\begin{aligned} \bar{h}_1(\bar{X}, \bar{t}) &= d_1 + a_1 \sin \left[ \frac{2\pi}{\lambda} (\bar{X} - c\bar{t}) \right], & \text{upper wall,} \\ \bar{h}_2(\bar{X}, \bar{t}) &= -d_2 - a_2 \sin \left[ \frac{2\pi}{\lambda} (\bar{X} - c\bar{t}) + \phi \right], & \text{lower wall.} \end{aligned} \quad (6.7)$$

In above expressions  $c$  is the wave speed,  $a_1, a_2$  are the wave amplitudes,  $\lambda$  is the wavelength,  $d_1 + d_2$  is the width of the asymmetric channel, the phase difference  $\phi$  varies in the range  $0 \leq \phi \leq \pi$  ( $\phi = 0$  corresponds to symmetric channel with waves out of phase and  $\phi = \pi$  the waves are in phase) and further  $a_1, a_2, d_1, d_2$  and  $\phi$  satisfy the condition

$$a_1^2 + a_2^2 + 2a_1a_2 \cos \phi \leq (d_1 + d_2)^2. \quad (6.8)$$

The exchange of heat with ambient at the walls is given by

$$k \frac{\partial T}{\partial \bar{Y}} = -\eta_1(T - T_1) \text{ at } \bar{Y} = \bar{h}_1, \quad (6.9)$$

$$k \frac{\partial T}{\partial \bar{Y}} = -\eta_2(T - T_0) \text{ at } \bar{Y} = \bar{h}_2, \quad (6.10)$$

where  $\eta_1$  ( $\eta_2$ ) and  $T_1$  ( $T_0$ ) are the heat transfer coefficients and temperatures at the upper (lower) channel wall respectively.

The velocity  $\bar{\mathbf{V}}$  for two-dimensional flow is

$$\bar{\mathbf{V}} = (\bar{U}(\bar{X}, \bar{Y}, \bar{t}), \bar{V}(\bar{X}, \bar{Y}, \bar{t}), 0). \quad (6.11)$$

If  $(\bar{x}, \bar{y})$  and  $(\bar{u}, \bar{v})$  are the coordinates and velocity components in the wave frame  $(\bar{x}, \bar{y})$  then we have the following transformations:

$$\bar{x} = \bar{X} - c\bar{t}, \quad \bar{y} = \bar{Y}, \quad \bar{u}(\bar{x}, \bar{y}) = \bar{U}(\bar{X}, \bar{Y}, \bar{t}) - c, \quad \bar{v}(\bar{x}, \bar{y}) = \bar{V}(\bar{X}, \bar{Y}, \bar{t}), \quad T(\bar{x}, \bar{y}) = T(\bar{X}, \bar{Y}, \bar{t}). \quad (6.12)$$

Employing these transformations and introducing the following dimensionless variables

$$\begin{aligned} x &= \frac{2\pi\bar{x}}{\lambda}, \quad y = \frac{\bar{y}}{d_1}, \quad u = \frac{\bar{u}}{c}, \quad v = \frac{\bar{v}}{c}, \quad p = \frac{2\pi d_1^2 \bar{p}}{c\lambda(\mu + \xi)}, \\ h_1 &= \frac{\bar{h}_1}{d_1}, \quad h_2 = \frac{\bar{h}_2}{d_1}, \quad t = \frac{2\pi c\bar{t}}{\lambda}, \quad \mathbf{S} = \frac{d_1}{\mu c} \bar{\mathbf{S}}, \quad \theta = \frac{T - T_0}{T_1 - T_0}, \end{aligned} \quad (6.13)$$

and the stream function  $\psi(x, y)$  by

$$u = \frac{\partial \psi}{\partial y}, \quad v = -\delta \frac{\partial \psi}{\partial x}, \quad (6.14)$$

Eq. (6.4) is satisfied identically and Eqs. (6.5) and (6.6) help in writing the following equations in terms of stream function  $\psi$  as

$$\delta \text{Re} \left[ \left( \frac{\partial \psi}{\partial y} \frac{\partial}{\partial x} - \frac{\partial \psi}{\partial x} \frac{\partial}{\partial y} \right) \left( \frac{\partial \psi}{\partial y} \right) \right] + \frac{(\mu + \xi)}{\mu} \frac{\partial p}{\partial x} = \delta^2 \frac{\partial^3 \psi}{\partial x^2 \partial y} + \frac{\partial^3 \psi}{\partial y^3} + \delta \frac{\partial S_{xx}}{\partial x} + \frac{\partial S_{xy}}{\partial y}, \quad (6.15)$$

$$-\delta^3 \text{Re} \left[ \left( \frac{\partial \psi}{\partial y} \frac{\partial}{\partial x} - \frac{\partial \psi}{\partial x} \frac{\partial}{\partial y} \right) \left( \frac{\partial \psi}{\partial x} \right) \right] + \frac{(\mu + \xi)}{\mu} \frac{\partial p}{\partial y} = -\delta^2 \left[ \delta^2 \frac{\partial^3 \psi}{\partial x^3} + \frac{\partial^3 \psi}{\partial x \partial y^2} \right] + \delta^2 \frac{\partial S_{xy}}{\partial x} + \delta \frac{\partial S_{yy}}{\partial y}, \quad (6.16)$$

$$\begin{aligned} \delta \text{Re} \left[ \frac{\partial \psi}{\partial y} \frac{\partial}{\partial x} - \frac{\partial \psi}{\partial x} \frac{\partial}{\partial y} \right] \theta &= \frac{1}{\text{Pr}} \left( \delta^2 \frac{\partial^2}{\partial x^2} + \frac{\partial^2}{\partial y^2} \right) \theta \\ &+ Ec \left[ \delta \frac{\partial^2 \psi}{\partial x \partial y} (S_{xx} - S_{yy}) + \left( \frac{\partial^2 \psi}{\partial y^2} - \delta^2 \frac{\partial^2 \psi}{\partial x^2} \right) S_{xy} \right], \end{aligned} \quad (6.17)$$

where Eq. (6.2) gives

$$\begin{aligned} \delta \left( 2 \frac{\xi}{\mu} \frac{\partial^2 \psi}{\partial x \partial y} \right) &= S_{xx} + \delta We \left[ \frac{\partial \psi}{\partial y} \frac{\partial}{\partial x} - \frac{\partial \psi}{\partial x} \frac{\partial}{\partial y} \right] S_{xx} - \delta We (2e) S_{xx} \frac{\partial^2 \psi}{\partial x \partial y} \\ &- We \left[ (1+e) \frac{\partial^2 \psi}{\partial y^2} - \delta^2 (1-e) \frac{\partial^2 \psi}{\partial x^2} \right] S_{xy}, \end{aligned} \quad (6.18)$$

$$\begin{aligned} \frac{\xi}{\mu} \left( \frac{\partial^2 \psi}{\partial y^2} - \delta^2 \frac{\partial^2 \psi}{\partial x^2} \right) &= S_{xy} + \delta We \left[ \frac{\partial \psi}{\partial y} \frac{\partial}{\partial x} - \frac{\partial \psi}{\partial x} \frac{\partial}{\partial y} \right] S_{xy} + \frac{We}{2} \left[ (1-e) \frac{\partial^2 \psi}{\partial y^2} + (1+e) \delta^2 \frac{\partial^2 \psi}{\partial x^2} \right] S_{xx} \\ &- \frac{We}{2} \left[ (1+e) \frac{\partial^2 \psi}{\partial y^2} - (1-e) \delta^2 \frac{\partial^2 \psi}{\partial x^2} \right] S_{yy}, \end{aligned} \quad (6.19)$$

$$\begin{aligned} -\delta \left( 2 \frac{\xi}{\mu} \frac{\partial^2 \psi}{\partial x \partial y} \right) &= S_{yy} + \delta We \left[ \frac{\partial \psi}{\partial y} \frac{\partial}{\partial x} - \frac{\partial \psi}{\partial x} \frac{\partial}{\partial y} \right] S_{yy} + \delta We (2e) S_{yy} \frac{\partial^2 \psi}{\partial x \partial y} \\ &+ We \left[ (1-e) \frac{\partial^2 \psi}{\partial y^2} + (1+e) \delta^2 \frac{\partial^2 \psi}{\partial x^2} \right] S_{xy}. \end{aligned} \quad (6.20)$$

In the above equations the dimensionless wave number  $\delta$ , the Reynolds number  $\text{Re}$ , the Weissenberg number  $We$ , the Prandtl number  $\text{Pr}$  and the Eckert number  $Ec$  are defined as follows:

$$\delta = \frac{2\pi d_1}{\lambda}, \quad \text{Re} = \frac{\rho c d_1}{\mu}, \quad We = \frac{m_1 c}{d_1}, \quad \text{Pr} = \frac{\mu c_p}{k}, \quad Ec = \frac{c^2}{(T_1 - T_0) c_p}. \quad (6.21)$$



Equations (6.9) and (6.10) give

$$\frac{\partial \theta}{\partial y} + Bi_1(\theta - 1) = 0 \text{ at } y = h_1, \quad (6.22)$$

$$\frac{\partial \theta}{\partial y} + Bi_2\theta = 0 \text{ at } y = h_2, \quad (6.23)$$

where  $Bi_1 = \eta_1 d_1/k$  and  $Bi_2 = \eta_2 d_1/k$  are the Biot numbers.

Under the assumption of long wavelength  $\delta \ll 1$  and low Reynolds number  $Re \rightarrow 0$  [6], Eqs. (6.15) and (6.16) are reduced to

$$\frac{(\mu + \xi)}{\mu} \frac{\partial p}{\partial x} = \frac{\partial^3 \psi}{\partial y^3} + \frac{\partial S_{xy}}{\partial y}, \quad (6.24)$$

$$\frac{(\mu + \xi)}{\mu} \frac{\partial p}{\partial y} = 0. \quad (6.25)$$

The above equation indicates that  $p$  is independent of  $y$ . Eliminating the pressure  $p$  from Eqs. (6.24) and (6.25) we arrive at

$$\frac{\partial^4 \psi}{\partial y^4} + \frac{\partial^2 S_{xy}}{\partial y^2} = 0. \quad (6.26)$$

Also Eq. (6.17) yields

$$\frac{\partial^2 \theta}{\partial y^2} + Br \left( \frac{\partial^2 \psi}{\partial y^2} \right) S_{xy} = 0, \quad (6.27)$$

in which the Brinkman number  $Br$  is

$$Br = Pr Ec. \quad (6.28)$$

Equations (6.18) – (6.20) become

$$S_{xx} = We(1 + e) \frac{\partial^2 \psi}{\partial y^2} S_{xy}, \quad (6.29)$$

$$S_{xy} + \frac{We}{2}(1 - e) \frac{\partial^2 \psi}{\partial y^2} S_{xx} - \frac{We}{2}(1 + e) \frac{\partial^2 \psi}{\partial y^2} S_{yy} = \frac{\xi}{\mu} \frac{\partial^2 \psi}{\partial y^2}, \quad (6.30)$$

$$S_{yy} = -We(1 - e) \frac{\partial^2 \psi}{\partial y^2} S_{xy}. \quad (6.31)$$

From Eqs. (6.29) – (6.31), we write

$$S_{xy} = \frac{\xi}{\mu} \left[ \frac{\partial^2 \psi}{\partial y^2} - We^2(1 - e^2) \left( \frac{\partial^2 \psi}{\partial y^2} \right)^3 \right], \quad (6.32)$$

and thus Eq. (6.24) takes the form

$$\frac{\partial^3 \psi}{\partial y^3} - \alpha_1 We^2(1 - e^2) \frac{\partial}{\partial y} \left[ \left( \frac{\partial^2 \psi}{\partial y^2} \right)^3 \right] = \frac{dp}{dx}, \quad (6.33)$$

where  $\alpha_1 = \frac{\gamma_1}{1+\gamma_1}$  and  $\gamma_1 = \frac{\xi}{\mu}$ .

The conditions for the dimensionless stream function in wave frame are [27]

$$\psi = \frac{F}{2}, \quad \frac{\partial \psi}{\partial y} = -1, \quad \text{at } y = h_1(x), \quad (6.34)$$

$$\psi = -\frac{F}{2}, \quad \frac{\partial \psi}{\partial y} = -1, \quad \text{at } y = h_2(x), \quad (6.35)$$

where

$$F = \int_{h_2(x)}^{h_1(x)} \frac{\partial \psi}{\partial y} dy = \psi(h_1(x)) - \psi(h_2(x)). \quad (6.36)$$

## 6.4 Solution scheme

The resulting equation (6.26) is highly non-linear. It seems difficult to find exact solution of this equation. Therefore our interest now is to obtain the series solution for small Weissenberg parameter  $We^2$ . Hence we expand  $\psi$ ,  $\theta$ ,  $S_{xy}$ ,  $p$  and  $F$  in the forms

$$\begin{aligned} \psi &= \psi_0 + (We^2)\psi_1 + \dots, \\ \theta &= \theta_0 + (We^2)\theta_1 + \dots, \\ S_{xy} &= S_{0xy} + (We^2)S_{1xy} + \dots, \\ p &= p_0 + (We^2)p_1 + \dots, \\ F &= F_0 + (We^2)F_1 + \dots \end{aligned} \quad (6.37)$$

Substituting Eqs. (6.37) into Eqs. (6.22), (6.23), (6.26), (6.27) and (6.32)-(6.35) and then collecting the terms of like powers of  $(We^2)$  we can write the following systems.

#### 6.4.1 Zeroth order system

$$\frac{\partial^4 \psi_0}{\partial y^4} = 0, \quad (6.38)$$

$$\frac{\partial^2 \theta_0}{\partial y^2} + \gamma_1 Br \left( \frac{\partial^2 \psi_0}{\partial y^2} \right)^2 = 0, \quad (6.39)$$

$$\frac{dp_0}{dx} = \frac{\partial^3 \psi_0}{\partial y^3}, \quad (6.40)$$

$$\psi_0 = \frac{F_0}{2}, \quad \frac{\partial \psi_0}{\partial y} = -1, \quad \frac{\partial \theta_0}{\partial y} + Bi_1(\theta_0 - 1) = 0, \quad \text{at } y = h_1(x), \quad (6.41)$$

$$\psi_0 = \frac{-F_0}{2}, \quad \frac{\partial \psi_0}{\partial y} = -1, \quad \frac{\partial \theta_0}{\partial y} + Bi_2 \theta_0 = 0, \quad \text{at } y = h_2(x). \quad (6.42)$$

#### 6.4.2 First order system

$$\frac{\partial^4 \psi_1}{\partial y^4} - \alpha_1(1 - e^2) \frac{\partial^2}{\partial y^2} \left( \frac{\partial^2 \psi_0}{\partial y^2} \right)^3 = 0, \quad (6.43)$$

$$\frac{\partial^2 \theta_1}{\partial y^2} + \gamma_1 Br \left[ 2 \frac{\partial^2 \psi_0}{\partial y^2} \frac{\partial^2 \psi_1}{\partial y^2} - (1 - e^2) \left( \frac{\partial^2 \psi_0}{\partial y^2} \right)^4 \right] = 0, \quad (6.44)$$

$$\frac{dp_1}{dx} = \frac{\partial^3 \psi_1}{\partial y^3} - \alpha_1(1 - e^2) \frac{\partial}{\partial y} \left( \frac{\partial^2 \psi_0}{\partial y^2} \right)^3, \quad (6.45)$$

$$\psi_1 = \frac{F_1}{2}, \quad \frac{\partial \psi_1}{\partial y} = 0, \quad \frac{\partial \theta_1}{\partial y} + Bi_1 \theta_1 = 0, \quad \text{at } y = h_1(x), \quad (6.46)$$

$$\psi_1 = \frac{-F_1}{2}, \quad \frac{\partial \psi_1}{\partial y} = 0, \quad \frac{\partial \theta_1}{\partial y} + Bi_2 \theta_1 = 0, \quad \text{at } y = h_2(x). \quad (6.47)$$

The next two subsections will develop the solutions of zeroth and first order systems.

### 6.4.3 Zeroth order solution

The solutions of Eqs. (6.39) and (6.40) satisfying the boundary conditions (6.41) and (6.42) are

$$\psi_0 = C_{01}y^3 + C_{02}y^2 + C_{03}y + C_{04}, \quad (6.48)$$

$$\theta_0 = B_{01}y^4 + B_{02}y^3 + B_{03}y^2 + B_{04}y + B_{05}, \quad (6.49)$$

where

$$C_{01} = \frac{-2(F_0 + h_1 - h_2)}{(h_1 - h_2)^3},$$

$$C_{02} = \frac{3(F_0 + h_1 - h_2)(h_1 + h_2)}{(h_1 - h_2)^3},$$

$$C_{03} = \frac{-h_1^3 - 6F_0h_1h_2 - 3h_1^2h_2 + 3h_1h_2^2 + h_2^3}{(h_1 - h_2)^3},$$

$$C_{04} = \frac{-(h_1 + h_2)(2h_1h_2(-h_1 + h_2) + F_0(h_1^2 - 4h_1h_2 + h_2^2))}{2(h_1 - h_2)^3},$$

$$D = (Bi_2 + Bi_1(-1 + Bi_2(h_1 - h_2))),$$

$$B_{01} = -3\gamma_1 Br C_{01}^2, \quad B_{02} = -4\gamma_1 Br C_{01} C_{02}, \quad B_{03} = -2\gamma_1 Br C_{02}^2,$$

$$B_{04} = \frac{1}{D} [4Bi_2 Br h_1 (C_{02}^2 + 3C_{01} C_{02} h_1 + 3C_{01}^2 h_1^2) \gamma_1 + Bi_1 \{ -4Br h_2 (C_{02}^2 + 3C_{01} C_{02} h_2 + 3C_{01}^2 h_2^2) \gamma_1 \\ + Bi_2 (1 + Br (2C_{02}^2 (h_1^2 - h_2^2) + 4C_{01} C_{02} (h_1^3 - h_2^3) + 3C_{01}^2 (h_1^2 - h_2^2)) \gamma_1) \}],$$

$$B_{05} = -\frac{1}{D} [Br \{ 4C_{01} C_{02} (3h_1^2 (1 + Bi_2 h_2) - h_2^2 (3 + Bi_2 h_2)) + 3C_{01}^2 (4h_1^3 (1 + Bi_2 h_2) \\ - h_2^3 (4 + Bi_2 h_2)) + C_{02}^2 (-2h_2 (2 + Bi_2 h_2) + 4(h_1 + Bi_2 h_1 h_2)) \} \gamma_1 \\ + Bi_1 \{ 1 + Br h_1 (2C_{02}^2 (h_1 - 2h_2) + 4C_{01} C_{02} (h_1^2 - 3h_2^2) + 3C_{01}^2 (h_1^3 - 4h_2^3)) \gamma_1 \\ + Bi_2 h_2 (1 + Br h_1 (h_1 - h_2) (2C_{02}^2 + 4C_{01} C_{02} (h_1 + h_2) + 3C_{01}^2 (h_1^2 + h_1 h_2 + h_2^2)) \gamma_1) \}].$$

Expressions of longitudinal velocity and pressure gradient are

$$u_0 = 3C_{01}y^2 + 2C_{02}y + C_{03}, \quad (6.50)$$

$$\frac{dp_0}{dx} = 6C_{01}. \quad (6.51)$$

The non-dimensional pressure rise per wavelength ( $\Delta P_{\lambda_0}$ ) can be put into the form

$$\Delta P_{\lambda_0} = \int_0^{2\pi} \frac{dp_0}{dx} dx. \quad (6.52)$$

It is worth mentioning to note that the solution expressions at this order correspond to the Newtonian fluid.

#### 6.4.4 First order solution

Substituting Eqs. (6.48) and (6.49) into Eqs. (6.43 – 6.45), solving the resulting equations and then applying the corresponding boundary conditions we get the solutions for  $\psi_1$ ,  $u_1$ ,  $dp_1/dx$  and  $\theta_1$  in the forms presented below:

$$\psi_1 = C_{11}y^5 + C_{12}y^4 + C_{13}y^3 + C_{14}y^2 + C_{15}y + C_{16}, \quad (6.53)$$

$$u_1 = 5C_{11}y^4 + 4C_{12}y^3 + 3C_{13}y^2 + 2C_{14}y + C_{15}, \quad (6.54)$$

$$\theta_1 = B_{11}y^6 + B_{12}y^5 + B_{13}y^4 + B_{14}y^3 + B_{15}y^2 + B_{16}y + B_{17}, \quad (6.55)$$

$$\frac{dp_1}{dx} = - \left( \frac{12F_1}{(h_1 - h_2)^3} + 3(h_1 - h_2)^2 C_{11} \right), \quad (6.56)$$

where

$$\begin{aligned}
C_{11} &= -\frac{54}{5}(e^2 - 1)C_{01}^3\alpha_1, \\
C_{12} &= -18(e^2 - 1)C_{01}^2C_{02}\alpha_1, \\
C_{13} &= \frac{2}{5}\left[\frac{5F_1}{(h_2 - h_1)^3} + 9(e^2 - 1)C_{01}^2(10C_{02}(h_1 + h_2) + 3C_{01}(3h_1^2 + 4h_1h_2 + 3h_2^2))\alpha_1\right], \\
C_{14} &= \frac{3}{5(h_1 - h_2)^3}[5F_1(h_1 + h_2) - 6(e^2 - 1)C_{01}^2(h_1 - h_2)^3(6C_{01}(h_1 + h_2)(h_1^2 + 3h_1h_2 + h_2^2) \\
&\quad 5C_{02}(h_1^2 + 4h_1h_2 + h_2^2))\alpha_1], \\
C_{15} &= \frac{6}{5}h_1h_2\left[\frac{5F_1}{(h_2 - h_1)^3} + 3(e^2 - 1)C_{01}^2(10C_{02}(h_1 + h_2) + 3C_{01}(4h_1^2 + 7h_1h_2 + 4h_2^2))\alpha_1\right], \\
C_{16} &= -\frac{F_1(h_1 + h_2)(h_1^2 - 4h_1h_2 + h_2^2)}{2(h_2 - h_1)^3}, \\
B_{11} &= -\frac{8}{5}BrC_{01}(27(e^2 - 1)C_{01}^3 + 5C_{11})\gamma_1, \\
B_{12} &= -\frac{4}{5}Br(108(e^2 - 1)C_{01}^3C_{02} + 5C_{02}C_{11} + 9C_{01}C_{12})\gamma_1, \\
B_{13} &= -2Br(36(e^2 - 1)C_{01}^2C_{02}^2 + 2C_{02}C_{12} + 3C_{01}C_{13})\gamma_1, \\
\\
B_{14} &= -4Br(C_{02}C_{13} + C_{01}(8(e^2 - 1)C_{02}^3 + C_{14}))\gamma_1, \\
B_{15} &= -4BrC_{02}(2(e^2 - 1)C_{02}^3 + C_{14})\gamma_1, \\
B_{16} &= \frac{1}{5D}[2Br\gamma_1\{-2Bi_1h_2(20(e^2 - 1)C_{02}^4 + 120(e^2 - 1)C_{01}C_{02}^3h_2 + 360(e^2 - 1)C_{01}^2C_{02}^2h_2^2 \\
&\quad + 3C_{01}h_2(5C_{14} + h_2(10C_{13} + h_2(15C_{12} + 4(27(e^2 - 1)C_{01}^3 + 5C_{11})h_2)))) + 5C_{02} \\
&\quad \times (2C_{14} + h_2(3C_{13} + h_2(4C_{12} + (108(e^2 - 1)C_{01}^3 + 5C_{11})h_2)))) + Bi_2(20(e^2 - 1)C_{02}^4 \\
&\quad \times (h_1(2 + Bi_1h_1) - Bi_1h_2^2) + 80(e^2 - 1)C_{01}C_{02}^3(h_1^2(3 + Bi_1h_1) - Bi_1h_2^3) + 180(e^2 - 1) \\
&\quad \times C_{01}^2C_{02}^2(h_1^3(4 + Bi_1h_1) - Bi_1h_2^4) + 2C_{02}(5C_{14}h_1(2 + Bi_1h_1) + 5C_{13}h_1^2(3 + Bi_1h_1) \\
&\quad + 5C_{12}h_1^3(4 + Bi_1h_1) - 5Bi_1C_{14}h_2^2 - 5Bi_1C_{13}h_2^3 - 5Bi_1C_{12}h_2^4 + (108(e^2 - 1)C_{01}^3 + 5C_{11}) \\
&\quad \times (h_1^4(5 + Bi_1h_1) - Bi_1h_2^5)) - C_{01}(10C_{14}(h_1^2(3 + Bi_1h_1) - Bi_1h_2^3) + 15C_{13}(h_1^3(4 + Bi_1h_1) \\
&\quad - Bi_1h_2^4) + 2(9C_{12}h_1^4(5 + Bi_1h_1) - 9Bi_1C_{12}h_2^5) + 2(27(e^2 - 1)C_{01}^3 + 5C_{11}) \\
&\quad \times (h_1^5(6 + Bi_1h_1) - Bi_1h_2^6))\}]\gamma_1,
\end{aligned}$$

$$\begin{aligned}
B_{17} = & -\frac{2Br\gamma_1}{5D}[80(e^2-1)C_{01}C_{02}^3(h_1^2(3+Bi_1h_1)+Bi_2h_1^2(3+Bi_1h_1)h_2-3(1+Bi_1h_1)h_2^2 \\
& -Bi_2(1+Bi_1h_1)h_2^3+180(e^2-1)C_{01}^2C_{02}^2(h_1^3(4+Bi_1h_1)+Bi_2h_1^3(4+Bi_1h_1)h_2 \\
& -4(1+Bi_1h_1)h_2^3-Bi_2(1+Bi_1h_1)h_2^4)+20(e^2-1)C_{02}^4(Bi_1h_1^2(1+Bi_2h_2) \\
& -h_2(2+Bi_2h_2)+h_1(2+2Bi_2h_2-Bi_1h_2(2+Bi_2h_2))) + C_{01}(10C_{14} \\
& \times(h_1^2(3+Bi_1h_1)+Bi_2h_1^2(3+Bi_1h_1)h_2-3(1+Bi_1h_1)h_2^2-Bi_2(1+Bi_1h_1)h_2^3) \\
& +15C_{13}(h_1^3(4+Bi_1h_1)+Bi_2h_1^3(4+Bi_1h_1)h_2-4(1+Bi_1h_1)h_2^3-Bi_2(1+Bi_1h_1)h_2^4) \\
& +2(9C_{12}(h_1^4(5+Bi_1h_1)+Bi_2h_1^4(5+Bi_1h_1)h_2-5(1+Bi_1h_1)h_2^4-Bi_2(1+Bi_1h_1)h_2^5) \\
& +2(27(e^2-1)C_{01}^3+5C_{11})(h_1^5(6+Bi_1h_1)+Bi_2h_1^5(6+Bi_1h_1)h_2-6(1+Bi_1h_1)h_2^5 \\
& -Bi_2(1+Bi_1h_1)h_2^6))) + 2C_{02}(5C_{13}(h_1^2(3+Bi_1h_1)+Bi_2h_1^2(3+Bi_1h_1)h_2 \\
& -3(1+Bi_1h_1)h_2^2-Bi_2(1+Bi_1h_1)h_2^3+5C_{12}(h_1^3(4+Bi_1h_1)+Bi_2h_1^3(4+Bi_1h_1)h_2 \\
& -4(1+Bi_1h_1)h_2^3-Bi_2(1+Bi_1h_1)h_2^4)+(108(e^2-1)C_{01}^3+5C_{11})(h_1^4(5+Bi_1h_1) \\
& +Bi_2h_1^4(5+Bi_1h_1)h_2-5(1+Bi_1h_1)h_2^4-Bi_2(1+Bi_1h_1)h_2^5)+5C_{14}(Bi_1h_1^2(1+Bi_2h_2) \\
& -h_2(2+Bi_2h_2)+h_1(2+2Bi_2h_2-Bi_1h_2(2+Bi_2h_2))))].
\end{aligned}$$

The pressure rise per wavelength at this order ( $\Delta P_{\lambda_1}$ ) is

$$\Delta P_{\lambda_1} = \int_0^{2\pi} \frac{dp_1}{dx} dx. \quad (6.57)$$

The perturbation expressions of  $\psi$ ,  $\theta$ ,  $\Delta P_\lambda$  and  $dp/dx$  upto  $O(We^2)^1$  are

$$\begin{aligned}
\psi &= \psi_0 + (We^2)\psi_1. \\
\theta &= \theta_0 + (We^2)\theta_1. \\
\frac{dp}{dx} &= \frac{dp_0}{dx} + (We^2)\frac{dp_1}{dx}. \\
\Delta P_\lambda &= \Delta P_{\lambda_0} + (We^2)\Delta P_{\lambda_1}.
\end{aligned} \quad (6.58)$$

## 6.5 Discussion

### 6.5.1 Pumping characteristics

In this subsection the developed series solutions in the flow of the Johnson-Segalman fluid model are illustrated in the Figs. 6.1 – 6.14. In order to see the effects of emerging parameters  $We$ ,  $\gamma_1$ ,  $e$ ,  $\phi$ ,  $a$ ,  $b$  and  $d$  on axial pressure gradient  $dp/dx$ , we have plotted Figs. 6.1 – 6.7. It can be clearly seen from these Figs. that axial pressure gradient decreases for increasing values of Weissenberg number  $We$ , viscosity ratio parameter  $\gamma_1$ , phase difference  $\phi$  and channel width  $d$  whereas it increases by increasing the values of slip parameter  $e$ , upper wave amplitude  $a$  and lower wave amplitude  $b$ . Fig. 6.1 indicates that the pressure gradient is larger for Newtonian fluid ( $We = 0$ ) in comparison to that of Johnson-Segalman fluid ( $0 < We < 1$ ). Figs. 6.8 – 6.14 are prepared for the pressure rise  $\Delta p_\lambda$  per wavelength against volume flow rate  $\Theta$  for different values of  $We$ ,  $\gamma_1$ ,  $e$ ,  $\phi$ ,  $d$ ,  $b$  and  $a$  respectively. It is observed from these Figs. that with increase in  $We$ ,  $\gamma_1$ ,  $\phi$  and  $d$  the pressure rise per wavelength  $\Delta p_\lambda$  increases, while  $\Delta p_\lambda$  decreases by increasing  $e$ ,  $b$  and  $a$ . Moreover, pressure rise within one wavelength  $\Delta p_\lambda$  gives larger values for small volume flow rate (peristaltic pumping occurs in the region  $-1 < \Theta < 1$ ) and it gives smaller values for large  $\Theta$  i.e., augmented pumping occurs in the region  $1 < \Theta < 3$  (see Figs. 6.8, 6.9, 6.11 and 6.12) whereas it has opposite behavior in Figs. 6.10, 6.13 and 6.14.

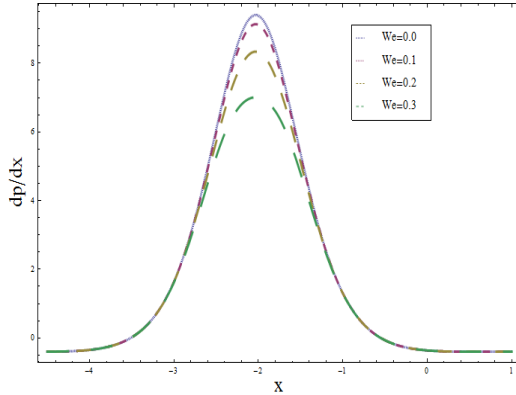


Fig. 6.1

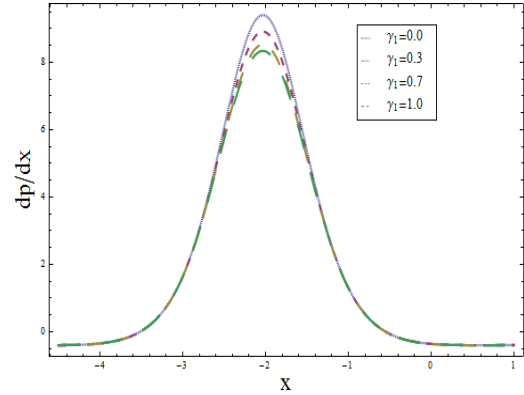


Fig. 6.2

Fig. 6.1: Pressure gradient  $dp/dx$  versus  $x$  for  $We$  when  $a = 0.5$ ,  $b = 0.7$ ,  $d = 1.2$ ,  $\gamma_1 = 1$ ,  $e = 0.8$ ,  $\phi = \pi/4$  and  $\Theta = 0.1$ .



Fig. 6.2: Pressure gradient  $dp/dx$  versus  $x$  for  $\gamma_1$  when  $a = 0.5$ ,  $b = 0.7$ ,  $d = 1.2$ ,  $e = 1$ ,  $We = 0.2$ ,  $\phi = \pi/4$  and  $\Theta = 0.1$ .

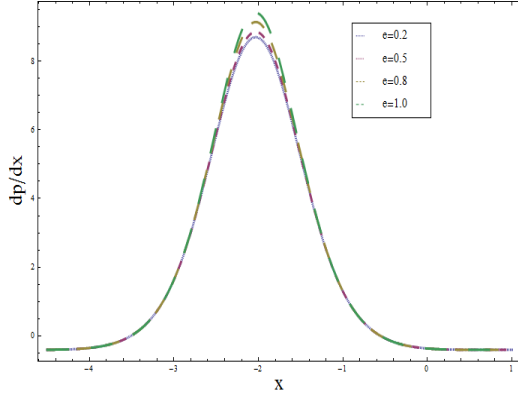


Fig. 6.3

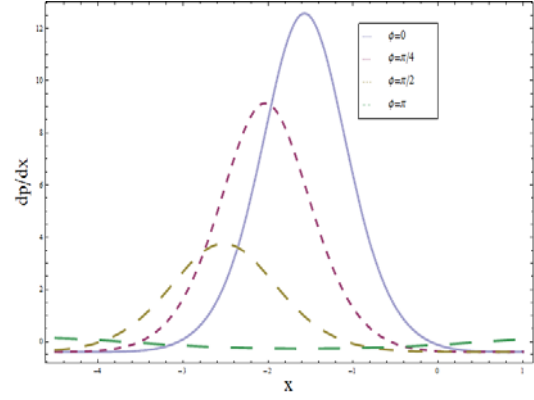


Fig. 6.4

Fig. 6.3: Pressure gradient  $dp/dx$  versus  $x$  for  $e$  when  $a = 0.5$ ,  $b = 0.7$ ,  $d = 1.2$ ,  $We = 0.1$ ,  $\phi = \pi/4$ ,  $\gamma_1 = 1$  and  $\Theta = 0.1$ .

Fig. 6.4: Pressure gradient  $dp/dx$  versus  $x$  for  $\phi$  when  $a = 0.5$ ,  $b = 0.7$ ,  $d = 1.2$ ,  $We = 0.1$ ,  $\gamma_1 = 1$ ,  $e = 0.8$  and  $\Theta = 0.1$ .

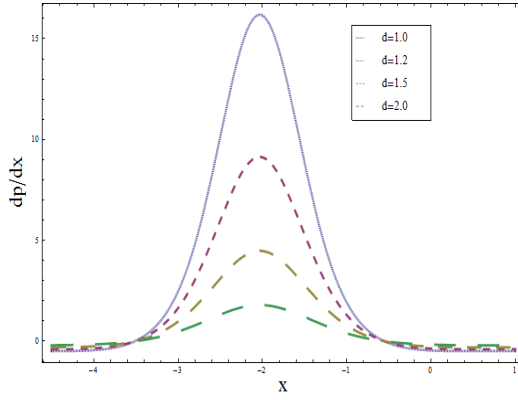


Fig. 6.5

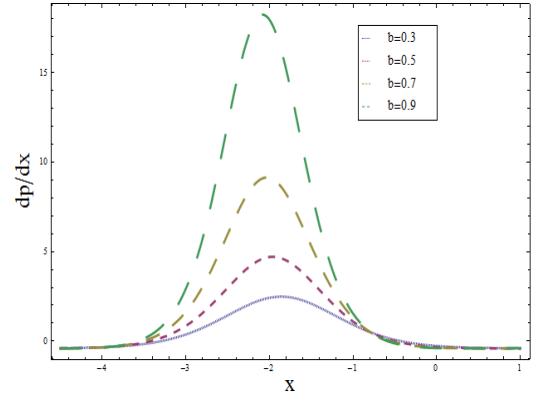


Fig. 6.6

Fig. 6.5: Pressure gradient  $dp/dx$  versus  $x$  for  $d$  when  $a = 0.5$ ,  $b = 0.7$ ,  $\phi = \pi/4$ ,  $\gamma_1 = 1$ ,  $We = 0.1$ ,  $e = 0.8$  and  $\Theta = 0.1$ .

Fig. 6.6: Pressure gradient  $dp/dx$  versus  $x$  for  $b$  when  $a = 0.5$ ,  $d = 1.2$ ,  $\phi = \pi/4$ ,  $\gamma_1 = 1$ ,  $We = 0.1$ ,  $e = 0.8$  and  $\Theta = 0.1$ .

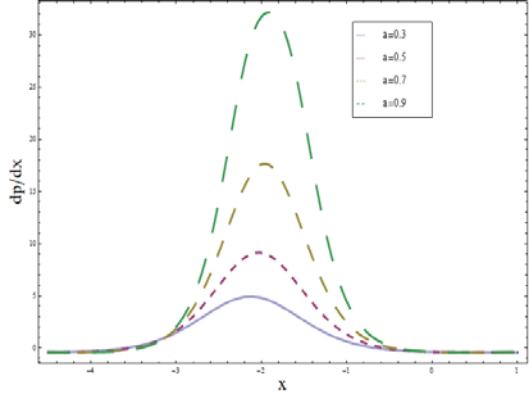


Fig. 6.7

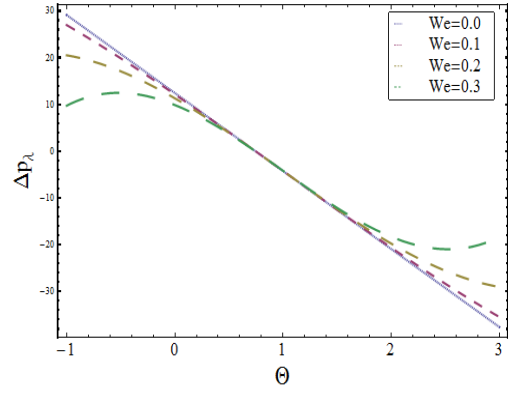


Fig. 6.8

Fig. 6.7: Pressure gradient  $dp/dx$  versus  $x$  for  $a$  when  $b = 0.7$ ,  $d = 1.2$ ,  $\phi = \pi/4$ ,  $\gamma_1 = 1$ ,  $We = 0.1$ ,  $e = 0.8$  and  $\Theta = 0.1$ .

Fig. 6.8:  $\Delta p_\lambda$  versus  $\Theta$  for  $We$  when  $a = 0.5$ ,  $b = 0.7$ ,  $d = 1.2$ ,  $\gamma_1 = 1$ ,  $e = 0.8$  and  $\phi = \pi/4$ .

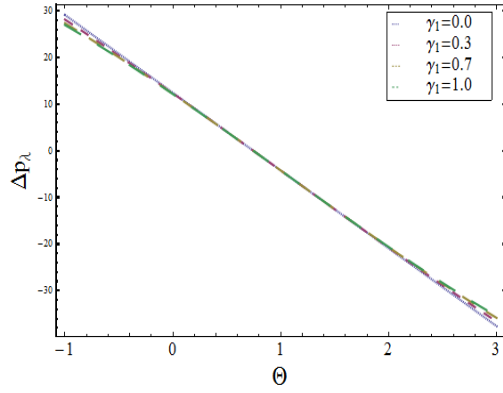


Fig. 6.9

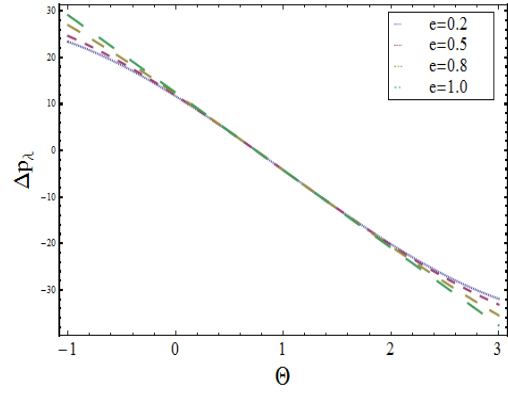


Fig. 6.10

Fig. 6.9:  $\Delta p_\lambda$  versus  $\Theta$  for  $\gamma_1$  when  $a = 0.5$ ,  $b = 0.7$ ,  $d = 1.2$ ,  $We = 0.1$ ,  $e = 0.8$  and  $\phi = \pi/4$ .

Fig. 6.10:  $\Delta p_\lambda$  versus  $\Theta$  for  $e$  when  $a = 0.5$ ,  $b = 0.7$ ,  $d = 1.2$ ,  $\gamma_1 = 1$ ,  $We = 0.1$  and  $\phi = \pi/4$ .

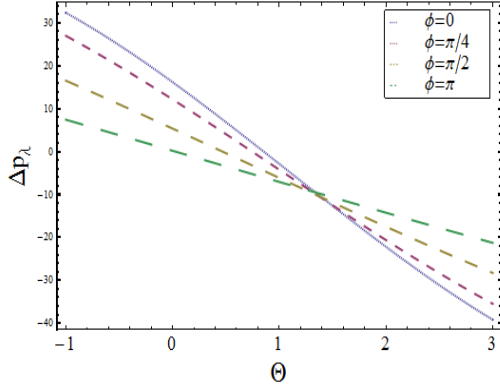


Fig. 6.11

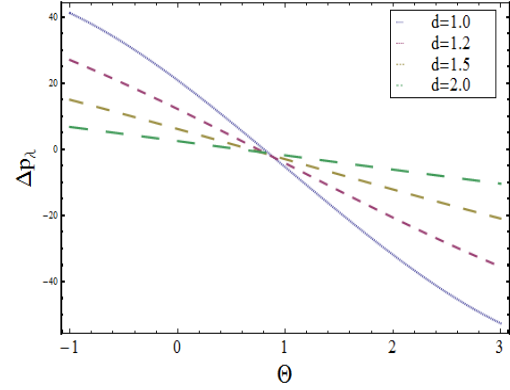


Fig. 6.12

Fig. 6.11:  $\Delta p_\lambda$  versus  $\Theta$  for  $\phi$  when  $a = 0.5$ ,  $b = 0.7$ ,  $d = 1.2$ ,  $\gamma_1 = 1$ ,  $e = 0.8$  and  $We = 0.1$ .

Fig. 6.12:  $\Delta p_\lambda$  versus  $\Theta$  for  $d$  when  $a = 0.5$ ,  $b = 0.7$ ,  $We = 0.1$ ,  $\gamma_1 = 1$ ,  $e = 0.8$  and  $\phi = \pi/4$ .

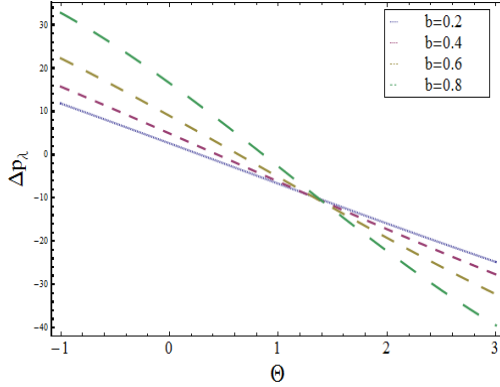


Fig. 6.13

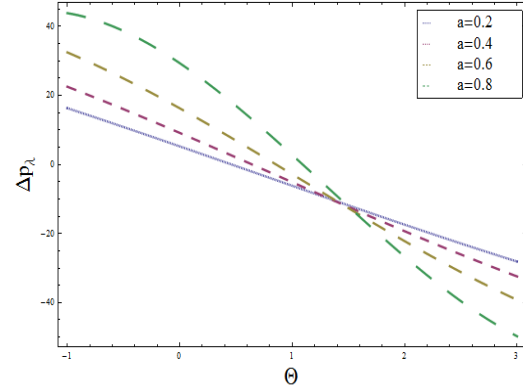


Fig. 6.14

Fig. 6.13:  $\Delta p_\lambda$  versus  $\Theta$  for  $b$  when  $a = 0.5$ ,  $d = 1.2$ ,  $We = 0.1$ ,  $\gamma_1 = 1$ ,  $e = 0.8$  and  $\phi = \pi/4$ .

Fig. 6.14:  $\Delta p_\lambda$  versus  $\Theta$  for  $a$  when  $b = 0.7$ ,  $d = 1.2$ ,  $We = 0.1$ ,  $\gamma_1 = 1$ ,  $e = 0.8$  and  $\phi = \pi/4$ .

### 6.5.2 Velocity behavior

This subsection addresses the behavior of velocity profile through Figs. 6.15 – 6.17. It is observed that with the increase in  $We$  and  $\gamma_1$  the velocity profile decreases in the narrow part of the channel. However the velocity increases in the wider part of the channel (see Figs. 6.15 and 6.16). Opposite behavior is noted in Fig. 6.17 for different values of  $e$ .

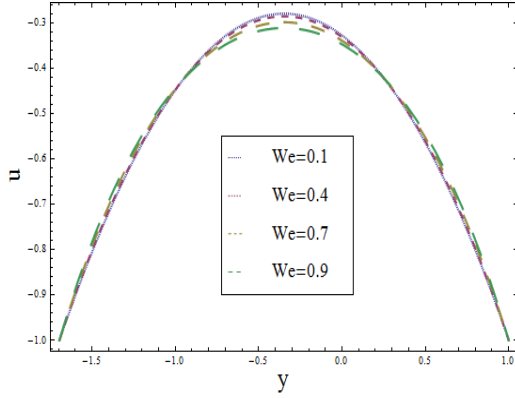


Fig. 6.15

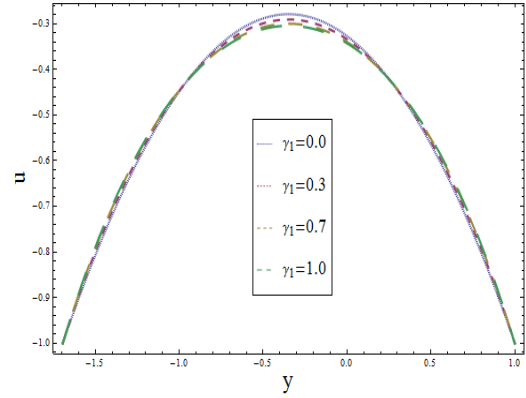


Fig. 6.16

Fig. 6.15: Velocity profile  $u$  for  $We$  when  $a = 0.5$ ,  $b = 0.7$ ,  $d = 1.2$ ,  $\phi = \pi/4$ ,  $e = 0.2$ ,  $\gamma_1 = 1$ ,  $\Theta = 0.8$  and  $x = 0$ .

Fig. 6.16: Velocity profile  $u$  for  $\gamma_1$  when  $a = 0.5$ ,  $b = 0.7$ ,  $d = 1.2$ ,  $\phi = \pi/4$ ,  $e = 0.2$ ,  $We = 0.8$ ,  $\Theta = 0.8$  and  $x = 0$ .

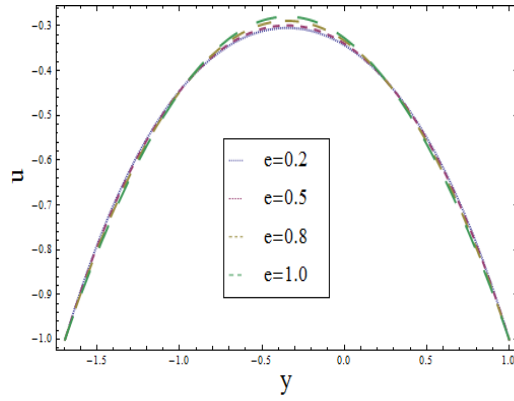


Fig. 6.17

Fig. 6.17: Velocity profile  $u$  for  $e$  when  $a = 0.5$ ,  $b = 0.7$ ,  $d = 1.2$ ,  $\phi = \pi/4$ ,  $We = 0.8$ ,  $\gamma_1 = 1$ ,  $\Theta = 0.8$  and  $x = 0$ .

### 6.5.3 Temperature profile

Here the effects of various emerging parameters on the temperature profile  $\theta$  are discussed. Figs. 6.18 and 6.22 show a decrease in the fluid temperature due to the increase in Weissenberg number  $We$  and Biot number  $Bi_1$  (due to the convective condition at the upper wall) respectively. It is worth mentioning to point out that the fluid temperature  $\theta$  generally increases when the values of viscosity ratio parameter  $\gamma_1$ , the slip parameter  $e$ , Brinkman number  $Br$  and the Biot number  $Bi_2$  (due to the convective condition at the lower wall) are increased (see Figs. 6.19 – 6.21 and 6.23).

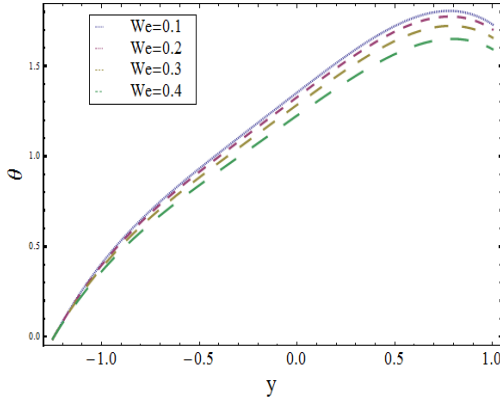


Fig. 6.18

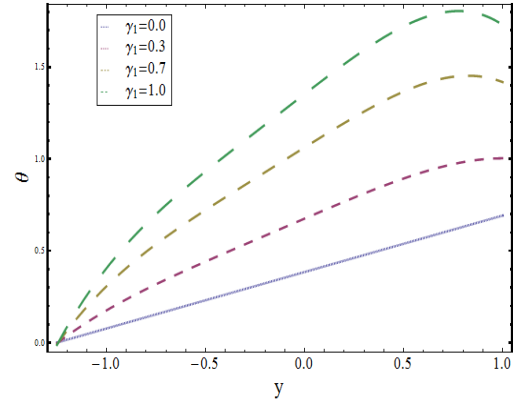


Fig. 6.19

Fig. 6.18: Temperature profile  $\theta$  for  $We$  when  $a = 0.3$ ,  $b = 0.5$ ,  $d = 1$ ,  $\phi = \pi/4$ ,  $\Theta = 1.5$ ,  $x = 0$ ,  $e = 0.8$ ,  $Br = 1$ ,  $\gamma_1 = 1$ ,  $Bi_1 = 1$  and  $Bi_2 = 10$ .

Fig. 6.19: Temperature profile  $\theta$  for  $\gamma_1$  when  $a = 0.3$ ,  $b = 0.5$ ,  $d = 1$ ,  $\phi = \pi/4$ ,  $\Theta = 1.5$ ,  $x = 0$ ,  $e = 0.8$ ,  $Br = 1$ ,  $We = 0.1$ ,  $Bi_1 = 1$  and  $Bi_2 = 10$ .

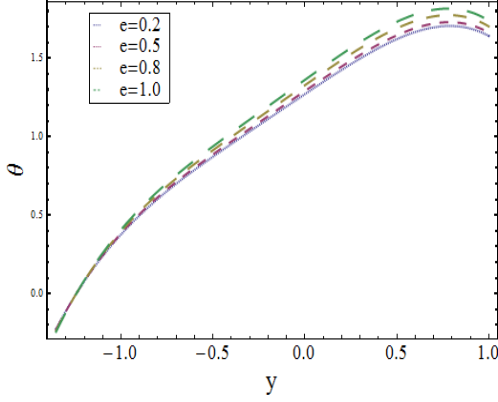


Fig. 6.20

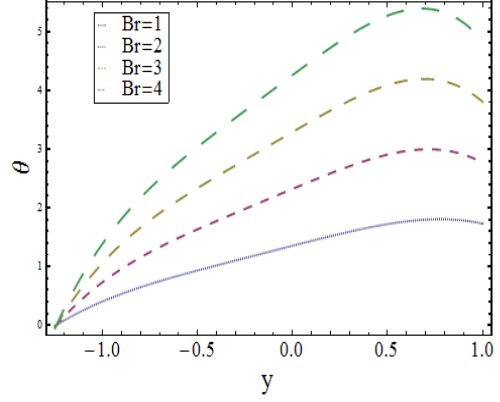


Fig. 6.21

Fig. 6.20: Temperature profile  $\theta$  for  $e$  when  $a = 0.3$ ,  $b = 0.5$ ,  $d = 1$ ,  $\phi = \pi/4$ ,  $\Theta = 1.5$ ,  $x = 0$ ,  $We = 0.2$ ,  $Br = 1$ ,  $\gamma_1 = 1$ ,  $Bi_1 = 1$  and  $Bi_2 = 10$ .

Fig. 6.21: Temperature profile  $\theta$  for  $Br$  when  $a = 0.3$ ,  $b = 0.5$ ,  $d = 1$ ,  $\phi = \pi/4$ ,  $\Theta = 1.5$ ,  $x = 0$ ,  $e = 0.8$ ,  $We = 0.1$ ,  $\gamma_1 = 1$ ,  $Bi_1 = 1$  and  $Bi_2 = 10$ .

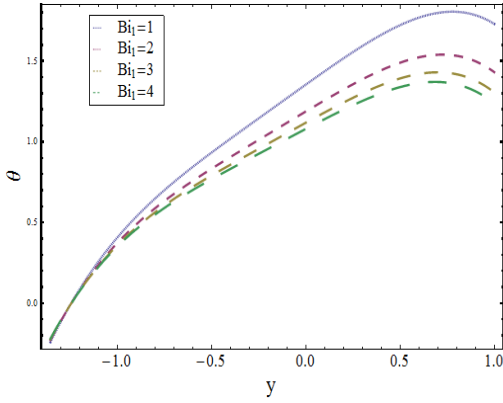


Fig. 6.22

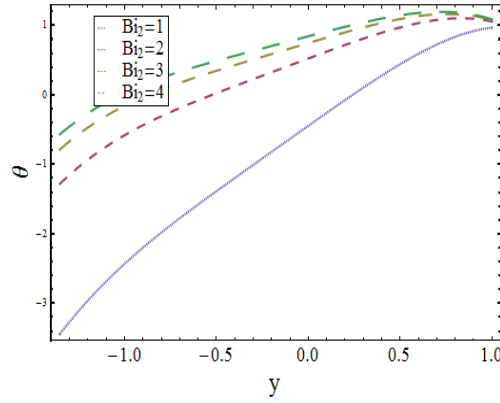


Fig. 6.23

Fig. 6.22: Temperature profile  $\theta$  for  $Bi_1$  when  $a = 0.3$ ,  $b = 0.5$ ,  $d = 1$ ,  $\phi = \pi/4$ ,  $\Theta = 1.5$ ,  $x = 0$ ,  $e = 0.8$ ,  $Br = 1$ ,  $\gamma_1 = 1$ ,  $We = 0.1$  and  $Bi_2 = 10$ .

Fig. 6.23: Temperature profile  $\theta$  for  $Bi_2$  when  $a = 0.3$ ,  $b = 0.5$ ,  $d = 1$ ,  $\phi = \pi/4$ ,  $\Theta = 1.5$ ,  $x = 0$ ,  $e = 0.8$ ,  $Br = 1$ ,  $\gamma_1 = 1$ ,  $Bi_1 = 10$  and  $We = 0.1$ .

#### 6.5.4 Trapping

In general the shape of streamlines is similar to that of a boundary wall in the wave frame due to stationary walls. Nevertheless, some streamlines split and enclose a bolus under certain conditions and this bolus moves as a whole with the wave. This phenomenon is known as trapping. Figs. 6.24 and 6.25 show the streamlines for three different values of  $We$  and viscosity ratio parameter  $\gamma_1$ . The streamlines near the channel walls strictly follow the wall waves, which are mainly generated by the relative movement of the walls. A bolus is formed in the center region. These Figs. reveal that by increasing the values of  $We$  and  $\gamma_1$  the size of the trapping bolus decreases. Fig. 6.26 gives the sketch of the streamlines for various values of the slip parameter  $e$ . It is noticed that the size of the trapping bolus increases with an increase in the slip parameter  $e$ .

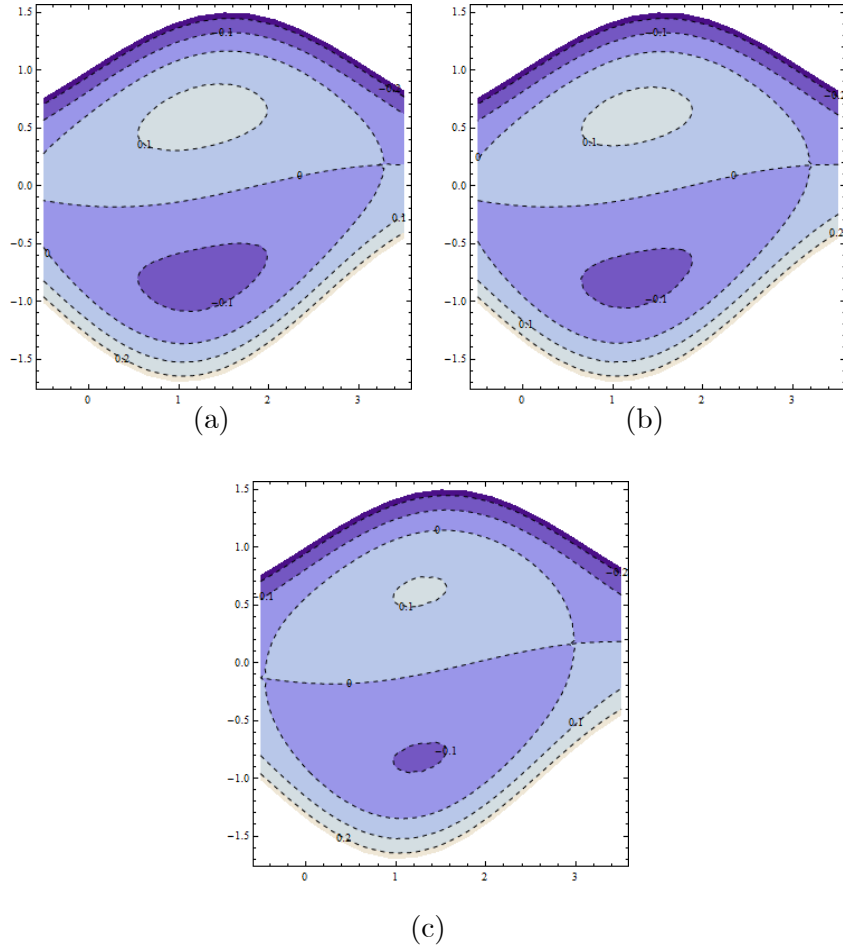


Fig. 6.24: Streamlines for (a)  $We = 0.1$ , (b)  $We = 0.5$ , (c)  $We = 0.9$ . The other parameters are chosen as  $a = 0.5$ ,  $b = 0.7$ ,  $d = 1$ ,  $\phi = \pi/6$ ,  $\gamma_1 = 1$ ,  $e = 0.8$  and  $\Theta = 1.5$ .



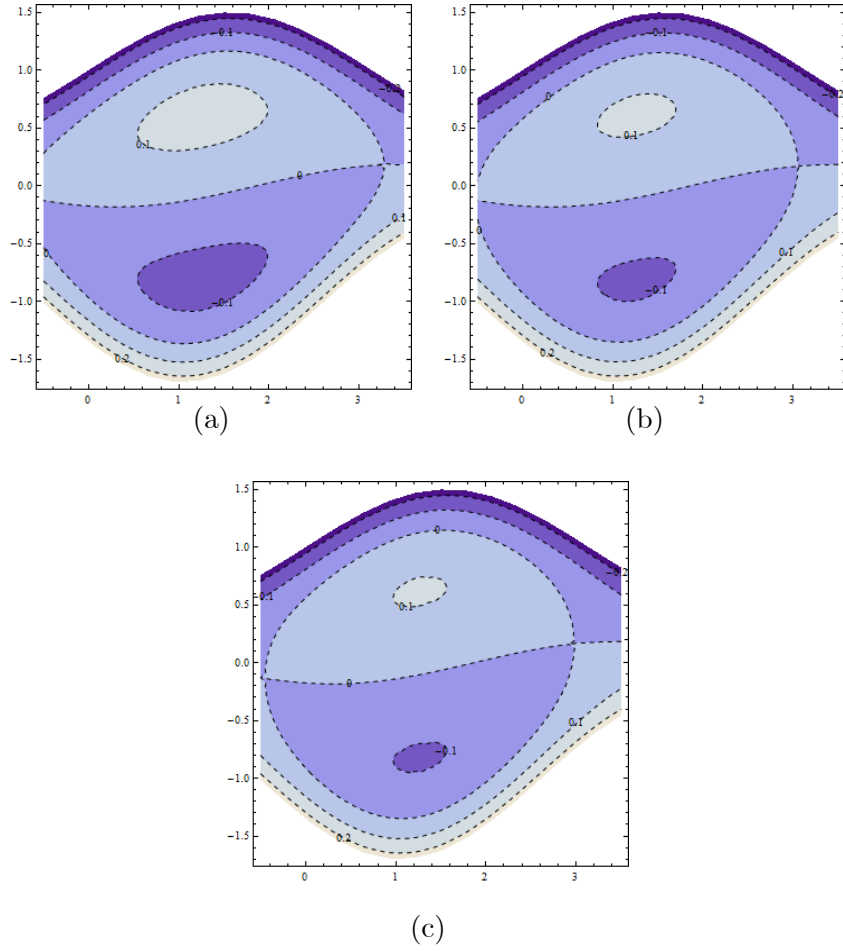


Fig. 6.25: Streamlines for (a)  $\gamma_1 = 0$ , (b)  $\gamma_1 = 0.6$ , (c)  $\gamma_1 = 1$ . The other parameters are chosen as  $a = 0.5$ ,  $b = 0.7$ ,  $d = 1$ ,  $\phi = \pi/6$ ,  $We = 0.9$ ,  $e = 0.8$  and  $\Theta = 1.5$ .

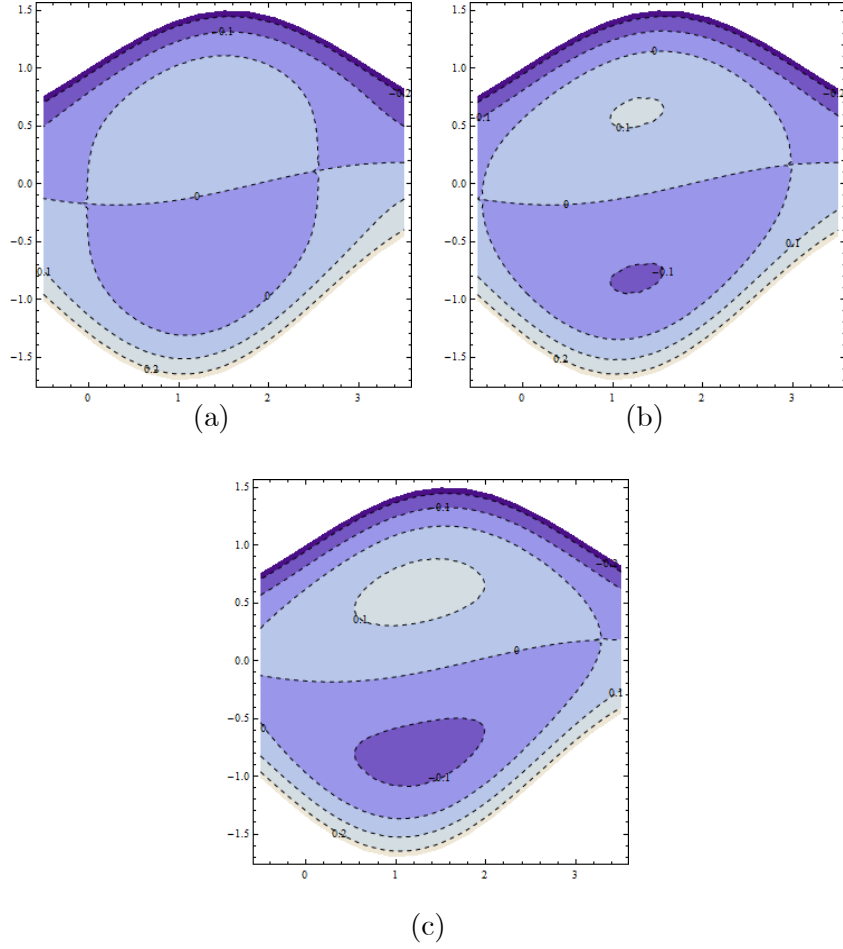


Fig. 6.26: Streamlines for (a)  $e = 0.3$ , (b)  $e = 0.8$ , (c)  $e = 1$ . The other parameters are chosen as  $a = 0.5$ ,  $b = 0.7$ ,  $d = 1$ ,  $\phi = \pi/6$ ,  $\gamma_1 = 1$ ,  $We = 0.9$  and  $\Theta = 1.5$ .

## 6.6 Closing remarks

In this chapter peristaltic motion of Johnson-Segalman fluid in an asymmetric channel with convective conditions is investigated. Behaviors of the velocity and temperature profiles, pumping and trapping phenomena are discussed. It is noticed that Biot number at the lower wall  $Bi_2$ , viscosity ratio parameter  $\gamma_1$ , slip parameter  $e$  and Brinkman number  $Br$  together enhance the thermal stability of the flow. Further an increase in the Weissenberg number  $We$  and Biot number at the upper channel wall  $Bi_1$  decrease the temperature profile.

## Chapter 7

# Convective heat transfer analysis on power-law fluid in a channel with peristalsis

### 7.1 Introduction

The peristaltic flow of power law fluid in an asymmetric channel is discussed. The flow is generated because of peristaltic waves propagating along the channel walls. Heat transfer is examined through convective conditions of channel walls. Mathematical model is presented employing lubrication approach. The differential equations governing the flow are nonlinear and admit non-unique solutions. There exists two different physically meaningful solutions one of which satisfying the boundary conditions at the upper wall and the other at the lower wall. The effects of Biot numbers and the power-law nature of the fluid on the longitudinal velocity, temperature and pumping characteristics are studied in detail. The streamlines pattern and trapping are given due attention. Important conclusions have been pointed out.

### 7.2 Problem formulation and flow equations

The flow of incompressible power-law fluid in an asymmetric channel with convective effects is considered (see Fig. 2.1). The  $\bar{X}$  and  $\bar{Y}$  axes are selected along and perpendicular to the

channel walls respectively. The flow created is due to the imposition of the following sinusoidal waves:

$$\begin{aligned}\bar{h}_1(\bar{X}, \bar{t}) &= d_1 + a_1 \cos \frac{2\pi}{\lambda}(\bar{X} - c\bar{t}), & \text{upper wall,} \\ \bar{h}_2(\bar{X}, \bar{t}) &= -d_2 - a_2 \cos \left( \frac{2\pi}{\lambda}(\bar{X} - c\bar{t}) + \phi \right), & \text{lower wall.}\end{aligned}\quad (7.1)$$

In above expressions  $c$  is the wave speed,  $a_1$ ,  $a_2$  are the waves amplitudes,  $\lambda$  is the wavelength,  $d_1 + d_2$  the width of the asymmetric channel, the phase difference  $\phi$  varies in the range  $0 \leq \phi \leq \pi$ . Here  $\phi = 0$  corresponds to symmetric channel with waves out of phase and  $\phi = \pi$  the waves are in phase. Further  $a_1$ ,  $a_2$ ,  $d_1$ ,  $d_2$  and  $\phi$  satisfy the condition

$$a_1^2 + a_2^2 + 2a_1a_2 \cos \phi \leq (d_1 + d_2)^2. \quad (7.2)$$

Conservation of mass for an incompressible fluid is given by

$$\text{div } \bar{\mathbf{V}} = 0. \quad (7.3)$$

The equations of motion and energy are

$$\rho \frac{d\bar{\mathbf{V}}}{d\bar{t}} = -\text{grad } \bar{p} + \text{div } \bar{\mathbf{S}}, \quad (7.4)$$

$$\rho c_p \frac{dT}{d\bar{t}} = k \nabla^2 T + \Phi, \quad (7.5)$$

in which  $\bar{\mathbf{V}}$  is the velocity,  $\rho$  is density of the fluid,  $\frac{d}{d\bar{t}}$  is material time derivative,  $T$  the fluid temperature,  $c_p$  the specific heat,  $k$  the thermal conductivity of the material, the viscous dissipation effects  $\Phi$ ,  $\bar{p}$  the pressure,  $\bar{\mathbf{S}}$  the extra stress tensor and  $\nabla^2 = \left( \frac{\partial^2}{\partial \bar{X}^2} + \frac{\partial^2}{\partial \bar{Y}^2} \right)$  (the over bar refers to a dimensional quantity).

The exchange of heat with ambient at the walls is given by

$$k \frac{\partial T}{\partial \bar{Y}} = -\eta_1(T - T_a) \text{ at } \bar{Y} = \bar{h}_1, \quad (7.6)$$

$$k \frac{\partial T}{\partial \bar{Y}} = -\eta_2(T_a - T) \text{ at } \bar{Y} = \bar{h}_2, \quad (7.7)$$

where  $\eta_1$  and  $\eta_2$  are the heat transfer coefficients at the upper and lower channel walls respectively and  $T_a$  is the ambient temperature.

For two-dimensional flow of power-law fluid, we have the velocity  $\bar{\mathbf{V}}$  and extra stress tensor  $\bar{\mathbf{S}}$  in the forms:

$$\bar{\mathbf{V}} = [\bar{U}(\bar{X}, \bar{Y}, \bar{t}), \bar{V}(\bar{X}, \bar{Y}, \bar{t}), 0], \quad (7.8)$$

$$\bar{\mathbf{S}} = \mu \left| \text{tr} (\bar{\mathbf{A}}_1)^2 \right|^m \bar{\mathbf{A}}_1, \quad (7.9)$$

$$\bar{\mathbf{A}}_1 = \bar{\mathbf{L}} + \bar{\mathbf{L}}^*, \quad \bar{\mathbf{L}} = \text{grad } \bar{\mathbf{V}}. \quad (7.10)$$

Here  $\bar{\mathbf{A}}_1$  is the rate of deformation tensor,  $\mu$  the dynamic viscosity and  $\bar{\mathbf{L}}$  is the velocity gradient. Here  $m$  is the power-law index. The fluid behaves like shear-thinning or Newtonian or shear-thickening according to whether  $m < 0$  or  $m = 0$  or  $m > 0$ .

If  $(\bar{x}, \bar{y})$  and  $(\bar{u}, \bar{v})$  are the coordinates and velocity components in the wave frame  $(\bar{x}, \bar{y})$  then

$$\bar{x} = \bar{X} - c\bar{t}, \quad \bar{y} = \bar{Y}, \quad \bar{u}(\bar{x}, \bar{y}) = \bar{U}(\bar{X}, \bar{Y}, \bar{t}) - c, \quad \bar{v}(\bar{x}, \bar{y}) = \bar{V}(\bar{X}, \bar{Y}, \bar{t}), \quad T(\bar{x}, \bar{y}) = T(\bar{X}, \bar{Y}, \bar{t}). \quad (7.11)$$

Employing these transformations and introducing the dimensionless variables by

$$\begin{aligned} x &= \frac{\bar{x}}{\lambda}, \quad y = \frac{\bar{y}}{d_1}, \quad u = \frac{\bar{u}}{c}, \quad v = \frac{\bar{v}}{c}, \quad p = \frac{d_1}{c\mu\lambda} \left( \frac{d_1^2}{2c^2} \right)^m \bar{p}, \\ h_1 &= \frac{\bar{h}_1}{d_1}, \quad h_2 = \frac{\bar{h}_2}{d_1}, \quad t = \frac{c\bar{t}}{\lambda}, \quad \mathbf{S} = \frac{d_1}{\mu c} \left( \frac{d_1^2}{2c^2} \right)^m \bar{\mathbf{S}}, \quad \theta = \frac{T - T_a}{T_a} \end{aligned} \quad (7.12)$$

and the stream function  $\psi(x, y)$  through

$$u = \frac{\partial \psi}{\partial y}, \quad v = -\delta \frac{\partial \psi}{\partial x}, \quad (7.13)$$

continuity equation (7.3) is identically satisfied while Eqs. (7.4) and (7.5) yield

$$\delta \text{Re} \left[ \left( \frac{\partial \psi}{\partial y} \frac{\partial}{\partial x} - \frac{\partial \psi}{\partial x} \frac{\partial}{\partial y} \right) \left( \frac{\partial \psi}{\partial y} \right) \right] + \frac{\partial p}{\partial x} = \delta \frac{\partial S_{xx}}{\partial x} + \frac{\partial S_{xy}}{\partial y}, \quad (7.14)$$

$$-\delta^3 \text{Re} \left[ \left( \frac{\partial \psi}{\partial y} \frac{\partial}{\partial x} - \frac{\partial \psi}{\partial x} \frac{\partial}{\partial y} \right) \left( \frac{\partial \psi}{\partial x} \right) \right] + \frac{\partial p}{\partial y} = \delta^2 \frac{\partial S_{xy}}{\partial x} + \delta \frac{\partial S_{yy}}{\partial y}, \quad (7.15)$$

$$\delta \text{Re} \left[ \frac{\partial \psi}{\partial y} \frac{\partial}{\partial x} - \frac{\partial \psi}{\partial x} \frac{\partial}{\partial y} \right] \theta = \frac{1}{\text{Pr}} \left( \delta^2 \frac{\partial^2}{\partial x^2} + \frac{\partial^2}{\partial y^2} \right) \theta + Ec \left[ \delta \frac{\partial^2 \psi}{\partial x \partial y} (S_{xx} - S_{yy}) + \left( \frac{\partial^2 \psi}{\partial y^2} - \delta^2 \frac{\partial^2 \psi}{\partial x^2} \right) S_{xy} \right], \quad (7.16)$$

where the components of extra stress tensor from Eq. (7.9) are

$$S_{xx} = 2\delta \left[ \left| 4\delta^2 \left( \frac{\partial^2 \psi}{\partial x \partial y} \right)^2 + \left( \frac{\partial^2 \psi}{\partial y^2} - \delta^2 \frac{\partial^2 \psi}{\partial x^2} \right)^2 \right|^m \right] \frac{\partial^2 \psi}{\partial x \partial y}, \quad (7.17)$$

$$S_{xy} = \left[ \left| 4\delta^2 \left( \frac{\partial^2 \psi}{\partial x \partial y} \right)^2 + \left( \frac{\partial^2 \psi}{\partial y^2} - \delta^2 \frac{\partial^2 \psi}{\partial x^2} \right)^2 \right|^m \right] \left( \frac{\partial^2 \psi}{\partial y^2} - \delta^2 \frac{\partial^2 \psi}{\partial x^2} \right), \quad (7.18)$$

$$S_{yy} = -2\delta \left[ \left| 4\delta^2 \left( \frac{\partial^2 \psi}{\partial x \partial y} \right)^2 + \left( \frac{\partial^2 \psi}{\partial y^2} - \delta^2 \frac{\partial^2 \psi}{\partial x^2} \right)^2 \right|^m \right] \frac{\partial^2 \psi}{\partial x \partial y}. \quad (7.19)$$

In the above equations the dimensionless wave number  $\delta$ , the Reynolds number  $\text{Re}$ , the Prandtl number  $\text{Pr}$  and the Eckert number  $Ec$  are defined respectively as

$$\delta = \frac{d_1}{\lambda}, \quad \text{Re} = \frac{\rho c d_1}{\mu} \left( \frac{d_1^2}{2c^2} \right)^m, \quad \text{Pr} = \frac{\mu c_p}{k} \left( \frac{d_1^2}{2c^2} \right)^m, \quad Ec = \frac{c^2}{T_a c_p}, \quad (7.20)$$

and Eqs. (7.6) and (7.7) give

$$\frac{\partial \theta}{\partial y} + Bi_1 \theta = 0 \text{ at } y = h_1, \quad (7.21)$$

$$\frac{\partial \theta}{\partial y} - Bi_2 \theta = 0 \text{ at } y = h_2, \quad (7.22)$$

where  $Bi_1 = \eta_1 d_1 / k$  and  $Bi_2 = \eta_2 d_1 / k$  are the Biot numbers at the upper and lower channel walls respectively.

Under the assumption of long wavelength  $\delta \ll 1$  and low Reynolds number  $\text{Re} \rightarrow 0$  [6], Eqs. (7.14) and (7.15) become

$$\frac{\partial p}{\partial x} = \frac{\partial S_{xy}}{\partial y}, \quad (7.23)$$

$$\frac{\partial p}{\partial y} = 0. \quad (7.24)$$

The above equation indicates that  $p$  is independent of  $y$ . Eliminating the pressure  $p$  from (7.23)

and (7.24) we get the following governing equation

$$\frac{\partial^2 S_{xy}}{\partial y^2} = 0. \quad (7.25)$$

Also Eq. (7.16) takes the form

$$\frac{\partial^2 \theta}{\partial y^2} + Br \left( \frac{\partial^2 \psi}{\partial y^2} \right) S_{xy} = 0, \quad (7.26)$$

where

$$Br = \text{Pr} * Ec, \quad (7.27)$$

and  $S_{xy}$  is given by

$$S_{xy} = \left| \frac{\partial^2 \psi}{\partial y^2} \right|^{2m} \frac{\partial^2 \psi}{\partial y^2}. \quad (7.28)$$

The dimensionless forms of  $h_i$  ( $i = 1, 2$ ) are

$$h_1(x) = 1 + a \cos 2\pi x, \quad h_2(x) = -d - b \cos(2\pi x + \phi), \quad (7.29)$$

where  $a = a_1/d_1$ ,  $b = a_2/d_1$ ,  $d = d_2/d_1$  and  $\phi$  satisfies the following relation

$$a^2 + b^2 + 2ab \cos \phi \leq (1 + d)^2. \quad (7.30)$$

The conditions for the dimensionless velocity in wave frame are

$$u = -1, \quad \text{at } y = h_1(x) \text{ and } y = h_2(x). \quad (7.31)$$

### 7.3 Non-unique solutions of the problem

As the modulus sign appears in the leading equations, therefore the correct sign for this modulus has to be chosen. The researchers who have solved their problems for symmetric channel presented the solutions in the region between the middle line and the upper channel wall by taking the advantage of the symmetry about the center line. We found that the solution presented by such authors does not satisfy the conditions at lower channel wall because they

have taken  $n^{th}$  root to find the solution and lead to a non-unique solution. To determine the axial velocity in channel flow uniquely, a regularity condition is employed on the axis. Here we have analyzed two appropriate non-unique solutions from Eqs. (7.23) – (7.26) and (7.28). These solutions satisfy the corresponding boundary conditions.

The axial velocity attains a maximum value on the axis and similar regularity condition extends to asymmetric channel geometry. Thus, we choose for our problem

$$\frac{\partial u}{\partial y} = 0 \text{ for } y = \frac{h_1 + h_2}{2}. \quad (7.32)$$

As the maximum velocity  $u$  is on the middle line, we have

$$\frac{\partial u}{\partial y} < 0 \text{ for } y > \frac{h_1 + h_2}{2}, \quad (7.33)$$

and

$$\frac{\partial u}{\partial y} > 0 \text{ for } y < \frac{h_1 + h_2}{2}. \quad (7.34)$$

Integrating (7.23) with respect to  $y$ , removing modulus using (7.33), we have

$$\left(-\frac{\partial u}{\partial y}\right)^{2m+1} = -\left(\frac{dp}{dx}y + c_1\right) \text{ for } y > \frac{h_1 + h_2}{2} \quad (7.35)$$

Using (7.32) and taking  $n^{th}$  root (always to be taken for a positive quantity as the negative quantities lead to complex values which are not physically meaningful), Eq. (7.35) can be written as

$$\frac{\partial u}{\partial y} = \left|\frac{dp}{dx}\right|^{\frac{-2m}{2m+1}} \frac{dp}{dx} \left(y - \frac{h_1 + h_2}{2}\right)^{\frac{1}{2m+1}}, \quad y \geq \frac{h_1 + h_2}{2}. \quad (7.36)$$

Integrating (7.36) with respect to  $y$  and using (7.31), we get

$$u(y) = \left(\frac{2m+1}{2m+2}\right) \left|\frac{dp}{dx}\right|^{\frac{-2m}{2m+1}} \frac{dp}{dx} \left[ \left(y - \frac{h_1 + h_2}{2}\right)^{\frac{2m+2}{2m+1}} - \left(\frac{h_1 - h_2}{2}\right)^{\frac{2m+2}{2m+1}} \right] - 1, \quad y \geq \frac{h_1 + h_2}{2}. \quad (7.37)$$

Here the flow problem in an asymmetric channel is conducted, therefore, solution given in Eq. (7.37) does not satisfy the condition at the lower channel wall  $y = h_2$  and can not be used for  $y < \frac{h_1 + h_2}{2}$ . In this region, a physically meaningful solution is found by using (7.31), (7.32) and



(7.34) as follows:

$$u(y) = \left( \frac{2m+1}{2m+2} \right) \left| \frac{dp}{dx} \right|^{\frac{-2m}{2m+1}} \frac{dp}{dx} \left[ \left( \frac{h_1+h_2}{2} - y \right)^{\frac{2m+2}{2m+1}} - \left( \frac{h_1-h_2}{2} \right)^{\frac{2m+2}{2m+1}} \right] - 1, \quad y \leq \frac{h_1+h_2}{2}. \quad (7.38)$$

In order to study trapping phenomenon, a solution in terms of stream function ( $u = \partial\psi/\partial y$ ) is required. The volume flow rate  $F$  in wave frame of reference is given by

$$F = \int_{h_2}^{h_1} u \, dy = \int_{h_2}^{h_1} \frac{\partial\psi}{\partial y} dy = \psi|_{y=h_1} - \psi|_{y=h_2}, \quad (7.39)$$

$$\begin{aligned} F &= \int_{h_2}^{(h_1+h_2)/2} u \, dy + \int_{(h_1+h_2)/2}^{h_1} u \, dy \\ &= -\frac{4m+2}{4m+3} \left| \frac{dp}{dx} \right|^{\frac{-2m}{2m+1}} \frac{dp}{dx} \left( \frac{h_1-h_2}{2} \right)^{\frac{4m+3}{2m+1}} - (h_1-h_2). \end{aligned} \quad (7.40)$$

Thus we take the boundary conditions for  $\psi$  as

$$\begin{aligned} \psi|_{y=h_1} &= F/2, \quad \psi|_{y=h_2} = -F/2 \text{ and} \\ \psi &= 0 \text{ at } y = (h_1+h_2)/2. \end{aligned} \quad (7.41)$$

Therefore the solution in terms of stream function satisfying the boundary conditions (7.41) is obtained as

$$\begin{aligned} \psi &= -\left( \frac{4m+3}{4m+4} \right) (F + h_1 - h_2) \left( \frac{2}{h_1 - h_2} \right)^{\frac{4m+3}{2m+1}} \\ &\times \left[ \begin{aligned} &\left( \frac{2m+1}{4m+3} \right) \left( y - \frac{h_1+h_2}{2} \right)^{\frac{4m+3}{2m+1}} \\ &- \left( \frac{h_1-h_2}{2} \right)^{\frac{2m+2}{2m+1}} \left( y - \frac{h_1+h_2}{2} \right) \end{aligned} \right] - \left( y - \frac{h_1+h_2}{2} \right), \quad y \geq \frac{h_1+h_2}{2}, \end{aligned} \quad (7.42)$$

$$\begin{aligned} \psi &= \left( \frac{4m+3}{4m+4} \right) (F + h_1 - h_2) \left( \frac{2}{h_1 - h_2} \right)^{\frac{4m+3}{2m+1}} \\ &\times \left[ \begin{aligned} &\left( \frac{2m+1}{4m+3} \right) \left( \frac{h_1+h_2}{2} - y \right)^{\frac{4m+3}{2m+1}} \\ &- \left( \frac{h_1-h_2}{2} \right)^{\frac{2m+2}{2m+1}} \left( \frac{h_1+h_2}{2} - y \right) \end{aligned} \right] - \left( \frac{h_1+h_2}{2} - y \right), \quad y \leq \frac{h_1+h_2}{2}, \end{aligned} \quad (7.43)$$

When the power-law index ‘ $m$ ’ takes the value 0, our solutions (7.42) and (7.43) reduce to a single unique solution given by

$$\begin{aligned} \psi &= -2 \frac{(F + h_1 - h_2)}{(h_1 - h_2)^3} \\ &\times \left[ \begin{aligned} &\left(y - \frac{h_1 + h_2}{2}\right)^3 \\ &- 3 \left(\frac{h_1 - h_2}{2}\right)^2 \left(y - \frac{h_1 + h_2}{2}\right) \end{aligned} \right] - \left(y - \frac{h_1 + h_2}{2}\right), \quad h_2 \leq y \leq h_1. \end{aligned} \quad (7.44)$$

This solution coincides with that of Mishra and Rao [27] for peristaltic flow of a Newtonian fluid in an asymmetric channel.

From Eq. (7.40), we have

$$\frac{dp}{dx} = - \left( \frac{4m+3}{4m+2} \right)^{2m+1} |-(F + h_1 - h_2)|^{2m} (q + h_1 - h_2) \left( \frac{2}{h_1 - h_2} \right)^{4m+3}. \quad (7.45)$$

The instantaneous flux  $Q$  in the laboratory frame is

$$\begin{aligned} Q &= \int_{h_2}^{h_1} (u + 1) dy = \int_{h_2}^{h_1} u dy + \int_{h_2}^{h_1} dy \\ &= F + h_1 - h_2. \end{aligned} \quad (7.46)$$

The average flux over one period ( $\Omega = \lambda/c$ ) of the peristaltic wave is

$$\Theta = \frac{1}{\Omega} \int_0^\Omega Q dt = \frac{1}{\Omega} \int_0^\Omega (F + h_1 - h_2) dt = F + 1 + d. \quad (7.47)$$

Also the solution of Eq. (7.26) subject to boundary conditions (7.21) and (7.22) is given by

$$\begin{aligned} \theta(y) = & -\frac{1}{(A_3(3m+2)(4m+3))} [2^{-\frac{6m+5}{2m+1}} Br \left( \frac{dp}{dx} \right)^2 (2m+1) \left| \frac{dp}{dx} \right|^{-\frac{4m}{2m+1}} \\ & \times \{ A_1(h_1 - h_2)^{\frac{2m+3}{2m+1}} A_4(-1 + Bi_2(h_2 - y)) + A_2(-h_1 + h_2)^{\frac{2m+3}{2m+1}} \\ & \times A_5(1 + Bi_1(h_1 - y)) + A_3(2m+1)(-h_1 + h_2 + 2y)^{\frac{4(m+1)}{2m+1}} \\ & \times (2^{-\frac{1}{2m+1}} \frac{dp}{dx} (-h_1 - h_2 + 2y)^{\frac{1}{2m+1}} \left| \frac{dp}{dx} \right|^{-\frac{2m}{2m+1}})^{2m} \}], \quad y \geq \frac{h_1 + h_2}{2} \quad (7.48) \end{aligned}$$

$$\begin{aligned} \theta(y) = & \frac{1}{(A_3(3m+2)(4m+3))} [2^{-\frac{6m+5}{2m+1}} Br \left( \frac{dp}{dx} \right)^2 (2m+1) \left| \frac{dp}{dx} \right|^{-\frac{4m}{2m+1}} \\ & \times \{ A_1(h_1 - h_2)^{\frac{2m+3}{2m+1}} A_5(1 + Bi_1(h_1 - y)) + A_2(-h_1 + h_2)^{\frac{2m+3}{2m+1}} \\ & \times A_4(-1 + Bi_2(h_2 - y)) - A_3(2m+1)(h_1 + h_2 - 2y)^{\frac{4(m+1)}{2m+1}} \\ & \times (2^{-\frac{1}{2m+1}} \frac{dp}{dx} (h_1 + h_2 - 2y)^{\frac{1}{2m+1}} \left| \frac{dp}{dx} \right|^{-\frac{2m}{2m+1}})^{2m} \}], \quad y \leq \frac{h_1 + h_2}{2} \quad (7.49) \end{aligned}$$

where

$$\begin{aligned} A_1 &= \left( 2^{-\frac{1}{2m+1}} \left( \frac{dp}{dx} \right) (h_1 - h_2)^{\frac{1}{2m+1}} \left| \frac{dp}{dx} \right|^{-\frac{2m}{2m+1}} \right)^{2m}, \\ A_2 &= \left( 2^{-\frac{1}{2m+1}} \left( \frac{dp}{dx} \right) (-h_1 + h_2)^{\frac{1}{2m+1}} \left| \frac{dp}{dx} \right|^{-\frac{2m}{2m+1}} \right)^{2m}, \\ A_3 &= Bi_1 + Bi_2 + Bi_1 Bi_2 (h_1 - h_2), \\ A_4 &= 8 + 12m + Bi_1 (h_1 - h_2) (2m + 1), \\ A_5 &= 8 + 12m + Bi_2 (h_1 - h_2) (2m + 1). \end{aligned}$$

## 7.4 Results and discussion

This section deals with the graphical results for various parameters involved in the solution such as the power-law fluid parameter  $m$ , phase difference  $\phi$ , Brinkman number  $Br$  and Biot numbers  $Bi_1$  and  $Bi_2$ . Fig. 7.1 reveals the effects of phase difference  $\phi$  on pressure gradient  $dp/dx$  for different values of  $m$ . We observed that by increasing the values of phase difference  $\phi$  the pressure gradient  $dp/dx$  decreases. It is also noted that the magnitude of the pressure gradient for shear-thickening fluid ( $m = 0.05$ ) is larger when compared to that of Newtonian

( $m = 0.00$ ) and shear-thinning ( $m = -0.05$ ) fluids. Fig. 7.2 shows the effects of power-law fluid parameter  $m$  on pressure gradient  $dp/dx$ . It is found that the pressure gradient  $dp/dx$  is higher for a shear-thinning fluid ( $m = -0.05$ ) than for a shear-thickening fluid ( $m = 0.00$ ) in the wider part of the channel whereas the pressure gradient  $dp/dx$  for a Newtonian fluid ( $m = 0.00$ ) lies between. On the other hand, the opposite behavior is observed in the narrow part of the channel i.e. the pressure gradient  $dp/dx$  is higher for the shear-thickening ( $m = 0.05$ ) fluid when compared to the shear-thinning ( $m = -0.05$ ) fluid in the narrow part of the channel. However the case of Newtonian fluid ( $m = 0.00$ ) lies in between. Figs. 7.3 and 7.4 are plotted to see the effects of power law fluid parameter  $m$  and phase difference  $\phi$  on pressure rise per wavelength  $\Delta p_\lambda$  versus the flow rate  $\Theta$ . It is observed that the pressure rise per wavelength  $\Delta p_\lambda$  is larger for shear-thickening ( $m = 0.05$ ) fluid when compared to that of a Newtonian ( $m = 0.00$ ) and shear-thinning ( $m = -0.05$ ) fluids in the peristaltic pumping region ( $\Delta p_\lambda > 0, \Theta > 0$ ) and free pumping region ( $\Delta p_\lambda = 0$ ). While in the copumping region ( $\Delta p_\lambda > 0, \Theta < 0$ ), the pressure rise per wavelength  $\Delta p_\lambda$  is larger for the shear-thinning ( $m = -0.05$ ) fluid when compared with that of the shear-thickening ( $m = 0.05$ ) fluid. Whereas the case of a Newtonian fluid ( $m = 0.00$ ) lies in between. Hence it indicates that pumping increases as the fluid character changes from shear-thinning to Newtonian and then to shear-thickening. Fig. 7.4 (a-c) illustrates that the pressure rise per wavelength  $\Delta p_\lambda$  decreases in the peristaltic pumping region while it increases in the copumping region when we increase the phase difference  $\phi$ . It is also demonstrated that the pressure rise per wavelength  $\Delta p_\lambda$  is larger in magnitude for shear-thickening ( $m = 0.05$ ) fluid when compared with that of the Newtonian ( $m = 0.00$ ) and shear-thinning ( $m = -0.05$ ) fluids for various values of phase difference  $\phi$ .

The effects of various values of power-law fluid parameter  $m$  on the longitudinal velocity  $u(y)$  are shown in Fig. 7.5. It is evident from this Fig. that the magnitude of the longitudinal velocity  $u(y)$  is larger at the center of channel for the shear-thinning ( $m = -0.05$ ) fluid when compared to that for the Newtonian ( $m = 0.00$ ) and shear-thickening ( $m = 0.05$ ) fluids. Also the magnitude of the longitudinal velocity  $u(y)$  is larger near the channel walls for the shear-thickening ( $m = 0.05$ ) fluid than the shear-thinning ( $m = -0.05$ ) fluid. The case of a Newtonian fluid ( $m = 0.00$ ) lies in between. Fig. 7.6 (a-c) shows the effects of Brinkman number  $Br$  on temperature profile  $\theta(y)$  with variation in the power-law fluid parameter  $m$ . It is confirmed

that by increasing the values of Brinkman number  $Br$  the temperature profile  $\theta(y)$  increases gradually. It is also noteworthy that the temperature profile  $\theta(y)$  for shear-thinning ( $m = -0.01$ ) fluid is larger in magnitude when compared to that of Newtonian ( $m = 0.00$ ) and shear-thickening ( $m = 0.01$ ) fluids when we increase the values of Brinkman number  $Br$  (see Fig. 7.6 (a-c)). Fig. 7.7 is sketched to see the effects of power-law fluid parameter  $m$  on the temperature profile  $\theta(y)$ . It is noticed that the temperature profile  $\theta(y)$  is larger for a shear-thinning ( $m = -0.03$ ) fluid when compared with a shear-thickening ( $m = 0.03$ ) fluid. The case of Newtonian fluid ( $m = 0.00$ ) lies in between. Fig. 7.8 (a-c) is plotted to perceive the effects of Biot number  $Bi_1$  on the temperature profile  $\theta(y)$  for shear thinning ( $m = -0.01$ , Fig. 7.8 (a)), Newtonian ( $m = 0.00$ , Fig. 7.8 (b)) and shear-thickening ( $m = 0.01$ , Fig. 7.8 (c)) fluids. The temperature profile  $\theta(y)$  decreases gradually by increasing values of Biot number  $Bi_1$  near the upper wall while it has no significant effect near the lower wall of the channel. It is also noted that the temperature profile  $\theta(y)$  for a shear-thinning ( $m = -0.01$ ) fluid is higher in magnitude than that of the Newtonian ( $m = 0.00$ ) and shear-thickening ( $m = 0.01$ ) fluids. Fig. 7.9 (a-c) witnesses that the temperature profile  $\theta(y)$  decreases when we increase the Biot number  $Bi_2$  near the lower wall of the channel whereas it has no significant effect near the upper wall of the channel. Here we have considered the non-uniform temperature fields within the fluid as the values of the Biot numbers are much larger than 0.01 because the problems with uniform temperature fields within the fluid (i.e. when Biot number is less than 0.01) are simple in nature.

Another interesting phenomenon of peristalsis is trapping, the formulation of internally circulating bolus of fluid which moves along with the wave. The effects of power-law fluid parameter  $m$  on the streamlines in the wave frame for  $a = 0.3$ ,  $b = 0.5$ ,  $d = 1$ ,  $\phi = \pi/4$  and  $\Theta = 1.31$  show that the trapped bolus appearing in the center region and the bolus size decreases as the power-law fluid parameter  $m$  decreases (see Fig. 7.10). We observe that the streamlines for different phase shifts  $\phi$  and different  $m$  with  $a = 0.5$ ,  $b = 0.5$ ,  $d = 1$  and  $\Theta = 1.27$  produce results similar to those given by Mishra and Rao [27], where the trapped bolus shifts towards left and decreases in size as  $\phi$  increases (see Figs. 7.11 and 7.12). Further the trapping is more for shear-thickening fluid when compared with shear-thinning fluid. Fig. 7.13 shows the streamlines for shear-thinning fluid with  $a = 0.3$ ,  $b = 0.5$ ,  $d = 1$  and  $\Theta = 1.27$  for different

values of  $\phi$ . It is revealed that trapping exists only for  $\phi = 0$  and the trapping disappears as  $\phi$  increases. Whereas for shear-thickening fluid the trapping exists for all phase shifts  $\phi$  even when walls are moving in phase ( $\phi = \pi$ ) (see Fig. 7.14).

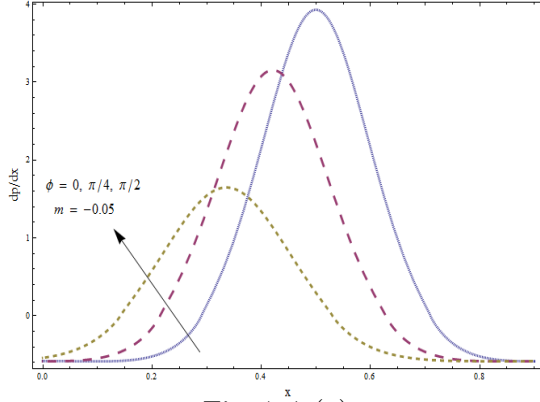


Fig. 7.1 (a)

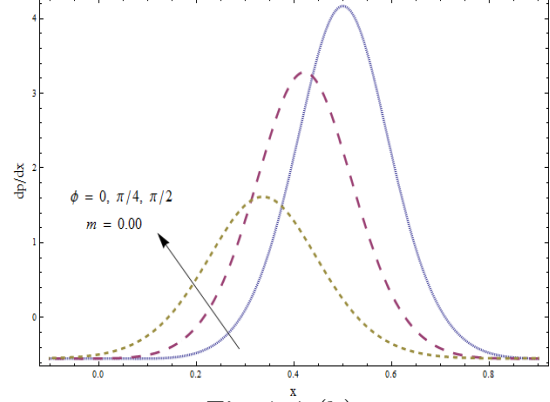


Fig. 7.1 (b)

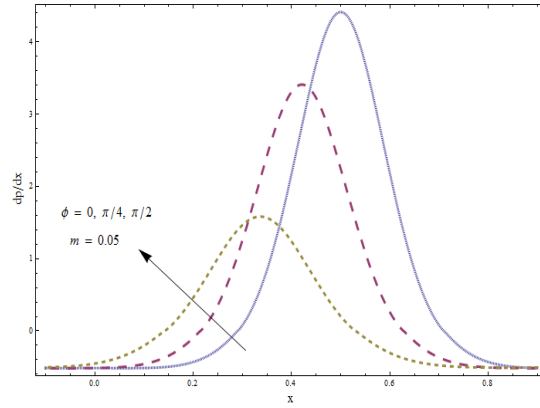


Fig. 7.1 (c)

Fig. 7.1: Variation in  $dp/dx$  for  $\phi$  when  $a = 0.3$ ,  $b = 0.5$ ,  $d = 1$ ,  $\Theta = 0.2$  with (a)  $m = -0.05$ , (b)  $m = 0.00$  and (c)  $m = 0.05$ .

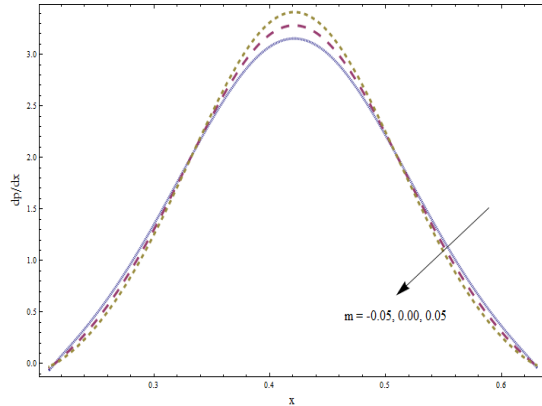


Fig. 7.2

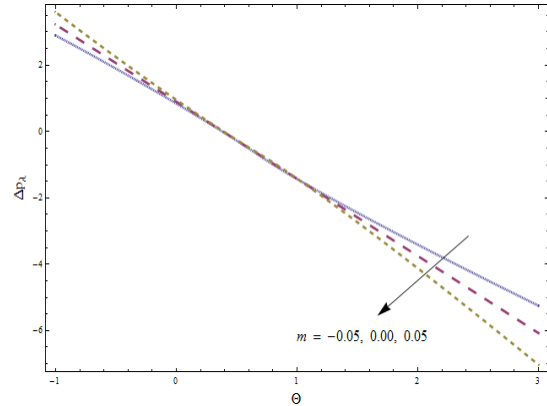


Fig. 7.3

Fig. 7.2: Variation in  $dp/dx$  for  $m$  when  $a = 0.3$ ,  $b = 0.5$ ,  $d = 1$ ,  $\Theta = 0.2$  and  $\phi = \pi/4$ .

Fig. 7.3: Variation in  $\Delta p_\lambda$  versus  $\Theta$  for  $m$  when  $a = 0.3$ ,  $b = 0.5$ ,  $d = 1$  and  $\phi = \pi/4$ .

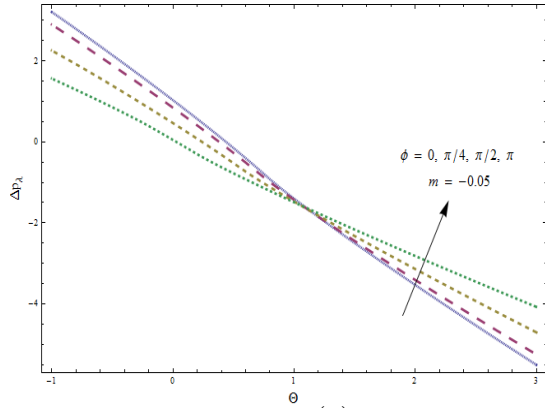


Fig. 7.4 (a)

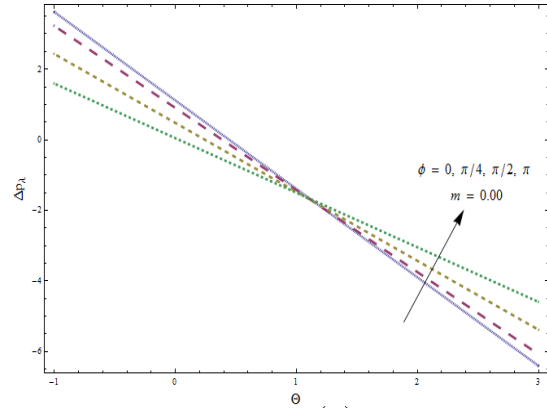


Fig. 7.4 (b)

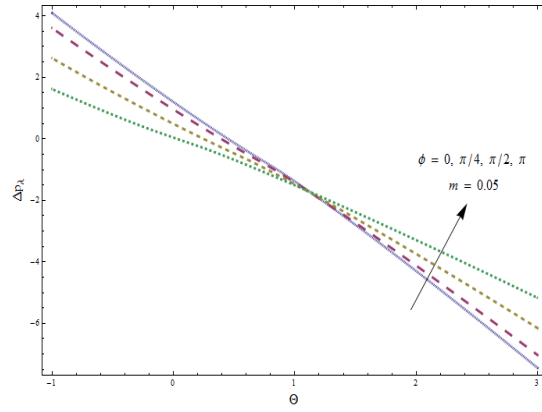


Fig. 7.4 (c)

Fig. 7.4: Variation in  $\Delta p_\lambda$  versus  $\Theta$  for  $\phi$  when  $a = 0.3$ ,  $b = 0.5$ ,  $d = 1$  with (a)  $m = -0.05$ , (b)  $m = 0.00$  and (c)  $m = 0.05$ .



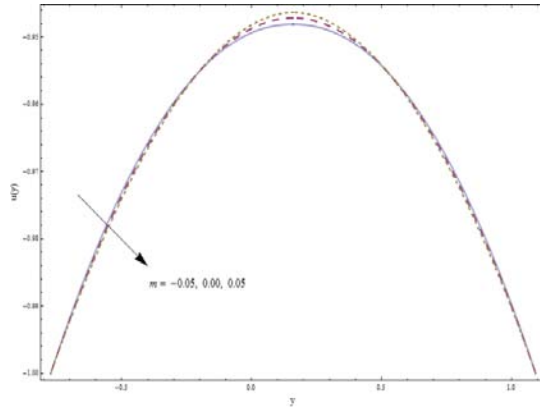


Fig. 7.5

Fig. 7.5: Longitudinal velocity  $u(y)$  for  $m$  when  $a = 0.3$ ,  $b = 0.5$ ,  $d = 1$ ,  $\Theta = 0.2$  and  $\phi = \pi/4$ .

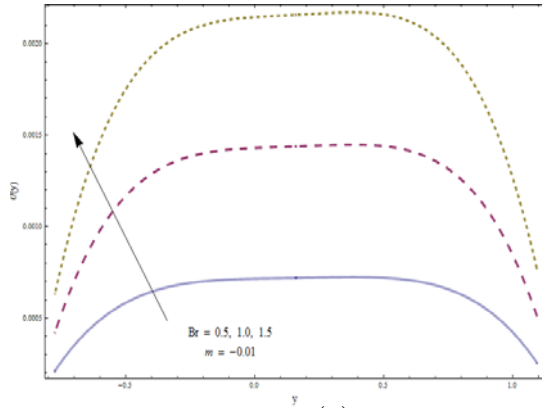


Fig. 7.6 (a)

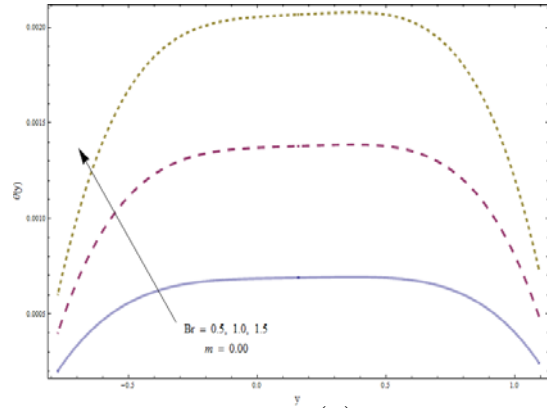


Fig. 7.6 (b)

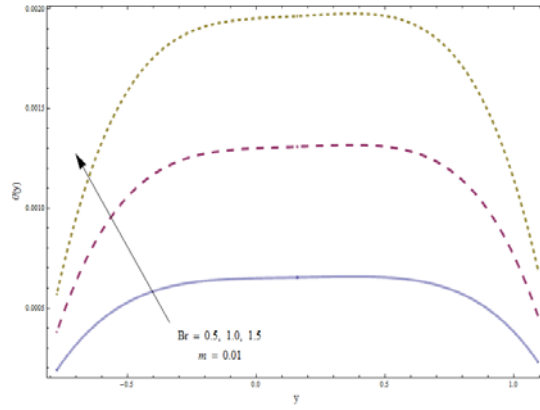


Fig. 7.6 (c)

Fig. 7.6: Temperature profile  $\theta(y)$  for  $Br$  when  $a = 0.3$ ,  $b = 0.5$ ,  $d = 1$ ,  $\Theta = 0.2$ ,  $\phi = \pi/4$ ,  $Bi_1 = 8$ ,  $Bi_2 = 10$  with (a)  $m = -0.01$ , (b)  $m = 0.00$  and (c)  $m = 0.01$ .

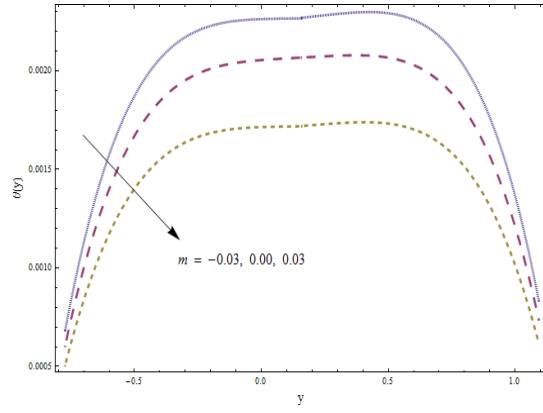


Fig. 7.7

Fig. 7.7: Temperature profile  $\theta(y)$  for  $m$  when  $a = 0.3$ ,  $b = 0.5$ ,  $d = 1$ ,  $\Theta = 0.2$ ,  $\phi = \pi/4$ ,  $Bi_1 = 8$ ,  $Bi_2 = 10$  and  $Br = 1.5$ .

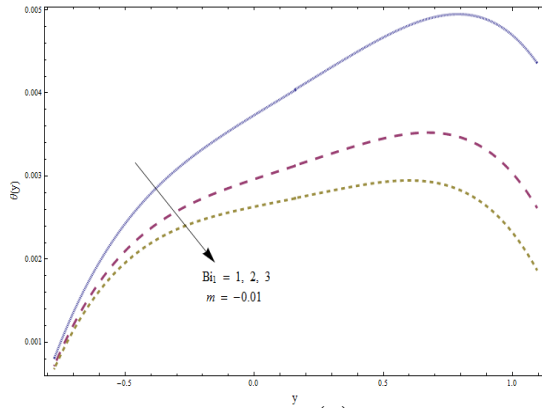


Fig. 7.8 (a)

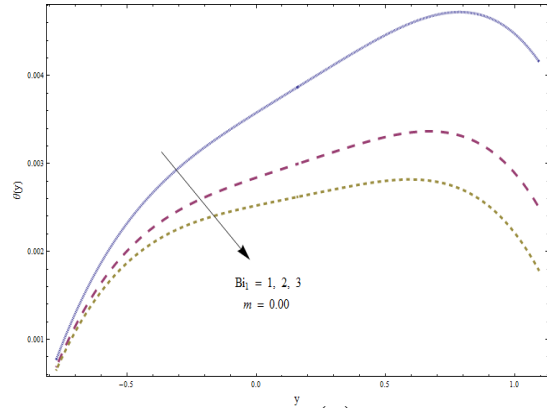


Fig. 7.8 (b)

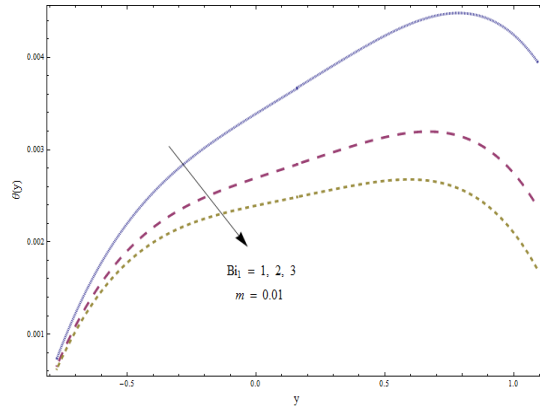


Fig. 7.8 (c)

Fig. 7.8: Temperature profile  $\theta(y)$  for  $Bi_1$  when  $a = 0.3$ ,  $b = 0.5$ ,  $d = 1$ ,  $\Theta = 0.2$ ,  $\phi = \pi/4$ ,  $Br = 1.5$ ,  $Bi_2 = 10$  with (a)  $m = -0.01$ , (b)  $m = 0.00$  and (c)  $m = 0.01$ .

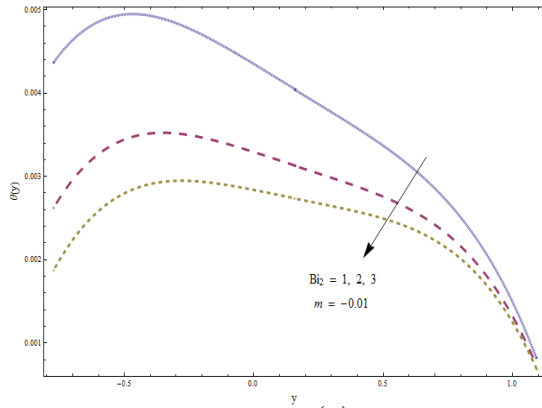


Fig. 7.9 (a)

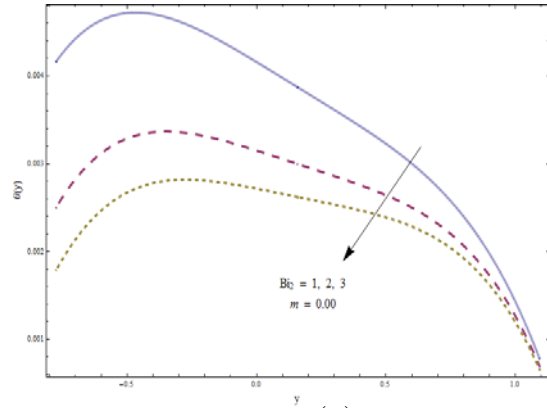


Fig. 7.9 (b)

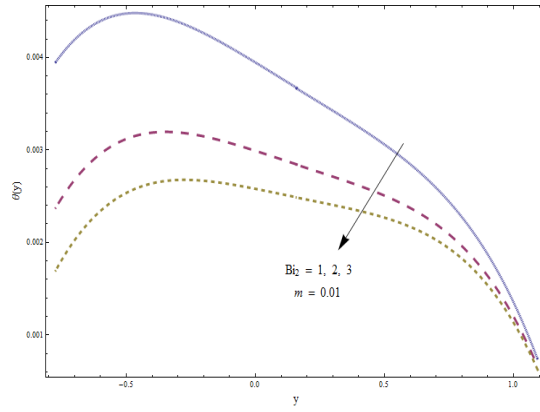


Fig. 7.9 (c)

Fig. 7.9: Temperature profile  $\theta(y)$  for  $Bi_2$  when  $a = 0.3$ ,  $b = 0.5$ ,  $d = 1$ ,  $\Theta = 0.2$ ,  $\phi = \pi/4$ ,  $Br = 1.5$ ,  $Bi_1 = 10$  with (a)  $m = -0.01$ , (b)  $m = 0.00$  and (c)  $m = 0.01$ .

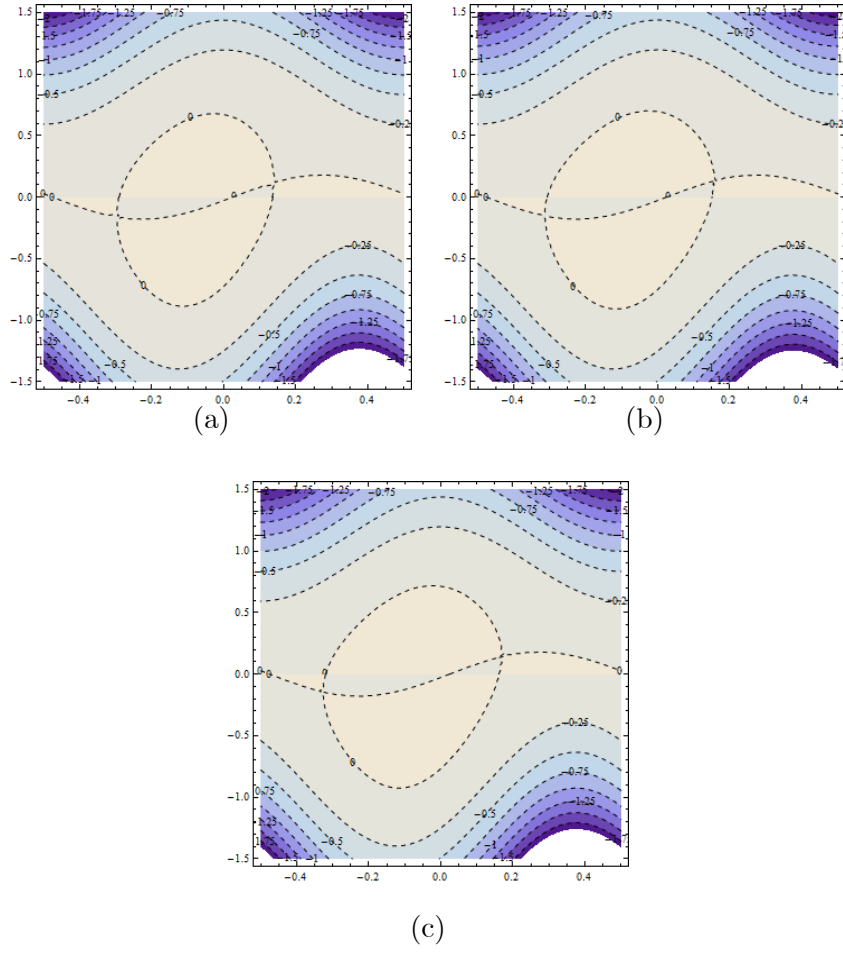


Fig. 7.10: The streamlines in wave frame for (a)  $m = -0.05$ , (b)  $m = 0.00$  and (c)  $m = 0.05$ .

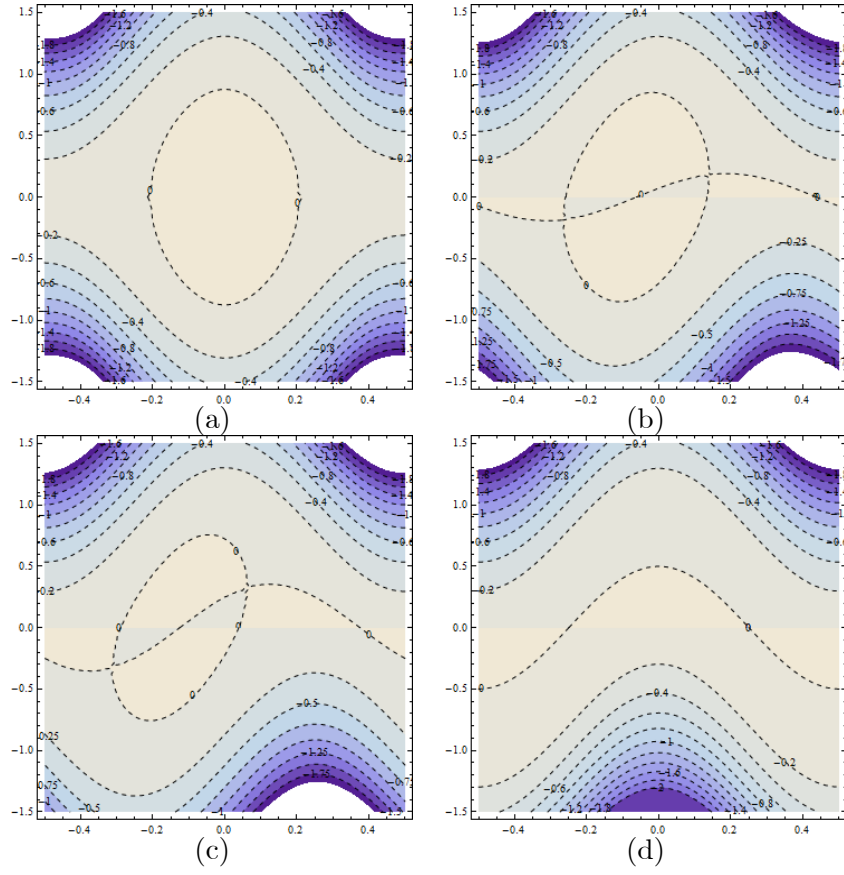


Fig. 7.11: The streamlines in wave frame for symmetric channel when  $m = -0.05$  with (a)  $\phi = 0$ , (b)  $\phi = \pi/4$ , (c)  $\phi = \pi/2$  and (d)  $\phi = \pi$ .

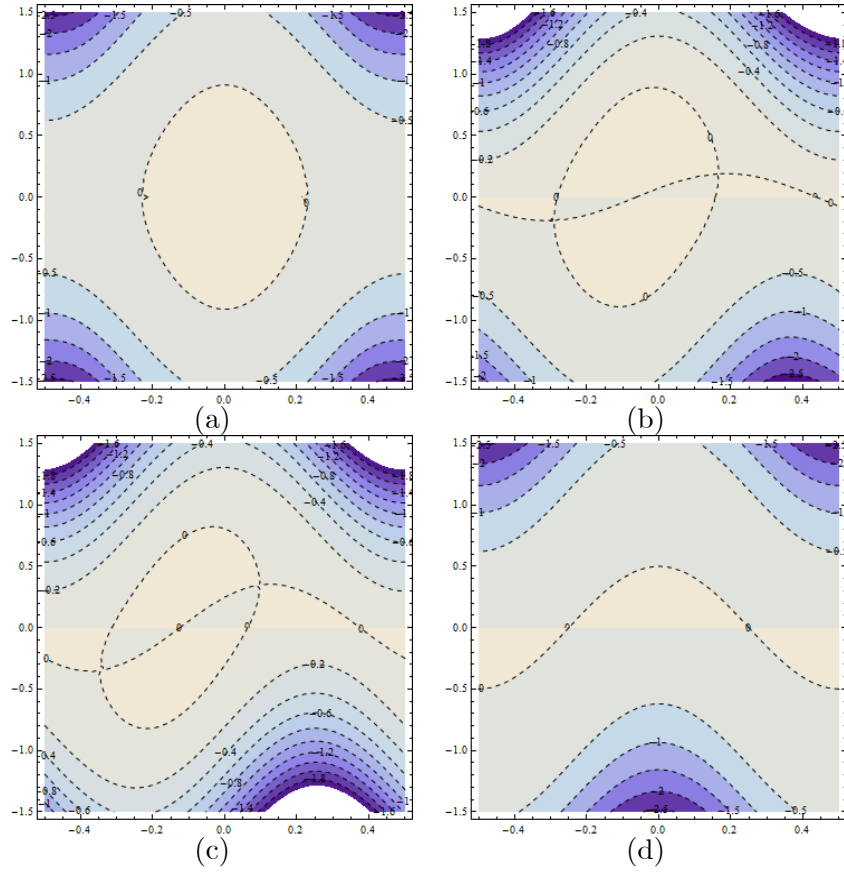


Fig. 7.12: The streamlines in wave frame for symmetric channel when  $m = 0.05$  with (a)

$\phi = 0$ , (b)  $\phi = \pi/4$ , (c)  $\phi = \pi/2$  and (d)  $\phi = \pi$ .



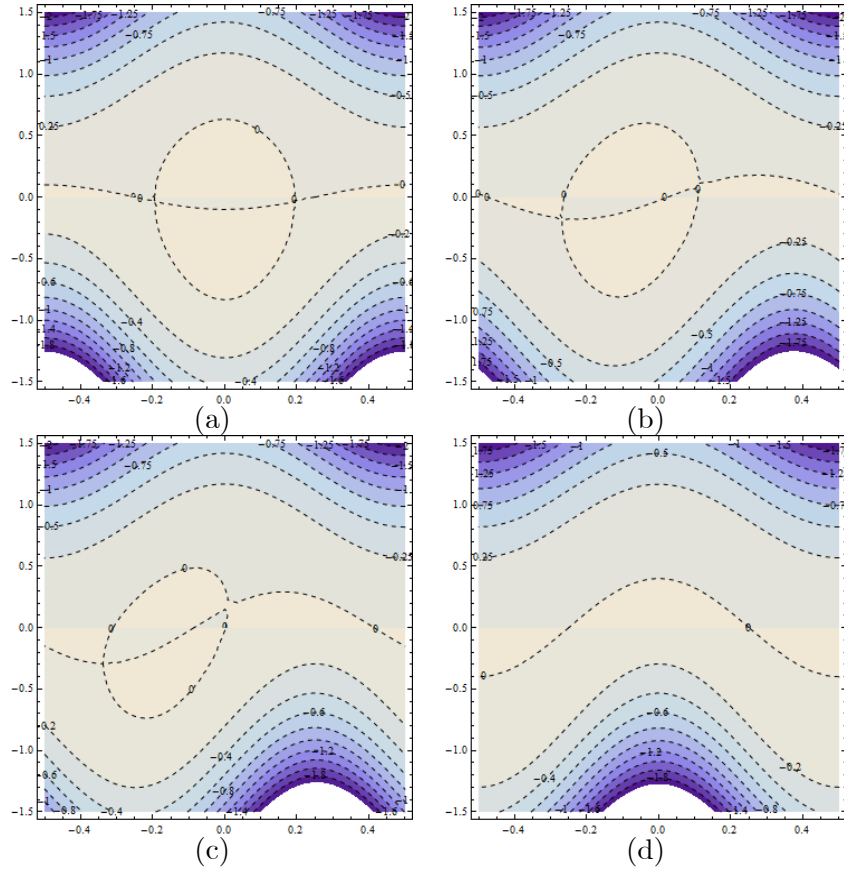


Fig. 7.13: The streamlines in wave frame for asymmetric channel when  $m = -0.05$  with (a)

$\phi = 0$ , (b)  $\phi = \pi/4$ , (c)  $\phi = \pi/2$  and (d)  $\phi = \pi$ .

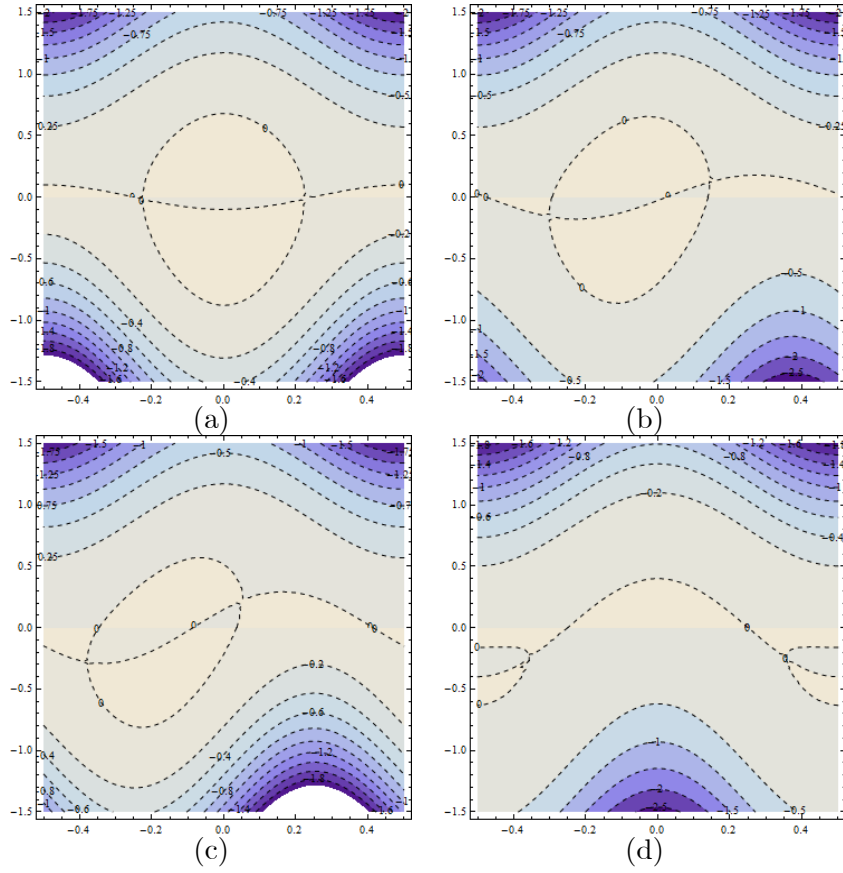


Fig. 7.14: The streamlines in wave frame for asymmetric channel when  $m = 0.05$  with (a)  $\phi = 0$ , (b)  $\phi = \pi/4$ , (c)  $\phi = \pi/2$  and (d)  $\phi = \pi$ .

## 7.5 Concluding remarks

We have presented the peristaltic motion of power-law fluid in an asymmetric channel with convective conditions at the channel walls. Closed form non-unique solutions of velocity, temperature and stream function are computed. By choosing different material parameters, the behaviors of the shear-thinning, shear-thickening and Newtonian fluids are compared and discussed. Typical features of peristaltic flow, e.g. pumping and trapping, are observed from the presented results. The thermal study reveals that a combined increase in Biot numbers and power-law fluid parameter decreases the temperature of fluid. On the other hand the Brinkman

number enhances the temperature of fluid.

## Chapter 8

# Exact solution for peristaltic transport of micropolar fluid in a channel with convective conditions and heat source/sink

### 8.1 Introduction

This chapter investigates the peristaltic transport of an incompressible micropolar fluid in an asymmetric channel with heat source/sink and convective boundary conditions. Mathematical formulation is completed in a wave frame of reference. Long wavelength and low Reynolds number approach is adopted. The solutions for velocity, microrotation component, axial pressure gradient, temperature, stream function and pressure rise over a wavelength are obtained. Velocity and temperature distributions are analyzed for different parameters of interest.

### 8.2 Flow equations

We consider the peristaltic transport of an incompressible micropolar fluid in a two-dimensional asymmetric channel of width  $d_1 + d_2$  (see Fig. 2.1). In Cartesian coordinate system the  $\bar{X}$ -axis is taken along the walls of the channel and  $\bar{Y}$ -axis perpendicular to the  $\bar{X}$ -axis. The flow created

is due to the propagation of sinusoidal waves parallel to the channel walls. The shapes of such waves are given by

$$\begin{aligned}\bar{h}_1(\bar{X}, \bar{t}) &= d_1 + a_1 \cos \frac{2\pi}{\lambda}(\bar{X} - c\bar{t}), & \text{upper wall,} \\ \bar{h}_2(\bar{X}, \bar{t}) &= -d_2 - a_2 \cos \left( \frac{2\pi}{\lambda}(\bar{X} - c\bar{t}) + \phi \right), & \text{lower wall.}\end{aligned}\quad (8.1)$$

In above expressions  $c$  is the wave speed,  $a_1, a_2$  are the waves amplitudes,  $\lambda$  is the wavelength,  $d_1 + d_2$  is the width of the asymmetric channel, the phase difference  $\phi$  varies in the range  $0 \leq \phi \leq \pi$  ( $\phi = 0$  corresponds to symmetric channel with waves out of phase and  $\phi = \pi$  the waves are in phase) and further  $a_1, a_2, d_1, d_2$  and  $\phi$  satisfy the condition

$$a_1^2 + a_2^2 + 2a_1a_2 \cos \phi \leq (d_1 + d_2)^2. \quad (8.2)$$

Let  $(\bar{U}, \bar{V})$  be the velocity components in a fixed frame of reference  $(\bar{X}, \bar{Y})$ . The flow in fixed frame of reference is unsteady. However if observed in a coordinate system moving at the wave speed  $c$  (wave frame)  $(\bar{x}, \bar{y})$  it can be treated as steady. The coordinates and velocities in the two frames are related through the following expressions:

$$\begin{aligned}\bar{x} &= \bar{X} - c\bar{t}, \quad \bar{y} = \bar{Y}, \quad \bar{u}(\bar{x}, \bar{y}) = \bar{U}(\bar{X}, \bar{Y}, \bar{t}) - c, \\ \bar{v}(\bar{x}, \bar{y}) &= \bar{V}(\bar{X}, \bar{Y}, \bar{t}), \quad T(\bar{x}, \bar{y}) = T(\bar{X}, \bar{Y}, \bar{t}),\end{aligned}\quad (8.3)$$

where  $\bar{u}$  and  $\bar{v}$  indicate the velocity components in the wave frame.

The equations governing without body force and body couple are given by

$$\text{div } \bar{\mathbf{v}} = 0. \quad (8.4)$$

$$\rho(\bar{\mathbf{v}} \cdot \nabla) \bar{\mathbf{v}} = -\nabla \bar{p} + k^* \nabla \times \bar{\mathbf{w}} + (\mu + k^*) \nabla^2 \bar{\mathbf{v}}, \quad (8.5)$$

$$\rho \bar{j}(\bar{\mathbf{v}} \cdot \nabla) \bar{\mathbf{w}} = -2k^* \bar{\mathbf{w}} + k^* \nabla \times \bar{\mathbf{v}} - \check{e}(\nabla \times \nabla \times \bar{\mathbf{w}}) + (\check{a} + \check{c} + \check{e}) \nabla(\nabla \cdot \bar{\mathbf{w}}), \quad (8.6)$$

$$\rho c_p \frac{dT}{d\bar{t}} = k \nabla^2 T + Q_0, \quad (8.7)$$

in which  $\bar{\mathbf{v}}$  is the velocity,  $\bar{\mathbf{w}}$  the microrotation vector,  $\bar{p}$  the fluid pressure,  $\rho$  the fluid density,  $\bar{j}$  the microgyration parameter,  $d/d\bar{t}$  the material time derivative,  $T$  the fluid temperature,  $c_p$

the specific heat,  $k$  the thermal conductivity of the material, the constant heat source/sink parameter  $Q_0$ , and  $\nabla^2 = \left( \frac{\partial^2}{\partial X^2} + \frac{\partial^2}{\partial Y^2} \right)$  (The overbar refers to a dimensional quantity). The material constants  $\mu$ ,  $k^*$ ,  $\check{a}$ ,  $\check{c}$  and  $\check{e}$  satisfy the following inequalities [43]

$$2\mu + k^* \geq 0, \quad k^* \geq 0, \quad 3\check{a} + \check{c} + \check{e} \geq 0, \quad \check{e} \geq |\check{c}|. \quad (8.8)$$

The exchange of heat with the ambient temperature at the walls through Newton's law of cooling is given by

$$-k \frac{\partial T}{\partial \bar{y}} = \eta_1 (T - T_a) \quad \text{at} \quad \bar{y} = \bar{h}_1, \quad (8.9)$$

$$-k \frac{\partial T}{\partial \bar{y}} = \eta_2 (T_a - T) \quad \text{at} \quad \bar{y} = \bar{h}_2, \quad (8.10)$$

in which  $T_a$  is the ambient temperature and  $\eta_1$  and  $\eta_2$  are heat transfer coefficients at the upper and lower channel walls respectively.

For the flow under consideration, the velocity field is  $\bar{\mathbf{v}} = (\bar{u}, \bar{v}, 0)$  and microrotation vector is  $\bar{\mathbf{w}} = (0, 0, \bar{w})$ . We introduce dimensionless variables, the Reynolds number (Re), the wave number ( $\delta$ ), Prandtl number (Pr) and the Biot numbers as follows:

$$\begin{aligned} x &= \frac{\bar{x}}{\lambda}, \quad y = \frac{\bar{y}}{d_1}, \quad u = \frac{\bar{u}}{c}, \quad v = \frac{\bar{v}}{c\delta}, \quad w = \frac{d_1 \bar{w}}{c}, \\ t &= \frac{c}{\lambda} \bar{t}, \quad p = \frac{d_1^2 \bar{p}}{c\lambda\mu}, \quad j = \frac{\bar{j}}{d_1^2}, \quad \delta = \frac{d_1}{\lambda}, \quad h_1 = \frac{\bar{h}_1}{d_1}, \\ h_2 &= \frac{\bar{h}_2}{d_1}, \quad \theta = \frac{T - T_a}{T_a}, \quad \text{Re} = \frac{\rho c d_1}{\eta_0}, \quad \text{Pr} = \frac{\mu c_p}{k}, \\ \beta' &= \frac{Q_0 d_1^2}{k T_a}, \quad Bi_1 = \frac{\eta_1 d_1}{k}, \quad Bi_2 = \frac{\eta_2 d_1}{k}. \end{aligned} \quad (8.11)$$

The dimensionless formulation gives

$$\frac{\partial u}{\partial x} + \frac{\partial v}{\partial y} = 0, \quad (8.12)$$

$$\text{Re } \delta \left( u \frac{\partial}{\partial x} + v \frac{\partial}{\partial y} \right) u = -\frac{\partial p}{\partial x} + \frac{1}{1-N} \left( N \frac{\partial w}{\partial y} + \delta^2 \frac{\partial^2 u}{\partial x^2} + \frac{\partial^2 u}{\partial y^2} \right), \quad (8.13)$$

$$\text{Re } \delta \left( u \frac{\partial}{\partial x} + v \frac{\partial}{\partial y} \right) v = -\frac{\partial p}{\partial y} + \frac{\delta^2}{1-N} \left( -N \frac{\partial w}{\partial x} + \delta^2 \frac{\partial^2 v}{\partial x^2} + \frac{\partial^2 v}{\partial y^2} \right), \quad (8.14)$$

$$\begin{aligned} \frac{\text{Re } j \delta (1-N)}{N} \left( u \frac{\partial}{\partial x} + v \frac{\partial}{\partial y} \right) w &= -2w + \left( \delta^2 \frac{\partial v}{\partial x} - \frac{\partial u}{\partial y} \right) \\ &+ \frac{2-N}{m^2} \left( \delta^2 \frac{\partial^2 w}{\partial x^2} - \frac{\partial^2 w}{\partial y^2} \right), \end{aligned} \quad (8.15)$$

$$\text{Re Pr } \delta \left( u \frac{\partial}{\partial x} + v \frac{\partial}{\partial y} \right) \theta = \delta^2 \frac{\partial^2 \theta}{\partial x^2} + \frac{\partial^2 \theta}{\partial y^2} + \beta', \quad (8.16)$$

$$\frac{\partial \theta}{\partial y} + Bi_1 \theta = 0 \text{ at } y = h_1, \quad (8.17)$$

$$\frac{\partial \theta}{\partial y} - Bi_2 \theta = 0 \text{ at } y = h_2, \quad (8.18)$$

where  $N = k^*/(\mu + k^*)$  is the coupling number ( $0 \leq N \leq 1$ ),  $m^2 = d_1^2 k^* (2\mu + k^*) / (\check{e}(\mu + k^*))$  is the micropolar parameter [43],  $\beta'$  is the dimensionless heat source/sink parameter and  $\check{a}$ ,  $\check{c}$  do not appear in the governing equation as the microrotation vector is solenoidal. These equations reduce to the classical Navier-Stokes equation when  $k^* \rightarrow 0$ .

Equations (8.12) – (8.16) subject to long wavelength and low Reynolds number assumptions yield

$$\frac{\partial u}{\partial x} + \frac{\partial v}{\partial y} = 0, \quad (8.19)$$

$$N \frac{\partial w}{\partial y} + \frac{\partial^2 u}{\partial y^2} = (1-N) \frac{\partial p}{\partial x}, \quad (8.20)$$

$$\frac{\partial p}{\partial y} = 0, \quad (8.21)$$

$$-2w - \frac{\partial u}{\partial y} + \left( \frac{2-N}{m^2} \right) \frac{\partial^2 w}{\partial y^2} = 0, \quad (8.22)$$

$$\frac{\partial^2 \theta}{\partial y^2} + \beta' = 0, \quad (8.23)$$

where Eq. (8.21) indicates that  $p \neq p(y)$ .

The conditions in wave frame of reference are

$$u = -1, \quad \text{at } y = h_1(x), \ y = h_2(x), \quad (8.24)$$

$$w = 0, \quad \text{at } y = h_1(x), \ y = h_2(x), \quad (8.25)$$

where

$$h_1(x) = 1 + a \cos(2\pi x), \ h_2(x) = -d - b \cos(2\pi x + \phi), \quad (8.26)$$

### 8.3 Exact solution

With the help of Eq. (8.21), Eq. (8.20) can be written in the following form

$$\frac{\partial^2 u}{\partial y^2} = \frac{\partial}{\partial y} \left( (1 - N) \frac{dp}{dx} y - Nw \right). \quad (8.27)$$

Integration of the above equation yields

$$\frac{\partial u}{\partial y} = (1 - N) \frac{dp}{dx} y - Nw + C_1. \quad (8.28)$$

Putting above equation in Eq. (8.22) we get

$$\frac{\partial^2 w}{\partial y^2} - m^2 w = \chi^2 C_1 + \chi^2 (1 - N) \frac{dp}{dx} y. \quad (8.29)$$

The general solution of Eq. (8.29) is

$$w = -\frac{\chi^2 C_1}{m^2} - \frac{\chi^2}{m^2} (1 - N) \frac{dp}{dx} y + C_2 \cosh my + C_3 \sinh my. \quad (8.30)$$

Through Eqs. (8.28) and (8.30) we have

$$u = \frac{1}{2} \left( 1 + \frac{N\chi^2}{m^2} \right) (1 - N) \frac{dp}{dx} y^2 + C_1 \left( 1 + \frac{N\chi^2}{m^2} \right) y - \frac{C_2 N}{m} \sinh my - \frac{C_3 N}{m} \cosh my + C_4, \quad (8.31)$$

in which  $C_{1-4}$  are the constants of integration and  $\chi^2 = m^2/(2 - N)$ .

The arbitrary constants involved in Eq. (8.31) can be found with the help of boundary



conditions (8.24) and (8.25) and are given by

$$C_1 = \frac{L_7}{2L_6} \frac{dp}{dx}, \quad C_2 = \frac{L_8}{2L_6} \frac{dp}{dx}, \quad C_3 = \frac{L_9}{-4L_6} \frac{dp}{dx}, \quad C_4 = \frac{L_{10}}{4L_6} \frac{dp}{dx} + \frac{L_{11}}{4L_6}. \quad (8.32)$$

The exact solution of the energy equation (8.23) is given by

$$\theta = C_5 y^2 + C_6 y + C_7, \quad (8.33)$$

in which the constants  $C_{5-7}$  can be found with the help of boundary conditions (8.17) and (8.18) and are given by

$$C_5 = -\frac{\beta'}{2}, \quad C_6 = \frac{L_{13}}{2L_{12}}, \quad C_7 = -\frac{L_{14}}{2L_{12}}. \quad (8.34)$$

Using

$$F = \int_{h_2(x)}^{h_1(x)} u dy,$$

we find that

$$\frac{dp}{dx} = \frac{F - \frac{L_{11}}{4L_6}(h_1 - h_2)}{L}, \quad (8.35)$$

where

$$\begin{aligned} L = & \frac{L_2}{3}(h_1^3 - h_2^3) + \frac{L_1 L_7}{2L_6}(h_1^2 - h_2^2) + \frac{L_3 L_8}{4mL_6}(\cosh mh_1 - \cosh mh_2) \\ & - \frac{L_3 L_9}{4mL_6}(\sinh mh_1 - \sinh mh_2) + \frac{L_{10}}{4L_6}(h_1 - h_2). \end{aligned} \quad (8.36)$$

The corresponding stream function is

$$\psi = \frac{L_{11}}{4L_6} y + \frac{dp}{dx} \left[ L_2 \frac{y^3}{3} + \frac{L_1 L_7}{L_6} \frac{y^2}{2} + \frac{L_3 L_8}{4mL_6} \cosh my - \frac{L_3 L_9}{4mL_6} \sinh my + \frac{L_{10}}{4L_6} y \right], \quad (8.37)$$

where

$$\begin{aligned}
L_1 &= \frac{1}{2} \left( 1 + \frac{N\chi^2}{m^2} \right), \\
L_2 &= L_1(1 - N), \\
L_3 &= -\frac{N}{m}, \quad L_4 = -\frac{\chi^2}{m^2}, \quad L_5 = L_4(1 - N), \\
L_6 &= (h_1 - h_2)L_1 \cosh \left( \frac{h_1 - h_2}{2} \right) m - L_3L_4 \sinh \left( \frac{h_1 - h_2}{2} \right) m, \\
L_7 &= -(h_1 + h_2) \left[ (h_1 - h_2)L_2 \cosh \left( \frac{h_1 - h_2}{2} \right) m - L_3L_5 \sinh \left( \frac{h_1 - h_2}{2} \right) m \right], \\
L_8 &= (h_1 - h_2) \csc h \left( \frac{h_1 - h_2}{2} \right) m [L_3L_4L_5(\cosh mh_2 - \cosh mh_1) + (h_1 + h_2)L_2L_4 \sinh mh_1 \\
&\quad + 2L_1L_5(h_1 \sinh mh_2 - h_2 \sinh mh_1) - (h_1 - h_2)L_2L_4 \sinh mh_2], \\
L_9 &= (h_1 - h_2) \csc h \left( \frac{h_1 - h_2}{2} \right) m [(h_1 + h_2)L_2L_4(\cosh mh_1 - \cosh mh_2) \\
&\quad + 2L_1L_5(h_2 \cosh mh_1 - h_1 \cosh mh_2) + L_3L_4L_5(\sinh mh_2 - \sinh mh_1)], \\
L_{10} &= \csc h \left( \frac{h_1 - h_2}{2} \right) m [-L_2L_3L_5(h_1^2 + h_2^2) (L_2L_3L_4(h_1^2 + h_2^2) - 4h_1h_2L_1L_3L_5) \\
&\quad \times \cosh(h_1 - h_2)m + 2L_1L_3L_5(h_1^2 + h_2^2) \\
&\quad + (h_1 - h_2) \sinh(h_1 - h_2)m (2h_1h_2L_1L_2 - L_3^2L_4L_5)], \\
L_{11} &= \csc h \left( \frac{h_1 - h_2}{2} \right) m [2L_3L_4(\cosh(h_1 - h_2)m - 1) - 2(h_1 - h_2)L_1 \sinh(h_1 - h_2)m], \\
L_{12} &= (Bi_2 + Bi_1(-1 + Bi_2(h_1 - h_2))), \\
L_{13} &= 2Bi_2h_1\beta + Bi_1(-2h_2\beta + Bi_2(2 + (h_1 - h_2)(h_1 + h_2))), \\
L_{14} &= 2Bi_1(1 + Bi_2h_2) + 2h_1\beta - h_1\beta(2 + Bi_2(-2h_1 + h_2)) \\
&\quad + Bi_1h_1\beta(h_1 + Bi_2h_1h_2 - h_2(2 + Bi_2h_2)).
\end{aligned}$$

The dimensionless expression for the pressure rise per wavelength  $\Delta p_\lambda$  is

$$\Delta p_\lambda = \int_0^1 \left( \frac{dp}{dx} \right) dx. \tag{8.38}$$

## 8.4 Shear stress distribution at the walls

It is interesting to note that the stress tensor of the micropolar fluid is not symmetric. The non-dimensional shear stresses in the problem under consideration are given by

$$\tau_{xy} = \frac{\partial u}{\partial y} - \frac{N}{1-N}w, \quad (8.39)$$

$$\tau_{yx} = \frac{1}{1-N} \frac{\partial u}{\partial y} + \frac{N}{1-N}w. \quad (8.40)$$

## 8.5 Results and discussion

To discuss qualitatively the influence of embedding parameters of interest on flow quantities such as velocity  $u(y)$  and temperature distribution  $\theta(y)$ , we have prepared Tables 8.1 – 8.5 and Figs. 8.1 – 8.4. The effects of various parameters on pressure gradient  $dp/dx$ , pressure rise per wavelength  $\Delta p_\lambda$ , shear stresses at upper and lower walls and pumping and trapping are already investigated in ref. [74]. Hence we avoid to include such results here. Tables 8.1 and 8.2 show the effects of  $m$  and  $N$  on velocity profile. It is observed from the tabulated values that the velocity profile increases near the center of the channel and it has opposite behavior near the channel walls for increasing values of  $m$  and  $N$ . Fig. 8.1 discloses that by increasing the value of  $Bi_1$  the temperature profile  $\theta(y)$  decreases near the upper wall while it has no significant effect near the lower wall of channel. Also the temperature  $\theta(y)$  decreases near the lower wall by increasing the Biot number  $Bi_2$  and it has no effect on temperature profile near the upper wall of the channel (see Fig. 8.2). Figs. 8.3 and 8.4 portray the temperature distribution for different values of  $\beta'$ . It is found that the temperature distribution decreases when there is a sink and it increases when there is an external source. These results for different values of  $Bi_1$ ,  $Bi_2$  and  $\beta'$  are also confirmed from Tables 8.3 – 8.5 respectively.

**Table 8.1:** Values of the axial velocity  $u$  at  $x = -0.5$  for  $a = 0.5$ ,  $b = 0.5$ ,  $d = 1$ ,  $\Theta = 1.2$ ,

$\phi = \pi/2$ and $N = 0.3$									
$m$	$y = -1$	$y = -0.8$	$y = -0.6$	$y = -0.5$	$y = -0.2$	$y = 0$	$y = 0.1$	$y = 0.3$	$y = 0.5$
3	-1	0.0470	0.7982	1.0528	1.3092	1.0528	0.7982	0.0470	-1
5	-1	0.0384	0.7991	1.0579	1.3188	1.0579	0.7991	0.0384	-1
7	-1	0.0359	0.8006	1.0600	1.3208	1.0600	0.8006	0.0359	-1

**Table 8.2:** Values of the axial velocity  $u$  at  $x = -0.5$  for  $a = 0.5$ ,  $b = 0.5$ ,  $d = 1$ ,  $\Theta = 1.2$ ,

$\phi = \pi/2$ and $m = 4$									
$N$	$y = -1$	$y = -0.8$	$y = -0.6$	$y = -0.5$	$y = -0.2$	$y = 0$	$y = 0.1$	$y = 0.3$	$y = 0.5$
0.3	-1	0.0417	0.7985	1.0558	1.3153	1.0558	0.7985	0.0417	-1
0.4	-1	0.0335	0.7983	1.0602	1.3251	1.0602	0.7983	0.0335	-1
0.5	-1	0.0247	0.7980	1.0649	1.3357	1.0649	0.7980	0.0247	-1

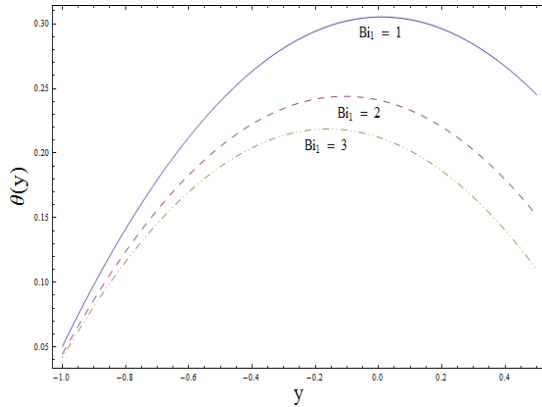


Fig. 8.1

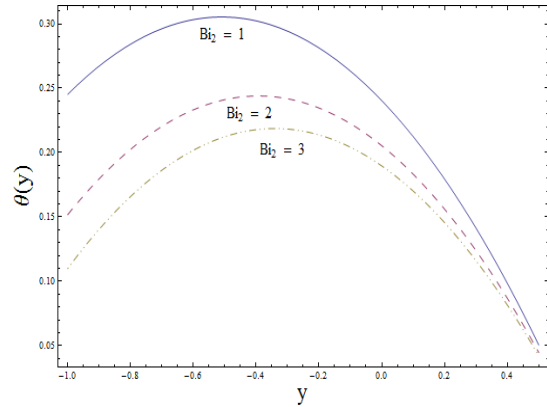


Fig. 8.2

Fig. 8.1: Plot showing  $\theta$  versus  $y$ . Here  $x = -0.5$ ,  $a = b = 0.5$ ,  $d = 1$ ,  $\Theta = 1.2$ ,  $\phi = \pi/2$ ,

$$Bi_2 = 10 \text{ and } \beta' = 0.5.$$

Fig. 8.2: Plot showing  $\theta$  versus  $y$ . Here  $x = -0.5$ ,  $a = b = 0.5$ ,  $d = 1$ ,  $\Theta = 1.2$ ,  $\phi = \pi/2$ ,

$$Bi_1 = 10 \text{ and } \beta' = 0.5.$$

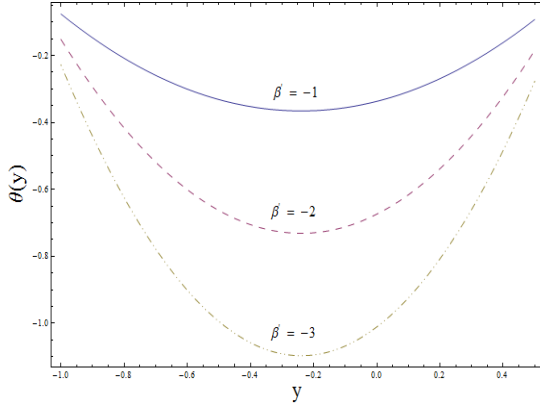


Fig. 8.3

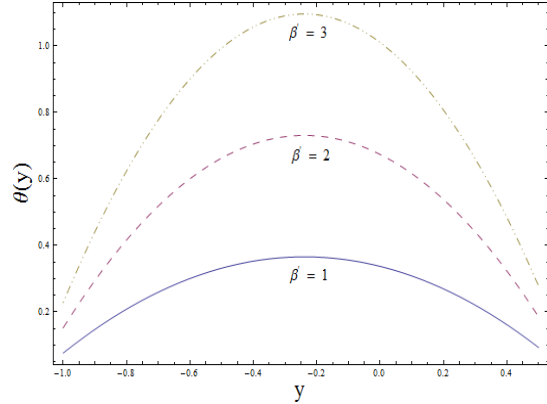


Fig. 8.4

Fig. 8.3: Plot showing  $\theta$  versus  $y$  for heat sink. Here  $x = -0.5$ ,  $a = b = 0.5$ ,  $d = 1$ ,  $\Theta = 1.2$ ,

$$\phi = \pi/2, Bi_1 = 8 \text{ and } Bi_2 = 10.$$

Fig. 8.4: Plot showing  $\theta$  versus  $y$  for heat source. Here  $x = -0.5$ ,  $a = b = 0.5$ ,  $d = 1$ ,  $\Theta = 1.2$ ,

$$\phi = \pi/2, Bi_1 = 8 \text{ and } Bi_2 = 10.$$

**Table 8.3:** Values of the temperature  $\theta$  at  $x = -0.5$  for  $a = b = 0.5$ ,  $d = 1$ ,  $\Theta = 1.2$ ,  $\phi = \pi/2$ ,  
 $Bi_2 = 10$  and  $\beta' = 0.5$

$Bi_1$	$y = -1$	$y = -0.8$	$y = -0.6$	$y = -0.5$	$y = -0.2$	$y = 0$	$y = 0.1$	$y = 0.3$	$y = 0.5$
1	0.05048	0.14144	0.21240	0.24038	0.29432	0.30529	0.30327	0.28423	0.24519
2	0.04464	0.12392	0.18321	0.20536	0.24177	0.24107	0.23321	0.20250	0.15179
3	0.04202	0.11608	0.17013	0.18965	0.21823	0.21228	0.20181	0.16586	0.10991

**Table 8.4:** Values of the temperature  $\theta$  at  $x = -0.5$  for  $a = b = 0.5$ ,  $d = 1$ ,  $\Theta = 1.2$ ,  $\phi = \pi/2$ ,

$$Bi_1 = 10 \text{ and } \beta' = 0.5$$

$Bi_2$	$y = -1$	$y = -0.8$	$y = -0.6$	$y = -0.5$	$y = -0.2$	$y = 0$	$y = 0.1$	$y = 0.3$	$y = 0.5$
1	0.24519	0.28423	0.30327	0.30529	0.28135	0.24038	0.21240	0.14144	0.05048
2	0.15179	0.20250	0.23321	0.24107	0.23464	0.20536	0.18321	0.12392	0.04464
3	0.10991	0.16586	0.20181	0.21228	0.21370	0.18965	0.17013	0.11608	0.04202

**Table 8.5:** Values of the temperature  $\theta$  at  $x = -0.5$  for  $a = b = 0.5$ ,  $d = 1$ ,  $\Theta = 1.2$ ,  $\phi = \pi/2$ ,

$Bi_1 = 8$ and $Bi_2 = 10$									
$\beta'$	$y = -1$	$y = -0.8$	$y = -0.6$	$y = -0.5$	$y = -0.2$	$y = 0$	$y = 0.1$	$y = 0.3$	$y = 0.5$
-1	-0.076	-0.208	-0.300	-0.332	-0.365	-0.337	-0.308	-0.220	-0.092
-2	-0.152	-0.416	-0.601	-0.663	-0.730	-0.674	-0.616	-0.440	-0.185
-3	-0.228	-0.625	-0.901	-0.994	-1.094	-1.011	-0.924	-0.661	-0.277
1	0.076	0.208	0.300	0.332	0.365	0.337	0.308	0.220	0.092
2	0.152	0.416	0.601	0.663	0.730	0.674	0.616	0.440	0.185
3	0.228	0.625	0.901	0.994	1.094	1.011	0.924	0.661	0.277

## 8.6 Concluding remarks

A mathematical model subject to long wavelength and low Reynolds number approximations is presented in order to study the effects of convective boundary conditions on peristaltic transport of micropolar fluid in an asymmetric channel with heat source/sink. Solution expressions of stream function, longitudinal velocity, temperature and pressure gradient are developed. It is concluded that velocity has maximum value near  $y = -0.2$  (due to asymmetry of the channel) while it decreases near the channel boundaries for increasing values of  $m$  and  $N$ . The thermal study discloses that with increase in Biot numbers at the lower wall  $Bi_2$  and the upper wall  $Bi_1$ , the fluid temperature decreases. It is worth mentioning that when we take very large values of Biot numbers, the case of prescribed surface temperature is deduced. It is also found that the temperature increases (decreases) when there is an increase in heat source (sink) parameter.

## Chapter 9

# Peristaltic flow of Sisko fluid in an asymmetric channel with convective boundary conditions

### 9.1 Introduction

This chapter deals with the peristaltic flow of Sisko fluid in an asymmetric channel with sinusoidal wave propagating down its walls. The channel walls in heat transfer process satisfy the convective conditions. The flow and heat transfer equations are modeled and non-dimensionalized. Analysis has been carried out subject to long wavelength and low Reynolds number considerations. The shear-thinning and shear-thickening properties of Sisko fluid in the present nonlinear analysis are examined. Comparison between the results of Sisko and viscous fluids is given. Velocity and temperature distributions, pressure gradient and streamline pattern are addressed with respect to different parameters of interest. Pumping and trapping phenomena are also analyzed.

### 9.2 Problem formulation and flow equations

We consider the flow of an incompressible Sisko fluid in an asymmetric channel (see Fig. 2.1). The  $\bar{X}$  and  $\bar{Y}$  axes are selected along and perpendicular to the channel walls respectively. The

flow created is due to the following sinusoidal waves:

$$\begin{aligned}\bar{h}_1(\bar{X}, \bar{t}) &= d_1 + a_1 \cos \frac{2\pi}{\lambda}(\bar{X} - c\bar{t}), & \text{upper wall,} \\ \bar{h}_2(\bar{X}, \bar{t}) &= -d_2 - a_2 \cos \left( \frac{2\pi}{\lambda}(\bar{X} - c\bar{t}) + \phi \right), & \text{lower wall.}\end{aligned}\quad (9.1)$$

In above expressions  $c$  is the wave speed,  $a_1, a_2$  are the waves amplitudes,  $\lambda$  is the wavelength,  $d_1 + d_2$  is the width of the asymmetric channel, the phase difference  $\phi$  varies in the range  $0 \leq \phi \leq \pi$  ( $\phi = 0$  corresponds to symmetric channel with waves out of phase and  $\phi = \pi$  the waves are in phase) and further  $a_1, a_2, d_1, d_2$  and  $\phi$  satisfy the condition

$$a_1^2 + a_2^2 + 2a_1a_2 \cos \phi \leq (d_1 + d_2)^2. \quad (9.2)$$

Incompressibility condition gives

$$\text{div } \bar{\mathbf{V}} = 0. \quad (9.3)$$

The equations of motion and energy are

$$\rho \frac{d\bar{\mathbf{V}}}{d\bar{t}} = -\text{grad } \bar{p} + \text{div } \bar{\mathbf{S}}, \quad (9.4)$$

$$\rho c_p \frac{dT}{d\bar{t}} = k \nabla^2 T + \bar{\boldsymbol{\tau}} \cdot (\text{grad } \bar{\mathbf{V}}), \quad (9.5)$$

in which  $\bar{\mathbf{V}}$  is the velocity,  $\rho$  is density of the fluid,  $d/d\bar{t}$  is material time derivative, body forces are absent,  $T$  the fluid temperature,  $c_p$  the specific heat,  $k$  the thermal conductivity of the material, the Cauchy stress tensor  $\bar{\boldsymbol{\tau}} = -\bar{p}\bar{\mathbf{I}} + \bar{\mathbf{S}}$ ,  $\bar{p}$  the pressure,  $\bar{\mathbf{S}}$  the extra stress tensor and  $\nabla^2 = \left( \frac{\partial^2}{\partial \bar{X}^2} + \frac{\partial^2}{\partial \bar{Y}^2} \right)$  (The overbar refers to a dimensional quantity).

The exchange of heat with ambient at the channel walls can be expressed in the forms

$$k \frac{\partial T}{\partial \bar{y}} = -\eta_1(T - T_1) \quad \text{at } \bar{y} = \bar{h}_1, \quad (9.6)$$

$$k \frac{\partial T}{\partial \bar{y}} = -\eta_2(T - T_0) \quad \text{at } \bar{y} = \bar{h}_2, \quad (9.7)$$

where  $\eta_1$  and  $\eta_2$ ,  $T_1$  and  $T_0$  are the heat transfer coefficients and the temperatures at the upper and lower channel walls respectively.



For two-dimensional flow of Sisko fluid, we have the velocity  $\bar{\mathbf{V}}$  and extra stress tensor  $\bar{\mathbf{S}}$  in the forms:

$$\bar{\mathbf{V}} = (\bar{U}(\bar{X}, \bar{Y}, \bar{t}), \bar{V}(\bar{X}, \bar{Y}, \bar{t}), 0), \quad (9.8)$$

$$\bar{\mathbf{S}} = \left[ \tilde{\alpha} + \tilde{\beta} \left| \sqrt{\bar{\Pi}} \right|^{\tilde{n}-1} \right] \bar{\mathbf{A}}_1, \quad (9.9)$$

$$\bar{\mathbf{A}}_1 = \bar{\mathbf{L}} + \bar{\mathbf{L}}^*, \quad \bar{\mathbf{L}} = \text{grad } \bar{\mathbf{V}}, \quad \bar{\Pi} = \frac{1}{2} \text{tr}(\bar{\mathbf{A}}_1^2). \quad (9.10)$$

Here  $\bar{\mathbf{A}}_1$  is the rate of deformation tensor,  $\bar{\Pi}$  the second invariant of the symmetric part of the velocity gradient,  $\tilde{n}$ ,  $\tilde{\alpha}$  and  $\tilde{\beta}$  the material parameters defined differently for different fluids. Note that for  $\tilde{n} = 1$ ,  $\tilde{\beta} = \mu$ ,  $\tilde{\alpha} = 0$  or  $\tilde{\beta} = 0$ ,  $\tilde{\alpha} = \mu$  the Newtonian fluid model is recovered, and for  $\tilde{\alpha} = 0$  the power-law model can be obtained.

If  $(\bar{x}, \bar{y})$  and  $(\bar{u}, \bar{v})$  are the coordinates and velocity components in the wave frame  $(\bar{x}, \bar{y})$  then we define

$$\bar{x} = \bar{X} - c\bar{t}, \quad \bar{y} = \bar{Y}, \quad \bar{u}(\bar{x}, \bar{y}) = \bar{U}(\bar{X}, \bar{Y}, \bar{t}) - c, \quad \bar{v}(\bar{x}, \bar{y}) = \bar{V}(\bar{X}, \bar{Y}, \bar{t}), \quad T(\bar{x}, \bar{y}) = T(\bar{X}, \bar{Y}, \bar{t}), \quad (9.11)$$

where  $(\bar{X}, \bar{Y})$  are the coordinates in the fixed frame. Employing these transformations and introducing the following dimensionless variables

$$\begin{aligned} x &= \frac{\bar{x}}{\lambda}, \quad y = \frac{\bar{y}}{d_1}, \quad u = \frac{\bar{u}}{c}, \quad v = \frac{\bar{v}}{c}, \quad p = \frac{d_1^2 \bar{p}}{c\mu\lambda}, \quad b^* = \frac{\tilde{\beta}}{\tilde{\alpha}(d_1/c)^{\tilde{n}-1}}, \\ h_1 &= \frac{\bar{h}_1}{d_1}, \quad h_2 = \frac{\bar{h}_2}{d_1}, \quad t = \frac{c\bar{t}}{\lambda}, \quad \mathbf{S} = \frac{d_1}{\mu c} \bar{\mathbf{S}}, \quad \theta = \frac{T - T_0}{T_1 - T_0} \end{aligned} \quad (9.12)$$

and the stream function  $\psi(x, y)$  by

$$u = \frac{\partial \psi}{\partial y}, \quad v = -\delta \frac{\partial \psi}{\partial x}, \quad (9.13)$$

Eq. (9.3) is satisfied identically and Eqs. (9.4) and (9.5) yield

$$\delta \text{Re} \left[ \left( \frac{\partial \psi}{\partial y} \frac{\partial}{\partial x} - \frac{\partial \psi}{\partial x} \frac{\partial}{\partial y} \right) \left( \frac{\partial \psi}{\partial y} \right) \right] + \frac{\partial p}{\partial x} = \delta \frac{\partial S_{xx}}{\partial x} + \frac{\partial S_{xy}}{\partial y}, \quad (9.14)$$

$$-\delta^3 \text{Re} \left[ \left( \frac{\partial \psi}{\partial y} \frac{\partial}{\partial x} - \frac{\partial \psi}{\partial x} \frac{\partial}{\partial y} \right) \left( \frac{\partial \psi}{\partial x} \right) \right] + \frac{\partial p}{\partial y} = \delta^2 \frac{\partial S_{xy}}{\partial x} + \delta \frac{\partial S_{yy}}{\partial y}, \quad (9.15)$$

$$\delta \text{Re} \left[ \frac{\partial \psi}{\partial y} \frac{\partial}{\partial x} - \frac{\partial \psi}{\partial x} \frac{\partial}{\partial y} \right] \theta = \frac{1}{\text{Pr}} \left( \delta^2 \frac{\partial^2}{\partial x^2} + \frac{\partial^2}{\partial y^2} \right) \theta + Ec \left[ \delta \frac{\partial^2 \psi}{\partial x \partial y} (S_{xx} - S_{yy}) + \left( \frac{\partial^2 \psi}{\partial y^2} - \delta^2 \frac{\partial^2 \psi}{\partial x^2} \right) S_{xy} \right], \quad (9.16)$$

where the components of extra stress tensor from Eq. (9.9) are

$$S_{xx} = 2\delta \left[ 1 + b^* \left| 4\delta^2 \left( \frac{\partial^2 \psi}{\partial x \partial y} \right)^2 + \left( \frac{\partial^2 \psi}{\partial y^2} - \delta^2 \frac{\partial^2 \psi}{\partial x^2} \right) \right|^{2(\tilde{n}-1)/2} \right] \frac{\partial^2 \psi}{\partial x \partial y}, \quad (9.17)$$

$$S_{xy} = \left[ 1 + b^* \left| 4\delta^2 \left( \frac{\partial^2 \psi}{\partial x \partial y} \right)^2 + \left( \frac{\partial^2 \psi}{\partial y^2} - \delta^2 \frac{\partial^2 \psi}{\partial x^2} \right) \right|^{2(\tilde{n}-1)/2} \right] \left( \frac{\partial^2 \psi}{\partial y^2} - \delta^2 \frac{\partial^2 \psi}{\partial x^2} \right), \quad (9.18)$$

$$S_{yy} = -2\delta \left[ 1 + b^* \left| 4\delta^2 \left( \frac{\partial^2 \psi}{\partial x \partial y} \right)^2 + \left( \frac{\partial^2 \psi}{\partial y^2} - \delta^2 \frac{\partial^2 \psi}{\partial x^2} \right) \right|^{2(\tilde{n}-1)/2} \right] \frac{\partial^2 \psi}{\partial x \partial y}. \quad (9.19)$$

In the above equations the dimensionless wave number  $\delta$ , the Reynolds number  $\text{Re}$ , the Prandtl number  $\text{Pr}$  and the Eckert number  $Ec$  are defined respectively as follows:

$$\delta = \frac{d_1}{\lambda}, \quad \text{Re} = \frac{\rho c d_1}{\mu}, \quad \text{Pr} = \frac{\mu c_p}{k}, \quad Ec = \frac{c^2}{(T_1 - T_0)c_p}. \quad (9.20)$$

Now Eqs. (9.6) and (9.7) give

$$\frac{\partial \theta}{\partial y} + Bi_1(\theta - 1) = 0 \text{ at } y = h_1, \quad (9.21)$$

$$\frac{\partial \theta}{\partial y} + Bi_2\theta = 0 \text{ at } y = h_2, \quad (9.22)$$

where  $Bi_1 = \eta_1 d_1/k$  and  $Bi_2 = \eta_2 d_1/k$  are the Biot numbers. Under the assumptions of long wavelength  $\delta \ll 1$  and low Reynolds number  $\text{Re} \rightarrow 0$  [6], Eqs. (9.14) and (9.15) become

$$\frac{\partial p}{\partial x} = \frac{\partial S_{xy}}{\partial y}, \quad (9.23)$$

$$\frac{\partial p}{\partial y} = 0. \quad (9.24)$$

The above equation indicates that  $p$  is independent of  $y$ . Eliminating the pressure  $p$  from Eqs.

(9.23) and (9.24) we get

$$\frac{\partial^2 S_{xy}}{\partial y^2} = 0. \quad (9.25)$$

Also Eq. (9.16) gives

$$\frac{\partial^2 \theta}{\partial y^2} + Br \left( \frac{\partial^2 \psi}{\partial y^2} \right) S_{xy} = 0, \quad (9.26)$$

where the Brinkman number  $Br$  is

$$Br = \text{Pr } Ec, \quad (9.27)$$

and  $S_{xy}$  is given by

$$S_{xy} = \left( 1 + b^* \left| \frac{\partial^2 \psi}{\partial y^2} \right|^{(\tilde{n}-1)} \right) \frac{\partial^2 \psi}{\partial y^2}. \quad (9.28)$$

The quantity  $\left( 1 + b^* \left| \frac{\partial^2 \psi}{\partial y^2} \right|^{(\tilde{n}-1)} \right)$  is called apparent viscosity. When the apparent viscosity decreases with increasing shear rate, we call the fluid shear-thinning. In the opposite case where the apparent viscosity increases as the fluid is subjected to a higher shear rate, the fluid is called shear-thickening. It turns out that the material relation (9.28) describes shear-thinning fluids for  $\tilde{n} < 1$  and shear-thickening fluids for  $\tilde{n} > 1$ . For  $\tilde{n} = 1$ , it reduces to Newtonian fluids.

The conditions for the dimensionless stream function in wave frame are

$$\psi = \frac{F}{2}, \quad \frac{\partial \psi}{\partial y} = -1, \quad \text{at } y = h_1(x), \quad (9.29)$$

$$\psi = -\frac{F}{2}, \quad \frac{\partial \psi}{\partial y} = -1, \quad \text{at } y = h_2(x). \quad (9.30)$$

with

$$F = \int_{h_2(x)}^{h_1(x)} \frac{\partial \psi}{\partial y} dy = \psi(h_1(x)) - \psi(h_2(x)). \quad (9.31)$$

The dimensionless forms of  $h_i$  ( $i = 1, 2$ ) are

$$h_1(x) = 1 + a \cos(2\pi x), \quad h_2(x) = -d - b \cos(2\pi x + \phi), \quad (9.32)$$

### 9.3 Method of solution

The resulting equation (9.25) is highly non-linear. For arbitrary values of parameters involving in this equation, the general solution in closed form seems impossible. Attention is thus focused

to the series solution for small parameter  $b^*$ . For that we expand  $\psi$ ,  $\theta$ ,  $S_{xy}$ ,  $p$  and  $F$  as follows:

$$\begin{aligned}
\psi &= \psi_0 + (b^*)\psi_1 + \dots, \\
\theta &= \theta_0 + (b^*)\theta_1 + \dots, \\
S_{xy} &= S_{0xy} + (b^*)S_{1xy} + \dots, \\
p &= p_0 + (b^*)p_1 + \dots, \\
F &= F_0 + (b^*)F_1 + \dots
\end{aligned} \tag{9.33}$$

Substitution of above equations into Eqs. (9.21–9.26), (9.28), (9.29), (9.30) and then collecting the terms of like powers of  $b^*$  we have:

### 9.3.1 Zeroth order system

$$\frac{\partial^4 \psi_0}{\partial y^4} = 0, \tag{9.34}$$

$$\frac{\partial^2 \theta_0}{\partial y^2} + Br \left( \frac{\partial^2 \psi_0}{\partial y^2} \right) S_{0xy} = 0, \tag{9.35}$$

$$\frac{dp_0}{dx} = \frac{\partial^3 \psi_0}{\partial y^3}, \tag{9.36}$$

$$\psi_0 = \frac{F_0}{2}, \quad \frac{\partial \psi_0}{\partial y} = -1, \quad \frac{\partial \theta_0}{\partial y} + Bi_1(\theta_0 - 1) = 0, \quad \text{at } y = h_1(x), \tag{9.37}$$

$$\psi_0 = \frac{-F_0}{2}, \quad \frac{\partial \psi_0}{\partial y} = -1, \quad \frac{\partial \theta_0}{\partial y} + Bi_2\theta_0 = 0, \quad \text{at } y = h_2(x). \tag{9.38}$$

### 9.3.2 First order system

$$\frac{\partial^2}{\partial y^2} \left[ \left( \frac{\partial^2 \psi_0}{\partial y^2} \right)^{\tilde{n}} + \frac{\partial^2 \psi_1}{\partial y^2} \right] = 0, \quad (9.39)$$

$$\frac{\partial^2 \theta_1}{\partial y^2} + Br \left[ 2 \left( \frac{\partial^2 \psi_0}{\partial y^2} \right) \left( \frac{\partial^2 \psi_1}{\partial y^2} \right) + \left( \frac{\partial^2 \psi_0}{\partial y^2} \right)^{\tilde{n}+1} \right] = 0, \quad (9.40)$$

$$\frac{dp_1}{dx} = \frac{\partial}{\partial y} \left[ \left( \frac{\partial^2 \psi_0}{\partial y^2} \right)^{\tilde{n}} + \frac{\partial^2 \psi_1}{\partial y^2} \right], \quad (9.41)$$

$$\psi_1 = \frac{F_1}{2}, \quad \frac{\partial \psi_1}{\partial y} = 0, \quad \frac{\partial \theta_1}{\partial y} + Bi_1 \theta_1 = 0, \quad \text{at } y = h_1(x), \quad (9.42)$$

$$\psi_1 = \frac{-F_1}{2}, \quad \frac{\partial \psi_1}{\partial y} = 0, \quad \frac{\partial \theta_1}{\partial y} + Bi_2 \theta_1 = 0, \quad \text{at } y = h_2(x). \quad (9.43)$$

In the next two subsections we will develop the solutions of above systems.

### 9.3.3 Zeroth order solution

The solutions of Eqs. (9.34) and (9.35) subject to the boundary conditions (9.37) and (9.38) are

$$\psi_0 = R_1 y^3 + R_2 y^2 + R_3 y + R_4, \quad (9.44)$$

$$\theta_0 = A_1 y^4 + A_2 y^3 + A_3 y^2 + A_4 y + A_5, \quad (9.45)$$

where

$$\begin{aligned}
R_1 &= \frac{-2(F_0 + h_1 - h_2)}{(h_1 - h_2)^3}, \\
R_2 &= \frac{3(F_0 + h_1 - h_2)(h_1 + h_2)}{(h_1 - h_2)^3}, \\
R_3 &= \frac{-h_1^3 - 6F_0h_1h_2 - 3h_1^2h_2 + 3h_1h_2^2 + h_2^3}{(h_1 - h_2)^3}, \\
R_4 &= \frac{-(h_1 + h_2)(2h_1h_2(-h_1 + h_2) + F_0(h_1^2 - 4h_1h_2 + h_2^2))}{2(h_1 - h_2)^3}, \\
B_1 &= Bi_2 + Bi_1(-1 + Bi_2(h_1 - h_2)), \\
B_2 &= 3h_1^2R_1^2 + 3h_1R_1R_2 + R_2^2, \quad B_3 = 3h_2^2R_1^2 + 3h_2R_1R_2 + R_2^2, \\
B_4 &= 3(h_1^4 - h_2^4)R_1^2 + 4(h_1^3 - h_2^3)R_1R_2 + 2(h_1^2 - h_2^2)R_2^2, \\
B_5 &= 1 + Bi_2h_2, \quad B_6 = -4h_1B_2B_5, \quad B_7 = 9h_2^2R_1^2 + 8h_2R_1R_2 + 2R_2^2, \\
B_8 &= B_3 + h_2R_1R_2 + R_2^2, \\
B_9 &= -3(h_1^3 - 4h_2^3)R_1^2 - 4(h_1^2 - 3h_2^2)R_1R_2 - 2(h_1^2 - h_2^2)R_2^2, \\
B_{10} &= 3(-h_1^3 + h_2^3)R_1^2 + 4(-h_1^2 + h_2^2)R_1R_2 + 2(-h_1 + h_2)R_2^2, \\
A_1 &= -3BrR_1^2, \quad A_2 = -4BrR_1R_2, \quad A_3 = -2BrR_2^2, \\
A_4 &= \frac{1}{B_1}[4Bi_2Brh_1B_2 + Bi_1\{-4Brh_2B_3 + Bi_2(1 + BrB_4)\}], \\
A_5 &= \frac{1}{B_1}[Br\{B_6 + h_2(B_7 + B_5B_8)\} + Bi_1\{-1 + Brh_1B_9 + Bi_2h_2(-1 + Brh_1B_{10})\}],
\end{aligned}$$

The longitudinal velocity and pressure gradient are given by

$$u_0 = 3R_1y^2 + 2R_2y + R_3, \quad (9.46)$$

$$\frac{dp_0}{dx} = 6R_1. \quad (9.47)$$

The non-dimensional pressure rise per wavelength ( $\Delta P_{\lambda_0}$ ) is given by

$$\Delta P_{\lambda_0} = \int_0^1 \frac{dp_0}{dx} dx. \quad (9.48)$$

We note that the solution expressions at this order correspond to the Newtonian fluid.

### 9.3.4 First order solution

Substituting Eq. (9.44) into Eqs. (9.39–9.41), solving the resulting equations and then applying the corresponding boundary conditions we get the solutions for  $\psi_1$ ,  $u_1$ ,  $dp_1/dx$  and  $\theta_1$  in the forms given below.

$$\begin{aligned}
\psi_1 = & \frac{1}{6B_{11}(h_1 - h_2)^3} [3F_1B_{11}(B_{16} - 6h_2y^2 + 4y^3 + 3h_1(h_2^2 - 4h_2y + 2y^2)) \\
& + 2^{\tilde{n}+1}\{2R_2^2B_{17}y^3 - 3h_2^2R_1y^2(B_{19} - 3\tilde{n}R_1B_{13}y) - 3h_2R_2y^2(B_{20} - B_{21}y) \\
& + h_2^3(3R_1R_2y(B_{22} - 2(R_2 + 3R_1y)^{\tilde{n}}) + R_2^2(B_{12} - (R_2 + 3R_1y)^{\tilde{n}}) \\
& - 9R_1^2y^2(B_{23} + (R_2 + 3R_1y)^{\tilde{n}})) + h_1^3(B_{24} - 3R_1R_2y(B_{25} - 2(R_2 + 3R_1y)^{\tilde{n}}) \\
& + 9R_1^2y^2(B_{26} + (R_2 + 3R_1y)^{\tilde{n}}) + R_2^2(-B_{13} + (R_2 + 3R_1y)^{\tilde{n}}) - 3h_2R_1(B_{27}y \\
& + \tilde{n}(B_{28} + B_{29}y))) - 3h_1^2(B_{30} - h_2^2R_1B_{17}(B_{31} + B_{32}y) + R_1y^2(B_{33} + B_{34}y) \\
& + h_2(-3R_1^2y^2(B_{35} - 3(R_2 + 3R_1y)^{\tilde{n}}) + R_2^2(-B_{13} + (R_2 + 3R_1y)^{\tilde{n}}) \\
& + R_1R_2y(B_{36} + 6(R_2 + 3R_1y)^{\tilde{n}}))) + 3h_1(-R_2y^2(B_{20} + B_{37}y) + h_2B_{17}y(B_{38} \\
& + B_{39}y + B_{40}y^2) + h_2^3R_1(-B_{27}y + \tilde{n}(B_{41} + B_{42}y)) + h_2^2(-3R_1^2y^2(B_{43} \\
& - 3(R_2 + 3R_1y)^{\tilde{n}}) + R_2^2(-B_{12} + (R_2 + 3R_1y)^{\tilde{n}}) \\
& + R_1R_2y(B_{44} + 6(R_2 + 3R_1y)^{\tilde{n}})))\}], \tag{9.49}
\end{aligned}$$

$$u_1 = M_1 + M_2y + M_3y^2 + M_4(R_2 + 3R_1y)^{\tilde{n}+1}, \tag{9.50}$$

$$\begin{aligned}
\frac{dp_1}{dx} = & -\frac{2}{(h_1 - h_2)^3B_{11}} [6F_1B_{11} + 2^{\tilde{n}}\{B_{14} + 2R_2^2(B_{12} - B_{13}) + 3h_2R_1R_2((\tilde{n} + 2)B_{12} \\
& + (\tilde{n} - 2)B_{13}) + 3h_1R_1(B_{15} - R_2((\tilde{n} - 2)B_{12} + (\tilde{n} + 2)B_{13}))\}], \tag{9.51}
\end{aligned}$$

with

$$\begin{aligned}
B_{11} &= (2 + 3\tilde{n} + \tilde{n}^2)R_1^2, \quad B_{12} = (3h_1R_1 + R_2)^{\tilde{n}}, \\
B_{13} &= (3h_2R_1 + R_2)^{\tilde{n}}, \quad B_{14} = -9\tilde{n}R_1^2(h_1^2B_{12} + h_2^2B_{13}), \\
B_{15} &= (\tilde{n} - 2)B_{12} + (\tilde{n} + 2)B_{13}, \quad B_{16} = h_1^3 - 3h_1^2h_2 + h_2^2, \\
B_{17} &= B_{12} - B_{13}, \quad B_{18} = B_{12} + B_{13}, \\
B_{19} &= R_2(4B_{17} + \tilde{n}(B_{12} + B_{18})), \quad B_{20} = R_2B_{17}, \\
B_{21} &= R_1(B_{12} + B_{17} + \tilde{n}B_{18}), \quad B_{22} = (\tilde{n} + 2)B_{12}, \\
B_{23} &= (\tilde{n} - 1)B_{13}, \quad B_{24} = 9h_2^2R_1^2(-B_{17} + \tilde{n}B_{18}), \\
B_{25} &= (\tilde{n} + 2)B_{13}, \quad B_{26} = (\tilde{n} - 1)B_{12}, \\
B_{27} &= -6R_1B_{17}, \quad B_{28} = -R_2B_{13}, \\
B_{29} &= 6R_1B_{18}, \quad B_{30} = 3h_2^2R_1^2(B_{17} + \tilde{n}B_{18}), \\
B_{31} &= (\tilde{n} - 4)R_2, \quad B_{32} = 3(\tilde{n} + 2)R_1, \\
B_{33} &= -R_2(-4B_{17} + \tilde{n}(B_{18} + B_{13})), \quad B_{34} = 3\tilde{n}R_1B_{12}, \\
B_{35} &= (\tilde{n} - 1)B_{12} + (2\tilde{n} + 4)B_{13}, \quad B_{36} = (2\tilde{n} - 8)B_{12} + (\tilde{n} + 2)B_{13}, \\
B_{37} &= R_1(-2B_{17} + \tilde{n}B_{18}), \quad B_{38} = 2R_2^2, \\
B_{39} &= (\tilde{n} - 4)R_1R_2, \quad B_{40} = 3(\tilde{n} + 2)R_1^2, \quad B_{41} = -R_2B_{12}, \\
B_{42} &= 3R_1(B_{12} + 2B_{13}), \quad B_{43} = (2\tilde{n} + 4)B_{12} + (\tilde{n} - 1)B_{13}, \\
B_{44} &= (\tilde{n} + 2)B_{12} + (2\tilde{n} - 8)B_{13},
\end{aligned}$$



$$\begin{aligned}
M_1 &= \frac{1}{B_{11}(h_1 - h_2)^3} [-6B_{11}F_1h_1h_2 + 2^{\tilde{n}}B_{17}h_1h_2(B_{38} + B_{32}h_1h_2R_1) \\
&\quad - 2^{\tilde{n}}R_1\{B_{27}h_1h_2(h_1^2 + h_2^2) + \tilde{n}B_{29}h_1^3h_2 - \tilde{n}B_{42}h_1h_2^3 + (B_{25}h_1^3 \\
&\quad - h_2(-B_{36}h_1^2 + h_2(B_{44}h_1 + B_{22}h_2)))R_2\}], \\
M_2 &= \frac{2}{B_{11}(h_1 - h_2)^3} [3B_{11}F_1(h_1 - h_2) + 2^{\tilde{n}}\{B_{17}B_{39}h_1h_2 + R_1(-B_{33}h_1^2 \\
&\quad + 3B_{26}h_1^3R_1 - h_2(-3B_{35}h_1^2R_1 + h_2(B_{19} + 3(B_{43}h_1 + B_{23}h_2)R_1))) \\
&\quad - B_{20}(h_1 + h_2)R_2\}], \\
M_3 &= \frac{1}{B_{11}(h_1 - h_2)^3} [6B_{11}F_1 + 2^{\tilde{n}}\{3B_{17}B_{40}h_1h_2 - 3B_{34}h_1^2R_1 \\
&\quad + 9\tilde{n}B_{13}h_2^2R_1^2 - 3B_{37}h_1R_2 + 3B_{21}h_2R_2 + 2B_{17}R_2^2\}], \\
M_4 &= \frac{2^{\tilde{n}}(\tilde{n} + 2)R_1}{B_{11}}.
\end{aligned}$$

Also

$$\theta_1 = L_1(R_2 + 3R_1y)^{\tilde{n}+3} + L_2y^4 + L_3y^3 + L_4y^2, \quad (9.52)$$

with

$$\begin{aligned}
L_1 &= \frac{2^{\tilde{n}+1}Br}{9B_{11}} \left( \frac{6(\tilde{n} + 1)}{\tilde{n} + 3} + \frac{B_{11}}{(\tilde{n} + 2)(\tilde{n} + 3)R_1^2} \right), \\
L_2 &= \frac{2BrR_1}{B_{11}(h_1 - h_2)^3} [6B_{11}F_1 + 2^{\tilde{n}}\{3B_{11}B_{40}h_1h_2 - 3B_{34}h_1^2R_1 \\
&\quad + 9B_{13}h_2^2\tilde{n}R_1^2 - 3B_{37}h_1R_2 + 3B_{21}h_2R_2 + 2B_{17}R_2^2\}], \\
L_3 &= \frac{4Br}{3B_{11}(h_1 - h_2)^3} [3B_{11}F_1(3h_1R_1 - 3h_2R_1 + 2R_2) \\
&\quad + 2^{\tilde{n}}\{-3R_1^2(B_{33}h_1^2 - 3B_{26}h_1^3R_1 + h_2(-3B_{35}h_1^2R_1 \\
&\quad + h_2(B_{19} + 3(B_{43}h_1 + B_{23}h_2)R_1))) - 3R_1(B_{34}h_1^2 \\
&\quad + B_{20}(h_1 + h_2) - 3B_{13}h_2^2\tilde{n}R_1)R_2 + 3(-B_{37}h_1 + B_{21}h_2)R_2^2 \\
&\quad + B_{17}(3B_{39}h_1h_2R_1 + 3B_{40}h_1h_2R_2 + 2R_2^3)\}], \\
L_4 &= \frac{-4BrR_2}{B_{11}(h_1 - h_2)^3} [3B_{11}F_1(h_2 - h_1) + 2^{\tilde{n}}\{-B_{17}B_{39}h_1h_2 \\
&\quad + R_1(B_{33}h_1^2 - 3B_{26}h_1^3R_1 + h_2(-3B_{35}h_1^2R_1 + h_2(B_{19} \\
&\quad + 3(B_{43}h_1 + B_{23}h_2)R_1))) + B_{20}(h_1 + h_2)R_2\}].
\end{aligned}$$

The pressure rise per wavelength ( $\Delta P_{\lambda_1}$ ) is given by

$$\Delta P_{\lambda_1} = \int_0^{2\pi} \frac{dp_1}{dx} dx. \quad (9.53)$$

The perturbation expressions of  $\psi$ ,  $\theta$ ,  $\Delta P_\lambda$  and  $dp/dx$  upto  $O(b^*)^1$  are

$$\begin{aligned} \psi &= \psi_0 + (b^*)\psi_1. \\ \theta &= \theta_0 + (b^*)\theta_1. \\ \frac{dp}{dx} &= \frac{dp_0}{dx} + (b^*)\frac{dp_1}{dx}. \\ \Delta P_\lambda &= \Delta P_{\lambda_0} + (b^*)\Delta P_{\lambda_1}. \end{aligned} \quad (9.54)$$

## 9.4 Results and discussion

### 9.4.1 Pumping characteristics

In this section the perturbed results of the Sisko fluid model are illustrated in Figs. 9.1 – 9.6. The variations of  $dp/dx$  for fixed values of involved parameters are sketched in the Figs. 9.1–9.3. The variation of axial pressure gradient ( $dp/dx$ ) for various values of the Sisko fluid parameter  $b^*$  is depicted in Fig. 9.1. The material parameter  $b^*$  occurring in the governing equation specifies the ratio of a power-law part to a viscous part in a Sisko fluid if  $\tilde{n} \neq 1$ . In the case of  $\tilde{n} \neq 1$ ,  $b^* = 0$  denotes a viscous fluid. It is observed from Fig. 9.1 that a negative pressure gradient in the wider part of the channel assists the flow, whereas in the narrow part positive pressure gradient repels the flow. Pumping of the peristalsis is more dominant in this case and flow is in the peristaltic direction. Fig. 9.2 is plotted to serve the effects of variation of the phase difference  $\phi$  on  $dp/dx$ . This Fig. reveals that the longitudinal pressure gradient  $dp/dx$  decreases by increasing the phase difference  $\phi$ . In Fig. 9.3 the axial distribution of the pressure gradient is portrayed for three different values of  $\tilde{n}$ . An interesting phenomenon observed from Fig. 9.3 is that the fluctuation in pressure gradient for a shear thickening fluid ( $\tilde{n} > 1$ ) is typically much higher than that for a shear thinning fluid ( $\tilde{n} < 1$ ) although all these phenomena reported above are alike for the Newtonian ( $\tilde{n} = 1$ ), shear-thinning and

shear-thickening fluids. Their difference can be observed without any difficulty from the total pressure rise per one wavelength. Note that the definition of pressure rise involves integration of  $dp/dx$ . The arising integral is not solvable analytically. Therefore the involved integral has been computed numerically. Figs. 9.4 – 9.6 illustrate the relation between pressure rise per wavelength  $\Delta p_\lambda$  and flow rate  $\Theta$  for various values of  $b^*$ ,  $\phi$  and  $\tilde{n}$ , respectively. It is observed that  $\Delta p_\lambda$  increases by increasing  $b^*$  and  $\tilde{n}$  (Figs. 9.4 and 9.6) and decreases with increasing  $\phi$  (Fig. 9.5). Effects of Sisko fluid parameter and phase differences are displayed in the Figs. 9.4 and 9.5 only for a shear-thickening fluid ( $\tilde{n} = 1.5$ ). There is a linear relationship between  $\Delta p_\lambda$  and  $\Theta$  for a Newtonian fluid as revealed in Fig. 9.6. A much greater pressure gradient is required for a shear thickening fluid ( $\tilde{n} > 1$ ) when compared with a shear thinning fluid ( $\tilde{n} < 1$ ). The case for a Newtonian fluid ( $\tilde{n} = 1$ ) lies in-between.

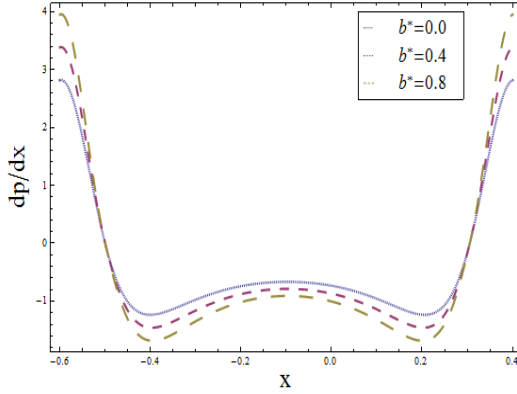


Fig. 9.1

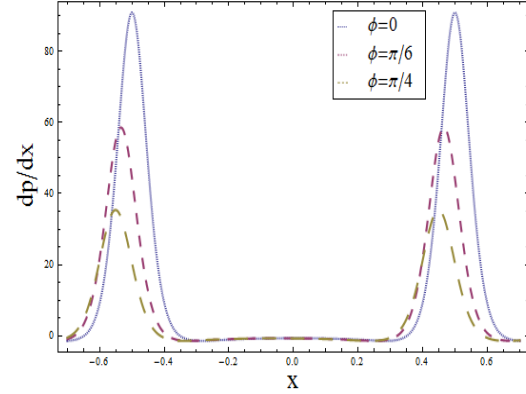


Fig. 9.2

Fig. 9.1: Plot of  $dp/dx$  for  $b^*$  with  $a = 1.0$ ,  $b = 0.7$ ,  $d = 1.2$ ,  $\tilde{n} = 1.5$ ,  $\phi = \pi/2$  and  $\Theta = 1$ .

Fig. 9.2: Plot of  $dp/dx$  for  $\phi$  with  $a = 1.0$ ,  $b = 0.7$ ,  $d = 1.2$ ,  $\tilde{n} = 1.5$ ,  $b^* = 0.2$  and  $\Theta = 1$ .

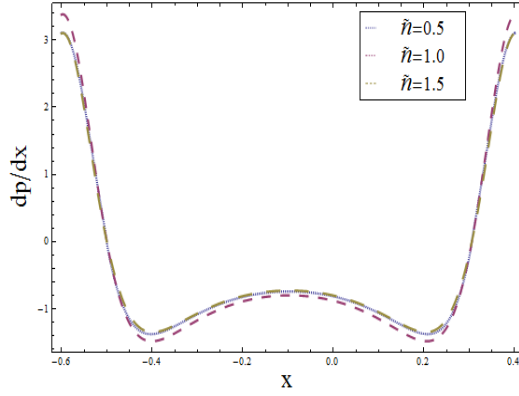


Fig. 9.3

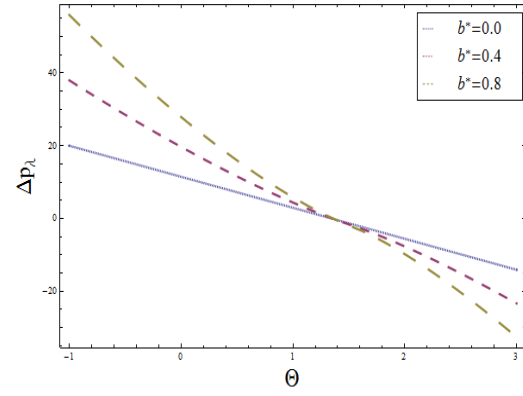


Fig. 9.4

Fig. 9.3: Plot of  $dp/dx$  for  $\tilde{n}$  with  $a = 1.0$ ,  $b = 0.7$ ,  $d = 1.2$ ,  $b^* = 0.2$ ,  $\phi = \pi/2$  and  $\Theta = 1$ .

Fig. 9.4: Plot of  $\Delta p_\lambda$  versus  $\Theta$  for  $b^*$  with  $a = 1.0$ ,  $b = 0.7$ ,  $d = 1.2$ ,  $\tilde{n} = 1.5$  and  $\phi = \pi/4$ .

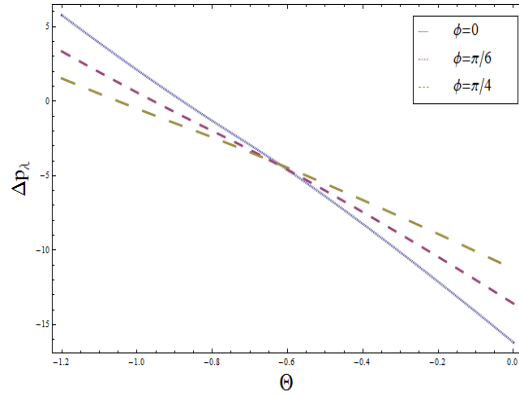


Fig. 9.5

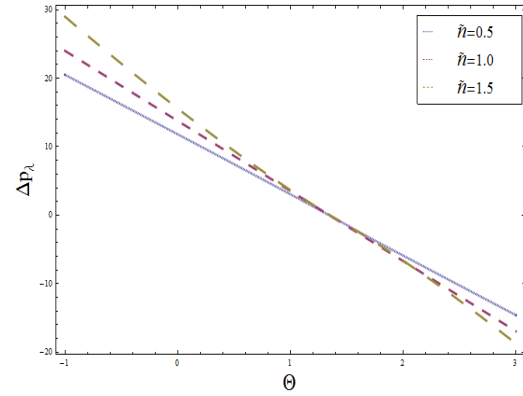


Fig. 9.6

Fig. 9.5: Plot of  $\Delta p_\lambda$  versus  $\Theta$  for  $\phi$  with  $a = 1.0$ ,  $b = 0.7$ ,  $d = 1.2$ ,  $\tilde{n} = 1.5$  and  $b^* = 0.2$ .

Fig. 9.6: Plot of  $\Delta p_\lambda$  versus  $\Theta$  for  $\tilde{n}$  with  $a = 1.0$ ,  $b = 0.7$ ,  $d = 1.2$ ,  $b^* = 0.2$  and  $\phi = \pi/4$ .

### 9.4.2 Velocity behavior

Figs. 9.7(a) and 9.7(b) display the effects of  $b^*$  on the velocity  $u$  for two different values of the power-law exponent  $\tilde{n} = 0.5$  and  $\tilde{n} = 1.5$ , respectively. It can be interpreted that an increase in  $b^*$  strengthens the power law effect of the Sisko fluid under observation. When we consider the case of  $\tilde{n} = 0.5$ , the boundary layers become thinner as  $b^*$  increases. On the other hand, an

increase in  $b^*$  thickens the boundary layer for the case when  $\tilde{n} = 1.5$ . The axial velocity profile is shown in Fig. 9.8 for three different values of power law index  $\tilde{n}$ . Here, to better observe the effect of rheology of fluid, we investigate a shear-thinning fluid ( $\tilde{n} = 0.5$ ) and a shear-thickening fluid ( $\tilde{n} = 1.5$ ) and compare the corresponding results with those of a Newtonian fluid. Apparently, sharp boundary layer is not developed near the walls of the channel for shear thickening fluid ( $\tilde{n} = 1.5$ ), whereas two thin boundary layers are formed near both walls of the channel for shear thinning fluid ( $\tilde{n} = 0.5$ ). Behavior of Newtonian fluid ( $\tilde{n} = 1$ ) lies in-between.

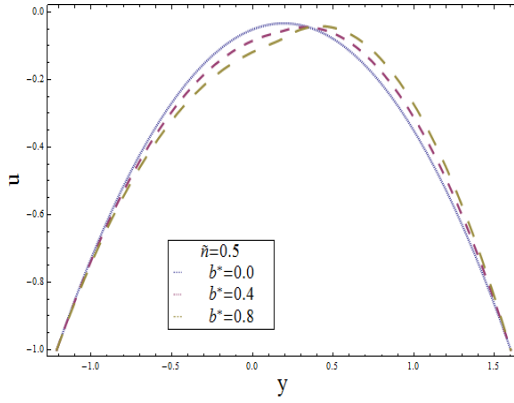


Fig. 9.7 (a)

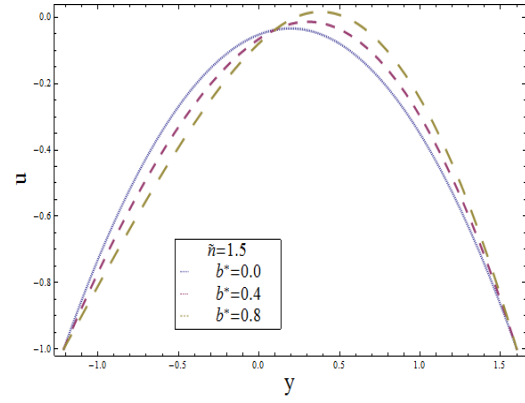


Fig. 9.7 (b)

Fig. 9.7 (a): Plot of  $u$  for  $b^*$  with  $a = 0.6$ ,  $b = 0.3$ ,  $d = 1.0$ ,  $\phi = \pi/4$ ,  $\Theta = 1$ ,  $x = 0$  and  $\tilde{n} = 0.5$ .

Fig. 9.7 (b): Plot of  $u$  for  $b^*$  with  $a = 0.6$ ,  $b = 0.3$ ,  $d = 1.0$ ,  $\phi = \pi/4$ ,  $\Theta = 1$ ,  $x = 0$  and  $\tilde{n} = 1.5$ .

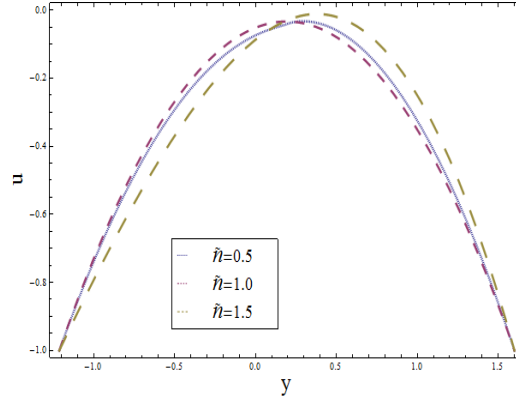


Fig. 9.8

Fig. 9.8: Plot of  $u$  for  $\tilde{n}$  with  $a = 0.6$ ,  $b = 0.3$ ,  $d = 1.0$ ,  $\phi = \pi/4$ ,  $\Theta = 1$ ,  $x = 0$  and  $b^* = 0.2$ .

#### 9.4.3 Temperature profile

Here the effects of various emerging parameters on the temperature profile  $\theta$  are discussed. Figs. 9.9 and 9.10 show an increase in the fluid temperature due to convective conditions (only for shear thickening fluid). It is noteworthy that the fluid temperature generally increases with increasing values of the material parameter  $b^*$  and the Brinkman number  $Br$ . Fig. 9.11 illustrates the effects of Biot number  $Bi_1$  on temperature profile  $\theta$  (for shear thickening fluid  $\tilde{n} = 1.5$ ). This Fig. reveals that by increasing the value of Biot number  $Bi_1$  the temperature profile  $\theta$  decreases at the upper wall of the channel while it does not show any effect near the lower wall of channel. Fig. 9.12 illustrates the effects of Biot number  $Bi_2$  on temperature profile  $\theta$  (for shear thickening fluid  $\tilde{n} = 1.5$ ). It is observed that the temperature  $\theta$  increases near the lower wall by increasing the Biot number  $Bi_2$ . The effect of different power values  $\tilde{n}$  on the temperature can also be clearly observed from Fig. 9.13. This Fig. indicates that the temperature for a shear thickening fluid ( $\tilde{n} = 1.5$ ) is higher than that of a shear thinning fluid ( $\tilde{n} = 0.5$ ). Also temperature for a Newtonian fluid ( $\tilde{n} = 1$ ) lies above these two.

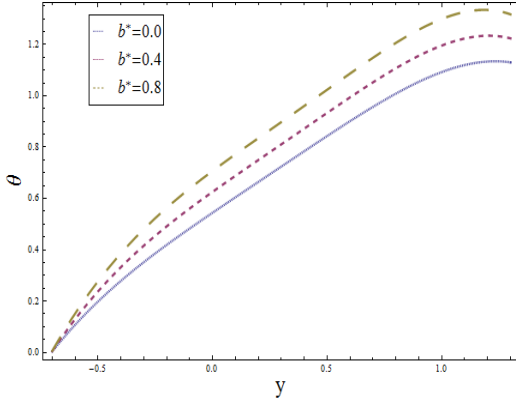


Fig. 9.9

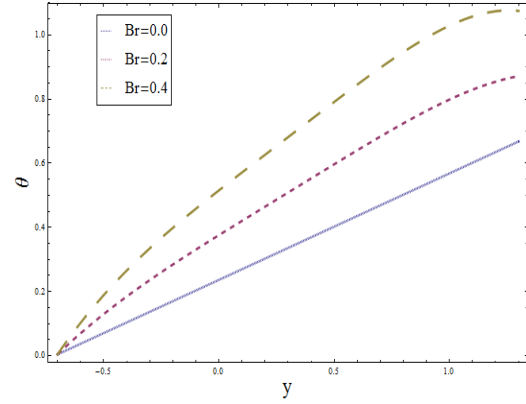


Fig. 9.10

Fig. 9.9: Plot of  $\theta$  for  $b^*$  with  $a = 0.3$ ,  $b = 0.3$ ,  $d = 0.6$ ,  $\phi = \pi/4$ ,  $\Theta = 1$ ,  $x = 0$ ,  $\tilde{n} = 1.5$ ,  
 $Br = 0.5$ ,  $Bi_1 = 1$  and  $Bi_2 = 10$ .

Fig. 9.10: Plot of  $\theta$  for  $Br$  with  $a = 0.3$ ,  $b = 0.3$ ,  $d = 0.6$ ,  $\phi = \pi/4$ ,  $\Theta = 1$ ,  $x = 0$ ,  $\tilde{n} = 1.5$ ,  
 $b^* = 0.2$ ,  $Bi_1 = 1$  and  $Bi_2 = 10$ .

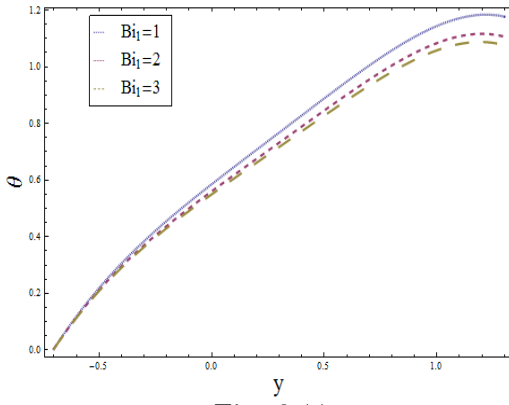


Fig. 9.11

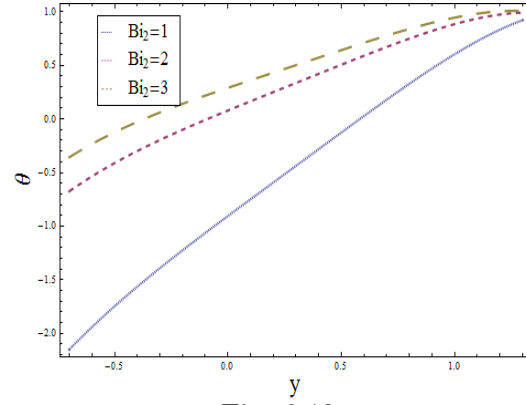


Fig. 9.12

Fig. 9.11: Plot of  $\theta$  for  $Bi_1$  with  $a = 0.3$ ,  $b = 0.3$ ,  $d = 0.6$ ,  $\phi = \pi/4$ ,  $\Theta = 1$ ,  $x = 0$ ,  $\tilde{n} = 1.5$ ,  
 $Br = 0.5$ ,  $b^* = 0.2$  and  $Bi_2 = 10$ .

Fig. 9.12: Plot of  $\theta$  for  $Bi_2$  with  $a = 0.3$ ,  $b = 0.3$ ,  $d = 0.6$ ,  $\phi = \pi/4$ ,  $\Theta = 1$ ,  $x = 0$ ,  $\tilde{n} = 1.5$ ,  
 $Br = 0.5$ ,  $b^* = 0.2$  and  $Bi_1 = 10$ .

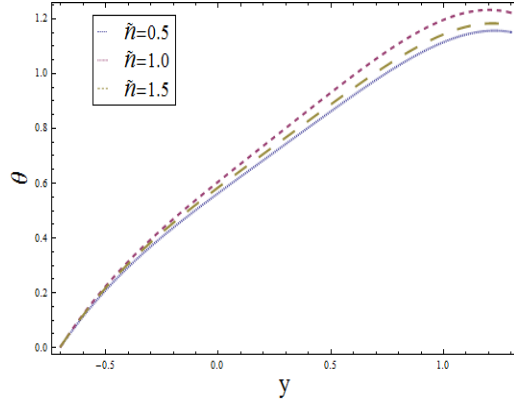


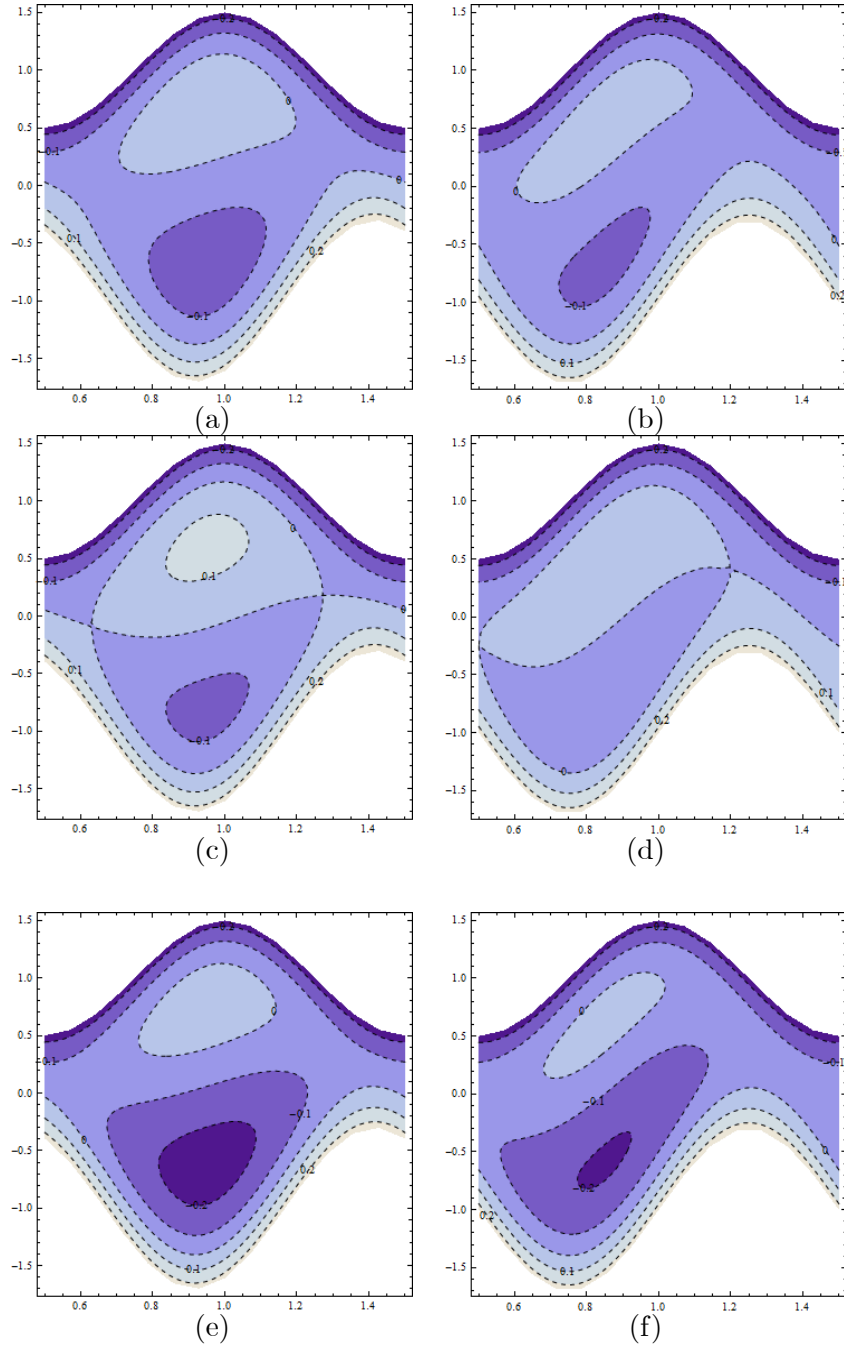
Fig. 9.13

Fig. 9.13: Plot of  $\theta$  for  $\tilde{n}$  with  $a = 0.3$ ,  $b = 0.3$ ,  $d = 0.6$ ,  $\phi = \pi/4$ ,  $\Theta = 1$ ,  $x = 0$ ,  $b^* = 0.2$ ,  $Br = 0.5$ ,  $Bi_1 = 1$  and  $Bi_2 = 10$ .

#### 9.4.4 Trapping

In general the shape of streamlines is similar to that of a boundary wall in the wave frame as the walls are stationary. However, some of the streamlines split and enclose a bolus under certain conditions and this bolus moves as a whole with the wave. This phenomenon is known as trapping. Fig. 9.14 shows the streamlines for three different power values  $\tilde{n} = 0.5$  (panels (a), (b)),  $\tilde{n} = 1$  (panels (c), (d)) and  $\tilde{n} = 1.5$  (panels (e), (f)) with two phase differences  $\phi = 0$  (left panels) and  $\phi = \pi/2$  (right panels). The streamlines near the channel walls strictly follow the wall waves, which are mainly generated by the relative movement of the walls. In the center region a bolus is formed. Comparisons among the flow fields obtained with different values of  $n$  show that the bolus rotation is faster for a shear-thickening fluid (panels (e) and (f)) than that for a shear-thinning fluid (panels (a) and (b)). The case of a Newtonian fluid lies in between.





## 9.5 Concluding remarks

In this chapter the peristaltic motion of the Sisko fluid in an asymmetric channel with convective conditions at the walls is investigated. By choosing different material parameters, the behaviors of the shear-thinning, shear-thickening and Newtonian fluids are compared and discussed. Typical features of peristaltic flow, e.g. pumping and trapping, are observed from the presented perturbed results. The thermal study reveals that a combine increase in Biot numbers, Brinkman number and non-Newtonian parameter enhances the thermal stability of the flow. To the best of our knowledge, such observation has never been reported for the peristaltic flows.

## Chapter 10

# Peristaltic motion of Carreau fluid in a channel with convective boundary conditions

### 10.1 Introduction

Peristaltic motion of Carreau fluid in an asymmetric channel with convective boundary conditions is investigated here. Mathematical formulation is first reduced in a wave frame of reference and then solutions are constructed. Results of the stream function, axial pressure gradient, temperature and pressure rise over a wavelength are obtained for small Weissenberg number. Velocity and temperature distributions are analyzed for different parameters of interest. A comparative study between the results of Newtonian and Carreau fluids is made.

### 10.2 Flow description

Consider the problem for an incompressible Carreau fluid in a two-dimensional asymmetric channel of width  $d_1 + d_2$  (see Fig. 2.1). The  $\bar{X}$  and  $\bar{Y}$  axes are the rectangular coordinates with  $\bar{X}$ -axis along the walls of the channel and  $\bar{Y}$ -axis perpendicular to the  $\bar{X}$ -axis. The flow

created is due to the imposition of the following sinusoidal waves:

$$\begin{aligned}\bar{h}_1(\bar{X}, \bar{t}) &= d_1 + a_1 \cos \frac{2\pi}{\lambda}(\bar{X} - c\bar{t}), & \text{upper wall,} \\ \bar{h}_2(\bar{X}, \bar{t}) &= -d_2 - a_2 \cos \left( \frac{2\pi}{\lambda}(\bar{X} - c\bar{t}) + \phi \right), & \text{lower wall.}\end{aligned}\quad (10.1)$$

In above expressions  $c$  is the wave speed,  $a_1, a_2$  are the wave amplitudes,  $\lambda$  is the wavelength,  $d_1 + d_2$  is the width of the asymmetric channel and the phase difference  $\phi$  varies in the range  $0 \leq \phi \leq \pi$  ( $\phi = 0$  corresponds to symmetric channel with waves out of phase and  $\phi = \pi$  the waves are in phase). Further  $a_1, a_2, d_1, d_2$  and  $\phi$  satisfy the condition

$$a_1^2 + a_2^2 + 2a_1a_2 \cos \phi \leq (d_1 + d_2)^2. \quad (10.2)$$

The Carreau fluid depends upon the shear rate by the following equation

$$\bar{\tau} = - \left[ \eta_\infty + (\eta_0 - \eta_\infty) \left( 1 + (\Gamma \bar{\gamma})^2 \right)^{\frac{\tilde{n}-1}{2}} \right] \bar{\gamma}, \quad (10.3)$$

where  $\bar{\tau}$  is the extra stress tensor,  $\eta_\infty$  the infinite shear-rate viscosity,  $\eta_0$  the zero shear-rate viscosity,  $\Gamma$  the time constant,  $\tilde{n}$  the dimensionless power law index and  $\bar{\gamma}$  is defined as

$$\bar{\gamma} = \sqrt{\frac{1}{2} \sum_i \sum_j \bar{\gamma}_{ij} \bar{\gamma}_{ji}} = \sqrt{\frac{1}{2} \Pi}. \quad (10.4)$$

Here  $\Pi$  is the second invariant of strain-rate tensor. Consider the constitutive equation (10.3) in the case for which  $\eta_\infty = 0$ , and so we can write

$$\bar{\tau} = -\eta_0 \left[ 1 + \left( \Gamma \bar{\gamma} \right)^2 \right]^{\frac{\tilde{n}-1}{2}} \bar{\gamma}. \quad (10.5)$$

Note that the above model reduces to Newtonian model for  $\tilde{n} = 1$  or  $\Gamma = 0$ . Here

$$\begin{aligned}\bar{\tau}_{\bar{X}\bar{X}} &= -\eta_0 \left[ 1 + \left( \frac{\tilde{n} - 1}{2} \right) \check{\Gamma}^2 \bar{\gamma}^2 \right] \frac{\partial \bar{U}}{\partial \bar{X}}, \\ \bar{\tau}_{\bar{X}\bar{Y}} &= -\eta_0 \left[ 1 + \left( \frac{\tilde{n} - 1}{2} \right) \check{\Gamma}^2 \bar{\gamma}^2 \right] \left( \frac{\partial \bar{U}}{\partial \bar{Y}} + \frac{\partial \bar{V}}{\partial \bar{X}} \right), \\ \bar{\tau}_{\bar{Y}\bar{Y}} &= -\eta_0 \left[ 1 + \left( \frac{\tilde{n} - 1}{2} \right) \check{\Gamma}^2 \bar{\gamma}^2 \right] \frac{\partial \bar{V}}{\partial \bar{Y}}.\end{aligned}$$

Incompressibility condition gives

$$\text{div } \bar{\mathbf{V}} = 0. \quad (10.6)$$

The equations of motion and energy are

$$\rho \frac{d\bar{\mathbf{V}}}{d\bar{t}} = -\text{grad } \bar{p} + \text{div } \bar{\boldsymbol{\tau}}, \quad (10.7)$$

$$\rho c_p \frac{dT}{d\bar{t}} = k \nabla^2 T + \bar{\boldsymbol{\tau}} \cdot (\text{grad } \bar{\mathbf{V}}), \quad (10.8)$$

where  $\bar{\mathbf{V}}$  is the velocity,  $\rho$  the density of fluid,  $\frac{d}{d\bar{t}}$  the material time derivative,  $T$  the fluid temperature,  $c_p$  the specific heat,  $k$  the thermal conductivity of the material, the Cauchy stress tensor  $\bar{\boldsymbol{\tau}}$ ,  $\bar{p}$  the pressure and  $\nabla^2 = \left( \frac{\partial^2}{\partial \bar{X}^2} + \frac{\partial^2}{\partial \bar{Y}^2} \right)$  (The over bar refers to a dimensional quantity).

Heat exchange at the walls is expressed as

$$k \frac{\partial T}{\partial \bar{Y}} = -\eta_1 (T - T_1) \quad \text{at } \bar{Y} = \bar{h}_1, \quad (10.9)$$

$$k \frac{\partial T}{\partial \bar{Y}} = -\eta_2 (T - T_0) \quad \text{at } \bar{Y} = \bar{h}_2, \quad (10.10)$$

where  $\eta_1$  and  $\eta_2$ ,  $T_1$  and  $T_0$  are the heat transfer coefficients and the temperatures at the upper and lower channel walls respectively. For two-dimensional flow of Carreau fluid, we have the velocity  $\bar{\mathbf{V}}$  in the form

$$\bar{\mathbf{V}} = (\bar{U}(\bar{X}, \bar{Y}, \bar{t}), \bar{V}(\bar{X}, \bar{Y}, \bar{t}), 0). \quad (10.11)$$

The transformations between laboratory and wave frames are

$$\begin{aligned}\bar{x} &= \bar{X} - c\bar{t}, \quad \bar{y} = \bar{Y}, \quad \bar{u}(\bar{x}, \bar{y}) = \bar{U}(\bar{X}, \bar{Y}, \bar{t}) - c, \\ \bar{v}(\bar{x}, \bar{y}) &= \bar{V}(\bar{X}, \bar{Y}, \bar{t}), \quad T(\bar{x}, \bar{y}) = T(\bar{X}, \bar{Y}, \bar{t}),\end{aligned}\tag{10.12}$$

Introducing

$$\begin{aligned}x &= \frac{\bar{x}}{\lambda}, \quad y = \frac{\bar{y}}{d_1}, \quad u = \frac{\bar{u}}{c}, \quad v = \frac{\bar{v}}{c\delta}, \quad t = \frac{c}{\lambda}\bar{t}, \quad p = \frac{d_1^2\bar{p}}{c\lambda\eta_0}, \quad We = \frac{\check{\Gamma}c}{d_1}, \\ h_1 &= \frac{\bar{h}_1}{d_1}, \quad h_2 = \frac{\bar{h}_2}{d_1}, \quad t = \frac{c\bar{t}}{\lambda}, \quad \tau_{xx} = \frac{\lambda}{c\eta_0}\bar{\tau}_{\bar{x}\bar{x}}, \quad \tau_{xy} = \frac{d_1}{c\eta_0}\bar{\tau}_{\bar{x}\bar{y}}, \quad \dot{\gamma} = \frac{\bar{\gamma}d_1}{c}, \\ \tau_{yy} &= \frac{d_1}{c\eta_0}\bar{\tau}_{\bar{y}\bar{y}}, \quad \theta = \frac{T - T_0}{T_1 - T_0}, \quad \delta = \frac{d_1}{\lambda}, \quad Re = \frac{\rho cd_1}{\eta_0}, \quad Pr = \frac{\mu c_p}{k}, \\ Ec &= \frac{c^2}{(T_1 - T_0)c_p},\end{aligned}\tag{10.13}$$

along with Eq. (10.12) and defining the stream function  $\psi(x, y)$  by

$$u = \frac{\partial\psi}{\partial y}, \quad v = -\frac{\partial\psi}{\partial x},\tag{10.14}$$

equation (10.6) is satisfied identically and Eqs. (10.7) and (10.8) yield

$$\delta Re \left[ \left( \frac{\partial\psi}{\partial y} \frac{\partial}{\partial x} - \frac{\partial\psi}{\partial x} \frac{\partial}{\partial y} \right) \left( \frac{\partial\psi}{\partial y} \right) \right] + \frac{\partial p}{\partial x} = -\delta^2 \frac{\partial\tau_{xx}}{\partial x} - \frac{\partial\tau_{xy}}{\partial y},\tag{10.15}$$

$$-\delta^3 Re \left[ \left( \frac{\partial\psi}{\partial y} \frac{\partial}{\partial x} - \frac{\partial\psi}{\partial x} \frac{\partial}{\partial y} \right) \left( \frac{\partial\psi}{\partial x} \right) \right] + \frac{\partial p}{\partial y} = -\delta^2 \frac{\partial\tau_{xy}}{\partial x} - \delta \frac{\partial\tau_{yy}}{\partial y},\tag{10.16}$$

$$\begin{aligned}\delta Re \left[ \frac{\partial\psi}{\partial y} \frac{\partial}{\partial x} - \frac{\partial\psi}{\partial x} \frac{\partial}{\partial y} \right] \theta &= \frac{1}{Pr} \left( \delta^2 \frac{\partial^2}{\partial x^2} + \frac{\partial^2}{\partial y^2} \right) \theta \\ &+ Ec \left[ \delta \frac{\partial^2\psi}{\partial x\partial y} (\tau_{xx} - \tau_{yy}) + \left( \frac{\partial^2\psi}{\partial y^2} - \delta^2 \frac{\partial^2\psi}{\partial x^2} \right) \tau_{xy} \right],\end{aligned}\tag{10.17}$$

where the components of extra stress tensor through Eq. (10.5) are

$$\tau_{xx} = -2 \left[ 1 + \frac{\tilde{n} - 1}{2} We^2 \dot{\gamma}^2 \right] \frac{\partial^2\psi}{\partial x\partial y},\tag{10.18}$$

$$\tau_{xy} = - \left[ 1 + \frac{\tilde{n} - 1}{2} We^2 \dot{\gamma}^2 \right] \left( \frac{\partial^2 \psi}{\partial y^2} - \delta^2 \frac{\partial^2 \psi}{\partial x^2} \right), \quad (10.19)$$

$$\tau_{yy} = 2\delta \left[ 1 + \frac{\tilde{n} - 1}{2} We^2 \dot{\gamma}^2 \right] \frac{\partial^2 \psi}{\partial x \partial y}, \quad (10.20)$$

$$\dot{\gamma} = \left[ 2\delta^2 \left( \frac{\partial^2 \psi}{\partial x \partial y} \right)^2 + \left( \frac{\partial^2 \psi}{\partial y^2} - \delta^2 \frac{\partial^2 \psi}{\partial x^2} \right)^2 + 2\delta^2 \left( \frac{\partial^2 \psi}{\partial x \partial y} \right)^2 \right]^{\frac{1}{2}}. \quad (10.21)$$

Here  $\delta$ ,  $Re$ ,  $We$ ,  $Pr$  and  $Ec$  are the wave, Reynolds, Weissenberg, Prandtl and Eckert numbers respectively. Equations (10.9) and (10.10) give

$$\frac{\partial \theta}{\partial y} + Bi_1(\theta - 1) = 0 \text{ at } y = h_1, \quad (10.22)$$

$$\frac{\partial \theta}{\partial y} + Bi_2\theta = 0 \text{ at } y = h_2, \quad (10.23)$$

where  $Bi_1 = \eta_1 d_1 / k$  and  $Bi_2 = \eta_2 d_1 / k$  are the Biot numbers.

Long wavelength  $\delta \ll 1$  and low Reynolds number assumptions yield

$$\frac{\partial p}{\partial x} = \frac{\partial}{\partial y} \left[ \left( 1 + \frac{\tilde{n} - 1}{2} We^2 \left( \frac{\partial^2 \psi}{\partial y^2} \right)^2 \right) \frac{\partial^2 \psi}{\partial y^2} \right], \quad (10.24)$$

$$\frac{\partial p}{\partial y} = 0. \quad (10.25)$$

The above equation indicates that  $p \neq p(y)$ . Eliminating the pressure  $p$  from Eqs. (10.24) and (10.25) we get the governing equation for the stream function in the form

$$\frac{\partial^2}{\partial y^2} \left[ \left( 1 + \frac{\tilde{n} - 1}{2} We^2 \left( \frac{\partial^2 \psi}{\partial y^2} \right)^2 \right) \frac{\partial^2 \psi}{\partial y^2} \right] = 0. \quad (10.26)$$

Also Eq. (10.17) becomes

$$\frac{\partial^2 \theta}{\partial y^2} + Br \left( \frac{\partial^2 \psi}{\partial y^2} \right)^2 \left[ 1 + \frac{\tilde{n} - 1}{2} We^2 \left( \frac{\partial^2 \psi}{\partial y^2} \right)^2 \right] = 0, \quad (10.27)$$

where the Brinkman number

$$Br = Pr Ec, \quad (10.28)$$

The subjected conditions are

$$\psi = \frac{F}{2}, \quad \frac{\partial \psi}{\partial y} = -1, \quad \text{at } y = h_1(x), \quad (10.29)$$

$$\psi = -\frac{F}{2}, \quad \frac{\partial \psi}{\partial y} = -1, \quad \text{at } y = h_2(x). \quad (10.30)$$

### 10.3 Perturbation solution

For perturbation solution, we expand  $\psi$ ,  $\theta$ ,  $dp/dx$  and  $F$  as follows:

$$\begin{aligned} \psi &= \psi_0 + We^2 \psi_1 + O(We^4), \\ \theta &= \theta_0 + We^2 \theta_1 + O(We^4), \\ dp/dx &= dp_0/dx + We^2(dp_1/dx) + O(We^4), \\ F &= F_0 + We^2 F_1 + O(We^4). \end{aligned}$$

Substitution of above equations into Eqs. (10.22 – 10.24), (10.26), (10.27), (10.29), (10.30) and then collecting the terms of like powers of  $We^2$  we arrived at

#### 10.3.1 System of order $We^0$

$$\frac{\partial^4 \psi_0}{\partial y^4} = 0, \quad (10.31)$$

$$\frac{\partial^2 \theta_0}{\partial y^2} + Br \left( \frac{\partial^2 \psi_0}{\partial y^2} \right)^2 = 0, \quad (10.32)$$

$$\frac{dp_0}{dx} = \frac{\partial^3 \psi_0}{\partial y^3}, \quad (10.33)$$

$$\psi_0 = \frac{F_0}{2}, \quad \frac{\partial \psi_0}{\partial y} = -1, \quad \frac{\partial \theta_0}{\partial y} + Bi_1(\theta_0 - 1) = 0, \quad \text{at } y = h_1(x), \quad (10.34)$$

$$\psi_0 = -\frac{F_0}{2}, \quad \frac{\partial \psi_0}{\partial y} = -1, \quad \frac{\partial \theta_0}{\partial y} + Bi_2 \theta_0 = 0, \quad \text{at } y = h_2(x). \quad (10.35)$$



### 10.3.2 System of order $We^2$

$$\frac{\partial^4 \psi_1}{\partial y^4} + \left( \frac{\tilde{n} - 1}{2} \right) \frac{\partial^2}{\partial y^2} \left( \frac{\partial^2 \psi_0}{\partial y^2} \right)^3 = 0, \quad (10.36)$$

$$\frac{\partial^2 \theta_1}{\partial y^2} + Br \left[ 2 \left( \frac{\partial^2 \psi_0}{\partial y^2} \right) \left( \frac{\partial^2 \psi_1}{\partial y^2} \right) + \left( \frac{\tilde{n} - 1}{2} \right) \left( \frac{\partial^2 \psi_0}{\partial y^2} \right)^4 \right] = 0, \quad (10.37)$$

$$\frac{dp_1}{dx} = \frac{\partial^3 \psi_1}{\partial y^3} + \left( \frac{\tilde{n} - 1}{2} \right) \frac{\partial}{\partial y} \left( \frac{\partial^2 \psi_0}{\partial y^2} \right)^3, \quad (10.38)$$

$$\psi_1 = \frac{F_1}{2}, \quad \frac{\partial \psi_1}{\partial y} = 0, \quad \frac{\partial \theta_1}{\partial y} + Bi_1 \theta_1 = 0, \quad \text{at } y = h_1(x), \quad (10.39)$$

$$\psi_1 = \frac{-F_1}{2}, \quad \frac{\partial \psi_1}{\partial y} = 0, \quad \frac{\partial \theta_1}{\partial y} + Bi_2 \theta_1 = 0, \quad \text{at } y = h_2(x). \quad (10.40)$$

### 10.3.3 Solution for system of order $We^0$

The solutions of the Eqs. (10.31) and (10.32) subject to the boundary conditions (10.34) and (10.35) are

$$\psi_0 = R_1 y^3 + R_2 y^2 + R_3 y + R_4, \quad (10.41)$$

$$\theta_0 = A_1 y^4 + A_2 y^3 + A_3 y^2 + A_4 y + A_5, \quad (10.42)$$

where

$$\begin{aligned} R_1 &= \frac{-2(F_0 + h_1 - h_2)}{(h_1 - h_2)^3}, \\ R_2 &= \frac{3(F_0 + h_1 - h_2)(h_1 + h_2)}{(h_1 - h_2)^3}, \\ R_3 &= \frac{-h_1^3 - 6F_0 h_1 h_2 - 3h_1^2 h_2 + 3h_1 h_2^2 + h_2^3}{(h_1 - h_2)^3}, \\ R_4 &= \frac{-(h_1 + h_2)(2h_1 h_2(-h_1 + h_2) + F_0(h_1^2 - 4h_1 h_2 + h_2^2))}{2(h_1 - h_2)^3}, \end{aligned}$$

$$\begin{aligned}
B_1 &= Bi_2 + Bi_1(-1 + Bi_2(h_1 - h_2)), \\
B_2 &= 3h_1^2 R_1^2 + 3h_1 R_1 R_2 + R_2^2, \quad B_3 = 3h_2^2 R_1^2 + 3h_2 R_1 R_2 + R_2^2, \\
B_4 &= 3(h_1^4 - h_2^4) R_1^2 + 4(h_1^3 - h_2^3) R_1 R_2 + 2(h_1^2 - h_2^2) R_2^2, \\
B_5 &= 1 + Bi_2 h_2, \quad B_6 = -4h_1 B_2 B_5, \quad B_7 = 9h_2^2 R_1^2 + 8h_2 R_1 R_2 + 2R_2^2, \\
B_8 &= B_3 + h_2 R_1 R_2 + R_2^2, \\
B_9 &= -3(h_1^3 - 4h_2^3) R_1^2 - 4(h_1^2 - 3h_2^2) R_1 R_2 - 2(h_1^2 - h_2^2) R_2^2, \\
B_{10} &= 3(-h_1^3 + h_2^3) R_1^2 + 4(-h_1^2 + h_2^2) R_1 R_2 + 2(-h_1 + h_2) R_2^2, \\
A_1 &= -3Br R_1^2, \quad A_2 = -4Br R_1 R_2, \quad A_3 = -2Br R_2^2, \\
A_4 &= \frac{1}{B_1} [4Bi_2 Br h_1 B_2 + Bi_1 \{-4Br h_2 B_3 + Bi_2(1 + Br B_4)\}], \\
A_5 &= \frac{1}{B_1} [Br \{B_6 + h_2(B_7 + B_5 B_8)\} + Bi_1 \{-1 + Br h_1 B_9 + Bi_2 h_2(-1 + Br h_1 B_{10})\}].
\end{aligned}$$

The longitudinal velocity and pressure gradient are

$$u_0 = 3R_1 y^2 + 2R_2 y + R_3, \quad (10.43)$$

$$\frac{dp_0}{dx} = 6R_1. \quad (10.44)$$

The non-dimensional pressure rise per wavelength ( $\Delta P_{\lambda_0}$ ) is given by

$$\Delta P_{\lambda_0} = \int_0^1 \frac{dp_0}{dx} dx. \quad (10.45)$$

We note that the solution expressions at this order are for the Newtonian fluid.

### 10.3.4 Solution for system of order $We^2$

Putting Eq. (10.41) into Eqs. (10.36 – 10.38), solving the resulting equations and then employing the corresponding boundary conditions we have

$$\psi_1 = M_1 y^5 + M_2 y^4 + M_3 y^3 + M_4 y^2 + M_5 y + M_6, \quad (10.46)$$

$$u_1 = 5M_1 y^4 + 4M_2 y^3 + 3M_3 y^2 + 2M_4 y + M_5, \quad (10.47)$$

$$\begin{aligned} \frac{dp_1}{dx} = & -\frac{2}{5(h_1 - h_2)^3} [30F_1 - (h_1 - h_2)^3(-1 + \tilde{n})(3(h_1 + h_2)R_1 + 2R_2) \\ & \times (9(2h_1^2 + h_1 h_2 + 2h_2^2)R_1^2 + 15(h_1 + h_2)R_1 R_2 + 5R_2^2)], \end{aligned} \quad (10.48)$$

$$\theta_1 = L_1 y^6 + L_2 y^5 + L_3 y^4 + L_4 y^3 + L_5 y^2 + L_6 y + L_7, \quad (10.49)$$

$$M_1 = -\frac{27}{5}(-1 + \tilde{n})R_1^3,$$

$$M_2 = -9(-1 + \tilde{n})R_1^2 R_2,$$

$$M_3 = -\frac{1}{5(h_1 - h_2)^3} [10F_1 - 9(h_1 - h_2)^3(-1 + \tilde{n})R_1^2(3(3h_1^2 + 4h_1 h_2 + 3h_2^2)R_1 + 10(h_1 + h_2)R_2)],$$

$$\begin{aligned} M_4 = & \frac{1}{5(h_1 - h_2)^3} [3(5F_1(h_1 + h_2) - 3(h_1 - h_2)^3(-1 + \tilde{n})R_1^2(6(h_1 + h_2)(h_1^2 + 3h_1 h_2 + h_2^2)R_1 \\ & + 5(h_1^2 + 4h_1 h_2 + h_2^2)R_2))], \end{aligned}$$

$$\begin{aligned} M_5 = & -\frac{1}{5(h_1 - h_2)^3} [3h_1 h_2(10F_1 - 3(h_1 - h_2)^3(-1 + \tilde{n})R_1^2(3(4h_1^2 + 7h_1 h_2 + 4h_2^2)R_1 \\ & + 10(h_1 + h_2)R_2))], \end{aligned}$$

$$\begin{aligned} M_6 = & -\frac{1}{10(h_1 - h_2)^3} [5F_1(h_1 + h_2)(h_1^2 - 4h_1 h_2 + h_2^2) \\ & + 18h_1^2(h_1 - h_2)^3 h_2^2(-1 + \tilde{n})R_1^2(6(h_1 + h_2)R_1 + 5R_2)], \end{aligned}$$

$$L_1 = -\frac{4}{5}BrR_1(10M_1 + 27(-1 + \tilde{n})R_1^3),$$

$$L_2 = -\frac{4}{5}Br(5M_1 R_2 + 9R_1(M_2 + 6(-1 + \tilde{n})R_1^2 R_2)),$$

$$L_3 = -2Br(3M_3 R_1 + 2R_2(M_2 + 9(-1 + \tilde{n})R_1^2 R_2)),$$

$$L_4 = -4Br(M_4 R_1 + M_3 R_2 + 4(-1 + \tilde{n})R_1 R_2^3),$$

$$L_5 = -4BrR_2(M_4 + (-1 + \tilde{n})R_2^3),$$

$$\begin{aligned}
L_6 = & \frac{2Br}{5B_1}[-2Bi_1h_2\{6h_2^4R_1(10M_1 + 27(-1 + \tilde{n})R_1^3) + 10R_2(M_4 + (-1 + \tilde{n})R_2^3) \\
& + 15h_2(M_4R_1 + M_3R_2 + 4(-1 + \tilde{n})R_1R_2^3) + 5h_2^3(5M_1R_2 + 9R_1(M_2 + 6(-1 + \tilde{n})R_1^2R_2)) \\
& + 10h_2^2(3M_3R_1 + 2R_2(M_2 + 9(-1 + \tilde{n})R_1^2R_2))\} + Bi_2\{2Bi_1h_1^6R_1(10M_1 + 27(-1 + \tilde{n})R_1^3) \\
& + 20h_1R_2(M_4 + (-1 + \tilde{n})R_2^3) + 10h_1^2(3M_3R_2 + M_4(3R_1 + Bi_1R_2) + (-1 + \tilde{n})R_2^3 \\
& \times (12R_1 + Bi_1R_2)) + 5h_1^4(2(5M_1 + 54(-1 + \tilde{n})R_1^3)R_2 + 2M_2(9R_1 + Bi_1R_2) \\
& + 3Bi_1R_1(M_3 + 6(-1 + \tilde{n})R_1R_2^2)) + 10h_1^3(M_3(6R_1 + Bi_1R_2) + 4R_2(M_2 \\
& + 9(-1 + \tilde{n})R_1^2R_2) + Bi_1R_1(M_4 + 4(-1 + \tilde{n})R_2^3)) + 2h_1^5(5M_1(12R_1 + Bi_1R_2) \\
& + 9(18(-1 + \tilde{n})R_1^4 + Bi_1R_1(M_2 + 6(-1 + \tilde{n})R_1^2R_2)))\} - Bi_1h_2^2(h_2^4(20M_1R_1 \\
& + 54(-1 + \tilde{n})R_1^4) + 10R_2(M_4 + (-1 + \tilde{n})R_2^3) + 10h_2(M_4R_1 + M_3R_2 \\
& + 4(-1 + \tilde{n})R_1R_2^3) + 2h_2^3(5M_1R_2 + 9R_1(M_2 + 6(-1 + \tilde{n})R_1^2R_2)) + 5h_2^2(3M_3R_1 + 2R_2(M_2 \\
& + 9(-1 + \tilde{n})R_1^2R_2)))\}]],
\end{aligned}$$

$$\begin{aligned}
L_7 = & \frac{2Br}{5B_1} [2Bi_1h_1^6(1 + Bi_2h_2)R_1(10M_1 + 27(-1 + \tilde{n})R_1^3) + 10h_1^2(1 + Bi_2h_2)(3M_3R_2 \\
& + M_4(3R_1 + Bi_1R_2) + (-1 + \tilde{n})R_2^3(12R_1 + Bi_1R_2)) + 5h_1^4(1 + Bi_2h_2)(2(5M_1 \\
& + 54(-1 + \tilde{n})R_1^3)R_2 + 2M_2(9R_1 + Bi_1R_2) + 3Bi_1R_1(M_3 + 6(-1 + \tilde{n})R_1R_2^2)) \\
& + 10h_1^3(1 + Bi_2h_2)(M_3(6R_1 + Bi_1R_2) + 4R_2(M_2 + 9(-1 + \tilde{n})R_1^2R_2) \\
& + Bi_1R_1(M_4 + 4(-1 + \tilde{n})R_2^3)) + 2h_1^5(1 + Bi_2h_2)(5M_1(12R_1 + Bi_1R_2) \\
& + 9(18(-1 + \tilde{n})R_1^4 + Bi_1R_1(M_2 + 6(-1 + \tilde{n})R_1^2R_2))) - h_2\{2Bi_2h_2^5R_1(10M_1 + 27(-1 + \tilde{n})R_1^3) \\
& + 20R_2(M_4 + (-1 + \tilde{n})R_2^3) + 10h_2(3M_3R_2 + M_4(3R_1 + Bi_2R_2) + (-1 + \tilde{n})R_2^3(12R_1 + Bi_2R_2)) \\
& + 5h_2^3(2(5M_1 + 54(-1 + \tilde{n})R_1^3)R_2 + 2M_2(9R_1 + Bi_2R_2) + 3Bi_2R_1(M_3 + 6(-1 + \tilde{n})R_1R_2^2)) \\
& + 10h_2^2(M_3(6R_1 + Bi_2R_2) + 4R_2(M_2 + 9(-1 + \tilde{n})R_1^2R_2) + Bi_2R_1(M_4 + 4(-1 + \tilde{n})R_2^3)) + 2h_2^4 \\
& \times (5M_1(12R_1 + Bi_2R_2) + 9(18(-1 + \tilde{n})R_1^4 + Bi_2R_1(M_2 + 6(-1 + \tilde{n})R_1^2R_2)))\} \\
& - h_1\{-20(1 + Bi_2h_2)R_2(M_4 + (-1 + \tilde{n})R_2^3) + Bi_1h_2(2Bi_2h_2^5R_1(10M_1 + 27(-1 + \tilde{n})R_1^3) \\
& + 20R_2(M_4 + (-1 + \tilde{n})R_2^3) + 10h_2(3M_3R_2 + M_4(3R_1 + Bi_2R_2) + (-1 + \tilde{n})R_2^3(12R_1 + Bi_2R_2)) \\
& + 5h_2^3(2(5M_1 + 54(-1 + \tilde{n})R_1^3)R_2 + 2M_2(9R_1 + Bi_2R_2) + 3Bi_2R_1(M_3 + 6(-1 + \tilde{n})R_1R_2^2)) \\
& + 10h_2^2(M_3(6R_1 + Bi_2R_2) + 4R_2(M_2 + 9(-1 + \tilde{n})R_1^2R_2) + Bi_2R_1(M_4 + 4(-1 + \tilde{n})R_2^3)) \\
& + 2h_2^4(5M_1(12R_1 + Bi_2R_2) + 9(18(-1 + \tilde{n})R_1^4 + Bi_2R_1(M_2 + 6(-1 + \tilde{n})R_1^2R_2))))\}].
\end{aligned}$$

The pressure rise per wavelength ( $\Delta P_{\lambda_1}$ ) is

$$\Delta P_{\lambda_1} = \int_0^{2\pi} \frac{dp_1}{dx} dx. \quad (10.50)$$

The perturbation expressions of  $\psi$ ,  $\theta$ ,  $\Delta P_\lambda$  and  $dp/dx$  upto  $We^2$  are

$$\begin{aligned}
\psi &= \psi_0 + We^2\psi_1. \\
\theta &= \theta_0 + We^2\theta_1. \\
\frac{dp}{dx} &= \frac{dp_0}{dx} + We^2\frac{dp_1}{dx}. \\
\Delta P_\lambda &= \Delta P_{\lambda_0} + We^2\Delta P_{\lambda_1}.
\end{aligned} \quad (10.51)$$

## 10.4 Results and discussion

To discuss qualitatively the behavior of embedding parameters of interest on flow quantities such as longitudinal velocity  $u$  and temperature distribution  $\theta$ , we have prepared Figs. 10.1 – 10.9. The effects of various parameters on pressure gradient  $dp/dx$ , pressure rise per wavelength  $\Delta p_\lambda$  and pumping and trapping are already investigated by Ali and Hayat [75]. Hence we avoid to include such results here. However the longitudinal velocity for different values of  $We$ ,  $\tilde{n}$ ,  $\phi$  and  $\Theta$  have been plotted in Figs. 9.1 – 9.4. Effects of  $We$  and  $\tilde{n}$  on the longitudinal velocity are indicated in the Figs. 10.1 and 10.2. These Figs. depict that velocity for Newtonian fluid (when  $We = 0.0$  and  $\tilde{n} = 1$ ) is greater than the Carreau fluid (when  $We = 0.3, 0.4$  and  $\tilde{n} = 0.398, 0.496$ ) in the narrow part of the channel. But in wider part of the channel we witness the opposite behavior. Fig. 10.3 designates the effect of phase angle  $\phi$  on longitudinal velocity  $u$ . This Fig. directs to the result that  $u$  decreases when  $\phi$  increases and such behavior is quite opposite in the other region. In Fig. 10.4, the effect of  $\Theta$  on longitudinal velocity is shown. It is perceived that with an increase in  $\Theta$ , the velocity increases. Fig. 10.5 confirms an increase in fluid temperature with maximum value along the centerline and minimum at the walls due to convective conditions. It is interesting to note that the fluid temperature generally increases with increasing values of the Brinkman number  $Br$ . Actually Brinkman number  $Br$  involves viscous dissipation effects which are due to the energy production and thus temperature enhances. Fig. 10.6 discloses that by increasing the value of  $Bi_1$  the temperature profile  $\theta$  decreases at the upper wall while it has no significant effect near the lower wall of channel. Also the temperature  $\theta$  increases near the lower wall by increasing the Biot number  $Bi_2$  and it has no effect on temperature profile near the upper wall of the channel (see Fig. 10.7). Here we have considered the values of Biot numbers much larger than 0.1 due to non-uniform temperature fields within the fluid. However problems involving small Biot numbers are thermally simple due to the uniform temperature fields within the fluid. Fig. 10.8 portrays the temperature distribution for numerous values of  $We$ . It is found that the temperature distribution is larger for the Newtonian fluid ( $We = 0$ ) when compared with the Carreau fluid ( $We = 0.2, 0.4$ ). Similar behavior is observed for the power-law index  $\tilde{n}$  in Fig. 10.9. Here for  $\tilde{n} = 1$  (Newtonian fluid), the temperature distribution is greater than the Carreau fluid (when  $\tilde{n} = 0.398, 0.496$ ). The behaviors of parameters on the heat transfer coefficient at the upper

wall have been observed in the Figures 10.10 – 10.13. The heat transfer coefficient is denoted by  $Z(x) = (h_1)_x \theta_y(h_1)$  which actually defines the rate of heat transfer or heat flux at the upper wall. The heat transfer coefficient  $Z(x)$  increases when the values of Brinkman number  $Br$  are set to be increased (see Fig. 10.10). Here  $Br = 0$  shows the absence of viscous dissipation effects. It is also note worthy that heat transfer coefficient  $Z(x)$  is higher when we consider the viscous dissipation effects (i.e. when  $Br \neq 0$ ). According to Fig. 10.11 the heat transfer coefficient  $Z(x)$  decreases by increasing  $We$ . Also heat transfer coefficient  $Z(x)$  is higher for Newtonian fluid ( $We = 0$ ) than the Carreau fluid ( $We \neq 0$ ). It is interesting to note that the heat transfer coefficient  $Z(x)$  increases for increasing values of Biot number  $Bi_1$  and  $Bi_2$  (see Figs. 10.12 and 10.13).

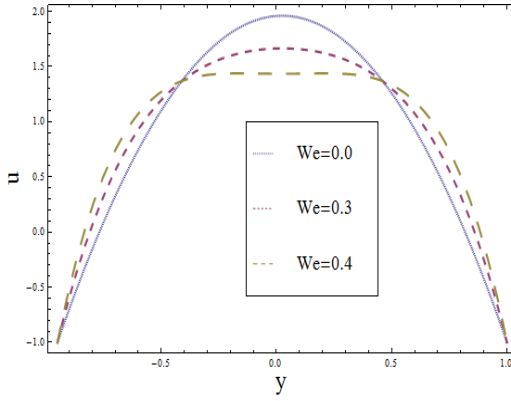


Fig. 10.1

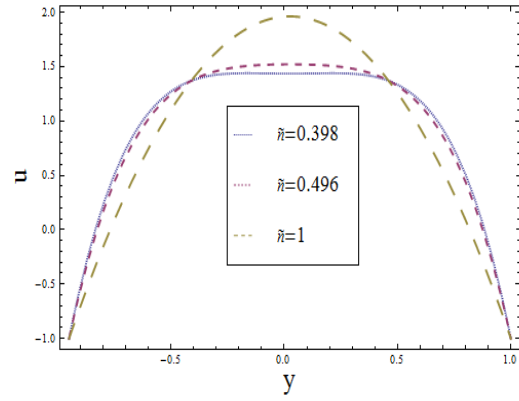


Fig. 10.2

Fig. 10.1: Plot showing  $u$  versus  $y$ . Here  $a = 0.6$ ,  $b = 0.3$ ,  $d = 1.1$ ,  $\Theta = 4$ ,  $\phi = \pi/6$ ,  $x = 0.25$  and  $\tilde{n} = 0.398$ .

Fig. 10.2: Plot showing  $u$  versus  $y$ . Here  $a = 0.6$ ,  $b = 0.3$ ,  $d = 1.1$ ,  $\Theta = 4$ ,  $\phi = \pi/6$ ,  $x = 0.25$  and  $We = 0.4$ .

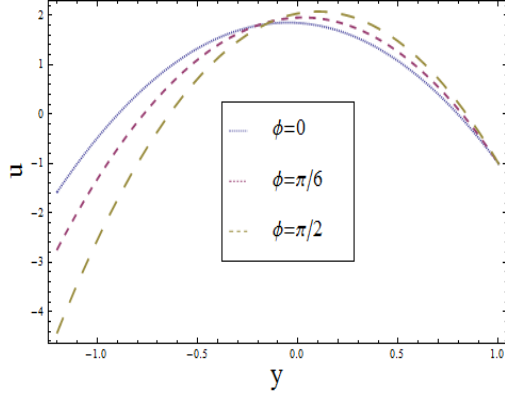


Fig. 10.3

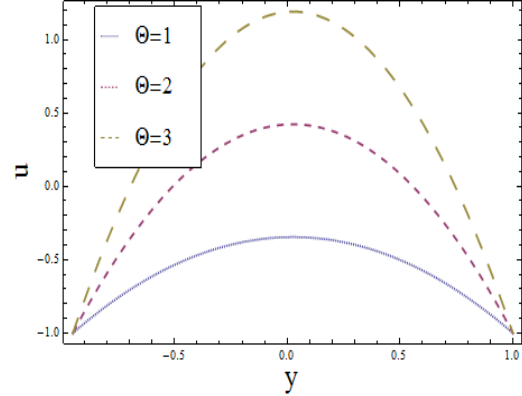


Fig. 10.4

Fig. 10.3: Plot showing  $u$  versus  $y$ . Here  $a = 0.6$ ,  $b = 0.3$ ,  $d = 1.1$ ,  $\Theta = 4$ ,  $\tilde{n} = 0.398$ ,  $x = 0.25$  and  $We = 0.4$ .

Fig. 10.4: Plot showing  $u$  versus  $y$ . Here  $a = 0.6$ ,  $b = 0.3$ ,  $d = 1.1$ ,  $\phi = \pi/6$ ,  $\tilde{n} = 0.398$ ,  $x = 0.25$  and  $We = 0.4$ .

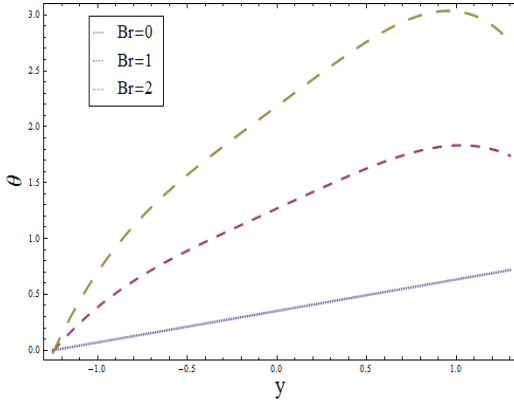


Fig. 10.5

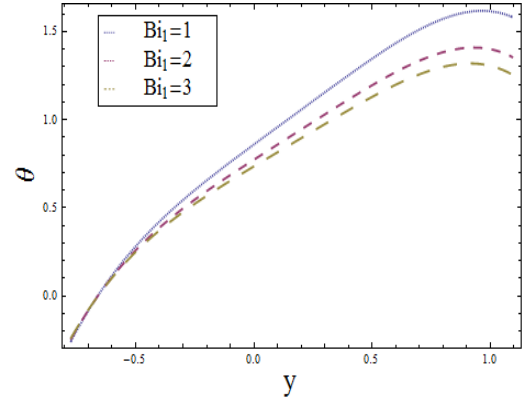


Fig. 10.6

Fig. 10.5: Plot showing  $\theta$  versus  $y$ . Here  $a = 0.3$ ,  $b = 0.5$ ,  $d = 1$ ,  $\phi = \pi/4$ ,  $\Theta = 1.5$ ,  $\tilde{n} = 0.398$ ,  $Bi_1 = 1$ ,  $Bi_2 = 10$ ,  $x = 0.2$  and  $We = 0.1$ .

Fig. 10.6: Plot showing  $\theta$  versus  $y$ . Here  $a = 0.3$ ,  $b = 0.5$ ,  $d = 1$ ,  $\phi = \pi/4$ ,  $\Theta = 1.5$ ,  $\tilde{n} = 0.398$ ,  $Br = 1$ ,  $Bi_2 = 10$ ,  $x = 0.2$  and  $We = 0.3$ .



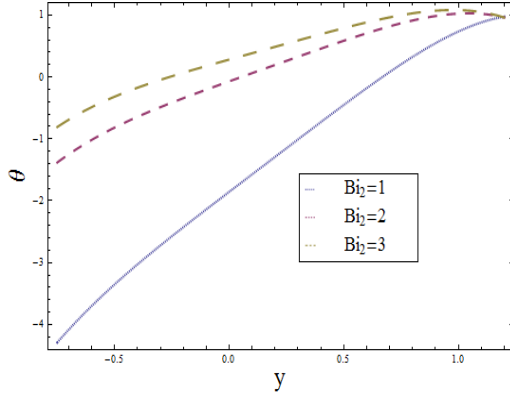


Fig. 10.7

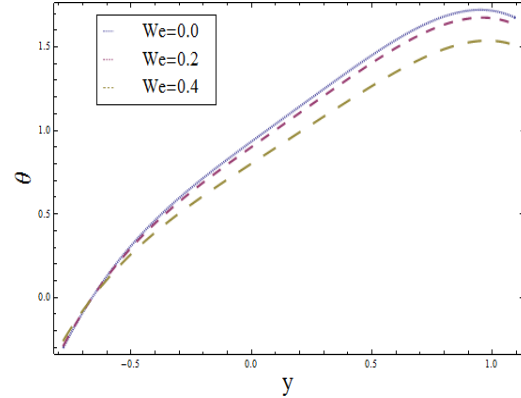


Fig. 10.8

Fig. 10.7: Plot showing  $\theta$  versus  $y$ . Here  $a = 0.3$ ,  $b = 0.5$ ,  $d = 1$ ,  $\phi = \pi/4$ ,  $\Theta = 1.5$ ,  $\tilde{n} = 0.398$ ,  $Bi_1 = 10$ ,  $Br = 1$ ,  $x = 0.2$  and  $We = 0.3$ .

Fig. 10.8: Plot showing  $\theta$  versus  $y$ . Here  $a = 0.3$ ,  $b = 0.5$ ,  $d = 1$ ,  $\phi = \pi/4$ ,  $\Theta = 1.5$ ,  $\tilde{n} = 0.398$ ,  $Bi_1 = 1$ ,  $Bi_2 = 10$ ,  $x = 0.2$  and  $Br = 1$ .

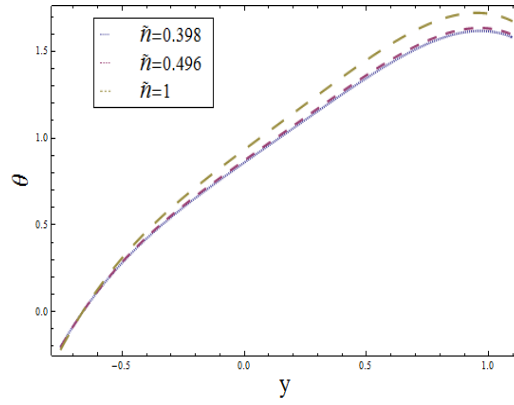


Fig. 10.9

Fig. 10.9: Plot showing  $\theta$  versus  $y$ . Here  $a = 0.3$ ,  $b = 0.5$ ,  $d = 1$ ,  $\phi = \pi/4$ ,  $\Theta = 1.5$ ,  $Br = 1$ ,  $Bi_1 = 1$ ,  $Bi_2 = 10$ ,  $x = 0.2$  and  $We = 0.1$ .

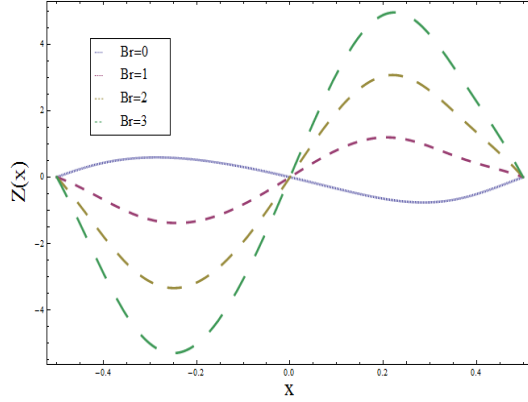


Fig. 10.10

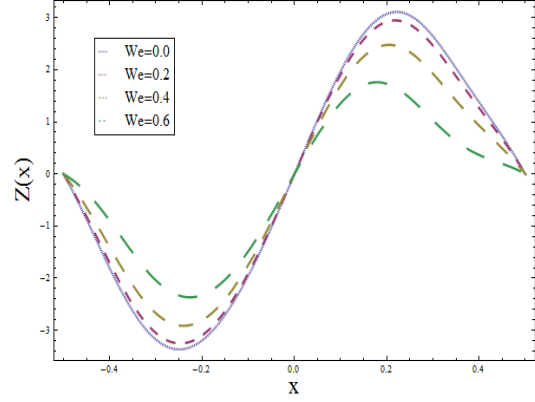


Fig. 10.11

Fig. 10.10: Plot showing  $Z(x)$  versus  $x$ . Here  $a = 0.3$ ,  $b = 0.5$ ,  $d = 1$ ,  $\phi = \pi/4$ ,  $\Theta = 1.5$ ,  $Bi_1 = 1$ ,  $Bi_2 = 10$ ,  $\tilde{n} = 0.398$  and  $We = 0.1$ .

Fig. 10.11: Plot showing  $Z(x)$  versus  $x$ . Here  $a = 0.3$ ,  $b = 0.5$ ,  $d = 1$ ,  $\phi = \pi/4$ ,  $\Theta = 1.5$ ,  $Br = 2$ ,  $Bi_1 = 1$ ,  $Bi_2 = 10$  and  $\tilde{n} = 0.398$ .

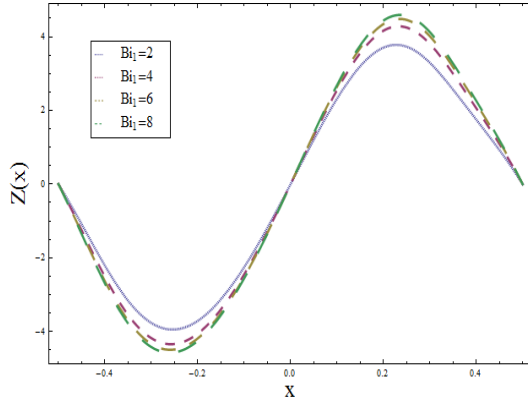


Fig. 10.12

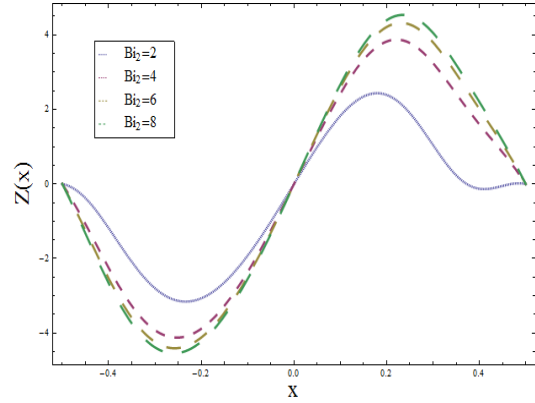


Fig. 10.13

Fig. 10.12: Plot showing  $Z(x)$  versus  $x$ . Here  $a = 0.3$ ,  $b = 0.5$ ,  $d = 1$ ,  $\phi = \pi/4$ ,  $\Theta = 1.5$ ,  $Br = 2$ ,  $Bi_2 = 10$ ,  $\tilde{n} = 0.398$  and  $We = 0.1$ .

Fig. 10.13: Plot showing  $Z(x)$  versus  $x$ . Here  $a = 0.3$ ,  $b = 0.5$ ,  $d = 1$ ,  $\phi = \pi/4$ ,  $\Theta = 1.5$ ,  $Br = 2$ ,  $Bi_1 = 10$ ,  $\tilde{n} = 0.398$  and  $We = 0.1$ .

## 10.5 Concluding remarks

A mathematical model subject to long wavelength and low Reynolds number approximations is presented in order to study the effects of convective boundary conditions on peristaltic transport of Carreau fluid in an asymmetric channel. Series expressions of stream function, longitudinal velocity and pressure gradient are developed. A comparative study is made between the Newtonian and Carreau fluids. It is concluded that in the narrow part of the channel, longitudinal velocity for Newtonian fluid is greater than the Carreau fluid while in the wider part of the channel the velocity for Newtonian fluid is lower than that of a Carreau fluid. The thermal study discloses that an increase in Biot number at the lower wall  $Bi_2$  and  $Br$  boosts the fluid temperature while it decreases for the Biot number at the upper wall of the channel  $Bi_1$ . Also the fluid temperature for a Newtonian fluid is higher than Carreau fluid. The heat transfer coefficient at the upper wall is an increasing function of Biot numbers.

## Chapter 11

# Convective heat and mass transfer analysis on peristaltic flow of Williamson fluid with Hall effects and Joule heating

### 11.1 Introduction

This chapter deals with the peristaltic flow of an incompressible and electrically conducting Williamson fluid in a symmetric planar channel with heat and mass transfer. Hall effects, viscous dissipation and Joule heating are also taken into consideration. Mathematical model is presented for long wavelength and low Reynolds number approximations. The differential equations governing the flow are highly nonlinear and thus perturbation solution for small Weissenberg number ( $0 < We < 1$ ) is presented. Effects of the heat and mass transfer Biot numbers and Hall parameter on the longitudinal velocity, temperature, concentration and pumping characteristics are studied in detail. The streamlines pattern and trapping are also given due attention. Main observations are presented in the concluding section.

## 11.2 Flow equations

The basic equations that govern the flow of an incompressible Williamson fluid in the presence of heat and mass transfer with viscous dissipation and Joule heating are

$$\nabla \cdot \bar{\mathbf{V}} = 0, \quad (11.1)$$

$$\rho \frac{d\bar{\mathbf{V}}}{dt} = -\nabla \bar{P} + \nabla \cdot \bar{\mathbf{S}} + \bar{\mathbf{J}} \times \bar{\mathbf{B}}, \quad (11.2)$$

$$\rho c_p \frac{d\bar{T}}{dt} = k \nabla^2 \bar{T} + \Phi + \frac{1}{\sigma} \bar{\mathbf{J}} \cdot \bar{\mathbf{J}}, \quad (11.3)$$

$$\rho \frac{d\bar{C}}{dt} = D \nabla^2 \bar{C} + \frac{Dk_T}{T_m} \nabla^2 \bar{T}, \quad (11.4)$$

where  $\bar{\mathbf{V}}$  is the velocity of fluid,  $\bar{\mathbf{J}}$  the current density,  $\bar{\mathbf{B}}$  the magnetic flux density,  $\bar{\mathbf{S}}$  the extra stress tensor representing the stresses resulting from a relative motion within a Williamson fluid,  $\rho$  the density of fluid,  $\bar{P}$  the pressure,  $c_p$  the specific heat at constant pressure,  $\sigma$  the electrical conductivity,  $\bar{T}$  the temperature of fluid,  $\bar{C}$  the concentration of fluid,  $T_m$  the mean temperature,  $k_T$  the thermal diffusion ratio,  $D$  the coefficient of mass diffusivity and  $\Phi$  the viscous dissipation factor.

The constitutive equation for the extra stress tensor  $\bar{\mathbf{S}}$  is

$$\bar{\mathbf{S}} = -[\eta_\infty + (\eta_0 - \eta_\infty)(1 - \check{\Gamma}\bar{\gamma})^{-1}]\bar{\gamma}, \quad (11.5)$$

where  $\eta_\infty$  is the infinite shear rate viscosity,  $\eta_0$  is the zero shear rate viscosity,  $\check{\Gamma}$  the time constant and  $\bar{\gamma}$  is defined by

$$\bar{\gamma} = \sqrt{\frac{1}{2} \sum_i \sum_j \bar{\gamma}_{ij} \bar{\gamma}_{ji}} = \sqrt{\frac{1}{2} \bar{\Pi}}. \quad (11.6)$$

Here  $\bar{\Pi}$  is the second invariant shear-rate tensor. By considering  $\eta_\infty = 0$  and  $\check{\Gamma}\bar{\gamma} < 1$  in the constitutive Eq. (5), we can write

$$\bar{\mathbf{S}} = -\eta_0[(1 - \check{\Gamma}\bar{\gamma})^{-1}]\bar{\gamma}, \quad (11.7)$$

in which Eq. (11.7) reduces to a Newtonian fluid when  $\check{\Gamma} = 0$ .

### 11.3 Problem formulation

Let us consider the peristaltic flow of an incompressible and electrically conducting Williamson fluid bounded in a two-dimensional infinite symmetric flexible channel of width  $2a$ . The flow is considered in the direction of  $\bar{X}$ -axis. Here  $\bar{Y}$ -axis is taken normal to the flow. A sinusoidal wave of amplitude  $b$  propagates along the channel walls with constant speed  $c$  along the direction of the  $\bar{X}$ -axis. A strong uniform magnetic field with magnetic flux density  $\bar{\mathbf{B}} = (0, 0, B_0)$  is applied and the Hall effects are taken into account. The induced magnetic field is neglected by assuming a very small magnetic Reynolds number ( $Re_m \ll 1$ ). Also it is assumed that there is no applied or polarization voltage so that the total electric field  $\bar{\mathbf{E}} = \mathbf{0}$ . The geometry of the wall surface is described by

$$\bar{H}(\bar{X}, \bar{t}) = \pm a \pm b \cos \left[ \frac{2\pi}{\lambda} (\bar{X} - c\bar{t}) \right]. \quad (11.8)$$

In the above equation  $a$  is the mean half width of the channel,  $b$  is the wave amplitude,  $\lambda$  is the wavelength,  $c$  is the velocity of propagation and  $\bar{t}$  is the time.

The generalized Ohm's law can be written as follows:

$$\bar{\mathbf{J}} = \sigma(\bar{\mathbf{E}} + \bar{\mathbf{V}} \times \bar{\mathbf{B}} - \check{\beta} \bar{\mathbf{J}} \times \bar{\mathbf{B}}), \quad (11.9)$$

where  $\check{\beta} = 1/en_e$  is the Hall factor,  $n_e$  the mass of electron and  $e$  is charge of the electron.

Eq. (11.9) can be solved in  $\bar{\mathbf{J}}$  to yield the Lorentz force vector in the form

$$\bar{\mathbf{J}} \times \bar{\mathbf{B}} = \frac{-\sigma B_0^2}{1 + \check{m}^2} [(\bar{U} - \hat{m}\bar{V})\hat{i} + (\hat{m}\bar{U} + \bar{V})\hat{j}], \quad (11.10)$$

where  $\bar{U}$  and  $\bar{V}$  are the  $\bar{X}$  and  $\bar{Y}$  components of the velocity vector and  $\hat{m} = \sigma B_0 \check{\beta}$  is the Hall parameter.

The boundary conditions in the fixed frame are given by

$$\begin{aligned} \frac{\partial \bar{U}}{\partial \bar{Y}} = 0, \quad \bar{T} = \bar{T}_0, \quad \bar{C} = \bar{C}_0, & \quad \text{at } \bar{Y} = 0, \\ \bar{U} = 0, \quad k \frac{\partial \bar{T}}{\partial \bar{Y}} = -h_t(\bar{T} - \bar{T}_1), \quad D \frac{\partial \bar{C}}{\partial \bar{Y}} = -h_m(\bar{C} - \bar{C}_1), & \quad \text{at } \bar{Y} = \bar{H}, \end{aligned} \quad (11.11)$$

in which  $k$  is the thermal conductivity,  $h_t$  the wall heat transfer coefficient and  $\bar{T}_1$  the temperature at the wall. Analogues to the convective heat transfer at the boundary, we use the mixed condition for the mass transfer as well. Therefore  $h_m$  is the mass transfer coefficient that is defined in almost the same way as the heat transfer coefficient (it is a parameter that is used to describe the ratio between actual mass flux of a specy into or out of the flowing fluid and the driving force that causes that flux) and  $\bar{C}_1$  is the concentration at the wall. Also  $\bar{T}_0$  and  $\bar{C}_0$  are the temperature and concentration at the center of the channel respectively.

Using the transformations

$$\begin{aligned}\bar{x} &= \bar{X} - c\bar{t}, \quad \bar{y} = \bar{Y}, \quad \bar{u}(\bar{x}, \bar{y}) = \bar{U}(\bar{X}, \bar{Y}, \bar{t}) - c, \quad \bar{v}(\bar{x}, \bar{y}) = \bar{V}(\bar{X}, \bar{Y}, \bar{t}), \\ \bar{T}(\bar{x}, \bar{y}) &= \bar{T}(\bar{X}, \bar{Y}, \bar{t}), \quad \bar{C}(\bar{x}, \bar{y}) = \bar{C}(\bar{X}, \bar{Y}, \bar{t}), \quad \bar{p}(\bar{x}, \bar{y}) = \bar{P}(\bar{X}, \bar{Y}, \bar{t}),\end{aligned}\quad (11.12)$$

the unsteady flow in the fixed frame  $(\bar{X}, \bar{Y})$  appears steady in the wave frame  $(\bar{x}, \bar{y})$ . Further  $(\bar{u}, \bar{v})$  and  $\bar{p}$  are the velocity components and pressure in the wave frame.

We define the following non-dimensionless quantities

$$\begin{aligned}x &= \frac{\bar{x}}{\lambda}, \quad y = \frac{\bar{y}}{a}, \quad u = \frac{\bar{u}}{c}, \quad v = \frac{\bar{v}}{c}, \quad t = \frac{c\bar{t}}{\lambda}, \quad p = \frac{a^2}{c\mu\lambda}\bar{p}, \quad \delta = \frac{a}{\lambda}, \\ \text{Re} &= \frac{\rho ca}{\mu}, \quad \dot{\gamma}^* = \frac{a}{c}\bar{\gamma}, \quad \theta = \frac{\bar{T} - \bar{T}_0}{\bar{T}_1 - \bar{T}_0}, \quad \phi = \frac{\bar{C} - \bar{C}_0}{\bar{C}_1 - \bar{C}_0}, \quad H = \frac{\bar{H}}{a}, \\ \mathbf{S} &= \frac{a}{\mu c}\bar{\mathbf{S}}, \quad \text{Pr} = \frac{\mu c_p}{k}, \quad M = \sqrt{\frac{\sigma}{\mu}}B_0a, \quad \text{Sc} = \frac{\mu}{\rho D}, \quad \text{Sr} = \frac{\rho D k_T (T_1 - T_0)}{T_m \mu (C_1 - C_0)}, \\ \text{Ec} &= \frac{c^2}{c_p(T_1 - T_0)}, \quad \text{Br} = \text{Pr} \text{Ec}, \quad \text{We} = \frac{\check{\Gamma}c}{a}, \quad \psi = \frac{\bar{\psi}}{ca}, \quad \gamma_t = \frac{h_t a}{k}, \quad \gamma_m = \frac{h_m a}{D},\end{aligned}\quad (11.13)$$

where  $\text{Re}$  is the Reynolds number,  $M$  the Hartman number,  $\text{Pr}$  the Prandtl number,  $\text{Sc}$  the Schmidt number,  $\text{Sr}$  the Soret number,  $\text{Ec}$  the Eckert number,  $\text{Br}$  the Brinkman number,  $\text{We}$  the Weissenberg number,  $\psi$  the stream function,  $\gamma_t$  the heat transfer Biot number and  $\gamma_m$  the mass transfer Biot number.

Using Eq. (11.12) and the above set of non-dimensional variables into Eqs. (11.1) – (11.4), the resulting equations in the wave frame of reference in terms of the stream function  $\psi$  ( $u =$

$\partial\psi/\partial y, v = -\delta\partial\psi/\partial x$  are

$$\begin{aligned} \delta \operatorname{Re} \left[ \left( \frac{\partial\psi}{\partial y} \frac{\partial}{\partial x} - \frac{\partial\psi}{\partial x} \frac{\partial}{\partial y} \right) \left( \frac{\partial\psi}{\partial y} \right) \right] &= -\frac{\partial p}{\partial x} + 2\delta \frac{\partial}{\partial x} \left( [1 + We\dot{\gamma}^*] \frac{\partial^2\psi}{\partial x\partial y} \right) \\ &+ \frac{\partial}{\partial y} \left( [1 + We\dot{\gamma}^*] \left( \frac{\partial^2\psi}{\partial y^2} - \delta^2 \frac{\partial^2\psi}{\partial x^2} \right) \right) - \delta \frac{\hat{m}M^2}{1 + \hat{m}^2} \left( \frac{\partial\psi}{\partial x} \right) \\ &- \frac{M^2}{1 + \hat{m}^2} \left( \frac{\partial\psi}{\partial y} + 1 \right), \end{aligned} \quad (11.14)$$

$$\begin{aligned} \delta^3 \operatorname{Re} \left[ \left( \frac{\partial\psi}{\partial y} \frac{\partial}{\partial x} - \frac{\partial\psi}{\partial x} \frac{\partial}{\partial y} \right) \left( \frac{\partial\psi}{\partial x} \right) \right] &= -\frac{\partial p}{\partial y} + \delta^2 \frac{\partial}{\partial x} \left( [1 + We\dot{\gamma}^*] \left( \frac{\partial^2\psi}{\partial y^2} - \delta^2 \frac{\partial^2\psi}{\partial x^2} \right) \right) \\ &- 2\delta^2 \frac{\partial}{\partial y} \left( [1 + We\dot{\gamma}^*] \frac{\partial^2\psi}{\partial x\partial y} \right) - \delta \frac{\hat{m}M^2}{1 + \hat{m}^2} \left( \frac{\partial\psi}{\partial y} + 1 \right) \\ &+ \delta^2 \frac{\hat{m}M^2}{1 + \hat{m}^2} \left( \frac{\partial\psi}{\partial x} \right), \end{aligned} \quad (11.15)$$

$$\begin{aligned} \delta \operatorname{Re} \left[ \frac{\partial\psi}{\partial y} \frac{\partial}{\partial x} - \frac{\partial\psi}{\partial x} \frac{\partial}{\partial y} \right] \theta &= \frac{1}{\operatorname{Pr}} \left( \delta^2 \frac{\partial^2}{\partial x^2} + \frac{\partial^2}{\partial y^2} \right) \theta + Ec[1 + We\dot{\gamma}^*] \\ &\times \left[ 4\delta^2 \left( \frac{\partial^2\psi}{\partial x\partial y} \right)^2 + \left( \frac{\partial^2\psi}{\partial y^2} - \delta^2 \frac{\partial^2\psi}{\partial x^2} \right)^2 \right] \\ &+ Ec \frac{M^2}{1 + \hat{m}^2} \left[ \delta^2 \left( \frac{\partial\psi}{\partial x} \right)^2 + \left( \frac{\partial\psi}{\partial y} + 1 \right)^2 \right], \end{aligned} \quad (11.16)$$

$$\delta \operatorname{Re} \left[ \frac{\partial\psi}{\partial y} \frac{\partial}{\partial x} - \frac{\partial\psi}{\partial x} \frac{\partial}{\partial y} \right] \phi = \frac{1}{Sc} \left( \delta^2 \frac{\partial^2}{\partial x^2} + \frac{\partial^2}{\partial y^2} \right) \phi + Sr \left( \delta^2 \frac{\partial^2}{\partial x^2} + \frac{\partial^2}{\partial y^2} \right) \theta, \quad (11.17)$$

with

$$\dot{\gamma}^* = \left[ 4\delta^2 \left( \frac{\partial^2\psi}{\partial x\partial y} \right)^2 + \left( \frac{\partial^2\psi}{\partial y^2} - \delta^2 \frac{\partial^2\psi}{\partial x^2} \right)^2 \right]^{\frac{1}{2}}. \quad (11.18)$$



For long wavelength  $\delta \ll 1$  and low Reynolds number  $Re \rightarrow 0$  [6], we finally obtain

$$0 = -\frac{\partial p}{\partial x} + \frac{\partial}{\partial y} \left( [1 + We\dot{\gamma}^*] \frac{\partial^2 \psi}{\partial y^2} \right) - \frac{M^2}{1 + \hat{m}^2} \left( \frac{\partial \psi}{\partial y} + 1 \right), \quad (11.19)$$

$$0 = -\frac{\partial p}{\partial y}, \quad (11.20)$$

$$0 = \frac{1}{Pr} \frac{\partial^2 \theta}{\partial y^2} + Ec \left[ \left( \frac{\partial^2 \psi}{\partial y^2} \right)^2 + We \left( \frac{\partial^2 \psi}{\partial y^2} \right)^3 + \frac{M^2}{1 + \hat{m}^2} \left( \frac{\partial \psi}{\partial y} + 1 \right)^2 \right], \quad (11.21)$$

$$0 = \frac{1}{Sc} \frac{\partial^2 \phi}{\partial y^2} + Sr \frac{\partial^2 \theta}{\partial y^2}. \quad (11.22)$$

Eq. (11.20) implies that  $p \neq p(y)$  and so we can write Eq. (11.19) in the form

$$0 = \frac{\partial^2}{\partial y^2} \left[ \left( [1 + We \frac{\partial^2 \psi}{\partial y^2}] \frac{\partial^2 \psi}{\partial y^2} \right) - \frac{M^2}{1 + \hat{m}^2} \psi \right]. \quad (11.23)$$

The nondimensional conditions in wave frame are given as follows:

$$\begin{aligned} \psi &= 0, \quad \frac{\partial^2 \psi}{\partial y^2} = 0, \quad \theta = 0, \quad \phi = 0, & \text{at } y = 0, \\ \psi &= F, \quad \frac{\partial \psi}{\partial y} = -1, \quad \frac{\partial \theta}{\partial y} + \gamma_t(\theta - 1) = 0, \quad \frac{\partial \phi}{\partial y} + \gamma_m(\phi - 1) = 0, & \text{at } y = H, \end{aligned} \quad (11.24)$$

where  $H(x) = 1 + \epsilon \cos(2\pi x)$ ,  $\epsilon = \frac{b}{a}$  ( $0 < \epsilon < 1$ ) is the amplitude ratio and  $F$  the dimensionless time mean flow rate in the wave frame. It is related to the dimensionless time mean flow rate  $\Theta$  in the laboratory frame through the relation  $\Theta = F + 1$ .

The non-dimensional expression for the pressure rise  $\Delta p_\lambda$  per wavelength  $\lambda$  is given by

$$\Delta p_\lambda = \int_0^{2\pi} \left( \frac{dp}{dx} \right) dx. \quad (11.25)$$

## 11.4 Series solution

In order to get closed form solutions of the Eqs. (11.21) – (11.24), we are looking for a regular perturbation technique in terms of the small parameter  $We$  as follows:

$$\psi = \psi_0 + We\psi_1 + We^2\psi_2 + \dots \quad (11.26)$$

$$F = F_0 + WeF_1 + We^2F_2 + \dots \quad (11.27)$$

$$\frac{dp}{dx} = \frac{dp_0}{dx} + We\frac{dp_1}{dx} + We^2\frac{dp_2}{dx} + \dots \quad (11.28)$$

$$\theta = \theta_0 + We\theta_1 + We^2\theta_2 + \dots \quad (11.29)$$

$$\phi = \phi_0 + We\phi_1 + We^2\phi_2 + \dots \quad (11.30)$$

Substituting Eqs. (11.26) – (11.30) into Eqs. (11.21) – (11.24) and then comparing the coefficients of like powers of  $We$  up to the first order and neglecting powers of order two and higher we have

### 11.4.1 System of order zero

$$0 = \left[ \frac{\partial^2}{\partial y^2} - \frac{M^2}{1 + \hat{m}^2} \right] \frac{\partial^2 \psi_0}{\partial y^2}, \quad (11.31)$$

$$0 = \frac{1}{Pr} \frac{\partial^2 \theta_0}{\partial y^2} + Ec \left[ \left( \frac{\partial^2 \psi_0}{\partial y^2} \right)^2 + \frac{M^2}{1 + \hat{m}^2} \left( \frac{\partial \psi_0}{\partial y} + 1 \right)^2 \right], \quad (11.32)$$

$$0 = \frac{1}{Sc} \frac{\partial^2 \phi_0}{\partial y^2} + Sr \frac{\partial^2 \theta_0}{\partial y^2}, \quad (11.33)$$

$$\psi_0 = 0, \quad \frac{\partial^2 \psi_0}{\partial y^2} = 0, \quad \theta_0 = 0, \quad \phi_0 = 0, \quad \text{at } y = 0,$$

$$\psi_0 = F_0, \quad \frac{\partial \psi_0}{\partial y} = -1, \quad \frac{\partial \theta_0}{\partial y} + \gamma_t(\theta_0 - 1) = 0, \quad \frac{\partial \phi_0}{\partial y} + \gamma_m(\phi_0 - 1) = 0, \quad \text{at } y = H \quad (11.34)$$

### 11.4.2 System of order one

$$0 = \frac{\partial^4 \psi_1}{\partial y^4} - \frac{M^2}{1 + \hat{m}^2} \frac{\partial^2 \psi_1}{\partial y^2} + \frac{\partial^2}{\partial y^2} \left( \frac{\partial^2 \psi_0}{\partial y^2} \right)^2, \quad (11.35)$$

$$0 = \frac{1}{\text{Pr}} \frac{\partial^2 \theta_1}{\partial y^2} + Ec \left[ 2 \left( \frac{\partial^2 \psi_0}{\partial y^2} \right) \left( \frac{\partial^2 \psi_1}{\partial y^2} \right) + \left( \frac{\partial^2 \psi_0}{\partial y^2} \right)^3 + \frac{M^2}{1 + \hat{m}^2} \left( 2 \left( \frac{\partial \psi_0}{\partial y} + 1 \right) \frac{\partial \psi_1}{\partial y} \right) \right], \quad (11.36)$$

$$0 = \frac{1}{Sc} \frac{\partial^2 \phi_1}{\partial y^2} + Sr \frac{\partial^2 \theta_1}{\partial y^2}, \quad (11.37)$$

$$\begin{aligned} \psi_1 &= 0, \quad \frac{\partial^2 \psi_1}{\partial y^2} = 0, \quad \theta_1 = 0, \quad \phi_1 = 0, & \text{at } y = 0, \\ \psi_1 &= F_1, \quad \frac{\partial \psi_1}{\partial y} = 0, \quad \frac{\partial \theta_1}{\partial y} + \gamma_t \theta_1 = 0, \quad \frac{\partial \phi_1}{\partial y} + \gamma_m \phi_1 = 0, & \text{at } y = H. \end{aligned} \quad (11.38)$$

Solving the resulting zeroth and first order systems we arrive at

$$\begin{aligned} \psi &= \frac{1}{A_1} [(\hat{\lambda} q \cos h(H\hat{\lambda}) + \sin h(H\hat{\lambda}))y - (H + F) \sin h(\hat{\lambda}y)] \\ &\quad - \frac{1}{12A_1^3} (H + F)^2 \hat{\lambda}^2 We [8y\hat{\lambda} + \hat{\lambda} \{ (6H - 9y) \cos h(H\hat{\lambda}) + y \cos h(3H\hat{\lambda}) \\ &\quad + H(\cos h((H - 2y)\hat{\lambda}) - 8 \cos h((H - y)\hat{\lambda}) + 2 \cos h((2H - y)\hat{\lambda}) - 2 \cos h((2H + y)\hat{\lambda}) \\ &\quad + \cos h((H + 2y)\hat{\lambda})) \} - 6 \sin h(H\hat{\lambda}) - \sin h((H - 2y)\hat{\lambda}) + 8 \sin h((H - y)\hat{\lambda}) \\ &\quad - \sin h((2H - y)\hat{\lambda}) + 6 \sin h(y\hat{\lambda}) + \sin h((2H + y)\hat{\lambda}) - \sin h((H + 2y)\hat{\lambda})], \end{aligned} \quad (11.39)$$

$$\frac{dp}{dx} = \frac{4\hat{\lambda}^5}{3A_1^3} We [(H + F)^2 (2 + \cos h(H\hat{\lambda})) \sin h^4(\frac{H\hat{\lambda}}{2})] - \frac{\hat{\lambda}^2}{A_1} (F\hat{\lambda} \cos h(H\hat{\lambda}) + \sin h(H\hat{\lambda})), \quad (11.40)$$

$$\begin{aligned}
\theta = & \frac{1}{4A_3}[-2\gamma_t y + (2\gamma_t H^2 y + Br(H+F)^2(A_2 - 5\gamma_t y))\hat{\lambda}^2 + Br(H+F)^2 y(H(1+A_2) \\
& - A_2 y)\hat{\lambda}^4 - y(-2\gamma_t + \gamma_t((-2+3Br)H^2 + 3BrF(F+2H))\hat{\lambda}^2 - Br(H+F)^2 \\
& \times (H(1+A_2) - A_2 y)\hat{\lambda}^4) \cos h(2H\hat{\lambda}) + 8Br(H+F)^2 \hat{\lambda}^2 \cos h(H\hat{\lambda})(-A_2 + \gamma_t y \\
& + A_2 \cos h(y\hat{\lambda})) + \hat{\lambda}(-BrA_2(H+F)^2 \hat{\lambda} \cos h(2y\hat{\lambda}) - 2y(2\gamma_t H + Br(H+F)^2 \hat{\lambda}^2) \\
& \times \sin h(2H\hat{\lambda}))] - \frac{Br(H+F)^3 \hat{\lambda}^4}{24A_4} We[-54A_2 + 81\gamma_t y + 3y(3y + H(-7 - 3\gamma_t(H-y))\hat{\lambda}^2 \\
& + 8(9A_2 - 16\gamma_t y + 2A_2(H-y)y\hat{\lambda}^2) \cos h(H\hat{\lambda}) - 2(9A_2 - 24\gamma_t y \\
& + 2y(H(3+2A_2) - 2A_2 y)\hat{\lambda}^2) \cos h(2H\hat{\lambda}) + y \cos h(4H\hat{\lambda})(\gamma_t(H^2 \hat{\lambda}^2 - 1) + H\hat{\lambda}^2) \\
& + A_2\{-y^2 \hat{\lambda}^2 \cos h(4H\hat{\lambda}) + \cos h((H-3y)\hat{\lambda}) - 8 \cos h((H-2y)\hat{\lambda}) - 27 \cos h((H-y)\hat{\lambda}) \\
& + 16 \cos h((2H-y)\hat{\lambda}) + 48 \cos h(y\hat{\lambda}) + 6 \cos h(2y\hat{\lambda}) - 37 \cos h((H+y)\hat{\lambda}) \\
& + 2 \cos h(2(H+y)\hat{\lambda}) - \cos h((H+3y)\hat{\lambda})\} - 8y\hat{\lambda}(2 + 3\gamma_t H) \sin h(H\hat{\lambda}) \\
& + 2y\hat{\lambda}(11 - 16\gamma_t H) \sin h(2H\hat{\lambda}) + \hat{\lambda}HA_2\{20 \sin h(2H\hat{\lambda}) - 16 \sin h(H\hat{\lambda}) - \sin h((H-3y)\hat{\lambda}) \\
& + 8 \sin h((H-2y)\hat{\lambda}) - \sin h((H-y)\hat{\lambda}) - \sin h(2(H-y)\hat{\lambda}) - 16 \sin h((2H-y)\hat{\lambda}) \\
& + 4 \sin h((3H-y)\hat{\lambda}) + 16 \sin h(y\hat{\lambda}) - 2 \sin h(2y\hat{\lambda}) + 9 \sin h((H+y)\hat{\lambda}) - 3 \sin h(2(H+y)\hat{\lambda}) \\
& + 4 \sin h((3H+y)\hat{\lambda}) + \sin h((H+3y)\hat{\lambda})\} - 8H\hat{\lambda}(A_2 - y) \sin h(3H\hat{\lambda}) \\
& - y\hat{\lambda}(1 + A_2) \sin h(4H\hat{\lambda})], \tag{11.41}
\end{aligned}$$

$$\begin{aligned}
\phi = & \frac{1}{4A_6}[-2y\gamma_m - (-2H^2y\gamma_m + Br(H+F)^2ScSr(A_5 - 5y\gamma_m))\hat{\lambda}^2 + Br(H+F)^2ScSry \\
& \times (y + H(-1 - A_5 + y\gamma_m))\hat{\lambda}^4 + y(2\gamma_m + (2H^2 + 3Br(H+F)^2ScSr)\gamma_m)\hat{\lambda}^2 \\
& - Br(H+F)^2ScSr(2H - y + H(H - y)\gamma_m)\hat{\lambda}^4) \cos h(2H\hat{\lambda}) \\
& - 8Br(H+F)^2ScSr\hat{\lambda}^2 \cos h(H\hat{\lambda}) \times (-A_5 + y\gamma_m + A_5 \cos h(y\hat{\lambda})) \\
& + \hat{\lambda}(Br(h+q)^2ScSrA_5\hat{\lambda} \cos h(2y\hat{\lambda}) + 2y(-2H\gamma_m + Br(H+F)^2ScSr\hat{\lambda}^2) \sin h(2H\hat{\lambda}))] \\
& + \frac{ScSr(H+F)^3\hat{\lambda}^4}{24A_7} We[-54A_5 + 81y\gamma_m + 3y(-7H + 3y + 3H(-H + y)\gamma_m)\hat{\lambda}^2 \\
& + 8(9A_5 - 16y\gamma_m + 2(H - y)yA_5\hat{\lambda}^2) \cos h(H\hat{\lambda}) - 2(9A_5 - 24y\gamma_m + 2y(5H - 2y \\
& + 2H(H - y)\hat{\lambda}^2) \cos h(2H\hat{\lambda}) - y\gamma_m \cos h(4H\hat{\lambda}) + A_5\{(H + y)y\hat{\lambda}^2 \cos h(4H\hat{\lambda}) \\
& + \cos h((H - 3y)\hat{\lambda}) - 8 \cos h((H - 2y)\hat{\lambda}) - 27 \cos h((H - y)\hat{\lambda}) \\
& + 16 \cos h((2H - y)\hat{\lambda}) + 48 \cos h(y\hat{\lambda}) + 6 \cos h(2y\hat{\lambda}) - 37 \cos h((H + y)\hat{\lambda}) \\
& + 2 \cos h(2(H + y)\hat{\lambda}) - \cos h((H + 3y)\hat{\lambda})\} - 8y\hat{\lambda}(2 - 3H\gamma_m) \sin h(H\hat{\lambda}) \\
& + 2y\hat{\lambda}(11 - 16H\gamma_m) \sin h(2H\hat{\lambda}) + 8Hy\hat{\lambda}\gamma_m \sin h(3H\hat{\lambda}) - y\hat{\lambda}(1 + 2H\gamma_m) \sin h(4H\hat{\lambda}) \\
& + H\hat{\lambda}A_5\{-16 \sin h(H\hat{\lambda}) + 20 \sin h(2H\hat{\lambda}) - 8 \sin h(3H\hat{\lambda}) - \sin h((H - 3y)\hat{\lambda}) \\
& + 8 \sin h((H - 2y)\hat{\lambda}) - \sin h((H - y)\hat{\lambda}) - \sin h(2(H - y)\hat{\lambda}) - 16 \sin h((2H - y)\hat{\lambda}) \\
& + 4 \sin h((3H - y)\hat{\lambda}) + 16 \sin h(y\hat{\lambda}) - 2 \sin h(2y\hat{\lambda}) + 9 \sin h((H + y)\hat{\lambda}) \\
& - 3 \sin h(2(H + y)\hat{\lambda}) + 4 \sin h((3H + y)\hat{\lambda}) + \sin h((H + 3y)\hat{\lambda})\}], \tag{11.42}
\end{aligned}$$

where

$$\begin{aligned}
\hat{\lambda} &= \sqrt{\frac{M^2}{1 + \hat{m}^2}}, \\
A_1 &= H\hat{\lambda} \cos h(H\hat{\lambda}) - \sin h(H\hat{\lambda}), \\
A_2 &= 1 + \gamma_t H, \quad A_3 = A_2 A_1^2, \\
A_4 &= A_3 A_1^2, \quad A_5 = 1 + \gamma_m H, \\
A_6 &= A_5 A_1^2, \quad A_7 = A_6 A_1^2.
\end{aligned}$$

## 11.5 Results and discussion

In this section we have presented a set of Figs. that describe qualitatively the effects of various parameters of interest on the flow quantities like axial pressure gradient  $dp/dx$ , pressure rise per wavelength  $\Delta p_\lambda$ , axial velocity  $u(y)$ , temperature distribution  $\theta(y)$  and concentration distribution  $\phi(y)$ . Figs. 11.1-11.3 display the variation of axial pressure gradient  $dp/dx$  with  $x$  for different values of Weissenberg number  $We$ , Hartman number  $M$  and Hall parameter  $\hat{m}$ . It is revealed that the magnitude of the pressure gradient decreases with the increase of Weissenberg number  $We$  and Hall parameter  $\hat{m}$  while it increases with an increase in the Hartman number  $M$ . It is also observed that the maximum pressure gradient occurs at the narrow part of the channel i.e.  $x = 0.5$ . Fig. 11.1 also shows that the pressure gradient  $dp/dx$  for the Newtonian fluid ( $We = 0$ ) is greater in magnitude when compared to that of a Williamson fluid ( $We > 0$ ). The pressure rise per wavelength  $\Delta p_\lambda$  against flow rate  $\Theta$  for different values of Weissenberg number  $We$ , Hartman number  $M$  and Hall parameter  $\hat{m}$  are shown in the Figs. 11.4-11.6. Note that Eq. (11.25) involves the integration of  $dp/dx$ . This integral is not solvable analytically so it is computed numerically by using "Mathematica". It is obvious from Figs. 11.4-11.6 that in the pumping region ( $\Delta p_\lambda > 0$ ), the pumping rate decreases by increasing Hall parameter  $\hat{m}$  and it increases for increasing values of Weissenberg number  $We$ , while in the co-pumping region ( $\Delta p_\lambda < 0$ ), the pumping rate decreases by increasing Hartman number  $M$  and it increases by increasing Hall parameter  $\hat{m}$  and the Weissenberg number  $We$ . For the free pumping case ( $\Delta p_\lambda = 0$ ), there is no noticeable difference. Figs. 11.7-11.9 are prepared to study the role of Weissenberg number  $We$ , Hartman number  $M$  and Hall parameter  $\hat{m}$  on the axial velocity  $u(y)$ . It is obvious from Fig. 11.9 that an increase in Hall parameter  $\hat{m}$ , the magnitude of the velocity  $u(y)$  increases at the center of the channel whereas it decreases near the channel walls. From Figs. 11.7 and 11.8 it is found that the Weissenberg number  $We$  and Hartman number  $M$  have opposite behavior when compared with Hall parameter  $\hat{m}$ . The variation of temperature distribution  $\theta(y)$  for several values of Weissenberg number  $We$ , Hartman number  $M$ , Hall parameter  $\hat{m}$ , the Brinkman number  $Br$  and heat transfer Biot number  $\gamma_t$  are plotted in Figs. 11.10-11.14. These Figs. depict an increase in the temperature field when Hartman number  $M$  and Brinkman number  $Br$  are increased. A decrease in the temperature field is noticed through increase in Weissenberg number  $We$ , Hall parameter  $\hat{m}$  and heat transfer Biot

number  $\gamma_t$ . Figs. 11.15-11.20 represent the concentration distribution  $\phi(y)$  for various values of Weissenberg number  $We$ , Hartman number  $M$ , Hall parameter  $\hat{m}$ , Schmidt number  $Sc$ , Soret number  $Sr$  and mass transfer Biot number  $\gamma_m$ . It can be noticed from these Figs. that the concentration distribution decreases by increasing the Hartman number  $M$ , Schmidt number  $Sc$  and the Soret number  $Sr$  while it increases when the Weissenberg number  $We$ , Hall parameter  $\hat{m}$  and mass transfer Biot number  $\gamma_m$  increase. Another fascinating phenomenon of peristalsis is known as trapping i.e. an internally circulating bolus of fluid is formed which travels along with the wave. The effects of Weissenberg number  $We$  on the streamlines for  $\epsilon = 0.2$ ,  $\hat{m} = 2$ ,  $\Theta = 0.5$ , and  $M = 1.5$  in the wave frame show that the trapped bolus size decreases when the Weissenberg number  $We$  increases (see Fig. 11.21). Further the trapping is more for Williamson fluid ( $We > 0$ ) when compared with Newtonian fluid ( $We = 0$ ). Fig. 11.22 depicts the streamlines for different values of Hartman number  $M$  when  $\epsilon = 0.2$ ,  $\hat{m} = 2$ ,  $\Theta = 0.5$  and  $We = 0.8$ . It is revealed that the size of trapped bolus increases with an increase in Hartman number  $M$ . Whereas for the Hall parameter  $\hat{m}$  the size of the trapped bolus decreases as shown in Fig. 11.23 when  $\epsilon = 0.2$ ,  $We = 0.8$ ,  $\Theta = 0.5$  and  $M = 1.5$ .

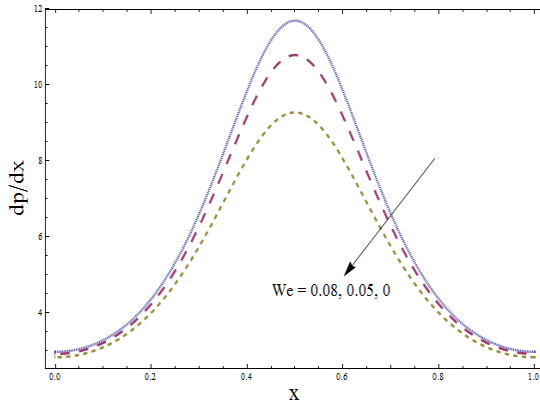


Fig. 11.1

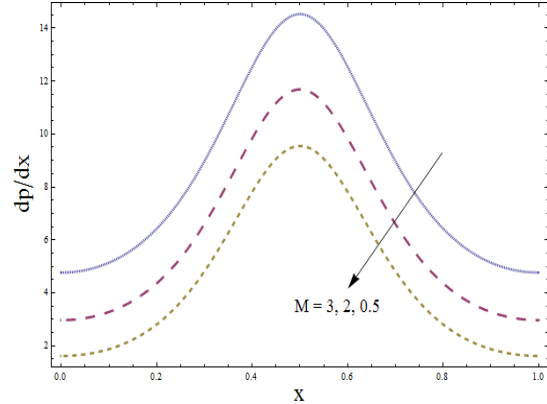


Fig. 11.2

Fig. 11.1: Variation in  $dp/dx$  for  $We$  when  $\epsilon = 0.2$ ,  $M = 2$ ,  $\hat{m} = 2$ , and  $\Theta = -1$ .

Fig. 11.2: Variation in  $dp/dx$  for  $M$  when  $\epsilon = 0.2$ ,  $We = 0.08$ ,  $\hat{m} = 2$ , and  $\Theta = -1$ .

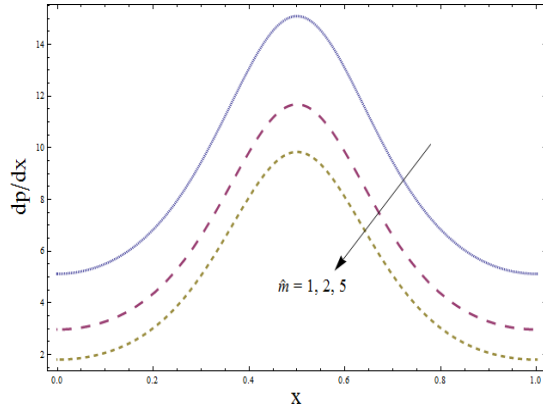


Fig. 11.3

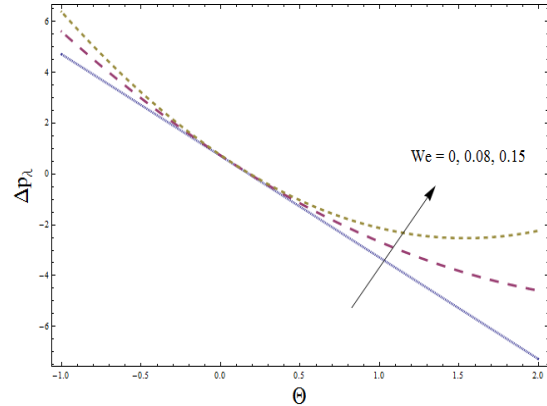


Fig. 11.4

Fig. 11.3: Variation in  $dp/dx$  for  $\hat{m}$  when  $\epsilon = 0.2$ ,  $M = 2$ ,  $We = 0.08$ , and  $\Theta = -1$ .

Fig. 11.4: Variation in  $\Delta p_\lambda$  versus  $\Theta$  for  $We$  when  $\epsilon = 0.2$ ,  $M = 1$  and  $\hat{m} = 1$ .

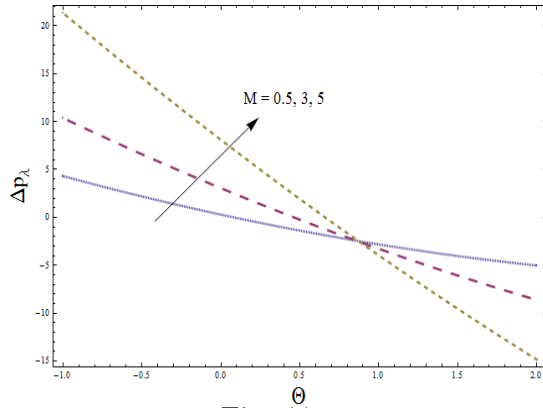


Fig. 11.5

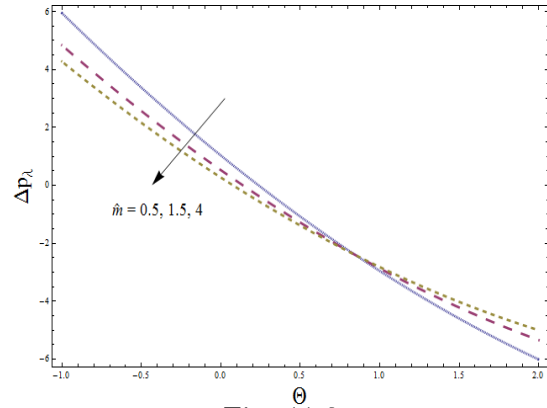


Fig. 11.6

Fig. 11.5: Variation in  $\Delta p_\lambda$  versus  $\Theta$  for  $M$  when  $\epsilon = 0.2$ ,  $We = 0.05$  and  $\hat{m} = 1.5$ .

Fig. 11.6: Variation in  $\Delta p_\lambda$  versus  $\Theta$  for  $\hat{m}$  when  $\epsilon = 0.2$ ,  $M = 1$  and  $We = 0.05$ .



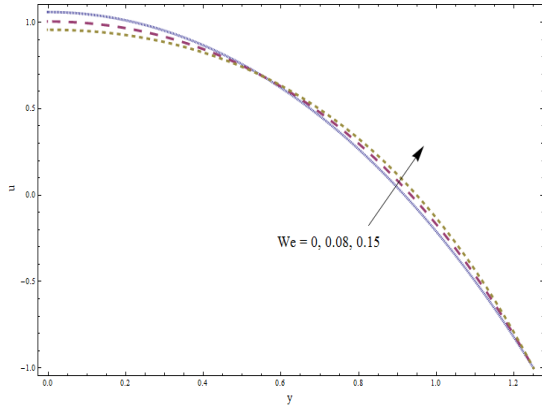


Fig. 11.7

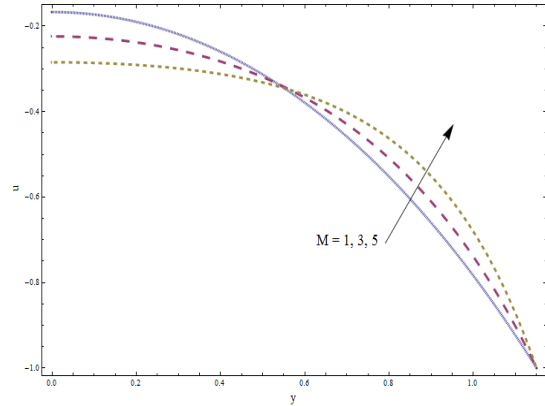


Fig. 11.8

Fig. 11.7: Axial velocity  $u(y)$  for  $We$  when  $\epsilon = 0.25$ ,  $\hat{m} = 2$ ,  $M = 2$ ,  $\Theta = 1.5$  and  $x = 0$ .

Fig. 11.8: Axial velocity  $u(y)$  for  $M$  when  $\epsilon = 0.15$ ,  $\hat{m} = 1$ ,  $We = 0.05$ ,  $\Theta = 0.5$  and  $x = 0$ .

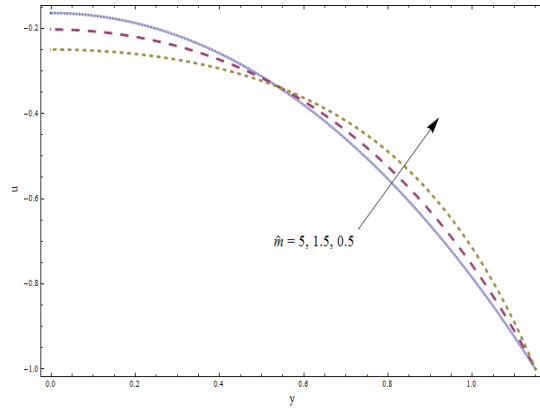


Fig. 11.9

Fig. 11.9: Axial velocity  $u(y)$  for  $\hat{m}$  when  $\epsilon = 0.15$ ,  $We = 0.05$ ,  $M = 3$ ,  $\Theta = 0.5$  and  $x = 0$ .

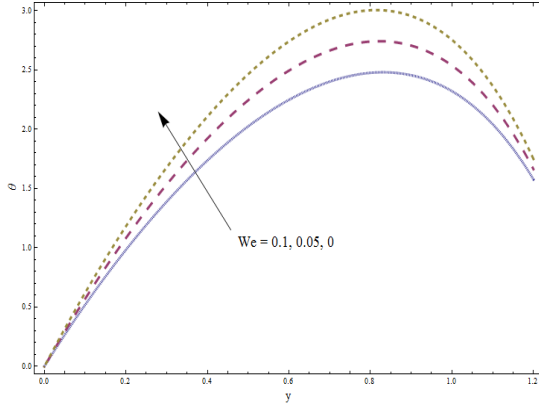


Fig. 11.10

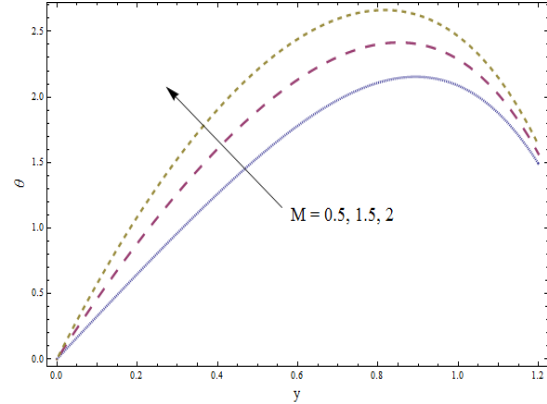


Fig. 11.11

Fig. 11.10: Temperature profile  $\theta(y)$  for  $We$  when  $\epsilon = 0.2$ ,  $M = 1.5$ ,  $Br = 2$ ,  $\Theta = 1.5$ ,  $x = 0$ ,  $\hat{m} = 1.5$  and  $\gamma_t = 10$ .

Fig. 11.11: Temperature profile  $\theta(y)$  for  $M$  when  $\epsilon = 0.2$ ,  $We = 0.08$ ,  $Br = 2$ ,  $\Theta = 1.5$ ,  $x = 0$ ,  $\hat{m} = 2$  and  $\gamma_t = 10$ .

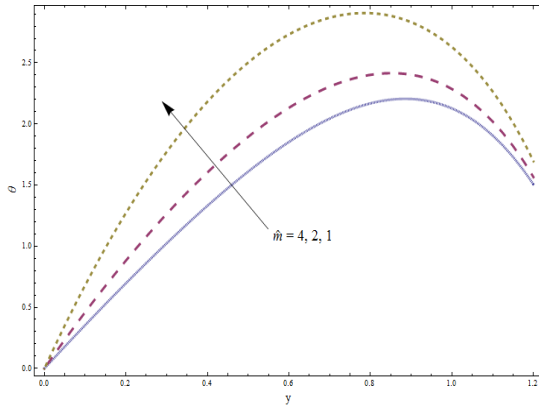


Fig. 11.12

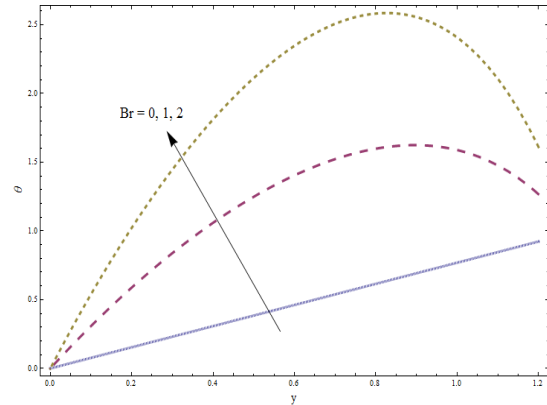


Fig. 11.13

Fig. 11.12: Temperature profile  $\theta(y)$  for  $\hat{m}$  when  $\epsilon = 0.2$ ,  $M = 1.5$ ,  $Br = 2$ ,  $\Theta = 1.5$ ,  $x = 0$ ,  $We = 0.08$  and  $\gamma_t = 10$ .

Fig. 11.13: Temperature profile  $\theta(y)$  for  $Br$  when  $\epsilon = 0.2$ ,  $M = 1.5$ ,  $We = 0.08$ ,  $\Theta = 1.5$ ,  $x = 0$ ,  $\hat{m} = 1.5$  and  $\gamma_t = 10$ .

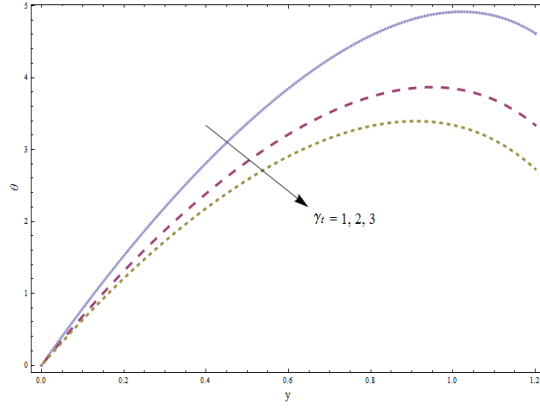


Fig. 11.14

Fig. 11.14: Temperature profile  $\theta(y)$  for  $\gamma_t$  when  $\epsilon = 0.2$ ,  $M = 1.5$ ,  $Br = 2$ ,  $\Theta = 1.5$ ,  $x = 0$ ,  $\hat{m} = 1.5$  and  $We = 0.08$ .

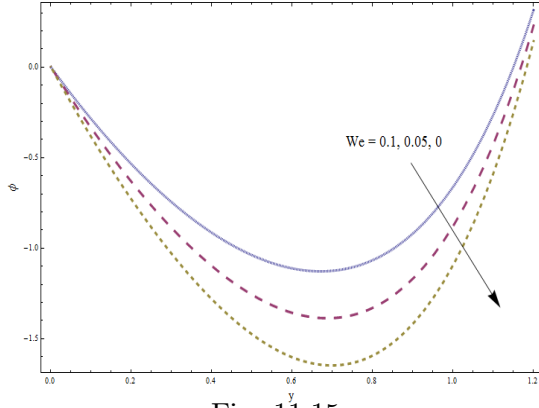


Fig. 11.15

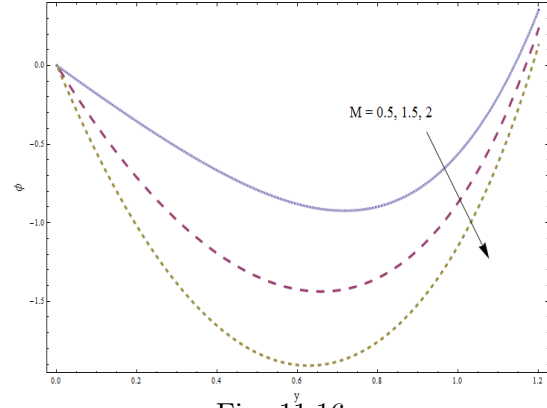


Fig. 11.16

Fig. 11.15: Concentration profile  $\phi(y)$  for  $We$  when  $\epsilon = 0.2$ ,  $M = 1.5$ ,  $Br = 2$ ,  $\Theta = 1.5$ ,  $x = 0$ ,  $\hat{m} = 2$ ,  $Sc = Sr = 1$  and  $\gamma_m = 10$ .

Fig. 11.16: Concentration profile  $\phi(y)$  for  $M$  when  $\epsilon = 0.2$ ,  $We = 0.08$ ,  $Br = 2$ ,  $\Theta = 1.5$ ,  $x = 0$ ,  $\hat{m} = 1.5$ ,  $Sc = Sr = 1$  and  $\gamma_m = 10$ .

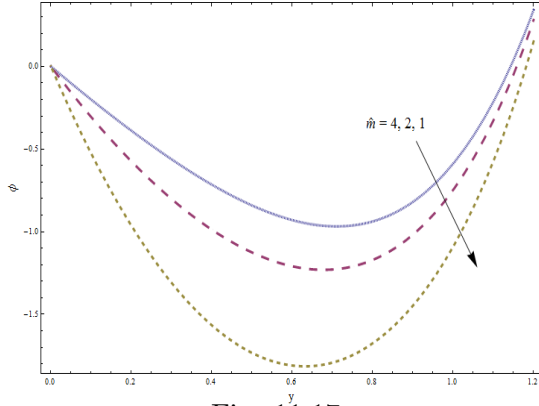


Fig. 11.17

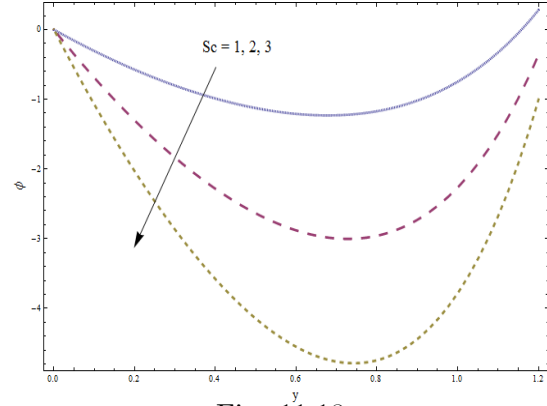


Fig. 11.18

Fig. 11.17: Concentration profile  $\phi(y)$  for  $\hat{m}$  when  $\epsilon = 0.2$ ,  $M = 1.5$ ,  $Br = 2$ ,  $\Theta = 1.5$ ,  $x = 0$ ,  $We = 0.08$ ,  $Sc = Sr = 1$  and  $\gamma_m = 10$ .

Fig. 11.18: Concentration profile  $\phi(y)$  for  $Sc$  when  $\epsilon = 0.2$ ,  $M = 1.5$ ,  $Br = 2$ ,  $\Theta = 1.5$ ,  $x = 0$ ,  $\hat{m} = 2$ ,  $We = 0.08$ ,  $Sr = 1$  and  $\gamma_m = 10$ .

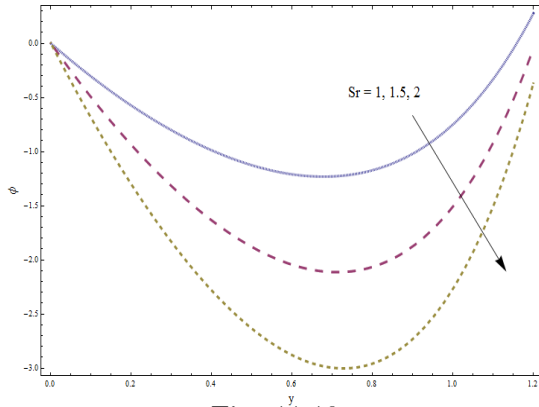


Fig. 11.19

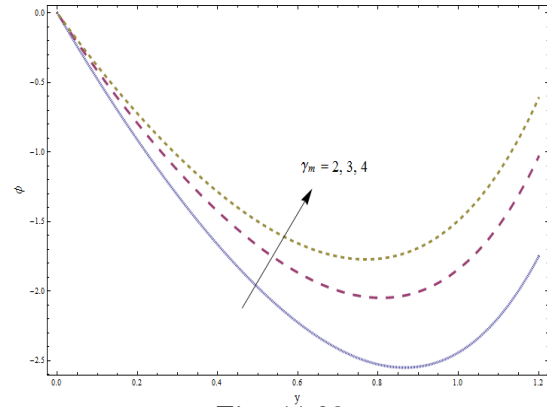


Fig. 11.20

Fig. 11.19: Concentration profile  $\phi(y)$  for  $Sr$  when  $\epsilon = 0.2$ ,  $M = 1.5$ ,  $Br = 2$ ,  $\Theta = 1.5$ ,  $x = 0$ ,  $\hat{m} = 2$ ,  $Sc = 1$ ,  $We = 0.08$  and  $\gamma_m = 10$ .

Fig. 11.20: Concentration profile  $\phi(y)$  for  $\gamma_m$  when  $\epsilon = 0.2$ ,  $M = 1.5$ ,  $Br = 2$ ,  $\Theta = 1.5$ ,  $x = 0$ ,  $\hat{m} = 2$ ,  $Sc = Sr = 1$  and  $We = 0.08$ .

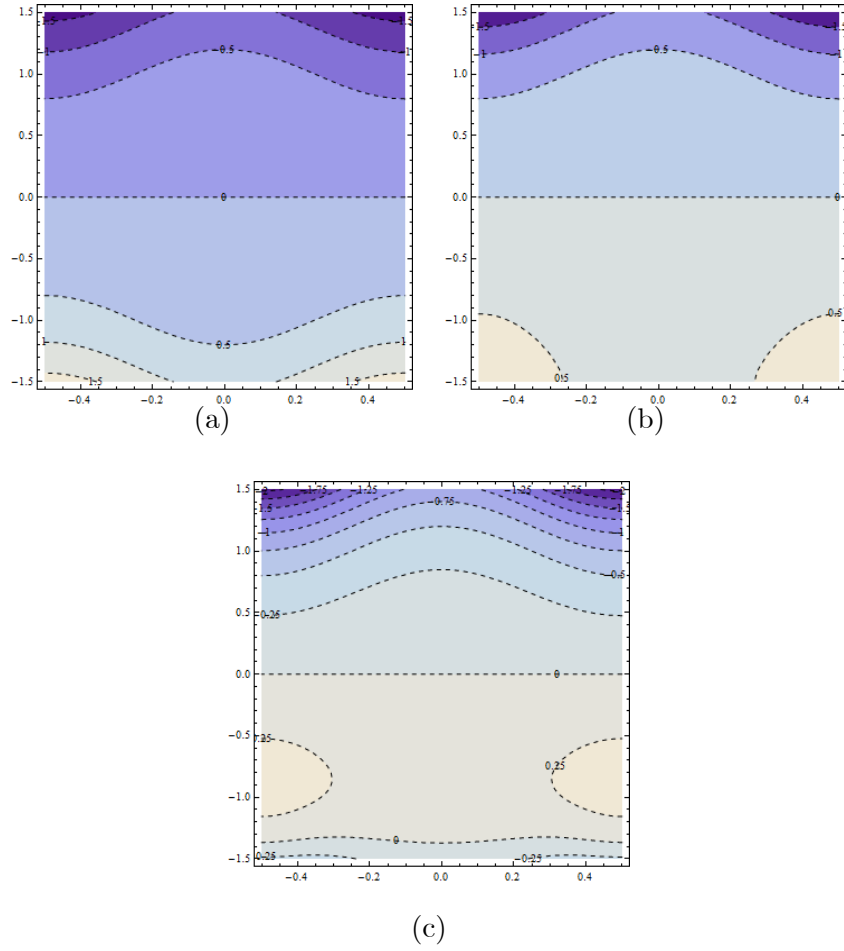


Fig. 11.21: The streamlines in wave frame for (a)  $We = 0.0$ , (b)  $We = 0.4$  and (c)  $We = 0.8$ .

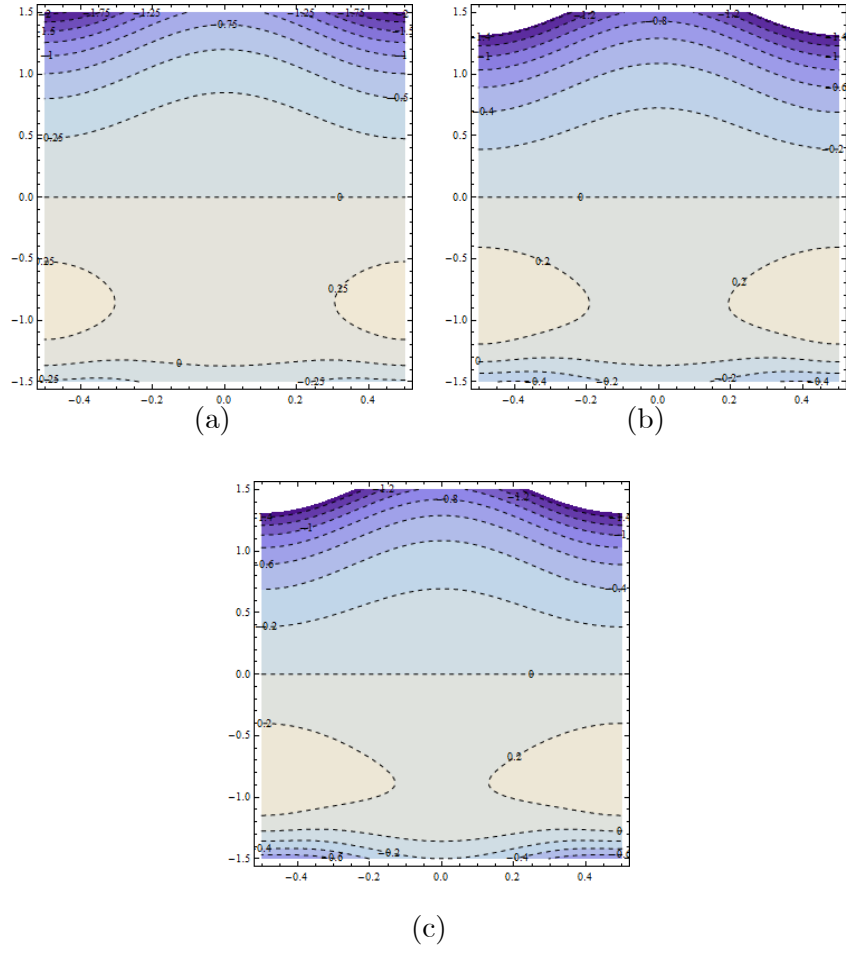


Fig. 11.22: The streamlines in wave frame for (a)  $M = 1.5$ , (b)  $M = 2$  and (c)  $M = 3$ .

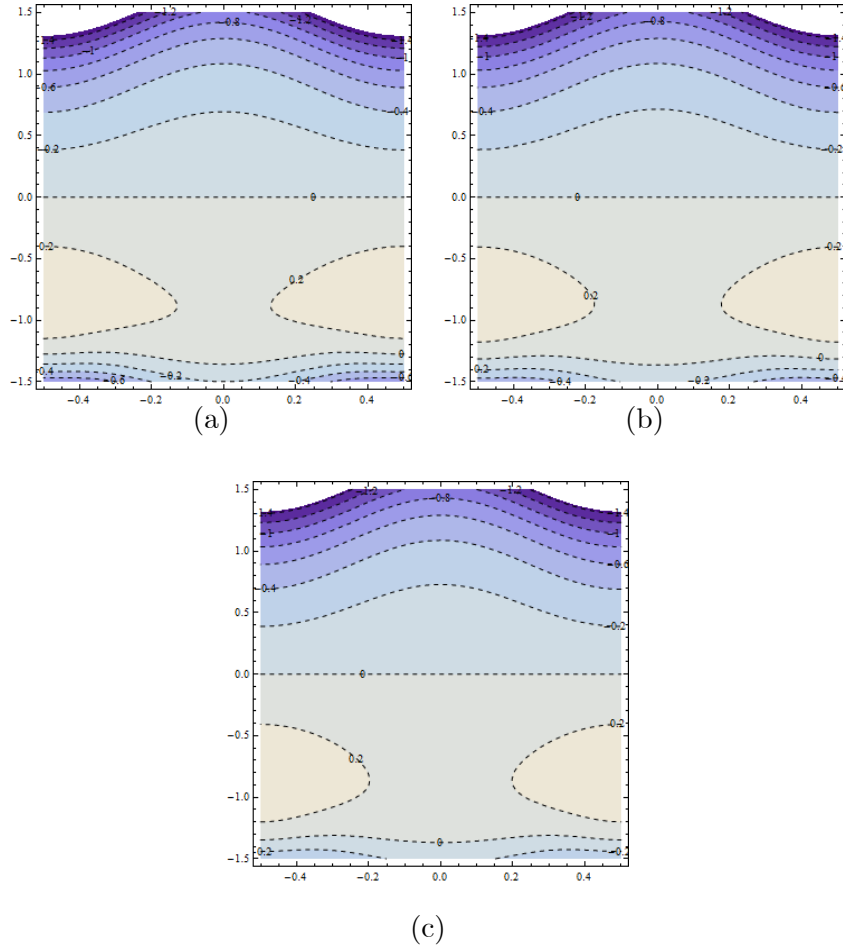


Fig. 11.23: The streamlines in wave frame for (a)  $\hat{m} = 0.5$ , (b)  $\hat{m} = 1$  and (c)  $\hat{m} = 1.5$ .

## 11.6 Concluding remarks

This chapter addresses the Joule heating, viscous dissipation and Hall effects in the peristaltic motion of Williamson fluid. The convective conditions for both heat and mass transfer at the channel walls are employed. The main observations have been summarized as follows.

- The axial pressure gradient  $dp/dx$  decreases with an increase in the Hall parameter  $\hat{m}$  while it decreases by increasing Hartman number  $M$ .
- Effect of Hartman number  $M$  on temperature  $\theta(y)$  is quite opposite to that of Hall parameter  $\hat{m}$  and Weissenberg number  $We$ .

- Effects of Hartman number  $M$ , Hall parameter  $\hat{m}$  and Weissenberg number  $We$  on the temperature  $\theta(y)$  and concentration  $\phi(y)$  are opposite.
- The variations of Hartman number  $M$  and Weissenberg number  $We$  on the longitudinal velocity  $u(y)$  are quite reverse to that of Hall parameter  $\hat{m}$ .
- An increase in the heat transfer Biot number  $\gamma_t$  decays the fluid temperature.
- The concentration of fluid increases when mass transfer Biot number  $\gamma_m$  is increased.
- In the absence of Joule heating effect the roles of Hartman number  $M$  and Hall parameter  $\hat{m}$  on the temperature  $\theta(y)$  and concentration  $\phi(y)$  distributions are reversed.



# Chapter 12

## Summary

Here the research conducted in this thesis is summarized through the contents of chapters' two to eleven. In all these chapters, the main focus is to investigate the novel idea of convective heat transfer for different non-Newtonian fluids exhibiting peristaltic motion in channels (symmetric or asymmetric). The channel asymmetry is produced by choosing the peristaltic waves along channel walls having different amplitudes and phase difference. Lubrication approximation is used for mathematical modelling. To obtain the series solutions for the stream function, temperature, concentration and pressure gradient, the regular and homotopy perturbation techniques are used. Exact solutions are also obtained in some chapters as well. Numerical integration is performed to calculate the pressure rise per wavelength. Variation of sundry parameters on the velocity, pressure gradient, pressure rise per wavelength, temperature, concentration and streamlines are shown graphically and discussed physically. The main observations of the conducted study are as follows:

- Pressure gradient increases when there is an increase in Deborah number, power-law fluid and Casson fluid parameters.
- Pressure gradient decreases by increasing the Sisko and couple stress fluid parameters, Weissenberg number, viscosity ratio, slip parameters, magnetic and Hall parameters.
- It is worth mentioning that the pressure rise per wavelength is enhanced in the peristaltic pumping region through larger Deborah number, upper and lower wave amplitudes, viscosity ratio parameter, Casson, couple stress parameter, power-law parameter, Sisko fluid

parameter, Hartman number and Weissenberg number. However pressure rise decays in the co-pumping region for these parameters.

- With an increase in phase difference, channel width, slip and Hall parameter, pressure rise per wavelength decreases in the peristaltic pumping region while these parameters have opposite effects in co-pumping region.
- The magnitude of the axial velocity increases at the center of channel for increasing values of couple stress fluid, power-law fluid, microrotation parameter and coupling number.
- In the narrow part of the channel, the magnitude of axial velocity decreases when there is an increase in Deborah number, Weissenberg number, Carreau fluid, Casson fluid, magnetic and Hall parameters.
- Temperature of the fluid decays with increasing Biot numbers at the upper and lower channel walls, Soret number, constructive chemical reaction parameter and Weissenberg number.
- By increasing Deborah number, Brinkman, Prandtl, Schmidt and Dufour numbers, temperature of the fluid enhances. Same is the case for Brownian motion, thermophoresis, couple stress fluid, viscosity ratio and Slip parameters, Sisko fluid, magnetic and Hall parameters and destructive chemical reaction parameters.
- The case of the prescribed surface temperature can be obtained as the special case of the presented studies for large values of Biot numbers.
- Concentration of the fluid increases when Brownian motion parameter and mass transfer Biot number are increased.
- An increase in Soret, Dufour and Schmidt numbers, fluid concentration decreases. Also there is a decrease in concentration for increasing values of thermophoresis, chemical reaction and magnetic and Hall parameters.
- Magnitude of heat transfer coefficient increases for Biot numbers at the upper and lower channel walls, Brinkman number, Brownian motion and thermophoresis parameter. On the other hand it decreases with an increase in Weissenberg number.

- Size of the trapped bolus decreases for Deborah number, phase difference, Casson fluid, Weissenberg number, Hall parameter, Couple stress fluid, viscosity ratio and slip parameters while it increases when flow rate, power-law fluid parameter, slip and magnetic parameters are increased.

All the chapters in this thesis provide the basis for the convective heat and mass transfer analysis in peristaltic flows with different rheological effects. These studies can be extended to discuss more complicated situations in the regime of peristalsis. The following problems will be discussed in future regarding to the peristaltic flows:

- Convective heat and mass transfer with Soret and Dufour effects.
- Effects of radiation, Joule heating and magnetohydrodynamics with convection.
- Nanofluid with different non-Newtonian fluids as base materials.
- Consideration of different flow geometries such as ducts, cylindrical tubes, annulus, curved channels etc.

# Bibliography

- [1] T. W. Latham, Fluid motion in a peristaltic pump, MIT Cambridge MA, (1966).
- [2] A. H. Shapiro, Pumping and retrograde diffusion in peristaltic waves, “Proceedings Workshop on ureteral reflux in children”. National Academy of Science (Natural Research Council) (1967) 109-126.
- [3] J. C. Burns and T. Parkes, Peristaltic motion, J. Fluid Mech. 29 (1967) 731-743.
- [4] Y. C. Fung and C. S. Yih, Peristaltic transport, J. Appl. Mech. 35 (1968) 669-675.
- [5] C. Barton and S. Raynor, Peristaltic flow in tubes, Bull. Math. Bio. 30 (1968) 663-680.
- [6] A. H. Shapiro, M. Y. Jaffrin and S. L. Weinberg, Peristaltic pumping with long wavelengths at low Reynolds number, J. Fluid Mech. 37 (1969) 799-825.
- [7] C. C. Yin and Y. C. Fung, Peristaltic wave in circular cylindrical tubes, J. Appl. Mech. 36 (1969) 579-587.
- [8] M. Y. Jaffrin and A. H. Shapiro, Peristaltic pumping, Ann. Rev. Fluid Mech. 3 (1971) 13-36.
- [9] T. F. Zien and S. Ostrach, A long wave approximation to peristaltic motion, J. Biomech. 3 (1970) 63-75.
- [10] H. S. Lew, Y. C. Fung and C. B. Lowenstein, Peristaltic carrying and mixing of chyme in the small intestine (An analysis of a mathematical model of peristalsis of the small intestine), J. Biomech. 4 (1971) 297-315.

- [11] H. S. Lew and Y. C. Fung, A study on the low Reynolds number in a valved vessel, J. Biomech. 4 (1971) 85-94.
- [12] M. Y. Jafrin, Inertia and streamline curvature effects on peristaltic pumping, Int. J. Eng. Sci. 11 (1973) 681-699.
- [13] R. E. Smelser, W. J. Shack and T. J. Lardner, The swimming of spermatozoa in an active channel, J. Biomech. 7 (1974) 349-355.
- [14] B. B. Gupta and V. Seshadri, Peristaltic pumping in non-uniform tubes, J. Biomech. 9 (1976) 105-109.
- [15] N. Liron, On peristaltic flow and its efficiency, Bull. Math. Bio. 38 (1976) 573-596.
- [16] V. K. Stud, G. S. Sephon and R. K. Mishra, Pumping action on blood flow by a magnetic field, Bull. Math. Bio. 39 (1977) 385-390.
- [17] L. M. Srivastava and V. P. Srivastava, Peristaltic transport of a two-layered model of physiological fluid, J. Biomech. 15 (1982) 257-265.
- [18] H. L. Agrawal and B. Anwaruddin, Peristaltic flow of blood in a branch, Ranchi Uni. Math. J. 15 (1984) 111-118.
- [19] S. Metry and G. Chauvet, A numerical computation of a 3D Stokes problem in the description of intestinal peristaltic waves, Simul. Practice Theory 2 (1995) 179-203.
- [20] A. R. Rao and S. Usha, Peristaltic transport of two immiscible viscous fluids in a circular tube, J. Fluid. Mech. 298 (1995) 271-285.
- [21] W. K. H. Chu and J. Fang, Peristaltic transport in a slip flow, Europ. Phys. J. B 16 (2000) 543-547.
- [22] O. Eytan, A. J. Jaffa and D. Elad, Peristaltic flow in a tapered channel: application to embryo transport within the uterine cavity, Medical Eng. Phys. 23 (2001) 475-482.
- [23] K. P. Selverov and H. A. Stone, Peristaltically driven channel flows with applications to ward micromixing, Phys. Fluids 13 (2001) 1837-1859.

- [24] E. F. El-Shehawey and S. Z. A. Husseny, Peristaltic transport of a magneto-fluid with porous boundaries, *Appl. Math. Comput.* 129 (2002) 421-440.
- [25] E. F. El-Shehawey, E. M. E. Elbarbary and N. S. Elgazery, Effects of inclined magnetic field on magneto fluid flow through a porous medium between two inclined wavy porous plates (numerical study), *Appl. Math. Comput.* 135 (2003) 85-103.
- [26] Kh. S. Mekheimer, Peristaltic flow of blood under effect of a magnetic field in a non-uniform channels, *Appl. Math. Comput.* 153 (2004) 763-777.
- [27] M. Mishra and A. R. Rao, Peristaltic transport in an asymmetric channel, *Z. Angew. Math. Phys. (ZAMP)* 54 (2003) 532-550.
- [28] E. E. Tzirtzilakis, A mathematical model for blood flow in magnetic field, *Phys. Fluids* 17 (2005) 077103-077117.
- [29] M. M. Teymoori and E. A. Sani, Design and simulation of a novel electrostatic peristaltic micromachined pump for drug delivery applications, *Sensors and Actuators A: Physical* 117 (2005) 222-229.
- [30] E. F. El-Shehawey, N. T. Eldabe, E. M. Elghazy and A. Ebaid, Peristaltic transport in an asymmetric channel through porous medium, *Appl. Math. Comput.* 182 (2006) 140-150.
- [31] V. P. Srivastava, Effects of an inserted endoscope on chyme movement in small intestine, *Appl. Appl. Math.* 2 (2007) 79-91.
- [32] T. T. Nguyen, M. Pham and N. S. Goo, Development of a peristaltic micropump for biomedical applications based on Mini LIPCA, *J. Bionic Eng.* 5 (2008) 135-141.
- [33] A. Ebaid, Effects of magnetic field and wall slip conditions on the peristaltic transport of a Newtonian fluid in an asymmetric channel, *Phys. Lett. A* 37 (2008) 4493-4499.
- [34] N. Ali, Q. Hussain, T. Hayat and S. Asghar, Slip effects on the peristaltic transport of MHD fluid with variable viscosity, *Phys. Lett. A* 372 (2008) 1477-1489.
- [35] J. J. Lozano and M. Sen, Streamline topologies of two-dimensional peristaltic flow and their bifurcations, *Chem. Eng. Processing: Process Intensification* 49 (2010) 704-715.

- [36] S. W. Walker and M. J. Shelley, Shape optimization of peristaltic pumping, *J. Comput. Phys.* 229 (2010) 1260-1291.
- [37] Kh. S. Mekheimer and A. N. Abdel-Wahab, Net annulus flow of a compressible viscous liquid with peristalsis, *J. Aerospace Eng.* 25 (2011) 660-669.
- [38] M. Keimanesh, M. M. Rashidi, A. J. Chamkha and R. Jafari, Study of a third grade non-Newtonian fluid flow between two parallel plates using the multi-step differential transform method, *Computers Math. Appl.* 62 (2011) 2871-2891.
- [39] K. K. Raju and R. Devanathan, Peristaltic motion of a non-Newtonian fluid, *Rheol. Acta* 11 (1972) 170-178.
- [40] N. Casson, A flow equation for pigment oil-suspensions of the printing ink type In: C. C. Mill, editor, *Rheology of disperse system*, London: Pergamon Press (1959) 84-105.
- [41] K. K. Raju and R. Devanathan, Peristaltic motion of a non-Newtonian fluid Part II. Visco-elastic fluid, *Rheol. Acta* 13 (1974) 944-948.
- [42] M. W. Johnson and D. Segalman, A model for viscoelastic fluid behavior which allows non-affine deformation, *J. Non-Newtonian Fluid Mech.* 2 (1977) 255-270.
- [43] A. C. Eringen, Nonlinear theory of simple micro-elastic solids-I, *Int. J. Eng. Sci.* 2 (1964) 189-203.
- [44] A. C. Eringen, Theory of micropolar fluids, *J. Math. Mech.* 16 (1966) 1-16.
- [45] G. Bohme and R. Friedrich, Peristaltic flow of visco-elastic liquids, *J. Fluid Mech.* 128 (1983) 109-122.
- [46] L. M. Srivastava and V. P. Srivastava, Peristaltic transport of blood: Casson fluid II, *J. Biomech.* 17 (1984) 821-829.
- [47] L. M. Srivastava and V. P. Srivastava, Peristaltic transport of a non-Newtonian fluid: Applications to the vas deferens and small intestine, *Ann. Biomed. Eng.* 13 (1985) 137-153.

- [48] P. Chaturani and R. P. Samy, A study of non-Newtonian aspects of blood flow through stenosed arteries and its application in arterial diseases, *J. Biorheol.* 22 (1985) 521-531.
- [49] A. M. El Misery, E. F. El-Shehawey and A. A. Hakeem, Peristaltic motion of an incompressible generalized Newtonian fluid in a planar channel, *J. Phys. Soc. Japan* 65 (1996) 3524-3529.
- [50] A. M. Siddiqui and W. H. Schwarz, Peristaltic motion of a third order fluid in a planar channel, *Rheol. Acta* 32 (1993) 47-56.
- [51] A. M. Siddiqui and W. H. Schwarz, Peristaltic flow of a second order fluid in tubes, *J. Non-Newtonian Fluid Mech.* 53 (1994) 257-284.
- [52] H. Strohmer, A. Obruca, K. M. Rander and W. Feichtinger, Relationship of the individual uterine size and the endometrial thickness in stimulated cycles, *Fertil. Steril.* 61 (1994) 972-975.
- [53] S. Usha and A. R. Rao, Peristaltic transport of a two-layered power-law fluids, *J. Biomech. Eng.* 119 (1997) 483-488.
- [54] O. Eytan and D. Elad, Analysis of intra-uterine fluid motion induced by uterine contractions, *Bull. Math. Biol.* 61 (1999) 221-238.
- [55] J. C. Misra and S. K. Pandey, A mathematical model for oesophageal swallowing of a food-bolus, *Math. Comput. Model.* 33 (2001) 997-1009.
- [56] A. V. Mernone, J. N. Mazumdar and S. K. Lucas, A mathematical study of peristaltic transport of Casson fluid, *Math. Comput. Model.* 35 (2002) 894-912.
- [57] A. R. Rao and M. Mishra, Peristaltic transport of a power-law fluid in a porous tube, *J. Non-Newtonian Fluid Mech.* 121 (2004) 163-174.
- [58] P. N. Rani and G. Sarojamma, Peristaltic transport of a Casson fluid in an asymmetric channel, *Australian Phys. Eng. Sci. Med.* 27 (2004) 49-59.
- [59] K. Vajravelu, S. Sreenadh and V. R. Babu, Peristaltic pumping of a Herschel-Bulkley fluid in a channel, *Appl. Math. Comput.* 169 (2005) 726-735.



- [60] K. Vajravelu, S. Sreenadh and V. R. Babu, Peristaltic transport of a Herschel-Bulkley fluid in contact with a Newtonian fluid, *Quarterly J. Appl. Mech.* 64 (2006) 593-604.
- [61] M. H. Haroun, Effect of Deborah number and phase difference on peristaltic transport of a third-order fluid in an asymmetric channel, *Comm. Nonlinear Sci. Numer. Simul.* 12 (2007) 1464-1480.
- [62] T. Hayat and N. Ali, Peristaltically induced motion of MHD third grade fluid in a deformable tube, *Physica A* 370 (2006) 225-239.
- [63] T. Hayat, A. Afsar, M. Khan and S. Asghar, Peristaltic transport of a third order fluid under the effect of a magnetic field, *Comput. Math. Appl.* 53 (2007) 1074-1087.
- [64] T. Hayat, M. U. Qureshi and N. Ali, The influence of slip on the peristaltic motion of a third order fluid in an asymmetric channel, *Phys. Lett. A* 372 (2008) 2653-2664.
- [65] T. Hayat, Y. Khan, N. Ali and Kh. S. Mekheimer, Effect of an induced magnetic field on the peristaltic flow of a third order fluid, *Numer. Methods Partial Diff. Eqs.* 26 (2009) 345-360.
- [66] M. H. Haroun, Nonlinear peristaltic flow of a fourth grade fluid in an inclined asymmetric channel, *Comput. Mat. Sci.* 39 (2007) 324-333.
- [67] D. Tsiklauri and I. Beresnev, Non-Newtonian effects in the peristaltic flow of a Maxwell fluid, *Phys. Rev. E* 64 (2001) 036303-036331.
- [68] E. F. El-Shehawey, N. T. El-dabe and I. M. Eldesoky, Slip effects on the peristaltic flow of a non-Newtonian Maxwellian fluid, *Acta Mech.* 186 (2006) 141-159.
- [69] T. Hayat, N. Alvi and N. Ali, Peristaltic mechanism of a Maxwell fluid in an asymmetric channel, *Nonlinear Analysis: RWA* 9 (2008) 1474-1490.
- [70] T. Hayat, Y. Wang, K. Hutter, S. Asghar and A. M. Siddiqui, Peristaltic transport of an Oldroyd-B fluid in a planar channel, *Math. Prob. Eng.* 4 (2004) 347-376.
- [71] M. H. Haroun, Effect of relaxation and retardation time on peristaltic transport of the Oldroydian viscoelastic fluid, *J. Appl. Mech. Tech. Phys.* 46 (2005) 842-850.

- [72] T. Hayat, N. Ali and S. Asghar, Peristaltic motion of a Burger's fluid in a planar channel, *Appl. Math. Comput.* 186 (2007) 309-329.
- [73] N. T. M. Eldabe, M. F. El-Sayed, A. Y. Galy and H. M. Sayed, Peristaltically induced transport of a MHD biviscosity fluid in a non-uniform tube, *Physica A* 383 (2007) 253-266.
- [74] N. Ali and T. Hayat, Peristaltic flow of a micropolar fluid in an asymmetric channel, *Comp. Math. Appl.* 55 (2008) 589-608.
- [75] N. Ali and T. Hayat, Peristaltic motion of a Carreau fluid in an asymmetric channel, *Appl. Math. Comput.* 193 (2007) 535-552.
- [76] M. Kothandapani and S. Srinivas, Peristaltic transport of a Jeffrey fluid under the effect of magnetic field in an asymmetric channel, *Int. J. Nonlinear Mech.* 43 (2008) 915-924.
- [77] Y. Wang, T. Hayat, N. Ali and M. Oberlack, Magnetohydrodynamic peristaltic motion of Sisko fluid in a symmetric or asymmetric channel, *Physica A* 387 (2008) 347-362.
- [78] P. Hariharan, V. Seshadri and R. K. Banerjee, Peristaltic transport of non-Newtonian fluid in a diverging tube with different wave forms, *Math. Comput. Model.* 48 (2008) 998-1017.
- [79] S. Nadeem and N. S. Akbar, Peristaltic flow of Walter's B fluid in a uniform inclined tube, *J. Biorheol.* 24 (2010) 22-28.
- [80] N. Ali, M. Sajid, Z. Abbas and T. Javed, Non-Newtonian fluid flow induced by peristaltic waves in a curved channel, *Europ. J. Mech.-B/ Fluids* 29 (2010) 387-394.
- [81] Y. Abd elmaboud and Kh. S. Mekheimer, Nonlinear peristaltic transport of a second order fluid through a porous medium, *Appl. Math. Model.* 35 (2011) 2695-2710.
- [82] R. Ellahi, A. Riaz, S. Nadeem and M. Mushtaq, Series solutions of magnetohydrodynamic peristaltic flow of a Jeffrey fluid in eccentric cylinders, *Appl. Math. Inf. Sci.* 7 (2013) 1441-1449.
- [83] D. Tripathi, Numerical study on peristaltic transport of fractional bio-fluids, *J. Mech. Med. Biol.* 11 (2011) 1045-1058.

- [84] S. Nadeem, N. S. Akbar, T. Hayat and A. A. Hendi, Peristaltic flow of Walter's B fluid in endoscope, *Appl. Math. Mech.* 32 (2012) 689-700.
- [85] C. Fetecau, C. Fetecau, M. Jamil and A. Mahmood, Flow of fractional Maxwell fluid between coaxial cylinders, *Arch. Appl. Mech.* 81 (2011) 1153-1163.
- [86] S. Noreen, T. Hayat and A. Alsaedi, Study of slip and induced magnetic field on the peristaltic flow of pseudoplastic fluid, *Int. J. Phys. Sci.* 6 (2011) 8018-8026.
- [87] T. Hayat, N. Saleem, Y. Abd elmaboud and S. Asghar, Peristaltic flow of a second order fluid in the presence of an induced magnetic field, *Int. J. Numer. Meth. Fluids* 67 (2011) 537-558.
- [88] K. Yazdanpanh-Ardakani and H. Niroomand-Oscuii, New approach in modeling peristaltic transport of non-Newtonian fluid, *J. Mech. Med. Biol.* 13 (2013) DOI:10.1142/S0219519413500528.
- [89] S. Maiti and J. C. Misra, Peristaltic transport of a couple stress fluid: Some applications to hemodynamics, *J. Mech. Med. Biol.* 12 (2012) ID 1250048 (21 pages).
- [90] T. R. Rao and D. R. V. P. Rao, Peristaltic flow of a couple stress fluid through a porous medium in a channel at low Reynolds number, *Int. J. Appl. Math. Mech.* 8 (2012) 97-116.
- [91] T. Hayat, S. Noreen, N. Ali and S. Abbasbanday, Peristaltic motion of Phan-Thein-Tanner fluid in a planar channel, *Numer. Meth. Partial Diff. Eqs.* 28 (2012) 737-748.
- [92] T. Hayat and M. Javed, Exact solution to peristaltic transport of power-law fluid in asymmetric channel with compliant walls, *Appl. Math. Mech.* 31 (2010) 1231-1240.
- [93] A. Kalantari, K. Sadeghy and S. Sadeqi, Peristaltic flow of non-Newtonian fluids through curved channels: A numerical study, *Ann. Transac. Nordic Rheo. Soc.* 21 (2013) 163-170.
- [94] P. Hari Prabakaran, A. Kavitha, R. Saravana, R. H. Reddy and S. Sreenadh, Peritaltic transport of a fourth grade fluid between porous walls with suction and injection, *Int. J. Pure Appl. Math.* 86 (2013) 293-300.

- [95] N. S. Gad, Effect of Hall currents on interaction of pulsatile and peristaltic transport induced flows of a particle-fluid suspension, *Appl. Math. Comput.* 217 (2011) 4313-4320.
- [96] S. R. El Koumy, El Sayed I. Barakat and S. I. Abdelsalam, Hall and porous boundaries effects on peristaltic transport through porous medium of a Maxwell model, *Trans. Porous Media* 94 (2013) DOI:10.1007/s11242-012-0016-y.
- [97] R. Ellahi, A. Riaz and S. Nadeem, Three dimensional peristaltic flow of Williamson fluid in a rectangular duct, *Indian J. Phys.* 87 (2013) 1275-1281.
- [98] S. Nadeem, E. Maraj and N. S. Akbar, Investigation of peristaltic flow of Williamson nanofluid in a curved channel with compliant walls, *Appl. Nanosci.* (2013) DOI:10.1007/s13204-013-0234-9.
- [99] S. Akram, S. Nadeem and M. Hanif, Numerical and analytical treatment on peristaltic flow of Williamson fluid in the occurrence of induced magnetic field, *J. Magn. Magn. Mater.* 346 (2013) 142-151.
- [100] G. Radhakrishnamacharya and V. R. Murty, Heat transfer to peristaltic transport in a non-uniform channel, *Defence Sci. J.* 43 (1993) 275-280.
- [101] K. Vajravelu, G. Radhakrishnamacharya and V. Radhakrishnamurty, Peristaltic flow and heat transfer in a vertical porous annulus with long wave approximation, *Int. J. Nonlinear Mech.* 42 (2007) 754-759.
- [102] Kh. S. Mekheimer and Y. Abd elmaboud, The influence of heat transfer and magnetic field on peristaltic transport of a Newtonian fluid in a vertical annulus: Application of an endoscope, *Phys. Lett. A* 372 (2008) 1657-1665.
- [103] S. Srinivas and M. Kothandapani, Peristaltic transport in an asymmetric channel with heat transfer-A note, *Int. Commun. Heat Mass Transfer* 34 (2008) 514-522.
- [104] S. Srinivas and R. Gayathri, Peristaltic transport of a Newtonian fluid in a vertical asymmetric channel with heat transfer and porous medium, *Appl. Math. Comput.* 215 (2009) 185-196.

- [105] T. Hayat, M. U. Qureshi and Q. Hussain, Effect of heat transfer on the peristaltic flow of an electrically conducting fluid in a porous space, *Appl. Math. Model.* 33 (2009) 1862-1873.
- [106] S. Nadeem and N. S. Akbar, Effects of heat transfer on the peristaltic transport of MHD Newtonian fluid with variable viscosity: Application of Adomian decomposition method, *Comm. Nonlinear Sci. Numer. Simul.* 14 (2009) 3844-3855.
- [107] Kh. S. Mekheimer, S. Z. A. Husseny and Y. Abd Elmaboud, Effects of heat transfer and space porosity on peristaltic flow in a vertical asymmetric channel, *Numer. Methods Partial Diff. Eqs.* 26 (2010) 747-770.
- [108] C. Vasudev, U. R. Rao, M. V. S. Reddy and G. P. Rao, Effect of heat transfer on peristaltic transport of a Newtonian fluid through a porous medium in an asymmetric vertical channel, *Europ. J. Scientific Research* 44 (2010) 79-92.
- [109] S. Nadeem and S. Akram, Heat transfer in a peristaltic flow of MHD fluid with partial slip, *Comm. Nonlinear Sci. Numer. Simul.* 15 (2010) 312-321.
- [110] T. Hayat, M. Javed and S. Asghar, Slip effects in peristalsis, *Numer. Methods Partial Diff. Eqs.* 27 (2011) 1003-1015.
- [111] A. M. Sobh, S. S. Al Azab and H. H. Madi, Heat transfer in peristaltic flow of viscoelastic fluid in an asymmetric channel, *Appl. Math. Sci.* 4 (2010) 1583-1606.
- [112] S. Nadeem and N. S. Akbar, Influence of heat transfer on peristaltic flow of Jhonson-Segalman fluid in a non-uniform tube, *Int. J. Heat Mass Transfer* 36 (2009) 1050-1059.
- [113] S. Nadeem and N. S. Akbar, Effects of temperature dependent viscosity on peristaltic flow of a Jeffrey six constant fluid in a non-uniform vertical tube, *Comm. Nonlinear Sci. Numer. Simul.* 15 (2010) 3950-3964.
- [114] T. Hayat and S. Noreen, Peristaltic transport of fourth grade fluid with heat transfer and induced magnetic field, *C. R. Mecanique* 338 (2010) 518-528.
- [115] N. Ali, M. Sajid, T. Javed and Z. Abbas, Heat transfer analysis of peristaltic flow in a curved channel, *Int. J. Heat Mass Transfer* 53 (2010) 3319-3325.

- [116] N. T. M. Eldabe, M. F. El-Sayed, A. Y. Ghaly and H. M. Sayed, Mixed convective heat and mass transfer in a non-Newtonian fluid at a peristaltic surface with temperature dependent viscosity, *Arch. Appl. Mech.* 78 (2008) 599-624.
- [117] R. Muthuraj and S. Srinivas, Mixed convective heat and mass transfer in a vertical wavy channel with travelling thermal waves and porous medium, *Comp. Math. Appl.* 59 (2010) 3516-3528.
- [118] S. Nadeem, N. S. Akbar, N. Bibi and S. Ashiq, Influence of heat and mass transfer on peristaltic flow of a third order fluid in a diverging tube, *Comm. Nonlinear Sci. Numer. Simul.* 15 (2010) 2916-2931.
- [119] S. Nadeem and N. S. Akbar, Influence of radially varying MHD on the peristaltic flow in an annulus with heat and mass transfer, *J. Taiwan Institute Chemical Eng.* 41 (2010) 286-294.
- [120] T. Hayat, S. Hina and N. Ali, Simultaneous effects of slip and heat transfer on the peristaltic flow, *Commun. Nonlinear Sci. Numer. Simul.* 15 (2010) 1526-1537.
- [121] S. Srinivas, R. Gayathri and M. Kothandapani, Mixed convective heat and mass transfer in an asymmetric channel with peristalsis, *Comm. Nonlinear Sci. Numer. Simul.* 16 (2011) 1845-1862.
- [122] S. Srinivas and R. Muthuraj, Effects of chemical reaction and space porosity on MHD mixed convective flow in a vertical asymmetric channel with peristalsis, *Math. Computer Model.* 54 (2011) 1213-1227.
- [123] Kh. S. Mekheimer, N. Saleem, T. Hayat and A. A. Hendi, Simultaneous effects of induced magnetic field and heat and mass transfer on the peristaltic motion of second order fluid in a channel, *Int. J. Numer. Meth. Fluids* 70 (2011) 342-358.
- [124] Kh. S. Mekheimer and M. A. Elkot, Mathematical modelling of unsteady flow of a Sisko fluid through an anisotropically tapered elastic arteries with time-variant overlapping stenosis, *Appl. Math. Model.* 36 (2012) 5393-5407.

- [125] N. S. Akbar, T. Hayat, S. Nadeem and A. A. Hendi, Effects of slip and heat transfer on the peristaltic flow of a third order fluid in an inclined asymmetric channel, *Int. J. Heat and Mass Trans.* 54 (2011) 1654-1664.
- [126] K. Vajravelu, S. Sreenadh and P. Lakshminarayana, The influence of heat transfer on peristaltic transport of a Jeffrey fluid in a vertical porous stratum, *Commu. Nonlinear Sci. Numer. Simul.* 16 (2011) 3107-3125.
- [127] D. Tripathi, A mathematical model for swallowing of food bolus through the esophagus under the influence of heat transfer, *Int. J. Thermal Sci.* 51 (2012) 91-101.
- [128] T. Hayat, S. Hina and A. A. Hendi, Slip effects on peristaltic transport of a Maxwell fluid with heat and mass transfer, *J. Mech. Med. Biol.* 12 (2012) DOI:10.1142/S0219519412004375.
- [129] D. A. Nield and A. V. Kuznetsov, The Cheng-Minkowycz problem for the double diffusive natural convective boundary layer flow in a porous medium saturated by a nanofluid, *Int. J. Heat and Mass Trans.* 54 (2011) 374-378.
- [130] R. Ellahi, S. Aziz and A. Zeeshan, Non-Newtonian nanofluid flow through a porous medium between two coaxial cylinders with heat transfer and variable viscosity, *J. Porous Media* 16 (2013) 205-216.
- [131] R. Ellahi, The effects of MHD and temperature dependent viscosity on the flow of non-Newtonian nanofluid in a pipe: Analytical solutions, *Appl. Math. Model.* 37 (2013) 1451-1457.
- [132] N. T. Eldabe, S. M. Elshaboury, A. Hasan Alfaisal and M. A. Elogial, MHD peristaltic flow of a couple stress fluid with heat and mass transfer through a porous medium, *Inn. Syst. Des. Eng.* 3 (2012) ISSN 2222-2871.
- [133] S. Nadeem, A. Riaz, R. Ellahi and N. S. Akbar, Effects of heat and mass transfer on peristaltic flow of a nanofluid between eccentric cylinders, *Appl. Nanosci.* 4 (2013) 393-404.

- [134] T. Hayat, F. M. Abbasi and S. Obaidat, Peristaltic motion with Soret and Dufour effects, *Magnetohydrodynamics* 47 (2011) 295-302.
- [135] A. M. Sobh, Peristaltic slip flow of a viscoelastic fluid with heat and mass transfer in a tube, *Math. Prob. Eng.* 2012 (2012) ID 815747 (23 pages).
- [136] T. R. Rao and D. R. V. P. Rao, The influence of heat transfer on peristaltic transport of a couple stress fluid through a porous medium, *Advan. Appl. Sci. Research* 3 (2012) 2355-2368.
- [137] S. Srinivas, R. Muthuraj and J. Sakina, A note on the influence of heat and mass transfer on a peristaltic flow of a viscous fluid in a vertical asymmetric channel with wall slip, *Chem. Ind. Chem. Eng. Quarterly* 18 (2012) 483-493.
- [138] Y. Abd elmaboud, Kh. S. Mekheimer and A. I. Abdellateef, Thermal properties of couple stress fluid flow in an asymmetric channel with peristalsis, *J. Heat Trans.* 135 (2013) ID 044502.
- [139] M. F. El-Sayed, N. T. M. Eldabe and A. Y. Ghaly, Effect of chemical reaction, heat and mass transfer on non-Newtonian fluid flow through porous medium in a vertical peristaltic tube, *Transp. Porous Media*, 89 (2011) 185-212.
- [140] A. A. Shaaban and M. Y. Abou-Zeid, Effects of heat and mass transfer on MHD peristaltic flow of a non-Newtonian fluid through a porous medium between two coaxial cylinders, *Math. Prob. Eng.* 2013 (2013) ID 819683.
- [141] R. Saravana, R. Hemadri Reddy, S. Sreenadh, S. Vekataramana and A. Kavitha, Influence of slip, heat and mass transfer on the peristaltic transport of a third order fluid in an inclined asymmetric channel, *Int. J. Appl. Math. Mech.* 9 (2013) 51-86.
- [142] S. Hina, T. Hayat and A. Alsaedi, Slip effects on MHD peristaltic motion with heat and mass transfer, *Arab. J. Sci. Eng.* 39 (2014) 593-603.
- [143] R. Ellahi, M. M. Bhatti and K. Vafai, Effects of heat and mass transfer on peristaltic flow in a non-uniform rectangular duct, *Int. J. Heat Mass and Trans.* 71 (2014) 706-719.



- [144] T. K. Mitra and S. N. Prasad, On the influence of wall properties and Poiseuille flow in peristalsis, *J. Biomech.* 6 (1973) 681-693.
- [145] C. Davies and P. W. Carpenter, Instabilities in a plane channel flow between compliant walls, *J. Fluid Mech.* 352 (1997) 205-243.
- [146] M. H. Haroun, Effect of wall compliance on peristaltic transport of a Newtonian fluid in an asymmetric channel, *Math. Prob. Eng.* 2006 (2006) 61475-61493.
- [147] G. Radhakrishnamacharya and Ch. Srinivasulu, Influence of wall properties on peristaltic transport with heat transfer, *C. R. Mecanique* 335 (2007) 369-373.
- [148] P. Muthu, B. V. R. Kumar and P. Chandra, Peristaltic motion of micropolar fluid in circular cylindrical tubes: Effect of wall properties, *Appl. Math. Model.* 32 (2008) 2019-2033.
- [149] M. A. Abd Elnaby and M. H. Haroun, a new model for study the effect of wall properties on peristaltic transport of a viscous fluid, *Comm. Nonlinear Sci. Numer. Simul.* 13 (2008) 752-762.
- [150] T. Hayat, M. Javed and S. Asghar, MHD peristaltic motion of Jhonson-Segalman fluid in a channel with compliant walls, *Phys. Lett. A* 372 (2008) 5026-5036.
- [151] T. Hayat, M. Javed and N. Ali, MHD peristaltic transport of Jeffrey fluid in a channel with compliant walls and porous space, *Transport in Porous Media* 74 (2008) 259-274.
- [152] N. Ali, T. Hayat and S. Asghar, Peristaltic flow of a Maxwell fluid in a channel with compliant walls, *Chaos Solitons Fractals* 39 (2009) 407-416.
- [153] M. Kothandapani and S. Srinivas, On the influence of wall properties in the MHD peristaltic transport with heat transfer and porous medium, *Phys. Lett. A* 372 (2008) 4586-4591.
- [154] S. Srinivas, R. Gayathri and M. Kothandapani, The influence of slip conditions, wall properties and heat transfer on MHD peristaltic transport, *Comput. Phys. Commun.* 180 (2009) 2115-2122.

- [155] S. Srinivas and M. Kothandapani, The influence of heat and mass transfer on MHD peristaltic flow through a porous space with compliant walls, *Appl. Math. Comput.* 213 (2009) 197-208.
- [156] M. Mustafa, S. Hina, T. Hayat and A. Alsaedi, Influence of wall properties on the peristaltic flow of a nanofluid: Analytical and numerical solutions, *Int. J. Heat and Mass Trans.* 55 (2012) 4871-4877.
- [157] M. Mustafa, S. Hina, T. Hayat and A. Alsaedi, Slip effects on the peristaltic motion of nanofluid in a channel with wall properties, *ASME Journal of Heat Transfer*, 135 (2013) ID 041701 (7 pages).
- [158] N. T. M. Eldabe, A. S. Zaghrout, H. M. Shawky and A. S. Awad, Effects of chemical reaction with heat and mass transfer on peristaltic motion of power-law fluid in an asymmetric channel with wall's properties, *Int. J. Research and Reviews in Appl. Sci.* 15 (2013) 280-292.
- [159] T. Hayat, S. Hina, S. Asghar and S. Obaidat, Peristaltic flow of a Maxwell fluid in an asymmetric channel with wall properties, *Int. J. Phys. Sci.* 7 (2012) 2145-2155.
- [160] S. Hina, T. Hayat and A. Alsaedi, Heat and mass transfer effects on the peristaltic flow of Jhonson-Segalman fluid in a curved channel with compliant walls, *Int. J. Heat and Mass Trans.* 55 (2012) 3511-3521.